TUM School of Engineering and Design
Technische Universität München

Optimization of open-loop shallow geothermal systems

Smajil Halilović, M.Sc.

Vollständiger Abdruck der von der TUM School of Engineering and Design der Technischen Universität München zur Erlangung des akademischen Grades eines

Doktors der Ingenieurwissenschaften (Dr.-Ing.)

genehmigten Dissertation.

Vorsitz:
Prof. Dr.- Ing. Andreas Kremling

Prüfende der Dissertation:
1. Prof. Dr. rer. nat. Thomas Hamacher
2. Prof. Dr. rer. nat. Michael Ulbrich
3. Prof. Matthew D. Piggott, Ph.D.

Die Dissertation wurde am 20.11.2023 bei der Technischen Universität München eingereicht und durch die TUM School of Engineering and Design am 23.04.2024 angenommen.

Acknowledgements

Throughout my doctoral journey I have received support from many people to whom I would like to express my gratitude.

I thank my supervisor Prof. Thomas Hamacher for giving me the opportunity to do my PhD in the ENS chair and for the freedom to find my way, explore new research fields and learn. I would also like to thank my mentor Philipp Kuhn for his support and for his help with the administrative hurdles that I faced.

I am thankful to my longtime collaborators and co-authors for expanding my knowledge: Fabian Böttcher and Kai Zosseder from the Chair of Hydrogeology, and Leonhard Odersky, my office mate. This dissertation would not have been possible without their support.

I thank Prof. Matt Piggott and Stephan Kramer from Imperial College London for hosting me as a visiting researcher in their research group. This has been one of the most instructive and enriching experiences during my doctoral studies. I would also like to thank them for their collaboration on the publication that is included in this thesis.

To all my former and current colleagues, thank you for all the nice lunch and coffee breaks and for the fruitful and insightful discussions over the years. You have made coming to the office a pleasant experience that I looked forward to.

Finally, I thank my family for their unconditional support throughout my life. I dedicate this work to them.

Abstract

Open-loop shallow geothermal systems, also known as groundwater heat pumps, are a promising technology for reducing carbon emissions in the residential heating and cooling sector. To improve the efficiency and sustainability of these systems, it is important to optimize their design and operation. These systems simultaneously impact the geothermal resource, i.e. groundwater, and depend on its conditions. Consequently, these bidirectional interactions with groundwater must be carefully considered within the optimization process. In addition, since groundwater is a shared geothermal resource, there can be negative interactions between neighboring systems. Therefore, optimization approaches should not be limited to stand-alone systems, but also include simultaneous optimization of multiple neighboring systems to maximize the geothermal potential of groundwater. However, existing approaches for optimizing groundwater heat pumps are considerably limited, primarily due to the inherent complexity of the resulting optimization problems with constraints, which naturally take the form of partial differential equations.

This thesis presents a set of novel approaches for efficient and effective optimization of open-loop shallow geothermal systems. The approaches enable the optimization of individual systems as well as multiple neighboring systems, addressing key aspects such as optimal well placement and sizing. Two of the developed approaches are based on approximate analytical groundwater models, while the third is based on numerical groundwater simulation. The practical applicability of the new approaches in real-world scenarios is demonstrated through various case studies. Overall, this thesis provides valuable tools to a wide range of stakeholders, especially researchers and practitioners engaged in thermal groundwater management and optimization of shallow geothermal systems.

Zusammenfassung

Offene oberflächennahe geothermische Systeme, auch bekannt als Grundwasserwärmepumpen, sind eine vielversprechende Technologie zur Verringerung der Kohlendioxid-Emissionen im häuslichen Heiz- und Kühlsektor. Um die Effizienz und Nachhaltigkeit dieser Systeme zu verbessern, ist es wichtig, ihre Auslegung und ihren Betrieb zu optimieren. Diese Systeme beeinflussen gleichzeitig die geothermische Ressource, d. h. das Grundwasser, und sind von dessen Bedingungen abhängig. Daher müssen diese bidirektionalen Wechselwirkungen mit dem Grundwasser im Rahmen des Optimierungsprozesses sorgfältig berücksichtigt werden. Da es sich beim Grundwasser um eine gemeinsam genutzte geothermische Ressource handelt, kann es darüber hinaus zu negativen Wechselwirkungen zwischen benachbarten Systemen kommen. Daher sollten sich Optimierungsansätze nicht nur auf einzelne Systeme beschränken, sondern auch die gleichzeitige Optimierung mehrerer benachbarter Systeme umfassen, um das geothermische Potenzial des Grundwassers zu maximieren. Bestehende Ansätze zur Optimierung von Grundwasserwärmepumpen sind jedoch sehr eingeschränkt, vor allem aufgrund der inhärenten Komplexität der resultierenden Optimierungsprobleme mit Nebenbedingungen, die normalerweise die Form von partiellen Differentialgleichungen haben.

In dieser Arbeit wird eine Reihe neuartiger Ansätze zur effizienten und effektiven Optimierung von offenen oberflächennahen geothermischen Systemen vorgestellt. Die Ansätze ermöglichen die Optimierung einzelner Systeme sowie mehrerer benachbarter Systeme, wobei Schlüsselaspekte wie die optimale Platzierung und Dimensionierung von Brunnen berücksichtigt werden. Zwei der entwickelten Ansätze basieren auf annähernden analytischen Grundwassermodellen, während der dritte auf einer numerischen Grundwassersimulation beruht. Die praktische Anwendbarkeit der neuen Ansätze in realen Szenarien wird anhand verschiedener Fallstudien demonstriert. Insgesamt bietet diese Arbeit wertvolle Werkzeuge für ein breites Spektrum von Akteuren, insbesondere für Forscher und Praktiker, die sich mit dem thermischen Grundwassermanagement und der Optimierung von oberflächennahen geothermischen Systemen beschäftigen.

Contents

1 Introduction

1.1 Background and context

The European Union has established the goal of achieving CO_2 neutrality in all energy-related sectors by the year 2050 [1]. This transition requires significant transformations in the heating and cooling sector, which remains predominantly dependent on fossil fuels [2]. Among the viable technologies for decarbonizing this sector, shallow geothermal energy (SGE) systems emerge as a promising solution [3, 4], since they use renewable resources and are highly efficient [5]. SGE systems can be divided into two main types [6]: closed-loop systems, also known as ground source heat pumps (GSHP), and open-loop systems, usually referred to as groundwater heat pumps (GWHP). The difference between these two types lies in the nature of the heat carrier fluid circulation. In GSHP systems, an additional heat carrier fluid circulates in a closed loop to extract heat from the subsurface [7]. In contrast, GWHPs use groundwater directly as the heat carrier fluid that transfers heat from an aquifer to the heat pump [8]. The groundwater is extracted from one or more extraction (pumping) wells and, after heat exchange within the heat pump, is re-injected into the same aquifer via one or more injection wells [6, 8]. Further details on SGE systems, with a particular focus on GWHP systems, are provided in Section 2.1.

GWHP systems affect the aquifer both thermally and hydraulically [9]. At the same time, groundwater properties such as quantity, depth, and temperature play a crucial role in determining the feasibility and efficiency of GWHPs [10, 11]. Particularly, the efficiency is predominantly influenced by the groundwater temperature at the extraction wells [12]. Thus, these systems interact bidirectionally with their energy resource (groundwater) by both impacting it and simultaneously depending on it. In addition, groundwater is a shared shallow geothermal resource, which can lead to competing interests and potential negative interactions between neighboring systems [9].

To maximize the efficiency and sustainability of GWHP systems, as well as to fully exploit the potential of thermal groundwater utilization and thereby advance this technology, optimization of these systems becomes crucial. In addition, optimization of GWHPs is also important to enable active thermal groundwater management [13] and for urban energy planning purposes [14, 15]. In a broader context, the term "optimization of GWHPs" encompasses several dimensions, depending on the specific research questions and the level of analysis. For instance, at a granular level, optimization may involve enhancing heat pump components or well geometry. Moving up to the system level, optimization includes improving GWHP design (e.g. spatial arrangement of wells) and operation (pumping rates). At this level, optimization is not limited to individual systems only, but can also include simultaneous optimization of multiple neighboring systems with the goal of maximizing the geothermal potential of groundwater. Finally, GWHPs can be optimized as integral components of higher-level systems, such as urban energy systems. These three levels of analysis and optimization are illustrated in Figure 1.1. The main focus of this thesis is on the system level, i.e. on the optimization of GWHPs in terms of design and operational aspects. At this level, it is crucial to consider groundwater conditions and interactions within the optimization process due to the previously described bidirectional coupling between GWHPs and groundwater.

1.2 State of the art

Despite the significance of the aforementioned topic on system-level optimization of GWHPs, the existing research prior to the present thesis was remarkably limited. The existing body of research found in the literature can be divided into two groups. The first group includes simulation-based analyses of GWHP system designs. This involves comparative evaluation of a few different system configurations using detailed simulation

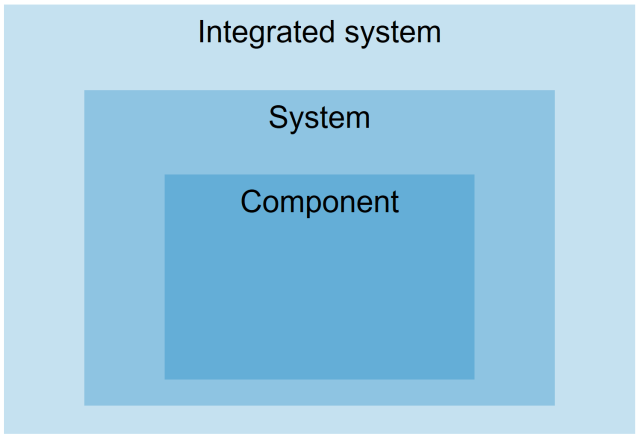

Figure 1.1 Analysis and optimization levels for GWHP systems.

models that involve numerical PDE (partial differential equation) groundwater simulations. Examples of such approaches include the works of Lo Russo and Civita [16], Zhou and Zhou [17], and Gao et al. [18]. Strictly speaking, these scenario-based approaches cannot be classified as mathematical optimization. This leads to a major drawback: these approaches generally result in only suboptimal solutions, since the design space (all feasible solutions) remains unexplored. The second major drawback of these approaches relates to the substantial time required to formulate relevant simulation scenarios and subsequently manually configure and run the corresponding simulations.

The second group of research studies involves the coupling of numerical groundwater simulation and derivative-free optimization algorithms for the purpose of GWHP optimization. Within this group, only two studies were identified prior to this thesis. Park et al [19] introduced an approach that optimizes the pumping rates of a GWHP system by coupling a numerical groundwater simulation tool and a genetic optimization algorithm. This approach is subsequently extended in [20] to include not only the optimization of pumping rates, but also the positioning of wells within a single GWHP system. The main drawback of these approaches is their high computational cost. Genetic algorithms and, more general, derivative-free algorithms require extensive number of iterations to find an optimum [21, 22]. In these approaches [19, 20], each iteration involves a computationally intensive numerical groundwater simulation. In addition, the number of optimization iterations usually increases exponentially with the number of optimization variables. Therefore, these approaches are limited to scenarios with only a few optimization variables. Moreover, due to the nature of genetic algorithms, the solution obtained is generally only a near-optimal solution, but not the global optimum [21].

Existing approaches exhibit several limitations and are insufficient for a comprehensive and efficient treatment of all aspects related to GWHP optimization. This inadequacy is particularly pronounced when dealing with the collective optimization of multiple neighboring systems due to the increased number of optimization variables in this case. In the existing literature that preceded this thesis, no study was found that considered such optimization scenarios. Therefore, there is a compelling need for novel approaches to optimize GWHP systems that are capable of overcoming the identified limitations.

1.3 Research objectives and questions

The main research objective of this thesis is to develop and evaluate novel approaches for the optimization of open-loop shallow geothermal systems, i.e. GWHP systems, that are both efficient and suitable for selected relevant applications. These approaches will also integrate groundwater-related considerations into the optimization process. By achieving this objective, the thesis will cover some of the previously identified research gaps and answer the following research questions:

1. **What are the viable approaches for the optimization of GWHP systems, and how do they compare in terms of efficiency and applicability?**

2. **How to optimize the design and operation of GWHP systems?** The optimal design/operation should minimize negative interactions between neighboring wells (systems) and thus maximize their efficiency and/or maximize the shallow geothermal potential of the area. This question includes the following sub-questions:
   a) How to optimize well locations of GWHP systems?
   b) How to determine the optimal number of GWHP wells to be installed?
   c) How to optimize the sizing (pumping rates) of GWHP wells?
3. **How to effectively integrate GWHPs into energy system optimization models?** This research question focuses on the integrated system level of optimization, which is different from the system-level focus of the other questions.

1.4 Structure

This thesis is based on five journal publications, which are listed below:

1. Halilovic, S., Odersky, L. and Hamacher, T., 2022. Integration of groundwater heat pumps into energy system optimization models. *Energy*, 238, p.121607. URL: https://doi.org/10.1016/j.energy.2021.121607
2. Halilovic, S., Böttcher, F., Zosseder, K. and Hamacher, T., 2023. Optimization approaches for the design and operation of open-loop shallow geothermal systems. *Advances in Geosciences*, 62, p.57-66. URL: https://doi.org/10.5194/adgeo-62-57-2023
3. Halilovic, S., Böttcher, F., Zosseder, K. and Hamacher, T., 2023. Optimizing the spatial arrangement of groundwater heat pumps and their well locations. *Renewable Energy*, 217, p.119148. URL: https://doi.org/10.1016/j.renene.2023.119148
4. Halilovic, S., Böttcher, F., Zosseder, K. and Hamacher, T., 2024. Spatial analysis of thermal groundwater use based on optimal sizing and placement of well doublets. *Energy*, 304, p.132058. URL: https://doi.org/10.1016/j.energy.2024.132058
5. Halilovic, S., Böttcher, F., Kramer, S.C., Piggott, M.D., Zosseder, K. and Hamacher, T., 2022. Well layout optimization for groundwater heat pump systems using the adjoint approach. *Energy Conversion and Management*, 268, p.116033. URL: https://doi.org/10.1016/j.enconman.2022.116033

The thesis is organized as follows. Chapter 2 provides fundamental insights on two topics: SGE systems and PDE constrained optimization. The following two chapters present the five publications. Chapter 3 addresses the relevance of GWHP systems in the context of the energy transition and features Publication 1. This publication introduces methods for integrating GWHP systems into energy system optimization models. Chapter 4 forms the core of this thesis and contains the remaining four publications. This chapter is dedicated to the optimization of GWHPs at the system level. Section 4.1 includes Publication 2, which performs a qualitative comparison of different optimization approaches for GWHP systems. Section 4.2 comprises Publications 3 and 4, which present novel GWHP optimization approaches that use analytical models to integrate groundwater-related aspects into the optimization process. Specifically, Publication 3 focuses on thermal groundwater considerations, while Publication 4 focuses on hydraulic groundwater aspects. Section 4.3 features Publication 5, which presents a novel approach that uses the adjoint method to determine optimal well layouts of GWHP systems. This approach uses PDE models to simulate groundwater flow and heat transport phenomena. Finally, Chapter 5 completes this thesis with concluding remarks and an outlook on future research directions.

Figure 1.2 provides a schematic overview of the core - in terms of publications and the research questions - content of the thesis, which includes Chapter 3 (Relevance of GWHPs) and Chapter 4 (Optimization of GWHPs). Some publications address one research (sub-)question, while others address multiple sub-questions simultaneously.

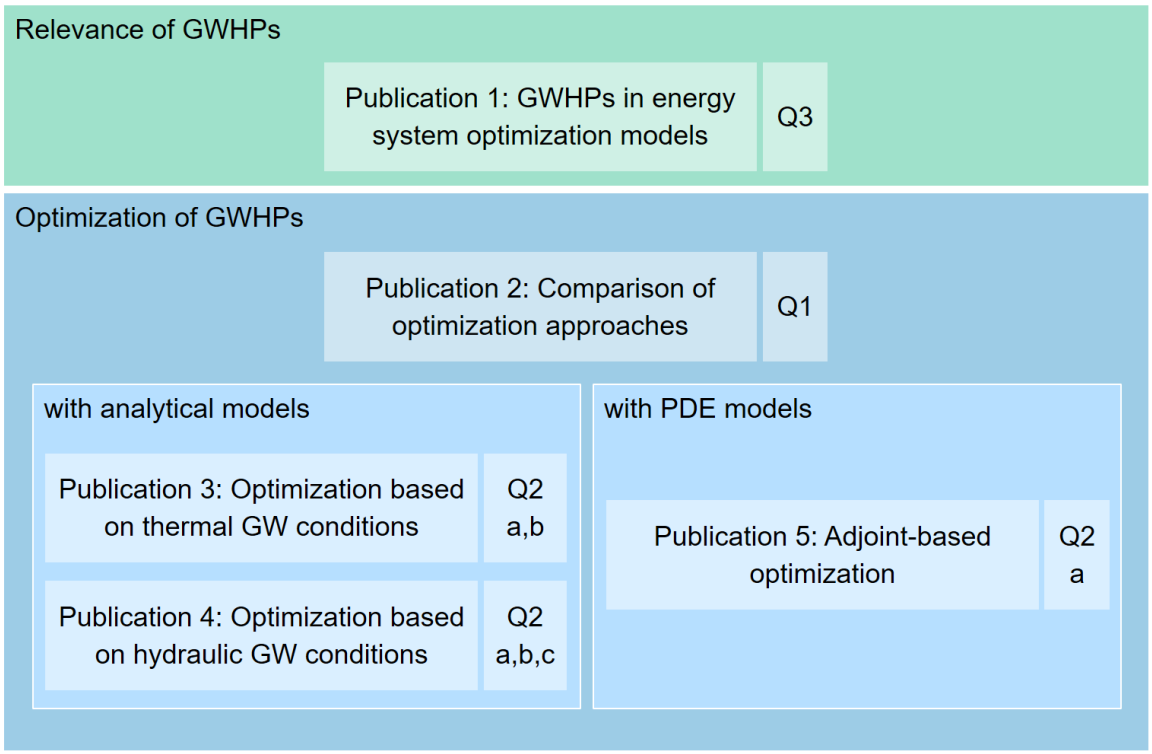

Figure 1.2 Schematic overview of the main part of the thesis (GW: groundwater).

2 Theoretical background

This chapter provides theoretical background on two topics: shallow geothermal energy (Section 2.1), with particular emphasis on open-loop systems, and PDE-constrained optimization (Section 2.2).

2.1 Shallow geothermal energy

Geothermal energy refers to the inherent thermal energy stored in geological materials such as rocks, sediments, groundwater, magma and other components beneath the Earth's surface [9,23]. This renewable, on the time scale of technical/societal systems [24], and sustainable energy resource can be used for both electricity generation and heating purposes. Geothermal energy can be classified based on exploration depth, temperature (enthalpy), or exergy [7,25]. However, it is important to note that the classification, especially with respect to temperature, is not universally standardized [26,27]. Based on the depth within the Earth's crust, geothermal energy can be classified into three main categories [9]:

- Shallow geothermal energy (<400 m) or very low temperature (enthalpy) geothermal energy. These geothermal resources, with typical temperatures below 30 °C, are used for direct heating and cooling applications in residential, agricultural, and industrial sectors.
- Medium geothermal energy (400-4000 m) or medium or low temperature geothermal energy. These geothermal systems can be used for both direct heating and electricity generation.
- Deep geothermal energy (4000-5000 m) or high temperature geothermal energy. These geothermal resources, with temperatures above 150 °C, are mainly used to generate electricity through flash steam or binary cycle power plants.

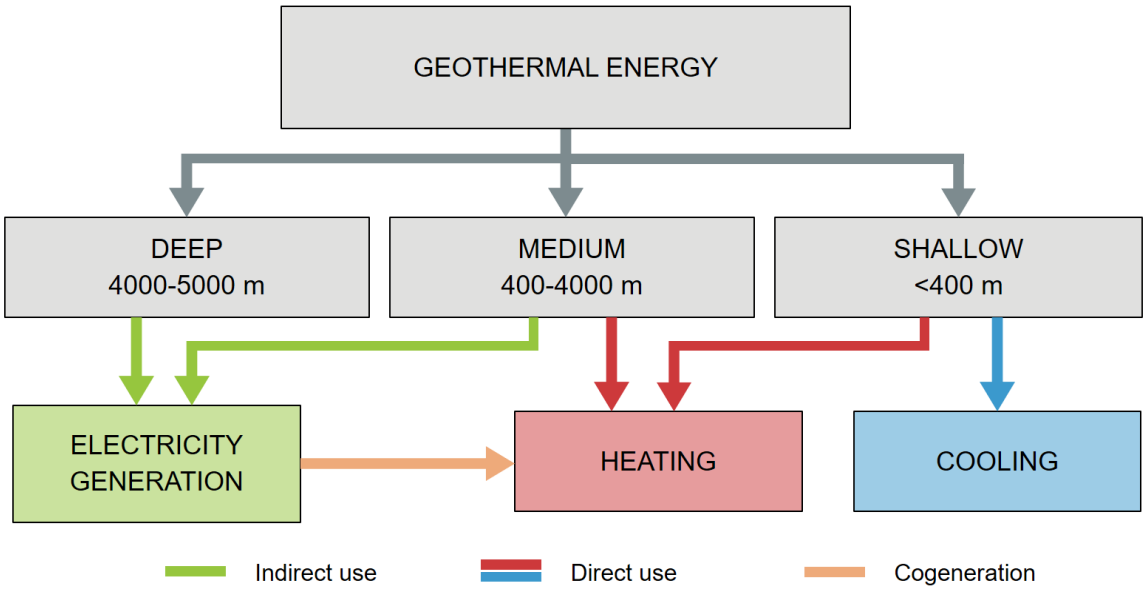

Figure 2.1 Classification of geothermal energy based on depth and type of end use (modified from [9]).

Figure 2.1 summarizes the classification of geothermal energy based on exploration depth and end use. As shown in the figure, only shallow geothermal energy systems can be used for cooling purposes due to the low

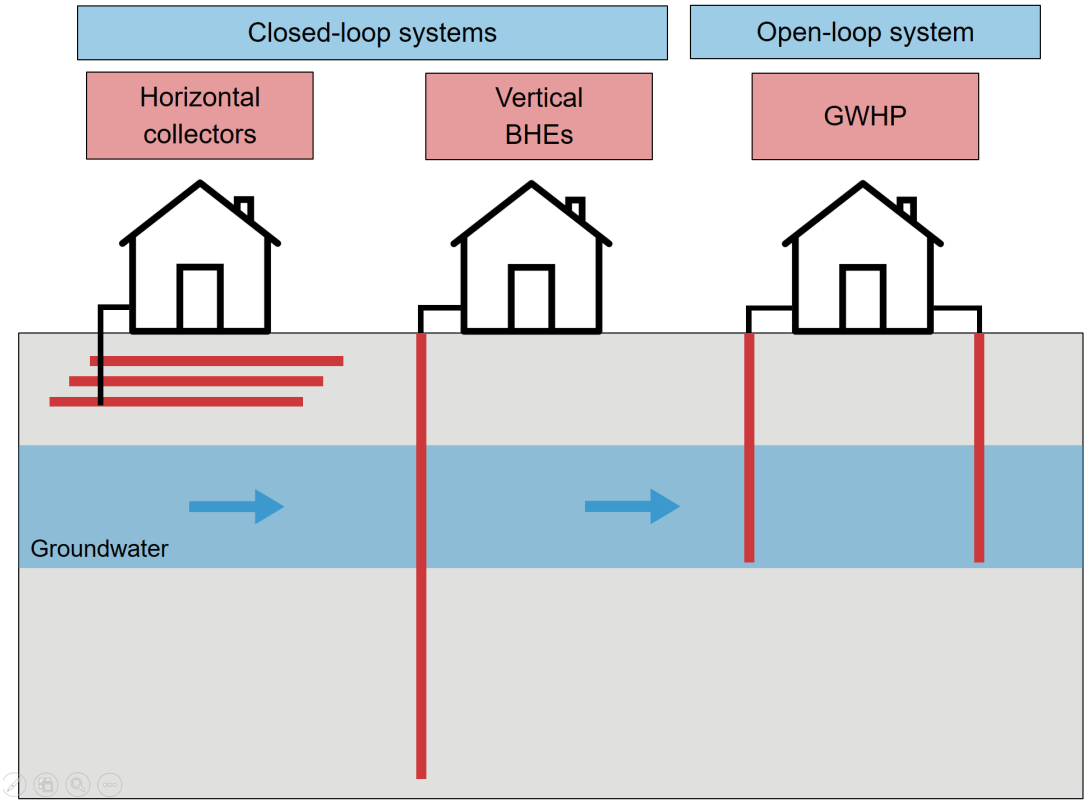

Figure 2.2 Main types of shallow geothermal systems.

temperatures in the shallow subsurface. These temperatures are similar to the annual average atmospheric temperature, and therefore SGE systems can be used for both heating and cooling applications throughout the year [10].

Based on the type of circulation of the heat carrier fluid, SGE systems can be divided into closed-loop and open-loop systems [5,6]. **Closed-loop systems**, also known as GSHP systems, use an auxiliary heat carrier fluid to exchange thermal energy with the subsurface [7]. This fluid circulates in a closed-loop system consisting of pipes that are integrated into geothermal heat exchangers. GSHP systems can be further divided into vertical and horizontal systems, depending on the type of geothermal heat exchangers [28, 29]: vertical borehole heat exchangers (BHEs) or horizontal collectors, respectively (Figure 2.2). **Open-loop systems**, known as GWHP systems, use groundwater as a heat carrier fluid to exchange thermal energy with the aquifer [8]. In these systems, groundwater circulates by being extracted and re-injected into an aquifer via "open" wells (Figure 2.2). Since GWHP systems are the focus of this thesis, the following section describes them in more detail.

In addition to these main types of SGE systems used directly for heating and/or cooling purposes, the shallow subsurface can also be used for seasonal thermal storage in the form of so-called underground thermal energy storage (UTES) systems [30]. There are two main types of UTES systems [31, 32]: borehole thermal energy storage (BTES) and aquifer thermal energy storage (ATES), which operate on the same principles as the GSHP and GWHP systems. The difference is that BTES and ATES systems store thermal energy underground for use at a later time. For example, a BTES system operates in cooling mode during the summer and stores the excess heat underground, which is then used for heating purposes during the following winter season.

2.1.1 Open-loop shallow geothermal systems

A typical residential GWHP system with a single extraction-injection well doublet is depicted in Figure 2.3. In larger systems, such as those for apartment complexes or hospitals, multiple extraction and injection wells can be installed [16]. As illustrated in the figure, a submersible pump is placed in the extraction well to pump groundwater from the aquifer. Once the heat is exchanged in the heat pump unit, the extracted groundwater is

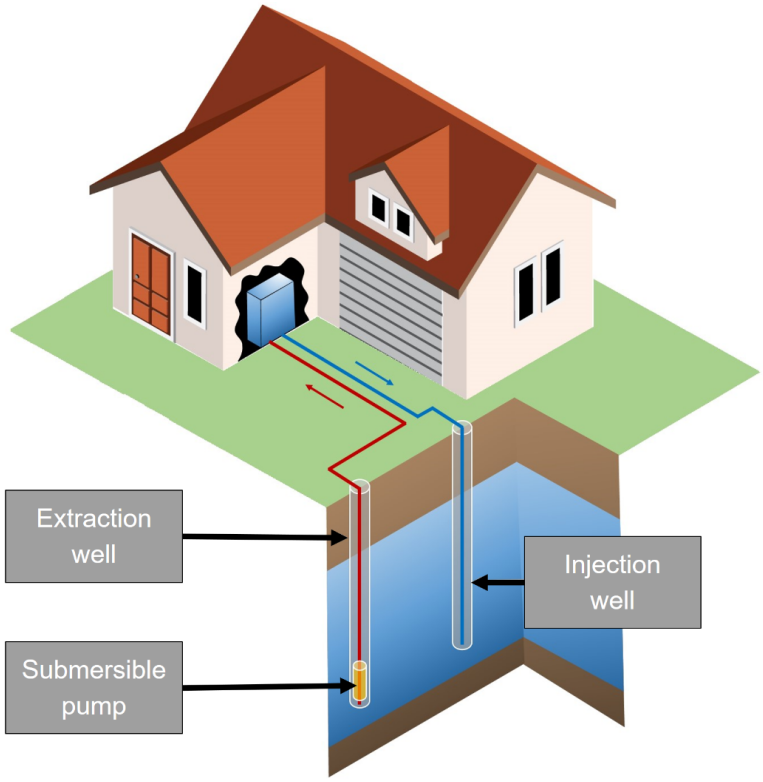

Figure 2.3 GWHP system and its main components (modified from [33]).

reintroduced into the same aquifer through the injection well [6]. Given their working principle, GWHP systems cause both hydraulic and thermal impacts on the groundwater body [9]. The hydraulic impacts are manifested as groundwater drawdown at the extraction wells and groundwater level rise at the injection wells [10], as shown in Figure 2.4. As a result, local groundwater flow patterns are also altered. The thermal effects are caused by the returned water at injection wells. The temperature of this water is different from that of the originally extracted water and depends on the operating mode of the system. In heating or cooling mode, the re-injected water is cooler or warmer, respectively. This results in thermal anomalies, i.e. so-called thermal plumes, in the aquifer that propagate downstream following the natural groundwater flow direction [34–36], as depicted in Figure 2.4.

The viability and efficiency of GWHP systems depend on several local groundwater parameters, including quality, quantity, depth, and temperature [10, 11]. Among these parameters, groundwater temperature at the extraction wells has the greatest influence on GWHP efficiency [12]. Consequently, it is essential to ensure that thermal plumes generated by an upstream GWHP system do not extend to the extraction wells of neighboring downstream systems, as this could negatively affect their operation [36]. To mitigate such negative thermal interactions between neighboring systems, certain regions have implemented specific regulations as part of the permitting process for new systems. For example, in Bavaria, Germany, the guidelines require that the induced temperature change at the extraction well of an existing downstream system must remain below 1 K [37].

Furthermore, groundwater, as a vital source of drinking water [38, 39], requires regulatory measures to protect against detrimental thermal alterations because these can affect its chemical, physical, and biological properties [40–43]. Currently, regulations for thermal groundwater use vary widely from country to country [7]. These regulations usually include criteria such as temperature limits and minimum spatial distances, for example, between GWHP wells and property boundaries. Prescribed groundwater temperature limits typically include both absolute minimum and maximum temperature values, as well as limitations on the extent of temperature changes caused by GWHPs [7]. For example, in the German federal state of Bavaria, these specified values are +5 °C, +20 °C, and ±6 K, respectively [44].

In addition to the aforementioned external factors concerning GWHP systems, such as thermal plumes or their environmental impacts on groundwater, there are also internal aspects that must be taken into account to ensure sustainable and efficient GWHP operation. In particular, pumping rates are technically limited by

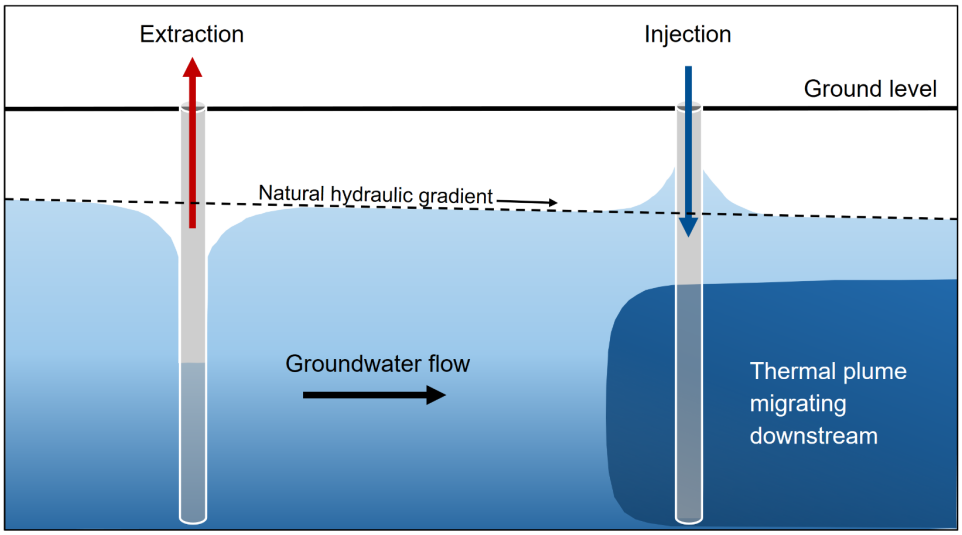

Figure 2.4 Hydraulic and thermal impacts of a GWHP system (modified from [10]).

the maximum drawdown allowed in extraction wells and the permissible groundwater rise in injection wells (Figure 2.4) [45]. The first restriction aims to prevent aquifer depletion [46], while the second aims to prevent groundwater flooding [47, 48], and thus this aspect also qualifies as an environmental concern. Furthermore, internal hydraulic and thermal breakthrough considerations are an essential part of GWHP system design and operation [49]. These breakthroughs occur when water re-injected at an injection well flows back into the extraction well of the same system. Thermal recycling of water decreases the efficiency of GWHP systems and therefore must be avoided or minimized [50]. To prevent hydraulic and thermal breakthroughs, it is important to space the wells adequately depending on the pumping rate and to position the injection well further downstream compared to the extraction well [51].

2.1.2 Groundwater simulation

Groundwater simulation models are required in order to optimize the design and operation of GWHP systems. In this context, they serve two purposes:

1. Evaluating the hydraulic and thermal impacts of GWHPs on groundwater, and
2. Determining the existing groundwater conditions, including parameters such as temperature, velocity, and hydraulic head.

These models are inherently numerical PDE models, since groundwater flow and heat transport in aquifers are governed by a system of PDEs. However, it is important to recognize the existence of analytical approximate models for estimating thermal plumes, which are reviewed in recent study [52]. This section will not discuss these analytical models further, but will focus on numerical groundwater simulation models. Therefore, this section provides background information on simulation models that are required for PDE-based optimization of GWHP systems (Section 4.3).

Groundwater represents a fully saturated porous medium, and its **3D flow** is described by the following PDEs [53, 54]:

$$S_0 \frac{\partial h}{\partial t} + \nabla \cdot \mathbf{q} = Q \tag{2.1a}$$

$$\mathbf{q} = -\mathbf{K} \cdot \nabla h \tag{2.1b}$$

where the hydraulic head h [m] and the Darcy velocity $\mathbf{q}$ [m/s] are the states (dependent variables). The parameters of the flow model are summarized in Table 2.1. The second PDE is the so-called Darcy's law, which describes the flow of a fluid through a porous medium [55]. Darcy's law implies that the flow is laminar [56].

This is the case with groundwater because the velocity range of groundwater varies greatly, but does not exceed a few meters per day [57].
The liquid sink/source term Q can be split into a supply term Q_h and a well-type SPC (singular point condition) term Q_{hw}, i.e. $Q = Q_h + Q_{hw}$. The well-type SPC term represents pumping (extraction) and injection wells as idealized point sinks/sources: $Q_{hw} = -\sum_w Q_w(t)\delta(\mathbf{x} - \mathbf{x}_w)$, where $Q_w(t)$ is the pumping rate (volume per unit time) of the well w at location $\mathbf{x}_w$, and $\delta(\mathbf{x} - \mathbf{x}_w) = \delta(x - x_w)\delta(y - y_w)\delta(z - z_w)$ is the 3D Dirac delta function associated with the well location $\mathbf{x}_w$. In the case of GWHP systems, $Q_w(t) > 0$ for extraction wells and $Q_w(t) < 0$ for injection wells. [53]
The PDE system (2.1) is solved to determine the states h and $\mathbf{q}$, considering a specified set of boundary conditions and an initial condition. Typically, this is done by substituting $\mathbf{q}$ from (2.1b) into (2.1a) and then solving for h only. Once the hydraulic head h has been determined, the Darcy velocity $\mathbf{q}$ can be calculated using equation (2.1b).

The **3D heat transport** in porous media is governed by the following PDE in divergence form [53, 54]:

$$\frac{\partial}{\partial t}\Big[\big(\varepsilon s\rho c + (1-\varepsilon)\rho^s c^s\big)(T - T_0)\Big] + \nabla\cdot(\rho c\mathbf{q}(T - T_0)) - \nabla\cdot(\mathbf{\Lambda}\cdot\nabla T) = Q_T + Q_{Tw} \tag{2.2}$$

and in convective form:

$$\big(\varepsilon s\rho c + (1-\varepsilon)\rho^s c^s\big)\frac{\partial T}{\partial t} + \rho c\mathbf{q}\cdot\nabla T - \nabla\cdot(\mathbf{\Lambda}\cdot\nabla T) = Q_T + Q_{Tw} - \rho c(T - T_0)Q \tag{2.3}$$

where the temperature of the porous medium T [K] is the state. A local thermodynamic equilibrium between the liquid and solid phases of the porous medium is assumed, meaning that T represents the groundwater temperature. The parameters of the heat transport model are summarized in Table 2.2, which gives their common values (or values of the constants) or orders of magnitude. It should be noted that the saturation $s = 1$, since groundwater is a fully saturated porous medium.
Q_T and Q_{Tw} are the thermal sink/source terms, Q_T being the supply term and Q_{Tw} the well-type SPC term. The well-type SPC term represents wells either as $Q_{Tw} = -\sum_w (T_w - T_0)\rho c Q_w(t)\delta(\mathbf{x} - \mathbf{x}_w)$ (divergence form) or $Q_{Tw} = -\sum_w (T_w - T)\rho c Q_w(t)\delta(\mathbf{x} - \mathbf{x}_w)$ (convective form), where $Q_w(t)$ is the pumping rate of the well w, and T_w is the prescribed temperature at well point $\mathbf{x}_w$. Regarding GWHP systems, only injection wells have a thermal impact on the groundwater, which means that $Q_w(t) < 0$ and $T_w = T_w^{\text{inj}}$ is the temperature of the re-injected water at the well w. [53]
The PDE (2.2) or (2.3) is solved for the state T, subject to specified boundary conditions and an initial condition. The difference between the divergence form and the convective form lies in the assumption of the specific heat capacities' dependence on temperature T. In the divergence form, the specific heat capacities are assumed to be independent of temperature, whereas no such assumption is made in the convective form [53].
The heat dispersion is described by the tensor of hydrodynamic thermodispersion $\mathbf{\Lambda}$, which is defined as follows [53]:

$$\mathbf{\Lambda} = \mathbf{\Lambda}_0 + \mathbf{\Lambda}_0^s + \rho c\mathbf{D}_{\text{mech}} \tag{2.4a}$$

$$\mathbf{\Lambda}_0 = \varepsilon s\Lambda\mathbf{I} \tag{2.4b}$$

$$\mathbf{\Lambda}_0^s = (1-\varepsilon)\Lambda^s\mathbf{I} \tag{2.4c}$$

$$\mathbf{D}_{\text{mech}} = \beta_T\|\mathbf{q}\|\mathbf{I} + (\beta_L - \beta_T)\frac{\mathbf{q}\otimes\mathbf{q}}{\|\mathbf{q}\|} \tag{2.4d}$$

with the parameters summarized in the second half of Table 2.2. Here, an axis-parallel isotropy is assumed for the thermal conductivity of solid.

Table 2.1 Parameters of the flow model [53].

Symbol	Parameter	Order of magnitude	Unit
S_0	Specific storage coefficient	10^{-4}	m^{-1}
$\mathbf{K}$	Tensor of hydraulic conductivity	10^{-4}	ms^{-1}
Q	General liquid sink/source function	10^{-4}	d^{-1}

In modeling scenarios where the horizontal extent of the regional groundwater flow field is much larger than the aquifer thickness B, vertical variations are often negligible. This allows the reduction of the full 3D equations to essentially horizontal 2D equations obtained by vertical averaging (integration) of the aquifer [53]. Here two cases have to be distinguished [53, 55]:

- unconfined aquifers: $B(x, y, t) = h(x, y, t) - f^{\mathrm{B}}(x, y)$,
- confined aquifers: $B(x, y) = f^{\mathrm{T}}(x, y) - f^{\mathrm{B}}(x, y)$,

where f^{B} and f^{T} are the functions describing the bottom and top surface (boundary) of the aquifer, respectively, and h is the previously described hydraulic head (Figure 2.5). The upper boundary of the aquifer is considered stationary in confined cases, whereas it is subject to movement in unconfined cases.

The resulting **2D** vertically averaged, essentially **horizontal**, groundwater **flow** in unconfined aquifers is described by the following PDEs [53, 54]:

$$(BS_0 + \varepsilon_e)\frac{\partial h}{\partial t} + \nabla \cdot \overline{\mathbf{q}} = \overline{Q} \tag{2.5a}$$

$$\overline{\mathbf{q}} = -B\mathbf{K} \cdot \nabla h \tag{2.5b}$$

$$B = h - f^{\mathrm{B}} \tag{2.5c}$$

where $\overline{\mathbf{q}}$ is the vertically averaged Darcy velocity, $\overline{\mathbf{q}} = B\mathbf{q}$. The parameter ε_e represents the specific yield. $\overline{Q}$ is the vertically averaged (depth-integrated) source/sink term, which can be split into a depth-integrated supply term $\overline{Q}_h$ and a depth-integrated well-type SPC term $\overline{Q}_{hw}$, i.e. $\overline{Q} = \overline{Q}_h + \overline{Q}_{hw}$. The well-type SPC term takes the following form: $\overline{Q}_{hw} = -\sum_w Q_w(t)\delta(\mathbf{x} - \mathbf{x}_w)$, where $\delta(\mathbf{x} - \mathbf{x}_w) = \delta(x - x_w)\delta(y - y_w)$ is the 2D Dirac delta function.

For confined aquifers, 2D horizontal, vertically averaged groundwater flow is described in a similar manner [54]:

$$BS_0\frac{\partial h}{\partial t} + \nabla \cdot \overline{\mathbf{q}} = \overline{Q} \tag{2.6a}$$

$$\overline{\mathbf{q}} = -B\mathbf{K} \cdot \nabla h\,. \tag{2.6b}$$

The PDE system (2.5) or (2.6) is solved for the hydraulic head h and the depth-integrated Darcy velocity $\overline{\mathbf{q}}$ in the same way as its 3D counterpart (2.1).

Table 2.2 Parameters of the heat transport model [53].

Symbol	Parameter	Value (Order of magnitude)	Unit
T_0	Reference temperature	273.15	K
ε	Porosity	0.3	-
s	Saturation	1	-
ρ	Liquid (water) density	1000	$\mathrm{kgm^{-3}}$
ρ^s	Solid density	2650	$\mathrm{kgm^{-3}}$
c	Liquid specific heat capacity	4200	$\mathrm{Jkg^{-1}K^{-1}}$
c^s	Solid specific heat capacity	950	$\mathrm{Jkg^{-1}K^{-1}}$
$\mathbf{\Lambda}$	Tensor of hydrodynamic thermodispersion	(10^0-10^1)	$\mathrm{Wm^{-1}K^{-1}}$
Q_T	Thermal supply term	(10^3-10^4)	$\mathrm{Jm^{-3}d^{-1}}$
Q_{Tw}	Thermal well-type SPC term	(10^8-10^9)	$\mathrm{Jm^{-3}d^{-1}}$
$\mathbf{\Lambda}_0$	Tensor of thermal conductivity of liquid	(10^{-1})	$\mathrm{Wm^{-1}K^{-1}}$
$\mathbf{\Lambda}_0^s$	Tensor of thermal conductivity of solid	(10^0)	$\mathrm{Wm^{-1}K^{-1}}$
$\mathbf{D}_{\mathrm{mech}}$	Tensor of mechanical dispersion	(10^{-4})	$\mathrm{m^2s^{-1}}$
Λ	Coefficient of thermal conductivity of liquid	0.65	$\mathrm{Jm^{-1}K^{-1}s^{-1}}$
Λ^s	Coefficient of thermal conductivity of solid	3	$\mathrm{Jm^{-1}K^{-1}s^{-1}}$
β_L	Longitudinal dispersivity	5	m
β_T	Transverse dispersivity	0.5	m
$\mathbf{I}$	Unity or identity matrix	1	-

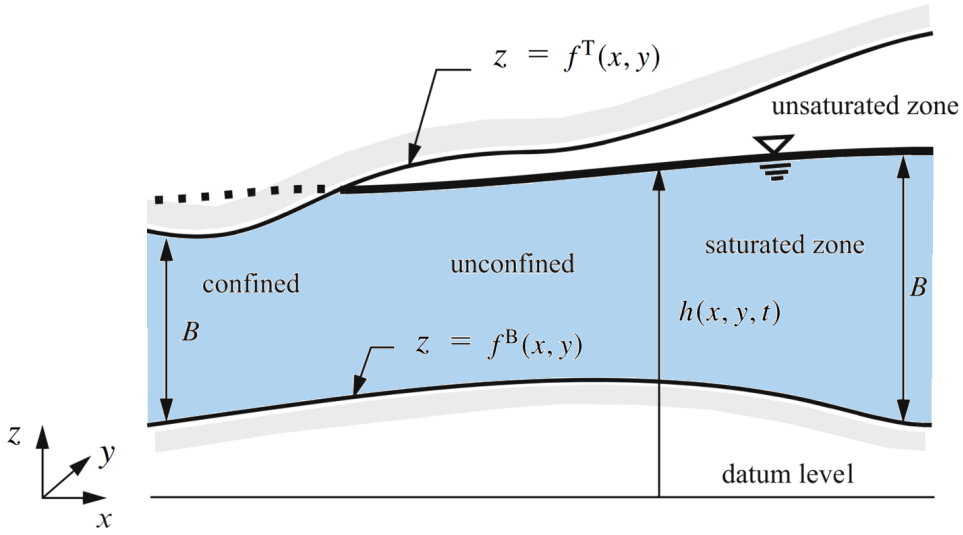

Figure 2.5 Confined and unconfined conditions in aquifers (modified from [53]).

The **2D horizontal**, vertically averaged **heat transport** in unconfined and confined aquifers is described by the following PDE in divergence form [53, 54]:

$$\frac{\partial}{\partial t}\Big[B\big(\varepsilon\rho c + (1-\varepsilon)\rho^s c^s\big)(T - T_0)\Big] + \nabla\cdot(\rho c\overline{\mathbf{q}}(T - T_0)) - \nabla\cdot(\overline{\mathbf{\Lambda}}\cdot\nabla T) = \overline{Q}_T + \overline{Q}_{Tw} \tag{2.7}$$

and in convective form:

$$B\big(\varepsilon\rho c + (1-\varepsilon)\rho^s c^s\big)\frac{\partial T}{\partial t} + \rho c\overline{\mathbf{q}}\cdot\nabla T - \nabla\cdot(\overline{\mathbf{\Lambda}}\cdot\nabla T) = \overline{Q}_T + \overline{Q}_{Tw} - \rho c(T - T_0)\overline{Q} \tag{2.8}$$

where $B = h - f^{\mathrm{B}}$ and $B = f^{\mathrm{T}} - f^{\mathrm{B}}$ for unconfined and confined cases, respectively. $\overline{\mathbf{\Lambda}}$ represents the depth-integrated tensor of hydrodynamic thermodispersion, and is defined in a similar way as its 3D counterpart $\mathbf{\Lambda}$. $\overline{Q}_T$ and $\overline{Q}_{Tw}$ are the depth-integrated supply and well-type SPC terms, respectively. The former is defined either as $\overline{Q}_{Tw} = -\sum_w (T_w - T_0)\rho c Q_w(t)\delta(\mathbf{x} - \mathbf{x}_w)$ (divergence form) or $\overline{Q}_{Tw} = -\sum_w (T_w - T)\rho c Q_w(t)\delta(\mathbf{x} - \mathbf{x}_w)$ (convective form), where δ is the 2D Dirac delta function.

In general, PDEs describing 3D and 2D groundwater flow and heat transport in aquifers exhibit bidirectional coupling because water density and hydraulic conductivity are affected by groundwater temperature [53]. However, when the temperature variations are in a relatively small range, these dependencies can be neglected [54]. Consequently, the PDE system can be solved sequentially: first the flow equations, followed by the heat transfer equation. This sequential approach considerably simplifies the numerical solution process.

2.2 PDE-constrained optimization

Various engineered and natural systems are characterized by underlying physical phenomena described by PDEs. In the energy domain, these include systems involving fluid dynamics (e.g. wind [58–60] and tidal energy [61–63], gas [64–66] and water distribution networks [67–69]), heat propagation (e.g. shallow [53, 54] and deep geothermal energy [70–73], thermal energy storage [74–76], district heating networks [77–79]), or electromagnetic phenomena (e.g. electric machines [80–83]). Optimization of these systems leads to optimization problems with PDE constraints, commonly referred to as PDE-constrained optimization (PDECO) problems. This also applies to GWHP optimization, since groundwater flow and heat transport are governed by PDEs, as described in the previous section. Therefore, this section provides mathematical background for PDE-based optimization of GWHP systems (Section 4.3).

A general PDECO problem can be stated as follows:

$$\min_{\boldsymbol{u},\boldsymbol{m}} \quad J(\boldsymbol{u},\boldsymbol{m}), \tag{2.9a}$$

$$\text{subject to} \quad \mathcal{F}(\boldsymbol{u},\boldsymbol{m}) = 0, \tag{2.9b}$$

$$g(\boldsymbol{u},\boldsymbol{m}) \leq 0, \tag{2.9c}$$

$$h(\boldsymbol{u},\boldsymbol{m}) = 0, \tag{2.9d}$$

where:

- $\mathcal{F}(\boldsymbol{u},\boldsymbol{m}) = 0$ is a PDE or a system of PDEs in a residual form, corresponding to the PDE constraints. These PDEs constitute the simulation problem or the so-called forward problem. In the context of optimization, PDE constraints are also referred to as state equations [84].
- $\boldsymbol{u}$ are **state variables** or states. These are the unknown (dependent) variables in the forward problem, i.e. the PDE solutions. Examples of state variables are temperature, velocity and electric field.
- $\boldsymbol{m}$ are **control (decision) variables** or controls. These are also referred to as design or inversion variables, depending on the optimization context [84]. In optimal control problems, $\boldsymbol{m}$ can represent source terms in the domain Ω or on the boundary $\partial\Omega$, corresponding to distributed and boundary control, respectively.
- $J(\boldsymbol{u},\boldsymbol{m}) \in \mathbb{R}$ is the functional of interest, which is equivalent to the objective function in the finite-dimensional optimization.
- g and h represent additional inequality and equality constraints, respectively, on controls and/or states.

In the forward problem, the control variables $\boldsymbol{m}$ are given and the corresponding states $\boldsymbol{u}$ are computed using a PDE solver. In the optimization problem (2.9), the process is reversed. Here, the task is to determine control variables $\boldsymbol{m}$ that result in states $\boldsymbol{u}$, which, in conjunction with these controls, minimize the specified functional of interest J and comply with the remaining optimization constraints g and h. The following two sections discuss different PDECO solution and discretization strategies.

2.2.1 PDECO solution strategies

There are two different strategies for solving PDECO problems: the full space method and the reduced space method [85, 86]. The former is alternatively referred to as the all-at-once or simultaneous analysis and design (SAND) method, while the latter is also known as the black-box or nested analysis and design (NAND) method [87, 88]. In the **full space method**, controls and states are treated as independent optimization variables. This means that the method solves a system of equations that represents the necessary first-order optimality conditions, the so-called Karush-Kuhn-Tucker (KKT) conditions, simultaneously for control and state variables [84]. Consequently, meeting the PDE constraint (2.9b) is only required in the last optimization iteration, eliminating the need to solve often computationally intensive PDEs in each iteration [88].

On the other side, the **reduced space method** treats only the controls as independent optimization variables, while the states are treated as implicit functions of these controls. This method offers the advantage of

integrating well-established algorithms and software for solving the state equation into the optimization process. In addition, the gradients required for optimization can be efficiently computed using adjoint PDE solvers, which are becoming increasingly popular and can be automatically generated through algorithmic differentiation. However, the main drawback of the reduced space method is that the PDE constraint (2.9b) must be satisfied in each optimization iteration, requiring repeated computationally intensive solutions of the state equation at each iteration. [84, 88]

In order to derive previously mentioned KKT conditions, we can formulate the Lagrangian functional $\mathcal{L}$ using the Lagrange multiplier field, also known as **adjoint or co-state variable** $\boldsymbol{\varphi}$ [84]. In the case of problem (2.9) without additional inequality and equality constraints, g and h, the Lagrangian functional is given as follows [89]:

$$\mathcal{L}(\boldsymbol{u}, \boldsymbol{m}, \boldsymbol{\varphi}) = J(\boldsymbol{u}, \boldsymbol{m}) - \boldsymbol{\varphi}^* \mathcal{F}(\boldsymbol{u}, \boldsymbol{m}), \tag{2.10}$$

where $\boldsymbol{\varphi}^* \mathcal{F}$ is an inner product or duality pairing. The first-order optimality conditions are obtained from the stationarity of the Lagrangian $\mathcal{L}$ with respect to the states $\boldsymbol{u}$, controls $\boldsymbol{m}$ and adjoints $\boldsymbol{\varphi}$ [89]:

$$\frac{\partial \mathcal{L}}{\partial \boldsymbol{\varphi}} = 0 \qquad \text{state equation,} \tag{2.11a}$$

$$\frac{\partial \mathcal{L}}{\partial \boldsymbol{u}} = 0 \qquad \text{adjoint equation,} \tag{2.11b}$$

$$\frac{\partial \mathcal{L}}{\partial \boldsymbol{m}} = 0 \qquad \text{control equation.} \tag{2.11c}$$

Using the definition of the Lagrangian $\mathcal{L}$, the previous equations result in the following optimality system:

$$\mathcal{F}(\boldsymbol{u}, \boldsymbol{m}) = 0 \qquad \text{state equation,} \tag{2.12a}$$

$$\left(\frac{\partial \mathcal{F}}{\partial \boldsymbol{u}}\right)^* \boldsymbol{\varphi} = \left(\frac{\partial J}{\partial \boldsymbol{u}}\right)^* \qquad \text{adjoint equation,} \tag{2.12b}$$

$$\left(\frac{\partial \mathcal{F}}{\partial \boldsymbol{m}}\right)^* \boldsymbol{\varphi} = \left(\frac{\partial J}{\partial \boldsymbol{m}}\right)^* \qquad \text{control equation,} \tag{2.12c}$$

where $(\partial \mathcal{F}/\partial \boldsymbol{u})^*$ denotes the adjoint operator of $(\partial \mathcal{F}/\partial \boldsymbol{u})$. In finite dimensions this adjoint operator corresponds to the conjugate transpose matrix [89]. The first equation (2.12a) is the same as the PDE constraint and is therefore called the state equation. The second and third equations are referred to as the adjoint and control equations, respectively. The adjoint equations, resulting from the Lagrangian stationarity condition with respect to the state variables, are PDEs characterized by linearity in the adjoint variables [90]. The full space method solves the coupled system of equations (2.12) for all variables simultaneously using either direct solvers or iterative solvers in combination with preconditioning techniques [91].

In the reduced space method, it is assumed that for each admissible $\boldsymbol{m}$ there is a unique solution $\boldsymbol{u}$ of the forward problem $\mathcal{F}(\boldsymbol{u}, \boldsymbol{m}) = 0$, i.e. there exist a mapping $\boldsymbol{m} \mapsto \boldsymbol{u}(\boldsymbol{m})$ that is defined implicitly by the PDE constraint [85]. By introducing $\boldsymbol{u}(\boldsymbol{m})$ into (2.9), the reduced problem is obtained:

$$\min_{\boldsymbol{m}} \qquad \hat{J}(\boldsymbol{m}) := J(\boldsymbol{u}(\boldsymbol{m}), \boldsymbol{m}), \tag{2.13a}$$

$$\text{subject to} \qquad g(\boldsymbol{u}(\boldsymbol{m}), \boldsymbol{m}) \leq 0, \tag{2.13b}$$

$$h(\boldsymbol{u}(\boldsymbol{m}), \boldsymbol{m}) = 0, \tag{2.13c}$$

where $\hat{J}(\boldsymbol{m})$ is the reduced functional of interest. Therefore, the only optimization variables in this case are the controls $\boldsymbol{m}$. In order to use gradient-based algorithms to solve the problem (2.13), it is necessary to compute the gradient of the reduced functional with respect to the control variables $\boldsymbol{m}$. The computation or estimation of this gradient can be done by different techniques, the most efficient one being the adjoint approach [92]. The gradient of the functional $\hat{J}$ with respect to controls $\boldsymbol{m}$ reads as follows:

$$\frac{\mathrm{d}\hat{J}}{\mathrm{d}\boldsymbol{m}} = \frac{\mathrm{d}J(\boldsymbol{u}(\boldsymbol{m}), \boldsymbol{m})}{\mathrm{d}\boldsymbol{m}} = \frac{\partial J}{\partial \boldsymbol{m}} + \frac{\partial J}{\partial \boldsymbol{u}} \frac{\mathrm{d}\boldsymbol{u}}{\mathrm{d}\boldsymbol{m}}. \tag{2.14}$$

The terms $\partial J/\partial \boldsymbol{u}$ and $\partial J/\partial \boldsymbol{m}$ in the previous equation can be computed analytically, which implies a negligible computational cost. On the other hand, the direct computation of the term $\mathrm{d}\boldsymbol{u}/\mathrm{d}\boldsymbol{m}$ is computationally challenging due to the inherent high dimensionality of the discretized states $\boldsymbol{u}$. This computationally intensive procedure is bypassed in the adjoint approach by using the following equation to calculate the gradient [89]:

$$\frac{\mathrm{d}\hat{J}}{\mathrm{d}\boldsymbol{m}} = \frac{\partial J}{\partial \boldsymbol{m}} - \boldsymbol{\varphi}^* \frac{\partial \mathcal{F}}{\partial \boldsymbol{m}}. \tag{2.15}$$

Equation (2.15) is derived from (2.14) as follows:

$$\frac{\mathrm{d}\hat{J}}{\mathrm{d}\boldsymbol{m}} = \frac{\partial J}{\partial \boldsymbol{m}} + \frac{\partial J}{\partial \boldsymbol{u}} \frac{\mathrm{d}\boldsymbol{u}}{\mathrm{d}\boldsymbol{m}} \tag{2.16a}$$

$$= \frac{\partial J}{\partial \boldsymbol{m}} + \boldsymbol{\varphi}^* \left(\frac{\partial \mathcal{F}}{\partial \boldsymbol{u}}\right) \frac{\mathrm{d}\boldsymbol{u}}{\mathrm{d}\boldsymbol{m}} \tag{2.16b}$$

$$= \frac{\partial J}{\partial \boldsymbol{m}} - \boldsymbol{\varphi}^* \frac{\partial \mathcal{F}}{\partial \boldsymbol{m}}. \tag{2.16c}$$

The first transformation is achieved by substituting the term $\partial J/\partial \boldsymbol{u}$ from the adjoint equation (2.12b). The second transformation is based on the sensitivity equation that is derived by differentiating the state equation (2.12a) [89]:

$$\nabla \mathcal{F}(\boldsymbol{u}, \boldsymbol{m}) = 0 \tag{2.17a}$$

$$\left(\frac{\partial \mathcal{F}}{\partial \boldsymbol{u}}\right) \frac{\mathrm{d}\boldsymbol{u}}{\mathrm{d}\boldsymbol{m}} + \frac{\partial \mathcal{F}}{\partial \boldsymbol{m}} = 0 \tag{2.17b}$$

$$\left(\frac{\partial \mathcal{F}}{\partial \boldsymbol{u}}\right) \frac{\mathrm{d}\boldsymbol{u}}{\mathrm{d}\boldsymbol{m}} = -\frac{\partial \mathcal{F}}{\partial \boldsymbol{m}}. \tag{2.17c}$$

A single optimization iteration in the reduced space method using the adjoint approach consists of the following steps [89]:

1. Based on the current values of the controls $\boldsymbol{m}$, the state equation (2.12a) is solved for the states $\boldsymbol{u}$.
2. These states are used to solve the adjoint equation (2.12b) to obtain the adjoints $\boldsymbol{\varphi}$.
3. The obtained adjoints are then used to calculate the gradient of the reduced functional from (2.15).
4. Based on the employed gradient-based optimization algorithm, the controls are updated using the calculated gradient.

The adjoint equation is linear in adjoint variables and does not contain derivatives with respect to controls. Therefore, it is usually less or equally computationally expensive compared to the state equation and requires only one solution to compute the gradient, regardless of the dimension of controls.

2.2.2 Discretization and optimization

PDECO problems have infinite-dimensional properties by nature. Therefore, in order to enable their computational solution by numerical methods, it is necessary to discretize them and thus reduce them to finite dimensions. Depending on the stage at which this discretization is performed in the PDECO solution procedure, two different approaches are possible [85,87]: the "discretize then optimize" (DTO) approach and the "optimize then discretize" (OTD) approach. In the former approach, the discretization is applied to the functional of interest and the constraints before the optimality conditions are derived, thereby yielding them in a discrete form. In contrast, in the latter approach, the optimality conditions are first derived in the continuous (infinite-dimensional) setting and then discretized. It is important to note that these two approaches generally do not produce the same results [84, 89]. Figure 2.6 shows the differences between DTO and OTD approaches.

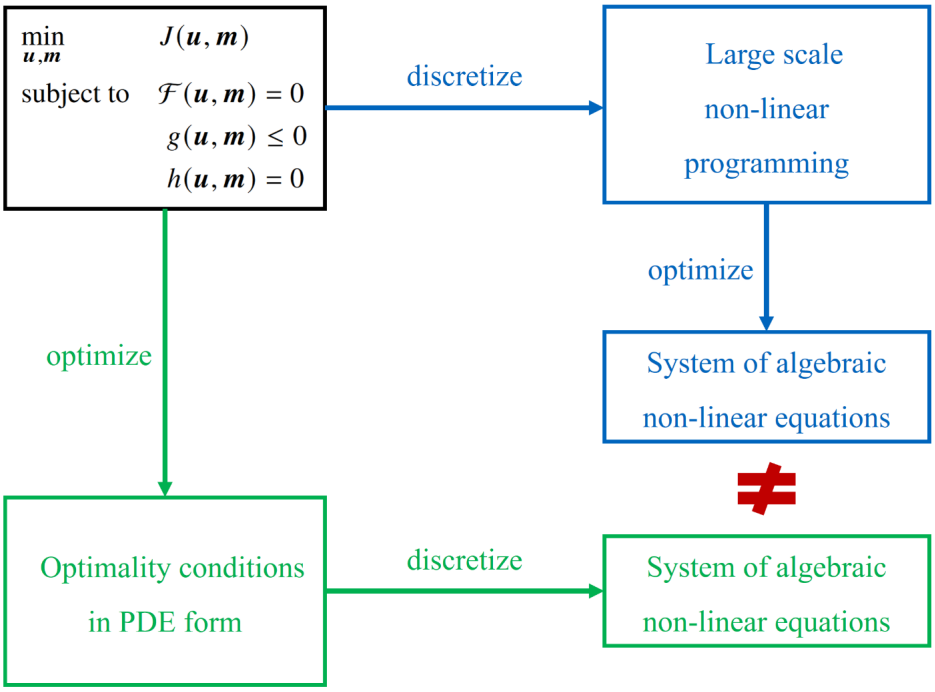

Figure 2.6 DTO and OTD approaches for solving PDECO problems.

The **DTO approach** offers the advantage of obtaining the exact gradient of the discrete objective functional, which ensures full convergence during the optimization process. In contrast, the **OTD approach** provides an approximated gradient that does not represent a true gradient of the continuous or discretized functional. Furthermore, the DTO approach allows the use of automatic differentiation to generate adjoint codes (discrete adjoint models), which simplifies their implementation. However, this approach often results in increased memory requirements and CPU time compared to manually written adjoint codes. On the other hand, the OTD approach provides clearer physical insights into the adjoint variables and the role of adjoint boundary conditions. It also allows for different discretizations (meshes) for the state and adjoint PDEs, which can make the adjoint code simpler and less memory intensive. These separate discretizations are particularly beneficial in shape optimization problems. [89, 92]

3 Relevance of GWHPs

As described previously, GWHP systems emerge as a promising technology for the decarbonization of heating and cooling sectors. To analyze this aspect and determine their potential for supplying heating and/or cooling demands in a given region, energy system optimization models (ESOMs) can be applied. ESOMs are widely used tools in the energy system modeling field to determine the optimal dispatch and expansion planning of technologies to achieve specified CO_2 reduction targets. In cases where GWHPs are a relevant and feasible technology in the considered area, their integration into the technology portfolio of the respective ESOM is required.

The first publication included in this thesis introduces and compares three different approaches for integrating (representing) GWHP systems in ESOMs. These approaches differ in their treatment of GWHP efficiency, i.e. modeling of COP (coefficient of performance), within the ESOM framework. The comparative analysis of the proposed approaches is performed on a real case study using an ESOM that models the heating system of the city of Munich. The results demonstrate that detailed modeling of heat pump efficiency results in GWHPs emerging as a key technology for reducing CO_2 emissions in the analyzed urban heating infrastructure. Therefore, **Publication 1** [93] serves a dual purpose: first, it confirms that GWHPs can make a significant contribution to the energy transition, and second, it highlights the importance of adequate representation of GWHPs (and heat pumps in general) in ESOMs. The publication also provides a comprehensive illustration of the appropriate approaches for this representation.

It should be noted that in Publication 1, the GWHP optimization level corresponds to the integrated system level. This leads to a relatively simple representation of GWHPs that does not include details about their operation, design, or interactions with groundwater. The impact of groundwater on GWHPs is accounted for by using groundwater temperature as a factor in estimating the COP. Nevertheless, the publication makes a significant progress in terms of the representation of heat pumps in ESOMs, compared to the previous research studies in this field.

Publication 1 - Integration of groundwater heat pumps into energy system optimization models

Authors: Smajil Halilović, Leonhard Odersky, Thomas Hamacher

Journal: Energy (Elsevier)

Status: Published - January 2022

Digital object identifier: https://doi.org/10.1016/j.energy.2021.121607

Author	Contribution
Smajil Halilović	Conceptualization, Methodology, Writing - original draft, Software, Investigation, Visualization
Leonhard Odersky	Writing - reviewing and editing, Data curation, Software, Visualization
Thomas Hamacher	Writing - reviewing and editing, Supervision

Energy 238 (2022) 121607

Contents lists available at ScienceDirect

Energy

journal homepage: www.elsevier.com/locate/energy

Integration of groundwater heat pumps into energy system optimization models

Smajil Halilovic*, Leonhard Odersky, Thomas Hamacher

Technical University of Munich, Chair of Renewable and Sustainable Energy Systems, Germany

ARTICLE INFO

Article history:
Received 1 November 2020
Received in revised form
18 July 2021
Accepted 24 July 2021
Available online 29 July 2021

Keywords:
Heat pump
Energy system
Optimization
Groundwater
Modelling

ABSTRACT

Heat pumps are one of the key technologies for the mitigation of carbon emissions in the heating sector. Therefore, they are an essential modelling component when analyzing future energy systems. The focus of this work are groundwater heat pumps and their integration into energy system optimization models. Three different integration approaches are introduced and compared to each other. The approaches differ in the representation of heat pumps efficiency: constant, time dependent and both time and spatially dependent. The comparison of the proposed approaches is conducted using an energy system model of the residential heating sector in Munich and two optimization scenarios: 70 % and 95 % emission reduction compared to 2014. Assuming constant efficiency of heat pumps throughout the year produces incorrect optimization results, whereas adding spatial component to the temporal one does not change cumulative results significantly. Thus, the second approach is the most suitable one due to its lower complexity compared to the last approach. However, if spatially distributed results are required, then the last approach is necessary. Finally, these integration approaches are applicable to all types of heat pumps.

1. Introduction

The building-related CO_2 emissions, i.e. CO_2 emissions from residential and non-residential buildings in all sectors, amounted to 208 Mt in 2017 in Germany [1]. Heating sector, i.e. space heating and hot water supply, accounted for around 83 % of those emissions and, thus, represents a significant potential for CO_2 emission reductions. The current aspiration of the German government is to reach around 66 % of CO_2 reductions in the building sector in 2030, compared to the 1990s level, on the way to an almost climate-neutral building stock in 2050 [2].

Heat pumps are one of the key technologies when considering future CO_2 reduction scenarios in the heating sector [3]. Hence, they are an essential component in numerous studies analyzing future energy systems. The majority of these studies assume constant efficiency, i.e. coefficient of performance, of heat pumps throughout the year. Table 1 shows examples of several studies together with the assumed constant efficiencies and corresponding types of heat pumps. More recently, the importance of temporal component in heat pumps efficiency has been emphasized in several works.

Ruhnau et al. [9] introduced a dataset consisting of national time series of heat demand and efficiency of heat pumps. This synthetic dataset provides data with hourly resolution for 16 European countries and years 2008–2018. The efficiency is calculated for three different heat pump types: air source (AHPs), ground source (GSHPs) and groundwater heat pumps (GWHPs). The main motivation for the temporal modelling of heat pumps efficiency, and also heat demand, is that the time variable electricity consumption of heat pumps will be important in future electricity systems with high penetration of heat pumps. On the other side, Conrad and Greif [10] introduced a dataset consisting of time series of efficiency and electric load demand of heat pumps, but for 32 building categories. The proposed methodology for the time series computation differs from the one in Ref. [9], but the motivation to model temporal variability is the same.

Both of the aforementioned works introduce methodologies to model time series of heat pumps efficiency and heat demand, but they stop there and do not use these time series further in an energy system model. Hence, the quantification of the improvements obtained with the inclusion of the time component in the efficiency modelling of heat pumps is missing. However, a couple of other studies analyze the impacts of different efficiency modelling of heat pumps. These are briefly described in the following.

Jarre et al. [11] analyzed the primary energy consumption of an

* Corresponding author.
E-mail address: smajil.halilovic@tum.de (S. Halilovic).

https://doi.org/10.1016/j.energy.2021.121607
0360-5442/

Table 1
Constant seasonal coefficient of performance (efficiency) of heat pumps in different studies.

Reference	Source side	Efficiency
Gerhardt et al. [4]	Air	3.8
	Soil	4.4
Karlsson et al. [5]	Air	2.7
Kruse et al. [6]	Air	3.03−3.45
	Soil	3.45−4.0
Quiggin and Buswell [7]	Air	2.65−3.0
Schlesinger et al. [8]	–	2.96−4.29

air-source heat pump used for space heating. The efficiency of heat pumps is calculated hourly and it depends on outdoor temperature and water supply temperature. This dependency is based on manufacturer data with an additional constant reduction factor. The authors concluded that using average annual or monthly values of primary energy factors underestimates primary energy savings compared with hourly values.

Petrović and Karlsson [12] investigated the impacts of a more detailed modelling of residential heat pumps when optimizing the future Danish energy system. The efficiency of heat pumps is modelled as a function of the source temperature, i.e. air and ground temperature, and installation of GSHPs is limited with the available space. The average seasonal values are used for the efficiency to decrease computational time. It was concluded that the improved representation of heat pumps efficiency influences the optimization results, such as technology mix or total costs in the future energy system. Moreover, the authors point out that the impact of even more detailed modelling of heat pumps efficiency should be further investigated in the future.

Pieper et al. [13] compared four different methods to estimate the efficiency of a large-scale heat pump used in district heating: constant, Lorenz, exergy and efficiency based on the method introduced by Kjær Jensen et al. [14]. These methods are implemented in an energy planning tool, which finds the cost-minimal configuration of a future district heating system for the considered development region in Copenhagen, Denmark. The results show that using constant, Lorenz or exergy efficiency can produce misleading results, which might lead to wrong investment decisions. The authors also pointed out that the impact of heat pumps efficiency estimation on the results of energy planning tools, i.e. energy system optimization models, is not addressed in the previous research works. Hence, they tried to close this research gap with their work using large-scale heat pumps for district heating as an application example. A similar analysis is conducted by Bach et al. [15], who investigated the integration of large-scale heat pumps into the district heating system of Greater Copenhagen, Denmark. The authors compared constant and season-dependent representations of heat pumps efficiency using an energy system optimization model. They found that the seasonal representation does not significantly change the overall model results for the investigated (water based) heat pumps.

Haikarainen et al. [16] presented a model for the long-term optimization of integrated electricity and heating sectors with hourly time resolution. The authors emphasized the importance of a high temporal resolution in energy system optimization models (ESOMs). The efficiency of the considered AHPs is modelled on an hourly basis and as a piece-wise linear function of the ambient air temperature. However, the focus of this work were not heat pumps but the whole technology portfolio. A comparison with a model with a lower temporal resolution was also not carried out.

Verda et al. [17] analyzed optimal configurations of heating systems in urban areas where district heating is the primary and GWHPs the alternative heating option. The efficiency of heat pumps is assumed to be constant during the heating season. The authors also took into account that the efficiency can be reduced by the existing upstream installations and thus the reduced groundwater inlet temperature. A probability-based optimization approach is used to select users to be disconnected from the district heating grid and to install a GWHP. However, it should be emphasized that the proposed model is not an ESOM.

The literature review shows that the integration of residential heat pumps into ESOMs has not yet been sufficiently investigated. Only one study [12] is found to analyze different representations of residential heat pumps in an ESOM. Other studies do not include an ESOM [9−11] or do not consider residential heat pumps [13,15]. Therefore, this work analyzes different representation/integration approaches of residential heat pumps in ESOMs. Compared to Ref. [12], it includes hourly modelling of the efficiency of heat pumps, more detailed modelling on the load side and consideration of the hot water supply and not only space heating via heat pumps. This contribution is important due to the significance of heat pumps in future energy scenarios, where incorrect heat pump representations can lead to significantly different optimization results and, thus, wrong conclusions or even political decisions.

The main objective of this paper is to introduce and compare different approaches for GWHP integration into ESOMs, where the approaches are applicable to all other types of heat pumps. The focus is on GWHPs for two reasons: lack of literature about GWHPs because research papers usually focus on GSHPs and AHPs, and the case study area (Munich, Germany) possesses high potential for GWHPs. The considered ESOM is an exemplary case study, but the introduced methodology can be applied to any location.

The paper is structured as follows: Section 2 provides basic information about GWHPs and their efficiency indicators. Section 3 describes the methodology, i.e. integration approaches of GWHPs into ESOMs (3.1), as well as the energy system optimization model and the used data (3.2). In Section 4, the proposed approaches are evaluated along with a critical reflection. A summary and outlook of the paper are provided in Section 5.

2. Efficiency of groundwater heat pumps

Groundwater heat pumps, also known as open-loop shallow geothermal systems, directly utilize the thermal energy of the aquifer. The working principle of a GWHP system is depicted in Fig. 1: warm groundwater is extracted at the extraction (pumping) well, the heat is then transferred to the demand side using heat exchangers of the heat pump and, finally, the cooled water is returned back into the aquifer at the injection well. In the case of cooling, the returned water will be warmer than the extracted one. The injection well has to be placed downstream and with a sufficient distance from the extraction well to avoid hydraulic and thermal breakthroughs [18]. In the case of a breakthrough, re-injected water will reach the extraction well and deteriorate the operation of a GWHP system [19].

The efficiency of (groundwater) heat pumps is one of major influencing factors on customers buying decision because it reflects operating costs directly. In addition, the efficiency will influence the CO_2 footprint of a heat pump. The two mainly used heat pump efficiency indicators are the coefficient of performance and the seasonal coefficient of performance [20].

The coefficient of performance (COP) is a dimensionless number defined as the ratio of the produced heating capacity Q_{hp} and the electric power input P_{hp} of the unit at specific temperature conditions, expressed in kW/kW [21]:

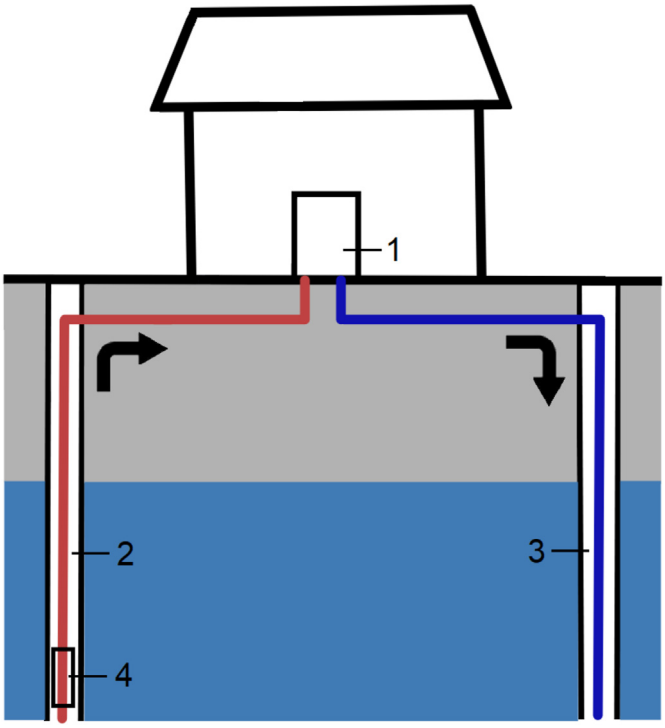

Fig. 1. Working principle of a GWHP system. Typical components of the system are: (1) Heat pump - main component with compressor and heat exchangers, (2) Extraction (pumping) well - where the warm groundwater is extracted from the aquifer, (3) (Re) injection well - where the cooled water is returned back to the aquifer, and (4) Submersible pump - used to pump the groundwater.

$$COP = \frac{Q_{hp}}{P_{hp}}. \quad (1)$$

For example, the COP value of 4 means that heat pumps produce 4 units of heat by using 1 unit of electricity. COP is a machine based indicator and takes into account only direct energetic inputs and outputs of heat pumps. Thus, COP can be used to compare heat pumps from different manufacturers when they are operating under identical conditions.

The seasonal coefficient of performance (SCOP) is the overall coefficient of performance of a heat pump using electricity, representative of the heating season, calculated as the reference annual heating demand divided by annual energy consumption for heating, expressed in kWh/kWh [21]. Compared to COP, SCOP usually includes auxiliary systems in the evaluation [20]. One such system is the submersible pump used to pump groundwater from below ground. This results in lower values of SCOP compared to COP.

Manufacturers usually define COP for a couple of operating points under optimal conditions. However, in reality, COP will have lower values because of non-ideal operating conditions. In addition to this, energy system modelers should take into account the extra energy needed for auxiliary components. Therefore, in this work the system's coefficient of performance (COP_s) will be used to model the efficiency of GWHP systems. COP_s is defined the same way as COP, i.e. for one operating point, but including all system components and not only the heat pump.

There are multiple factors influencing the COP_s, such as: local conditions (groundwater temperature and level), demand side (sink temperature), part load behaviour, and control strategy [22]. These factors are time dependent and thus COP_s will also vary over time, as can be seen from field measurements [23].

Two main approaches to model COP_s are identified in the literature. Both of them use temperature difference ΔT between source (groundwater) and sink (space heating/hot water supply) as a starting point. The first approach is using the ideal Carnot process to model the theoretical maximum COP based on ΔT values [10]. Thereafter these values are multiplied with scaling factors based on field measurements. This includes all additional efficiency losses and results in realistic COP_s values. Similar approach is used in Ref. [24] to benchmark the seasonal performance of heat pumps.

The second approach is using a quadratic function to model the dependence of theoretical COP on ΔT. This is used in works of Staffell et al. [20] and Fischer et al. [25], and most recently by Ruhnau et al. [9] and Mouzeviris and Papakostas [26]. In the first step, the coefficients of a quadratic function are fitted to the catalog data to obtain the theoretical correlation $COP = f(\Delta T)$. Thereafter these values are multiplied with a correction factor to match the field measurements. In this work the second approach and the coefficient/factor values from Ref. [9] are taken, as described in the following.

The theoretical dependence $COP = f(\Delta T)$ is fitted applying regression method on catalog data from Ref. [27] and for GWHPs is given by:

$$COP = 9.97 - 0.20 \cdot \Delta T + 0.0012 \cdot \Delta T^2, \quad (2)$$

where $\Delta T = T_l - T_s$, T_l is the sink (load) temperature and T_s the source temperature. In the second step, Ruhnau et al. [9] apply the correction factor f_{corr} to obtain realistic COP_s values:

$$COP_s = COP \cdot f_{corr}, \quad (3)$$

where $f_{corr} = 0.85$ is based on the field measurements from Ref. [28].

From (2) and (3) it follows that ΔT is the main influencing factor on the efficiency of heat pumps. In the case of GWHP systems, ΔT is the difference between the application temperature (space heating or domestic hot water (DHW)) and the groundwater temperature at extraction (pumping) well. There are different ways to model the temperature levels of space heating T_{sh} and domestic hot water supply T_{dhw}. The selection of temperature levels T_{sh} and T_{dhw} for the region of interest in this work is described in section 3.1.

Finally, groundwater temperatures T_s are required to compute COP from (2). It is common to set these temperatures at one constant level in modelling, e.g. 10 °C in Ref. [9]. However, field measurements from Germany [29] and China [30] show that temporal variations are present. In addition, spatial heterogeneity of the groundwater temperature field is also usually neglected. One of the goals in this work is to include the impact of resource (groundwater) on heat pumps efficiency. Therefore, different levels of complexity for the spatial and temporal component of groundwater temperature are considered in section 3.1.

3. Methodology

Fig. 2 depicts the overall methodology used to evaluate integration approaches of heat pumps into ESOMs. First, the efficiency of heat pumps is modelled in different ways, which corresponds to different integration approaches (section 3.1). In the second step, an ESOM for a residential heating sector is developed (section 3.2). Heat pumps are part of this ESOM and their efficiency is modelled differently according to the integration approaches. Finally, two optimization scenarios for reducing CO_2 emissions are simulated (section 3.2.2). Based on the optimization results, integration approaches are compared and evaluated.

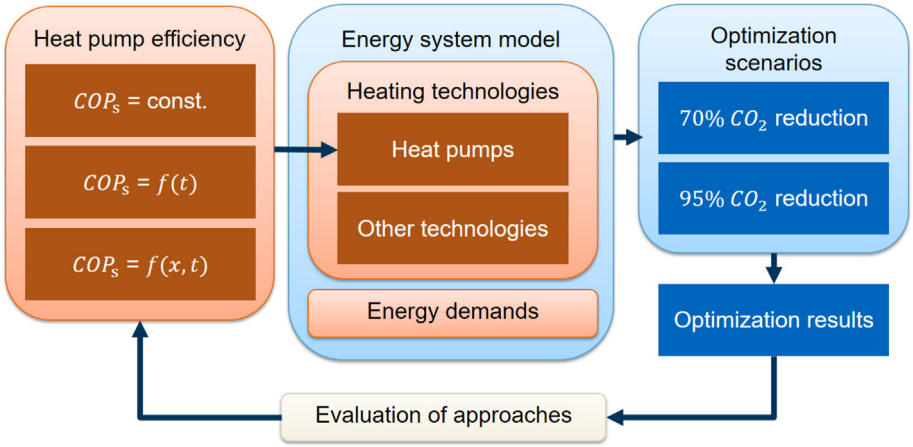

Fig. 2. Flow chart of the overall methodology.

3.1. Integration approaches

Motivated by the idea that more complex energy system models are also more accurate [31], different levels of complexity for the integration of heat pumps into energy system models are analyzed. Three different approaches to integrate GWHPs into ESOMs are considered:

1. COP_s = const.,
2. $COP_s = f(t)$,
3. $COP_s = f^i(t)$, where i denotes the i-th area/region.

For the sake of simplicity, these approaches are denoted as I, II and III, respectively. In the approach I, the performance of heat pump systems is considered constant for the whole energy system, i.e. urban area. This is a common approach in numerous energy system studies [10]. In this work, $COP_s = 4.0$ for GWHPs and $COP_s = 3.1$ for AHPs are used based on the study by Reinhold et al. [32]. It should be emphasized that AHP stands for air-to-water heat pumps within this work.

In the approach II, performance modelling of heat pumps is extended with a temporal component. In other words, COP_s is modelled as one time-series for the whole urban area. A detailed description of this approach is given in section 3.1.1.

In the approach III, a spatial component is added to the COP_s modelling. Here, the city is divided into regions, where each region has its own time-series for COP_s representation. A detailed description of this approach is given in section 3.1.2.

3.1.1. Temporal complexity

As previously stated in section 2, there are different approaches to model the space heating temperature T_{sh}. Conrad and Greif [10] apply weather compensation curves to describe the space heating temperatures T_{sh}, whereas Ruhnau et al. [9] apply linear heating curves and distinguish between radiator and floor heating. In both cases, T_{sh} depends on the ambient air temperature. In this work, the latter approach is applied:

$$\begin{aligned} T^r_{sh}(t) &= 40°C - 1.0 \cdot T_{abm}(t), \\ T^f_{sh}(t) &= 30°C - 0.5 \cdot T_{abm}(t), \end{aligned} \tag{4}$$

where T_{abm} is the ambient air temperature, T^r_{sh} and T^f_{sh} radiator and floor heating temperatures, respectively. Instead of time dependent temperatures, one can alternatively use constant values $T^r_{sh} = 55°C$ and $T^f_{sh} = 35°C$ as given in Ref. [33]. The obtained temperatures from (4) are combined into one temperature time-series applying the weighted average:

$$T_{sh}(t) = \frac{Q^r_{sh}(t) \cdot T^r_{sh}(t) + Q^f_{sh}(t) \cdot T^f_{sh}(t)}{Q_{sh}(t)}, \tag{5}$$

where Q^r_{sh} and Q^f_{sh} are radiator and floor heating demands, respectively, and $Q_{sh} = Q^r_{sh} + Q^f_{sh}$ the total space heating demand of the given area.

Differences are also present in the definition of the water heating temperature T_{dhw}. Conrad and Greif [10] define two constant levels for DHW supply, 50 °C for single family and 100 °C for multifamily houses, whereas Ruhnau et al. [9] define only one constant level $T_{dhw} = 50$ °C based on field measurements from Ref. [28]. Staffell et al. [20] assume the range 50–60 °C for domestic hot water temperatures. Temperatures for DHW supply T_{dhw} are independent from the ambient air temperature and thus considered constant. However, these values usually differ between small systems (single family houses) and large systems (multifamily houses). In this work, $T^s_{dhw} = 50°C$ for single family and $T^m_{dhw} = 65°C$ for multifamily houses are used, based on [33]. These values are also combined into one temperature as follows:

$$T_{dhw}(t) = \frac{Q^s_{dhw}(t) \cdot T^s_{dhw} + Q^m_{dhw}(t) \cdot T^m_{dhw}}{Q_{dhw}(t)}, \tag{6}$$

where Q^s_{dhw} and Q^m_{dhw} are single family and multifamily house DHW demands, respectively, and $Q_{dhw} = Q^s_{dhw} + Q^m_{dhw}$ the DHW demand of the given area. Although temperatures T^s_{dhw} and T^m_{dhw} are constants, the resulting mean DHW temperature $T_{dhw}(t)$ varies with time because of time dependent demands.

After the temperature levels T_{sh} and T_{dhw} are defined, they can be combined into one temperature T_l, which is then used in (2) to compute COP. The combined sink temperature T_l is the weighted average of T_{sh} and T_{dhw}, where weights are demands [20] or hourly shares [10] for space heating and DHW. In this work, the former approach is utilized:

$$T_l = \frac{Q_{sh} \cdot T_{sh} + Q_{dhw} \cdot T_{dhw}}{Q_{sh} + Q_{dhw}}, \tag{7}$$

where Q_{sh} and Q_{dhw} are demands for space heating and hot water, respectively.

Groundwater temperature T_{gw} at a given location is a function of the depth below the ground surface and time, which can be described by the following equation [34]:

$$T_{gw}(z,t) = T_m + \Delta T_s \cdot \exp\left(-2\pi\frac{z}{\Lambda}\right) \cdot \cos\left[2\pi\left(\frac{t}{t_0} - \frac{z}{\Lambda}\right)\right], \quad (8)$$

where z is the depth below the surface level, t time, T_m mean surface temperature, ΔT_s amplitude of the temperature variation on the surface, t_0 period of temperature oscillations, $\Lambda = 2\sqrt{\pi\alpha t_0}$ wavelength of one temperature oscillation, and α thermal diffusivity of the subsurface. In this work, the form of (8) is simplified by grouping certain parameters together as follows:

$$T_{gw}(t) = T_m - \Delta T_{gw} \cdot \cos\left[\frac{2\pi}{t_0}(t - t_d)\right], \quad (9)$$

where ΔT_{gw} is the amplitude of the groundwater temperature variation, t_d time delay constant, T_m and t_0 the same as before. The values of constant parameters in (9) are selected based on field measurements from Ref. [29] and given as follows: $T_m = 12$ °C, $\Delta T_{gw} = 2$ °C, $t_0 = 8760$ h, $t_d = 1800$ h.

It should be emphasized that the analytical formula for groundwater temperature is only an approximation and a numerical simulation of groundwater conditions would be required to account for all the complexities present in an urban aquifer. However, using an analytical formula for groundwater temperature in an ESOM is appropriate for several reasons:

- The majority of research studies, which use ESOMs to analyze future energy scenarios, assume constant groundwater temperature (usually 10 °C) for all locations and throughout the year. Therefore, this work improves the representation of groundwater temperatures and makes them more realistic by taking into account temporal and, in the approach III, also spatial dependencies.
- The applied analytical formula is parametrized with real field measurements and thus represents an estimation of the mixed groundwater temperature, which is extracted and used by a heat pump. Consequently, realistic seasonal changes are taken into account without explicitly using groundwater temperatures at different depths.
- A detailed modeling of the groundwater temperature and conditions, i.e. the use of a numerical model of the flow and heat transport in the porous media, is not suitable for ESOMs. The ESOMs are spatially aggregated models in which, for example, the entire city is represented as one location (site) that has one time-series for the heat demand and requires one time-series for the heat pump efficiency. This is due to the optimization part of ESOMs where it is not possible to optimize models with high spatial resolutions, e.g. to optimize a city model with a building resolution. Therefore, aggregated representations for the entire city or city regions (approach III) are required in ESOMs.
- Finally, the data required to build a numerical model for the groundwater simulation are usually difficult to obtain and were not available for the location considered in this work.

To maintain consistency, the same procedure has to be applied for AHP systems. In this case, the source temperature is the measured ambient air temperature $T_{abm}(t)$, whereas the load temperature $T_l(t)$ remains the same. Computation of theoretical COP for AHPs is the same as (2), but with different polynomial coefficients: 6.08, −0.09, 0.0005 [9]. Finally, applying (3) COP_s values for AHPs are obtained. The obtained COP_s values for GWHPs and AHPs over a period of one year are depicted in Fig. 3. It is evident that GWHPs significantly outperform AHPs during winter months. In addition, efficiency of both heat pump types decreases considerably during the summer period. This can be explained by the fact that there is only demand for DHW during summer months, which increases the load side temperature.

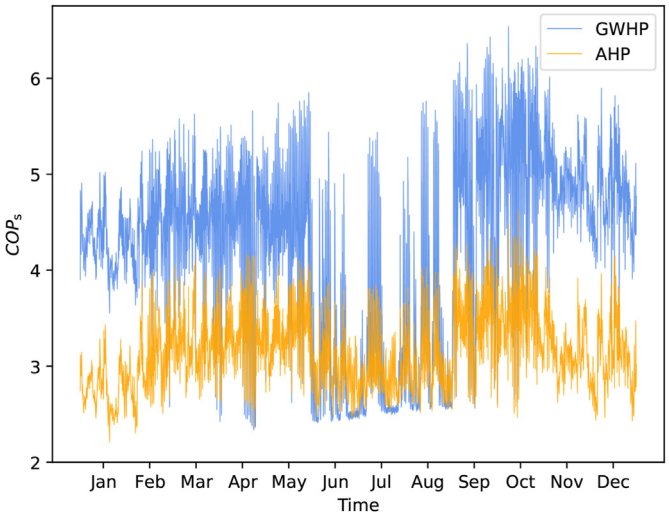

Fig. 3. COP_s variation over the year for GWHP (blue) and AHP systems (orange). (For interpretation of the references to colour in this figure legend, the reader is referred to the Web version of this article.)

It should be emphasized that instead of using weighted temperatures from (5), (6) and (7), one can compute COP_s for all different load sides independently. Fig. 4 shows computed COP_s of GWHPs and AHPs for four different load sides: space heating with radiators, floor heating, DHW supply for single and multifamily houses. It is evident that both types of heat pumps are more efficient for floor heating compared to radiators, especially during winter, and for DHW supply of single family compared to multifamily houses. This is due to the fact that lower load-side temperatures increase COP_s. It is also noticeable that GWHPs outperform AHPs in all cases, with the exception of the hot water supply of multifamily houses, where GWHPs do better in winter and worse in summer compared to AHPs. The COP_s of GWHPs for DHW looks smooth because load-side temperatures are constant and source-side temperatures are sinusoidal functions obtained from (9). To use the independently computed COP_s values in the ESOM, heat demands must be separated as well based on the load side. However, this is not considered further in this work for three reasons: (1) using equations (5)–(7) gives almost identical results (see Appendix A for a detailed comparison); and also (2) the results comparison is simplified; (3) computational time is reduced.

3.1.2. Spatial complexity

In the second extension, spatial complexity, i.e. heterogeneity, of GWHP system's performance at an urban scale is being considered. This is primarily motivated by the spatial heterogeneity of groundwater temperatures in urban aquifers. The city of Munich, which is the urban area of interest in this work, has already been analyzed for the shallow geothermal potential within the GRETA project [35]. One of the project outcomes is the map of groundwater temperatures in Munich, which is available at [36]. Based on these different groundwater temperature levels, the whole city is divided into separate regions as depicted in Fig. 5. The division is done using the clustering algorithm proposed by Siala and Mahfouz [37], which is a combination of the k-means++ and max-p regions

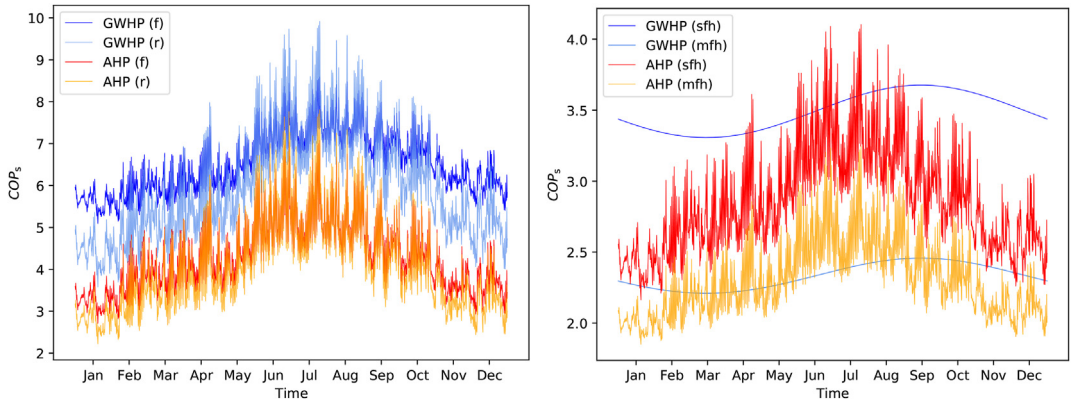

Fig. 4. COP_s variation over the year for GWHP and AHP systems, and different load sides: floor heating (f), radiator heating (r), DHW for single family (sfh) and multifamily houses (mfh).

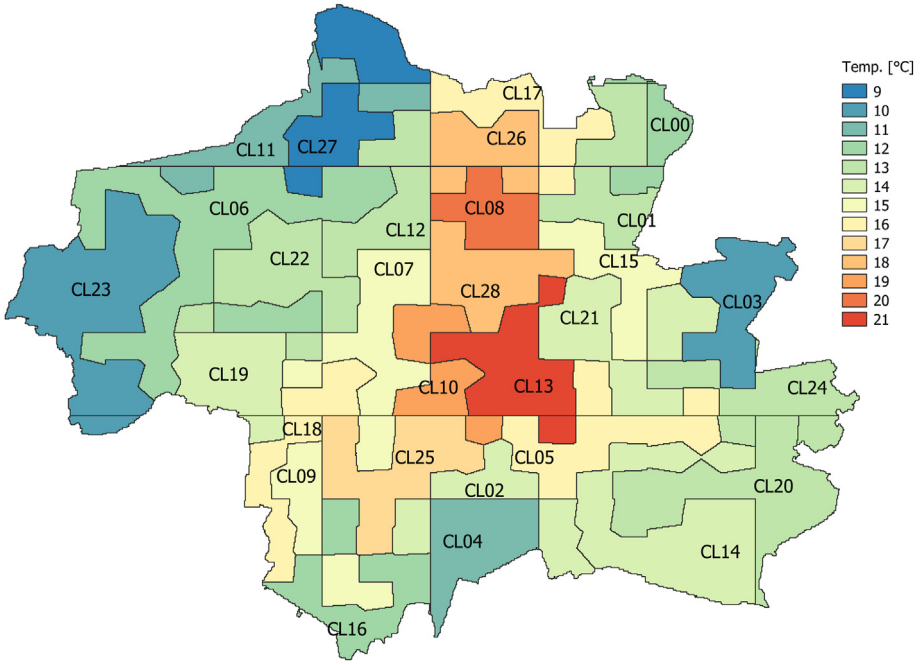

Fig. 5. Division of the city of Munich into separate regions based on the groundwater temperature.

algorithms.

Temperature levels for each of 29 identified city regions represent values that are based on measurements from April 2014 [36]. Therefore, equation (9) has to be first applied for each of regions to compute the mean surface temperature of each region:

$$T^i_{\mathrm{m}} = T^i_{\mathrm{gw}}(2520\mathrm{h}) + \Delta T_{\mathrm{gw}} \cdot \cos\left[\frac{2\pi}{t_0}(2520\mathrm{h} - t_{\mathrm{d}})\right], \tag{10}$$

where T^i_{m} is the mean surface temperature of region i, $i \in \{1, 2, \ldots, 29\}$, $T^i_{\mathrm{gw}}(2520\mathrm{h})$ groundwater temperature of region i measured in April ($t = 2520$ h), and the remaining parameters are the same as previously defined. Thereafter, inserting the obtained T^i_{m} values into (9), time-series of groundwater temperatures for each region $T^i_{\mathrm{gw}}(t)$ can be derived.

In addition, the separation of the city heat demand (and existing heating structure) by regions has to be considered. This means that each region i has its own:

- radiator heating demand $Q^{\mathrm{r},i}_{\mathrm{sh}}(t)$,
- floor heating demand $Q^{\mathrm{f},i}_{\mathrm{sh}}(t)$,
- total space heating demand $Q^{i}_{\mathrm{sh}}(t)$,
- single family house DHW demand $Q^{\mathrm{s},i}_{\mathrm{dhw}}(t)$,
- multifamily house DHW demand $Q^{\mathrm{m},i}_{\mathrm{dhw}}(t)$,
- total DHW demand $Q^{i}_{\mathrm{dhw}}(t)$.

These values are computed using a GIS tool, where, for instance, all single family houses geographically inside the region i are assigned to that region and their DHW demands are aggregated into $Q^{\mathrm{s},i}_{\mathrm{dhw}}(t)$. Thereafter, using different demands of each region and equations (5)–(7), load temperature levels $T^i_{\mathrm{sh}}(t)$, $T^i_{\mathrm{dhw}}(t)$ and $T^i_{\mathrm{l}}(t)$ for each region i can be computed. Finally, using $T^i_{\mathrm{l}}(t)$ and $T^i_{\mathrm{gw}}(t)$, time-series of GWHP performance $COP^i_{\mathrm{s}}(t)$ are estimated for all regions.

To maintain consistency, the same procedure is applied for AHP

systems. Ambient air temperatures are heterogeneously distributed in urban areas because of the well-known urban heat island effect [38]. However, here it is assumed that the source side, i.e. ambient air, is homogeneous throughout the city due to the lack of measurement data. Differences in COP_S time-series for AHP systems still exist between regions because of different demands and resulting load-side temperatures.

3.2. Energy system optimization model

In general, ESOMs are used to analyze future energy scenarios on different scales (urban, country, continent) and to solve the so-called unit commitment problem. The objective is usually to minimize costs and/or CO_2 emissions, while satisfying the energy demand at all times.

Within this work, an ESOM for the residential heating sector of the city of Munich has been developed and used. It should be emphasized that this in only an exemplary case study to analyze different integration approaches of heat pumps into ESOMs. By changing the input data, the approaches can be directly applied to other locations and system scales, e.g. country level. The considered model includes all relevant heating technologies for the city: district heating (DH), GWHPs, AHPs, pellet, gas, oil, solar-thermal and electric heating. GSHPs are excluded from the model because it is difficult to install them in the city of Munich: drilling regulations [39] limit borehole heat exchangers and there is usually not enough space for horizontal collectors.

The electricity system is simplified by electricity prices: retail price, tariff for heat pumps and feed-in tariff. In addition, photovoltaic modules (PVs) are included in the model as a competing technology to solar-thermal in the sense of available space. Heat and electricity demands are modelled with hourly resolution over a period of one year, which corresponds to optimization time step and period, respectively. Data and further assumptions used to build the model are described in section 3.2.3.

3.2.1. Optimization framework

The previously described model is developed using the modelling/optimization framework urbs, which is an open-source linear programming framework [40]. Urbs is based on multiple input - multiple output processes that are used to model different technologies [41]. Additional flexibility is provided through other framework components, such as energy storage, transmission, demand-side management and time-variable efficiency. The last one is used to model time-dependent COP_S of heat pumps in this work.

3.2.2. Optimization scenarios

In 2014, the heat-related CO_2 emissions from the Munich building stock amounted to 2.8 million t [32]. Residential buildings (single and multi-family houses) caused the majority of those emissions with around 80 %. Therefore, the focus is only on this sector within this work. Nonresidential sector is not considered as it requires separate analysis due to significantly different conditions.

In the study by Kenkmann et al. [42], three climate protection scenarios for Munich are identified: reference, moderate climate protection and the climate-neutral scenario. Similar to this, two different CO_2 mitigation scenarios are considered in this work: 70 % and 95 % reduction compared to the year 2014. These energy system optimization scenarios are used to evaluate and compare different GWHP integration approaches.

3.2.3. Data

The main data sources and underlying assumptions used to generate energy system optimization models are described in the following.

In the demand time-series, a distinction must be made between heat and electricity demand. Due to the limited access to real demand curves at the building level, both time-series are created synthetically. For the heat demand time-series the open-source tool UrbanHeatPro [43] is used. The tool generates synthetic heat demand time-series for one year for each building of a building list, taking into account all the necessary parameters, such as building classes and properties [44] or the ambient air temperature [45]. For the building database, data from Ref. [46] are used. The building stock consists of 121,832 residential buildings, of which 42,514 are multifamily houses and 79,318 single family houses. Finally, from the time-series of the individual buildings, time-series for the whole city or the individual regions are accumulated. The time-series obtained for space heating and hot water demand of the entire city are shown in Fig. 6. The demand for hot water is evenly distributed throughout the year, while the demand for space heating is inversely proportional to the ambient air temperature and is therefore much higher in winter. The estimated annual hot water and space heating demands for the city of Munich are 890.33 GWh and 5446.61 GWh, respectively. The electricity demand is synthesized using standard load profiles [47]. For this purpose the standard load curve is weighted according to the occupants of a building and the building class. Thereafter, the building time-series are summed up to obtain the demand of the entire city or selected regions.

Since suitable data about the existing generation capacities of different heating technologies in Munich were not available, they are generated synthetically. Based on the installed district heating capacity [48], an approximate installed heating capacity per heating type is generated using [49,50]. For the higher-resolution model, these heating capacities are divided according to the number of buildings and residents per region. The installed capacities of different heating technologies in 2014, as well as yearly heat and electricity demands, for all the regions and for the whole city of Munich are given in Table 2.

Data sources for groundwater temperatures are previously described in section 3.1.1 and section 3.1.2. For AHPs, air temperatures are required to compute COP_S. Here, the same temperatures are used as for the heat demand computation, i.e. the ambient air temperatures at 2 m above ground [45].

All cost relevant data are primarily based on the study by Stoffregen et al. [51]. The study is conducted for the region of Bavaria, where the city of Munich is also located. Therefore, this study has

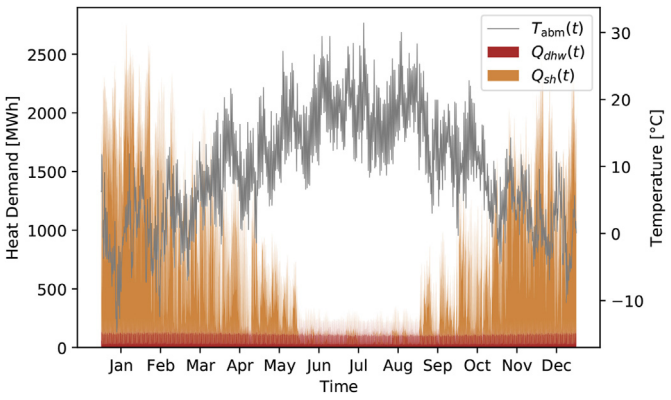

Fig. 6. Ambient air temperature and synthetic heat demands for the city of Munich. The hot water and space heating demands are denoted by $Q_{dhw}(t)$ and $Q_{sh}(t)$, respectively.

Table 2
Installed capacities and annual demands in 2014.

Region	Installed Capacity [MW]								Total Demand [MWh]	
	Oil	Gas	GWHP	AHP	Pellet	District heat	Solar- thermal	Electric Heater	Heat	Electricity
CL00	20.25	37.89	0.03	0.03	0.03	–	0.16	2.16	20,865.21	31,613.23
CL01	63.24	118.31	0.10	0.10	0.10	37.93	0.50	6.73	116,192.93	98,717.47
CL02	116.95	218.79	0.18	0.18	0.18	70.15	0.92	12.45	218,333.67	182,551.60
CL03	26.36	49.31	0.04	0.04	0.04	–	0.21	2.81	74,295.56	41,141.51
CL04	129.19	241.67	0.20	0.20	0.20	77.48	1.02	13.75	213,841.14	201,645.11
CL05	178.92	334.71	0.28	0.28	0.28	106.60	1.41	19.05	416,594.04	279,274.78
CL06	376.55	704.43	0.59	0.59	0.59	225.84	2.97	40.09	356,449.56	587,762.25
CL07	156.94	293.59	0.25	0.25	0.25	94.13	1.24	16.71	334,031.86	244,965.57
CL08	78.86	147.52	0.12	0.12	0.12	47.29	0.62	8.40	107,225.13	123,092.15
CL09	145.37	271.94	0.23	0.23	0.23	87.19	1.15	15.48	189,689.79	226,906.14
CL10	127.36	238.26	0.20	0.20	0.20	76.39	1.00	13.56	294,173.45	198,801.39
CL11	48.83	91.36	0.08	0.08	0.08	–	0.38	5.20	41,634.70	76,226.28
CL12	149.96	280.53	0.23	0.23	0.23	–	1.18	15.97	187,896.39	234,070.82
CL13	241.69	452.13	0.38	0.38	0.38	144.96	1.90	25.73	623,881.17	377,253.62
CL14	263.65	493.21	0.41	0.41	0.41	158.12	2.08	28.07	385,160.81	411,525.90
CL15	56.88	106.41	0.09	0.09	0.09	34.11	0.45	6.06	143,494.06	88,782.94
CL16	171.75	321.30	0.27	0.27	0.27	103.00	1.35	18.29	212,753.96	268,084.58
CL17	44.01	82.33	0.07	0.07	0.07	26.39	0.35	4.69	77,171.13	68,692.29
CL18	143.78	268.98	0.22	0.22	0.22	86.23	1.13	15.31	217,867.18	224,431.74
CL19	169.83	317.71	0.27	0.27	0.27	101.86	1.34	18.08	203,145.00	265,093.15
CL20	230.88	431.91	0.36	0.36	0.36	138.47	1.82	24.58	336,847.02	360,376.00
CL21	134.79	252.16	0.21	0.21	0.21	80.84	1.06	14.35	260,926.84	210,397.83
CL22	243.87	456.21	0.38	0.38	0.38	–	1.92	25.96	242,761.92	380,651.30
CL23	105.83	197.98	0.17	0.17	0.17	63.47	0.83	11.27	104,271.32	165,193.88
CL24	82.03	153.46	0.13	0.13	0.13	49.19	0.65	8.73	144,824.79	128,040.95
CL25	179.58	335.95	0.28	0.28	0.28	107.71	1.41	19.12	351,932.68	280,308.86
CL26	122.39	228.97	0.19	0.19	0.19	73.40	0.96	13.03	159,219.87	191,045.81
CL27	24.65	46.12	0.04	0.04	0.04	–	0.19	2.62	21,676.91	38,482.45
CL28	5.39	10.09	0.01	0.01	0.01	3.24	0.04	0.57	239,468.50	8420.35
Munich	3839.80	7183.20	6.00	6.00	6.00	1994.00	30.25	408.80	6,296,626.59	5,993,549.95

similar local conditions as the modelled area and represents a consistent and compact source of information. In addition, data about the district heating grid in Munich are obtained from the local provider [52] and the city gazette [53].

Specific CO_2 emissions of different energy carriers are obtained from different sources: [54] for electricity, [55] for district heating, [56] for pellet and [57] for the specific emissions of gas and oil. It should be emphasized that future developments of commodity prices and specific CO_2 emissions of different technologies, or the future development of heating demand, are not considered in this work. The focus here lies on the integration approaches of GWHPs into ESOMs and their impact on the optimization results, but not on the optimization scenarios itself. For the latter, one would require a detailed analysis of all relevant data, including future developments, which is beyond the scope of this paper.

4. Results

The integration approaches are compared based on the optimization results of the ESOM for different optimization scenarios. In addition, a critical reflection and possible future advancements of the methodology are provided in the following.

4.1. Comparison of different integration approaches

In order to evaluate different integration approaches of heat pumps into ESOMs, the results of CO_2 reduction scenarios are compared. The quantities used for the comparison are the installed capacities of heating technologies, as well as their utilization in the technology mix of the urban energy (heating) system. Figs. 7–9 show the results for all three integration approaches, and for both optimization scenarios.

Figs. 7 and 8 depict the new installed and the total capacities in the system, respectively, for all "integration approach - optimization scenario" combinations. The total capacities are the sum of the already available capacities in 2014 and the new installed capacities. If the technology is not utilized, i.e. it is replaced with other technologies, then its total capacity is set to zero. This means that the new installed capacities of such technologies are negative. These theoretically negative capacities are not depicted in Fig. 7 for the sake of simplicity. Analyzing Figs. 7 and 8 it can be stated that in both optimization scenarios the integration approach I significantly differs from the approaches II and III.

Applying the approach I will result in new installed capacities of AHPs in both scenarios, whereas this is not the case for approaches II and III. Also, new added capacities of GWHPs are smaller for the

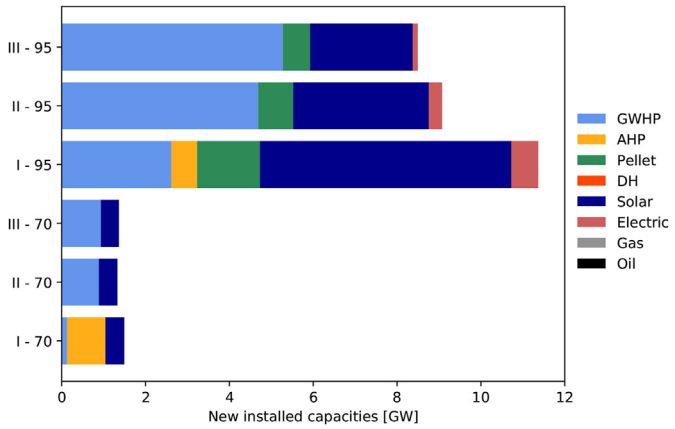

Fig. 7. New installed capacities of different heating technologies in the city of Munich. The horizontal bars represent different combinations of integration approach (I, II and III) and optimization scenarios (70 % or 95 % CO_2 reduction).

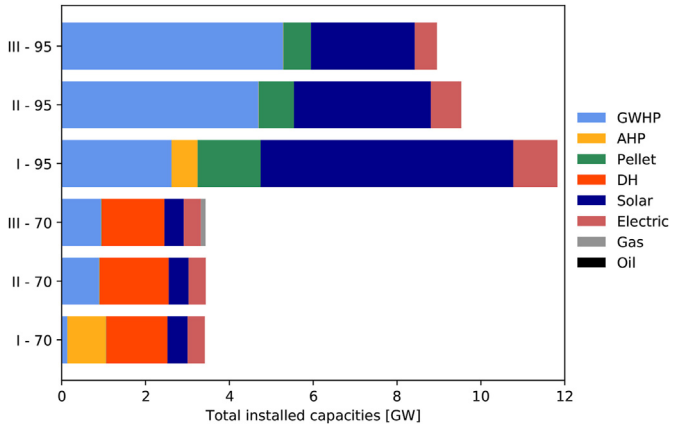

Fig. 8. Total installed capacities of different heating technologies in the city of Munich. The horizontal bars represent different combinations of integration approach (I, II and III) and optimization scenarios (70 % or 95 % CO_2 reduction).

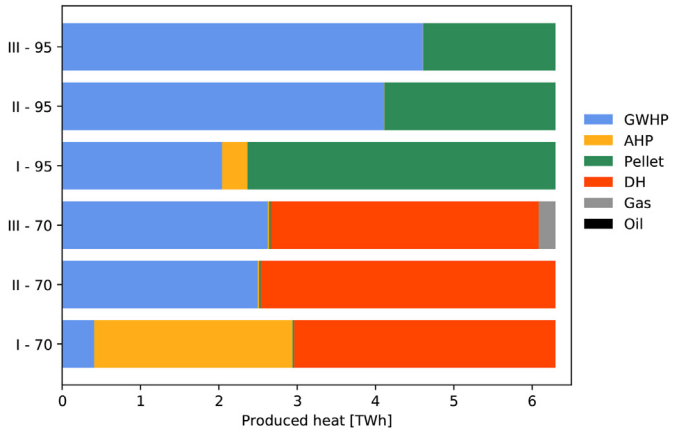

Fig. 9. Heat supply (production) from different technologies in the city of Munich in one year. The horizontal bars represent different combinations of integration approach (I, II and III) and optimization scenarios (70 % or 95 % CO_2 reduction).

approach I:

- 70 % CO_2 reduction: 0.128 GW (I), 0.886 GW (II), 0.935 GW (III),
- 95 % CO_2 reduction: 2.614 GW (I), 4.687 GW (II), 5.276 GW (III).

This can be explained by the fact that the approach I overestimates the efficiency of AHPs and underestimates the efficiency of GWHPs, which is also visible in Fig. 3. Therefore, using a constant COP_S value to model efficiency of heat pumps will result in misleading results from ESOMs. On the other hand, differences between approaches II and III are relatively small. This is especially the case for the 70 % CO_2 mitigation scenario. Thus, time-variable COP_S, i.e. the approach II, is sufficient to make statements about future energy-mix scenarios at the level of the entire system.

Previous statements can be reconfirmed when analyzing Fig. 9, which shows heat production of different technologies in the system over the whole year. All 6 ″approach - scenario” combinations are depicted here again. The labels correspond to the main technology in the household heat supply. For instance, “Gas” does not only mean heat produced from stand-alone gas heating, but also from combinations of gas and supporting systems such as solar-thermal or electric heating. Thus, supporting systems are not separately depicted in the figure. This is different compared to Figs. 7 and 8, but the same conclusions can be made again: approach I produces incorrect results, whereas approaches II and III are relatively similar. Furthermore, comparing the two optimization scenarios, the transition from district heating to pellets is noticeable. This is due to the assumption of constant specific CO_2 emission in the district heating energy-mix. For more realistic scenarios, one would require the future development of such emissions and other relevant factors, as already explained in section 3.2.3.

Based on Figs. 7–9, and the previous discussion, it can be concluded that the approach II is the most suitable approach when analyzing future scenarios for the entire system, i.e. the whole city or area of interest. This is because approach II produces comparable results to the approach III, despite being less complex/detailed and hence less computationally expensive. For instance, the optimization solver Gurobi [58] takes 48.13 s and 5043.89 s to solve 95 % CO_2 reduction scenario for the approaches II and III, respectively, when running on the machine Intel Xeon(R) Gold 6140 CPU @ 2.30 GHz x 72, 320 GB of RAM. In addition, loading data and generating the optimization model takes significantly longer in urbs for the approach III compared to II. However, if more detailed, i.e. spatially distributed, results are needed and not only the cumulative results for the entire energy system, the approach III will be necessary. On an urban system scale, such spatial results are important for city planers. On larger scales, region-based results are usually requested since regions may represent independent decision-makers, such as states or cities.

Fig. 10 shows the results of two optimization scenarios when applying the integration approach III. The heat production of different technologies is depicted separately for all 29 identified city regions. The technology labels used in the figure correspond to those from Fig. 9 and the numbering of regions coincides with that of Fig. 5. The transition from district heating to pellets between two scenarios is also easily noticeable here. In addition, some regions use gas heating in the 70 % CO_2 reduction scenario. These are mainly parts of the city where the district heating grid is not available. However, in the 95 % scenario GWHPs and pellets are the only viable heating technologies due to their low specific CO_2 emissions.

Region-based results, such as in Fig. 10, can be used by city planers to identify city regions where GWHPs might be the key technology for the future heat supply. This can help to prevent environmental issues or conflicting uses of groundwater caused by increased number of installations. Moreover, one can include groundwater protection zones and/or maximum pumping rates of GWHPs in the model prior to the optimization. This will limit the usage of GWHPs, but lead to even more realistic results. However, such considerations are beyond the scope of this work.

Finally, Fig. 11 shows time-series of heat supply for an exemplary week. The presented values correspond to the result of 95 % CO_2 reduction scenario and the approach II. These are hourly values of the heat supply for the whole city of Munich. Heat supply should be modelled in a way that different heating technologies are proportional to each other, i.e. that they always supply the same share of the total heating demand. For instance, if 75 % of households use GWHPs as their main heating systems, this percentage should remain the same during the whole year. In other words, one heating technology cannot be used to cover the base load on the city level and some other technologies to fulfill the remaining (peak) heat demand. Therefore, the so-called proportional processes are applied in the modelling framework urbs (see section 3.2.1) to obtain the correct heat supply behaviour, which can be seen in Fig. 11. The shares of different heating technologies are not predefined, but are set as an optimization result. It should be also emphasized that smoothing effects in the demand and corresponding supply curves are present due to the aggregation of individual household demands.

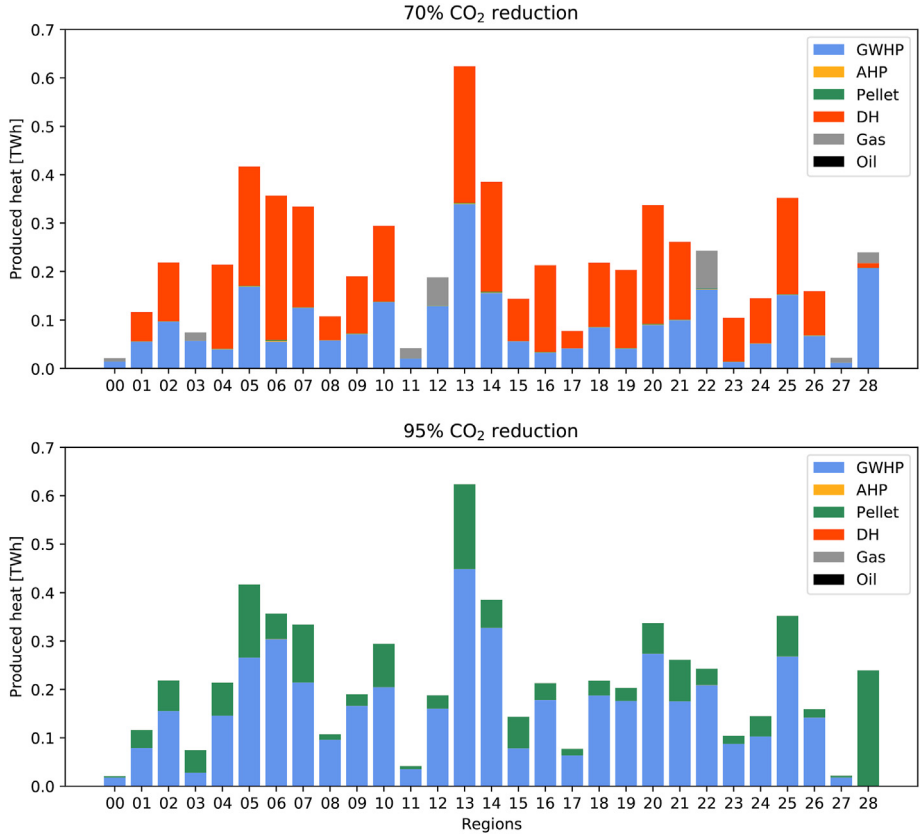

Fig. 10. Heat supply (production) from different technologies for each region of Munich in one year. The upper and lower diagrams represent results of the approach III for 70 % and 95 % CO_2 reduction optimization scenarios, respectively.

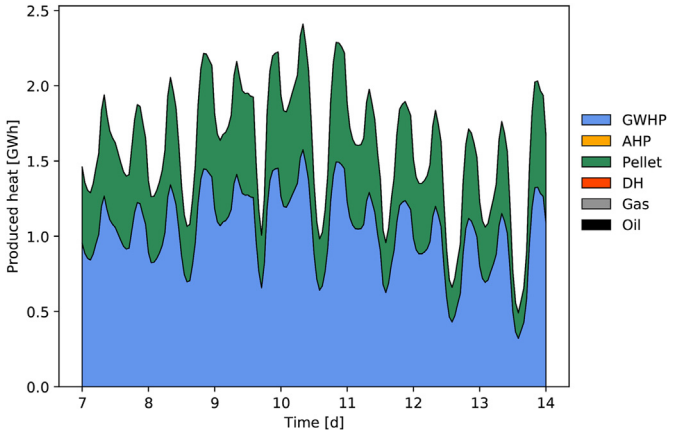

Fig. 11. Heat supply (production) from different technologies in the city of Munich during the second week of January. These are results from 95 % CO_2 reduction scenario when applying the approach II.

4.2. Critical reflection and future advancements

This paper focuses on different integration approaches of GWHPs into ESOMs and their impacts on the optimization results. However, the same integration approaches can be used for other types of heat pumps: ground and air source. AHPs are already considered in this work and modelled in the same fashion as GWHPs. In the case of GSHPs, one only has to change the coefficients in (2), according to Ref. [9], and to use soil temperatures. Therefore, the procedure introduced in this work is a general procedure for integration of heat pumps into ESOMs.

As previously stated, the focus of this work are heat pumps integration approaches, but not the optimization scenarios itself. For an analysis of future energy scenarios, a detailed analysis about future developments of heat demand, economical and environmental parameters is required. However, keeping these parameters constant, as in this work, facilitates analysis of the impact of different integration approaches.

Furthermore, it would be interesting to analyze impacts of heat pumps on the electricity system. Different integration approaches will result in different electricity demands of heat pumps, which might represent a high share of the total electricity demand in the energy system. An increase in the electricity demand may significantly change the energy-mix in the electricity sector and, hence, the specific CO_2 emissions of heat pumps. This is especially important for large scale systems, e.g. on a national level, where high penetration of heat pumps would significantly affect the electricity system. To analyze this interplay between electrified heating and the electricity sector, a detailed model of the electric energy system is required.

In the case of spatially heterogeneous efficiency of GWHPs, i.e. the integration approach III, only groundwater temperatures are used as an influencing factor from the source side. However, in reality there are other factors affecting the work/installation of GWHPs, such as groundwater thickness or drinking water protection zones. Increased number of installations might lead to negative interference between systems, which has to be avoided. In addition, the analytical formula (8) used in this work to compute groundwater temperatures is only an approximate estimation and does not consider numerous factors present in urban aquifers, which are

affecting the groundwater temperature. Including all these aspects in the model would result in a realistic (dynamic) thermal potential of groundwater, which enables strategic use of groundwater as an important energy resource. This requires coupling of energy system optimization models with numerical groundwater simulation (flow and heat transport) models, which is a complex task. Currently, within the project GEO.KW [59] such coupling schemes are being developed. Including the cooling in the model would also enable to analyze potential synergies between heating and cooling applications, since they can balance thermal usage of groundwater.

Finally, energy systems are complex socio-economical systems and thus a purely techno-economical model, which is used in this paper, is not sufficient to describe all aspects of the energy transition. This is especially the case for heating systems, where households individually decide on their heating technologies. In the future, it would be interesting to apply an agent-based modelling or sociodynamics approach, while still using techno-economical parameters from this work. Such models can provide policy recommendations that lead to the realization of CO_2 reduction goals.

5. Conclusions

In this work, different approaches to integrate GWHPs into energy system optimization models were analyzed. These approaches differ in the representation of GWHPs efficiency: (I) constant COP_S, (II) time-variable COP_S and (III) time-variable and spatially dependent COP_S. The energy system optimization model used in this work is the model of the residential heating sector in Munich. To analyze the impact of integration approaches on the optimization results of such a model, two different optimization scenarios were considered: 70 % and 95 % CO_2 reduction compared to the level from 2014.

In order to evaluate different approaches, the results of optimization scenarios were compared. In particular, the new installed capacities and the heat production from different technologies in the system are compared. The comparison shows that the more complex approaches, i.e. II and III, produce similar results, whereas the approach I yields significantly different and misleading results. The approach I, namely, overestimates the efficiency of AHPs and simultaneously underestimates the efficiency of GWHPs. The approach II is the most suitable for analyzing/obtaining optimization results on a cumulative/system level, since it is less complex and, thus, less computationally expensive than approach III. However, the approach III is necessary if regional (spatially distributed) results are required, e.g. for city planning or in large scale models. Additionally, it should be noted that the introduced integration approaches can be used for all types of heat pumps and also for different energy system scales and locations.

Since the electricity system was simplified by electricity price, the first future goal is to develop a detailed electricity system model and combine it with the heating model. This combined model can provide insights into interaction between heat pumps and electricity systems. In the spatial modelling, i.e. the approach III, only groundwater temperature was used as an important groundwater parameter. Adding other parameters, such as groundwater thickness or proximity of other installations, can provide more realistic and reliable results. Only techno-economical aspects of energy systems were considered in this work. In the future, the more detailed representation of heat pumps efficiency can be included in socio-economical models, e.g. agent-based, for an improved energy transition analysis.

Credit author statement

Smajil Halilovic: Conceptualization, Methodology, Writing – original draft, Software, Investigation, Visualization. Leonhard Odersky: Writing - reviewing and editing, Data curation, Software, Visualization. Thomas Hamacher: Writing - reviewing and editing, Supervision.

Declaration of competing interest

The authors declare that they have no known competing financial interests or personal relationships that could have appeared to influence the work reported in this paper.

Acknowledgement

The work presented in this paper has been supported by the German Federal Ministry for Economic Affairs and Energy (BMWi) within the scope of the research project GEO.KW (01184143/1).

Appendix A Separate efficiency values based on the load side

In section 3.1.1, it is stated that instead of using weighted load-side temperatures from (5), (6) and (7), one can compute COP_S for all different load sides separately. These separately calculated COP_S values can be included in the ESOM by dividing the heat demand according to the load side. However, the optimization results obtained by using weighted temperatures (simplified approach) are almost identical, as can be seen in Figure A.12 and Figure A.13.

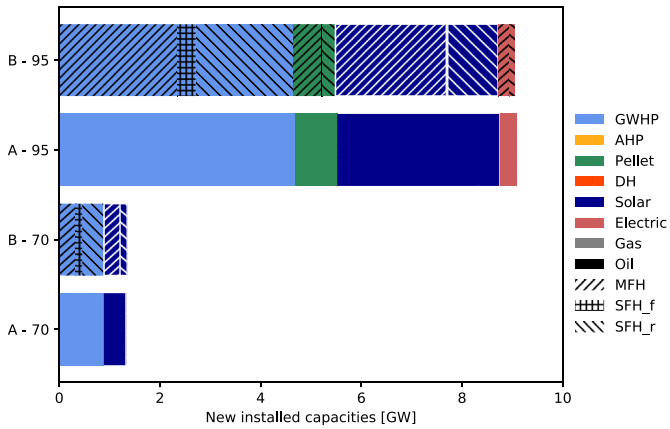

Fig. A.12. New installed capacities of different heating technologies in the city of Munich. The horizontal bars represent different combinations of COP_S estimation (A or B) and optimization scenarios (70 % or 95 % CO_2 reduction). The letters A and B correspond to the method used in this work with weighted averages of load-side temperatures and the method of using separate COP_S values for different load sides, respectively. Different hash patterns denote different load sides: multifamily houses (MFH), single family houses with floor heating (SFH_f) and single family houses with radiator heating (SFH_r).

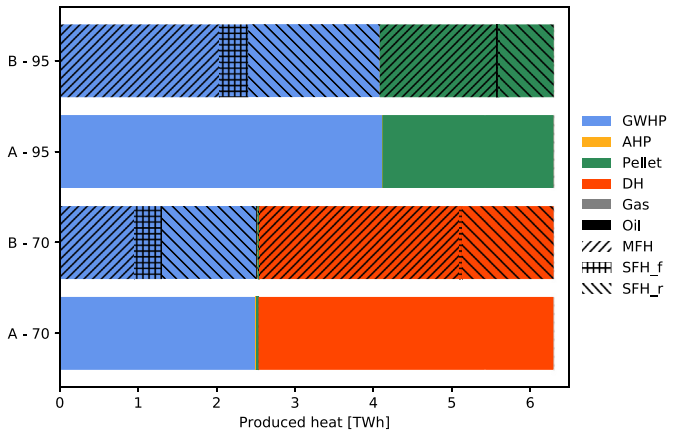

Fig. A.13. Heat supply (production) from different technologies in the city of Munich in one year. The horizontal bars represent different combinations of COP_s estimation (A or B) and optimization scenarios (70 % or 95 % CO_2 reduction). The letters A and B correspond to the method used in this work with weighted averages of load-side temperatures and the method of using separate COP_s values for different load sides, respectively. Different hash patterns denote different load sides: multifamily houses (MFH), single family houses with floor heating (SFH_f) and single family houses with radiator heating (SFH_r).

References

[1] BMWi Energieeffizienz. in Zahlen: entwicklungen und Trends in Deutschland. https://www.bmwi.de/Redaktion/DE/Publikationen/Energie/energieeffizienz-in-zahlen-2019.pdf?__blob=publicationFile&v=72; 2019. 2019.

[2] BMU Klimaschutzplan. Klimaschutzpolitische Grundsätze und Ziele der Bundesregierung, 2019. https://www.bmu.de/download/klimaschutzplan-2050/; 2020.

[3] Ruhnau O, Bannik S, Otten S, Praktiknjo A, Robinius M. Direct or indirect electrification? A review of heat generation and road transport decarbonisation scenarios for Germany 2050,. Energy 2019;166:989–99. https://doi.org/10.1016/J.ENERGY.2018.10.114.

[4] Gerhardt N, Sandau F, Scholz A, Hahn H, Scumacher P, Sager C, Bergk F, Kämper C, Knörr W, Kräck J, Lambrecht U, Antoni O, Hilpert J, Merkel K, Müller T. Interaktion EE-strom. Wärme und Verkehr 2015. https://www.iee.fraunhofer.de/content/dam/iee/energiesystemtechnik/de/Dokumente/Veroeffentlichungen/2015/Interaktion_EEStrom_Waerme_Verkehr_Endbericht.pdf.

[5] Karlsson M, Gebremedhin A, Klugman S, Henning D, Moshfegh B. Regional energy system optimization – potential for a regional heat market. Appl Energy 2009;86:441–51. https://doi.org/10.1016/j.apenergy.2008.09. 012.

[6] Kruse J, Hennes O, Wildgrube T, Lencz D, Hintermayer M, Gierkink M, Peter J, Lorenczik S. Dena-leitstudie integrierte energiewende: Teil B. https://www.dena.de/fileadmin/dena/Dokumente/Pdf/9261_dena-Leitstudie_Integrierte_Energiewende_lang.pdf; 2018.

[7] Quiggin D, Buswell R. The implications of heat electrification on national electrical supply-demand balance under published 2050 energy scenarios,. Energy 2016;98:253–70. https://doi.org/10.1016/j.energy.2015.11. 060.

[8] Schlesinger M, Hofer P, Kemmler A, Kirchner A, Koziel S, Ley A, Piegsa A, Seefeldt F, Straßburg S, Weinert K, Lindenberger D, Knaut A, Malischek R, Nick S, Panke T, Paulus S, Tode C, Wagner J, Lutz C, Lehr U, Ulrich P. Entwicklung der Energiemärkte - energiereferenzprognose. https://www.bmwi.de/Redaktion/DE/Publikationen/Studien/entwicklung-der-energiemaerkte-energiereferenzprognose-endbericht.pdf?__blob=publicationFile&v=7; 2014.

[9] Ruhnau O, Hirth L, Praktiknjo A. Time series of heat demand and heat pump efficiency for energy system modeling. Scientific data 2019;6:189. https://doi.org/10.1038/s41597-019-0199-y.

[10] Conrad J, Greif S. Modelling load profiles of heat pumps. Energies 2019;12:766. https://doi.org/10.3390/en12040766.

[11] Jarre M, Noussan M, Simonetti M. Primary energy consumption of heat pumps in high renewable share electricity mixes. Energy Convers Manag 2018;171:1339–51. https://doi.org/10.1016/j.enconman.2018.06. 067.

[12] Petrović SN, Karlsson KB. Residential heat pumps in the future Danish energy system. Energy 2016;114:787–97. https://doi.org/10.1016/j.energy. 2016.08.007.

[13] Pieper H, Ommen T, Kjær Jensen J, Elmegaard B, Brix Markussen W. Comparison of COP estimation methods for large-scale heat pumps used in energy planning. Energy 2020;205:117994. https://doi.org/10.1016/j.energy.2020.117994.

[14] Kjær Jensen J, Ommen T, Reinholdt L, Brix Markussen W, Elmegaard B, Heat pump COP. Part 2: generalized COP estimation of heat pump processes. 2018. https://doi.org/10.18462/IIR.GL.2018.1386.

[15] Bach B, Werling J, Ommen T, Münster M, Morales JM, Elmegaard B. Integration of large-scale heat pumps in the district heating systems of Greater Copenhagen. Energy 2016;107:321–34. https://doi.org/10.1016/j.energy.2016.04.029.

[16] Haikarainen C, Pettersson F, Saxén H. Optimized phasing of the development of a regional energy system. Energy 2020;206:118129. https://doi.org/10.1016/j.energy.2020.118129.

[17] Verda V, Guelpa E, Kona A, Lo Russo S. Reduction of primary energy needs in urban areas trough optimal planning of district heating and heat pump installations. Energy 2012;48:40–6. https://doi.org/10.1016/j.energy. 2012. 07.001.

[18] Clyde CG, Madabhushi GV. Spacing of wells for heat pumps. J Water Resour Plann Manag 1983;109:203–12. 10. 1061/(ASCE)0733-9496(1983)109:3(203).

[19] Milnes E, Perrochet P. Assessing the impact of thermal feedback and recycling in open-loop groundwater heat pump (GWHP) systems: a complementary design tool. Hydrogeol J 2013;21:505–14. https://doi.org/10.1007/s10040-012-0902-y.

[20] Staffell I, Brett D, Brandon N, Hawkes A. A review of domestic heat pumps,. Energy Environ Sci 2012;5:9291. https://doi.org/10.1039/c2ee22653g.

[21] DIN EN 14825:2016-10, Luftkonditionierer, Flüssigkeitskühlsätze und Wärmepumpen mit elektrisch angetriebenen Verdichtern zur Raumbeheizung und -kühlung_- Prüfung und Leistungsbemessung unter Teillastbedingungen und Berechnung der saisonalen Arbeitszahl. Deutsche Fassung EN_14825 2016:2016. https://doi.org/10.31030/2436322.

[22] Nolting L, Steiger S, Praktiknjo A. Assessing the validity of European labels for energy efficiency of heat pumps. J Build Eng 2018;18:476–86. https://doi.org/10.1016/j.jobe.2018.02.013.

[23] Zhu N, Hu P, Wang W, Yu J, Lei F. Performance analysis of ground water-source heat pump system with improved control strategies for building retrofit. Renew Energy 2015;80:324–30. https://doi.org/10.1016/j.renene.2015.02.021.

[24] Zottl A, Nordman R, Miara M. Benchmarking method of seasonal performance. http://sepemo.ehpa.org/deliverables/wp4/; 2012.

[25] Fischer D, Wolf T, Wapler J, Hollinger R, Madani H. Model-based flexibility assessment of a residential heat pump pool. Energy 2017;118:853–64. https://doi.org/10.1016/j.energy.2016.10.111.

[26] Mouzeviris GA, Papakostas KT. Comparative analysis of air-to-water and ground source heat pumps performances. Int J Sustain Energy 2021;40:69–84. https://doi.org/10.1080/14786451.2020. 1794864.

[27] PIW Planung. Und Installation: Wärmepumpen. https://www.stiebel-eltron.de/content/dam/ste/de/de/products/downloads/Planungsunterlagen/Planungshandbuch/Planungshandbuch_EE_Waermepumpen.pdf; 2019.

[28] Günther D, Miara M, Langner R, Helmling S, Wapler J. WP monitor feldmessung von Wärmepumpenanlagen. https://wp-monitoring.ise.fraunhofer.de/wp-monitor-plus/german/index/ergebnisse.html; 2014.

[29] Miara M, Günther D, Kramer T, Oltersdorf T, Wapler J. Wärmepumpen Effizienz: messtechnische Untersuchung von Wärmepumpenanlagen zur Analyse und Bewertung der Effizienz im realen Betrieb. https://wp-monitoring.ise.fraunhofer.de/wp-effizienz//download/wp_effizienz_endbericht_langfassung.pdf; 2011.

[30] Fei L, Pingfang H. Energy and exergy analysis of a ground water heat pump system. Phys Procedia 2012;24:169–75. https://doi.org/10.1016/j.phpro. 2012.02.026.

[31] Priesmann J, Nolting L, Praktiknjo A. Are complex energy system models more accurate? An intra-model comparison of power system optimization models. Appl Energy 2019;255:113783. https://doi.org/10.1016/j.apenergy.2019.113783.

[32] Reinhold N, Dufter C, Kleinertz B, von Roon S. Wärmewende münchen 2040 – handlungsempfehlungen. https://www.ffegmbh.de/kompetenzen/wissenschaftliche-analysen-system-und-energiemaerkte/energiesystem/713-waermewende-in-muenchen-2040-handlungsempfehlungen; 2018.

[33] Tiator I, Schenker M. Wärmepumpen, Wärmepumpenanlagen, 2. In: überarb aufl, Würzburg Vogel, editors; 2014. ISBN: 978-91-637-4473-0.

[34] Taylor CA, Stefan HG. Shallow groundwater temperature response to climate change and urbanization. J Hydrol 2009;375:601–12. https://doi.org/10.1016/j.jhydrol.2009.07.009.

[35] Casasso A, Piga B, Sethi R, Prestor J, Pestotnik S, Bottig M, Goetzl G, Zambelli P, D'Alonzo V, Vaccaro R, Capodaglio P, Olmedo M, Baietto A, Maragna C, Böttcher F, Zoesseder K. The GRETA project: the contribution of near-surface geothermal energy for the energetic self-sufficiency of Alpine regions,. Acque Sotterranee - Italian J Groundwater 2017;6. https://doi.org/10.7343/as-2017-265.

[36] Böttcher F. Potenzial der oberflächennahen Geothermie in München. http://greta.eurac.edu/maps/266; 2019.

[37] Siala K, Mahfouz MY. Impact of the choice of regions on energy system models. Energy Strat Rev 2019;25:75–85. https://doi.org/10.1016/j.esr. 2019.100362.

[38] Peng S, Piao S, Ciais P, Friedlingstein P, Ottle C, Bréon F-M, Nan H, Zhou L,

Myneni RB. Surface urban heat island across 419 global big cities. Environ Sci Technol 2012;46:696–703. https://doi.org/10.1021/es2030438.
[39] BWP. Leitfaden erdwärmesonden in bayern. https://www.stmwi.bayern.de/fileadmin/user_upload/stmwi/Themen/Energie_und_Rohstoffe/Dokumente_und_Cover/Leitfaden_Erdwaermesonden.pdf; 2012.
[40] Dorfner J. urbs: a linear optimisation model for distributed energy systems. https://github.com/tum-ens/urbs; 2020.
[41] Dorfner J. Open source modelling and optimisation of energy infrastructure at urban scale. PhD Thesis. Munich: Technical University of Munich; 2016.
[42] Kenkmann T, Hesse T, Hülsmann F, Timpe C, Hoppe K. Klimaschutzziel und –strategie München. https://www.oeko.de/publikationen/p-details/klimaschutzziel-und-strategie-muenchen-2050; 2020. 2017.
[43] Molar-Cruz A. UrbanHeatPro. https://github.com/tum-ens/UrbanHeatPro; 2020.
[44] IWU. TABULA web tool. 2016. http://webtool.building-typology.eu/.
[45] DWD. DWD Climate Data Center (CDC): hourly station observations of air temperature at 2 m above ground in °C for Germany, version v19.3. https://cdc.dwd.de/portal/202007291339/mapview; 2020.
[46] OpenStreetMap contributors. Planet dump retrieved from. https://planet.osm.org; 2017. https://www.openstreetmap.org.
[47] BDEW. Standardlastprofile strom. https://www.bdew.de/energie/standardlastprofile-strom/; 2020.
[48] SWM. Fernwärme und Rücklauftemperatur in modernen Niedertemperaturnetzen. https://www.swm.de/dam/jcr:7821c04d-9a95-44bf-9edb-2792c8c89f28/broschuere-fernwaerme-ruecklauftemperatur.pdf; 2015.
[49] Heilek C. Modellgestützte Optimierung des Neubaus und Einsatzes von Erzeugungsanlagen und Speichern für elektrische und thermische Energie im deutschen Energiesystem. PhD Thesis. Munich: Technical University of Munich; 2015.
[50] BDEW, Entwicklung des. Wärmeverbrauchs in Deutschland: basisdaten und Einflussfaktoren. https://www.bdew.de/service/anwendungshilfen/fakten-und-argumente-entwicklung-des-waermeverbrauchs-deutschland/; 2019.
[51] Stoffregen A, Hengstler J, Reuter B, Schuller O. Ökoeffizienzanalyse von Heiz- und Speichersystemen für private Haushalte. https://www.energieatlas.bayern.de/file/pdf/2096/LfU_Oekoeffizienzanalyse_20170217_final.pdf; 2017.
[52] SWM Preisblatt. Netzanschlüsse: der SWM Versorgungs GmbH. https://www.swm.de/dam/swm/dokumente/kundenservice/netzanschluss/preise-netzanschluesse.pdf; 2020.
[53] ALM. Amtsblatt der Landeshauptstadt münchen – Nr. 9/2020. https://www.muenchen.de/rathaus/Stadtrecht/Amtsblatt.html; 2020.
[54] Icha P, Kuhs G. Entwicklung der spezifischen Kohlendioxid-Emissionen des deutschen Strommix in den Jahren 1990-2019. https://www.umweltbundesamt.de/publikationen/entwicklung-der-spezifischen-kohlendioxid-6; 2020.
[55] LAK. Länderarbeitskreis Energiebilanzen: spezifische CO2-Emissionen der Strom- und Wärmeerzeugung. http://www.lak-energiebilanzen.de/spezifische-co2-emissionen-der-strom-und-waermeerzeugung/; 2019.
[56] Memmler M, Lauf T, Schneider S. Emissionsbilanz erneuerbarer Energieträger: bestimmung der vermiedenen Emissionen im Jahr. https://www.umweltbundesamt.de/publikationen/emissionsbilanz-erneuerbarer-energietraeger-2017; 2017. 2018.
[57] Lauf T, Memmler M, Schneider S. Emissionsbilanz erneuerbarer Energieträger: bestimmung der vermiedenen Emissionen im Jahr. https://www.umweltbundesamt.de/sites/default/files/medien/1410/publikationen/2019-11-07_cc-37-2019_emissionsbilanz-erneuerbarer-energien_2018.pdf; 2018. 2019.
[58] Gurobi L. Optimization, Gurobi optimizer reference manual. http://www.gurobi.com; 2020.
[59] Böttcher F, Davis K, Halilovic S, Odersky L, Pauw V, Schramm T, Zosseder K. Optimising the thermal use of groundwater for a decentralized heating and cooling supply in the city of Munich. Germany 2021. https://doi.org/10.5194/egusphere-egu21-14929. 10.5194/egusphere-egu21-14929.

4 Optimization of GWHPs

This chapter is dedicated to the central topic of this thesis, namely the optimization of GWHP systems at the system level. In Section 4.1, possible optimization approaches for GWHP systems are identified, classified and qualitatively compared. Subsequently, in Sections 4.2 and 4.3, three novel optimization approaches are introduced and analyzed using real case studies.

4.1 Optimization approaches

The task of optimizing GWHPs can be approached from several angles, depending on factors such as the level of abstraction in modeling physical phenomena, the conceptualization and formulation of the associated optimization problem, and the strategies used to solve the underlying problem. In this context, **Publication 2** [94] analyzes possible approaches for optimizing the design and operation of GWHP systems. To systematically perform this analysis, a novel classification scheme is introduced, dividing the identified optimization approaches into four different classes. These classes are distinguished based on the type of groundwater simulation model used, being PDE-based or simplified (e.g. analytical), and the choice of optimization algorithm, being gradient-based or derivative-free. Subsequently, a qualitative comparison of these classes is performed to evaluate their computational efficiency and applicability. In addition, the publication also reviews the existing approaches in the literature and underlines their limitations as well as possible future improvements. It should be noted that Publication 2 chronologically follows Publications 3 and 5, and thus also reviews the optimization approaches introduced in these earlier publications.

Publication 2 - Optimization approaches for the design and operation of open-loop shallow geothermal systems

Authors: Smajil Halilović, Fabian Böttcher, Kai Zosseder, Thomas Hamacher

Journal: Advances in Geosciences (Copernicus Publications)

Status: Published - December 2023

Digital object identifier: `https://doi.org/10.5194/adgeo-62-57-2023`

Author	Contribution
Smajil Halilović	Conceptualization, Writing – original draft, Methodology, Investigation, Visualization
Fabian Böttcher	Writing - reviewing and editing
Kai Zosseder	Writing - reviewing and editing
Thomas Hamacher	Writing - reviewing and editing, Supervision

Adv. Geosci., 62, 57–66, 2023
https://doi.org/10.5194/adgeo-62-57-2023

Advances in Geosciences
Open Access
EGU

Optimization approaches for the design and operation of open-loop shallow geothermal systems

Smajil Halilovic[1], **Fabian Böttcher**[2,3], **Kai Zosseder**[2], **and Thomas Hamacher**[1]

[1]Chair of Renewable and Sustainable Energy Systems, Technical University of Munich, Garching, Germany
[2]Chair of Hydrogeology, Technical University of Munich, Munich, Germany
[3]Department for Climate and Environmental Protection (RKU), City of Munich, Munich, Germany

Correspondence: Smajil Halilovic (smajil.halilovic@tum.de)

Received: 14 June 2023 – Revised: 15 October 2023 – Accepted: 12 December 2023 – Published: 19 December 2023

Abstract. The optimization of open-loop shallow geothermal systems, which includes both design and operational aspects, is an important research area aimed at improving their efficiency and sustainability and the effective management of groundwater as a shallow geothermal resource. This paper investigates various approaches to address optimization problems arising from these research and implementation questions about GWHP systems. The identified optimization approaches are thoroughly analyzed based on criteria such as computational cost and applicability. Moreover, a novel classification scheme is introduced that categorizes the approaches according to the types of groundwater simulation model and the optimization algorithm used. Simulation models are divided into two types: numerical and simplified (analytical or data-driven) models, while optimization algorithms are divided into gradient-based and derivative-free algorithms. Finally, a comprehensive review of existing approaches in the literature is provided, highlighting their strengths and limitations and offering recommendations for both the use of existing approaches and the development of new, improved ones in this field.

1 Introduction

Open-loop shallow geothermal systems, also known as groundwater heat pumps (GWHPs), have emerged as a promising solution for decarbonizing the residential heating and cooling sector (Russo et al., 2012). The performance of GWHPs is primarily influenced by groundwater temperature (Kim and Nam, 2016), which remains relatively stable throughout the year and is elevated in urban areas due to the subsurface urban heat island effect (Menberg et al., 2013; Epting and Huggenberger, 2013; Böttcher and Zosseder, 2021). These systems harness the thermal energy of the aquifer by extracting groundwater from one or more extraction wells and returning it to the same aquifer via injection wells after heat exchange in a heat pump (Florides and Kalogirou, 2007; Stauffer et al., 2014; García Gil et al., 2022). Since the temperature of the re-injected water is different from that of the extracted (lower in the heating and higher in the cooling case), this results in thermal plumes in the aquifer that propagate downstream along the groundwater flow direction. If these plumes reach the extraction wells of neighboring downstream GWHPs, this can result in either negative or positive thermal interference (Perego et al., 2022). Figure 1 provides an overview of potential thermal interferences that can occur between neighboring systems, depicting scenarios where the operation of downstream systems can be either degraded (negative interference) or enhanced (positive interference).

It is also important to recognize that GWHPs have a thermal impact on groundwater, which serves as a vital source of drinking water in many places (e.g. Blum et al., 2021). To mitigate the aforementioned negative interactions and improve the efficiency and sustainability of thermal groundwater use, resource management strategies need to be implemented (Epting et al., 2020). This includes optimizing the design, particularly well placement, and operation of GWHP systems, since the propagation of thermal plumes is affected by injection well locations, system operation (pumping rates), and aquifer characteristics. For example, optimal well placement can minimize negative thermal interference between neighboring GWHPs (Halilovic et al., 2022a) or

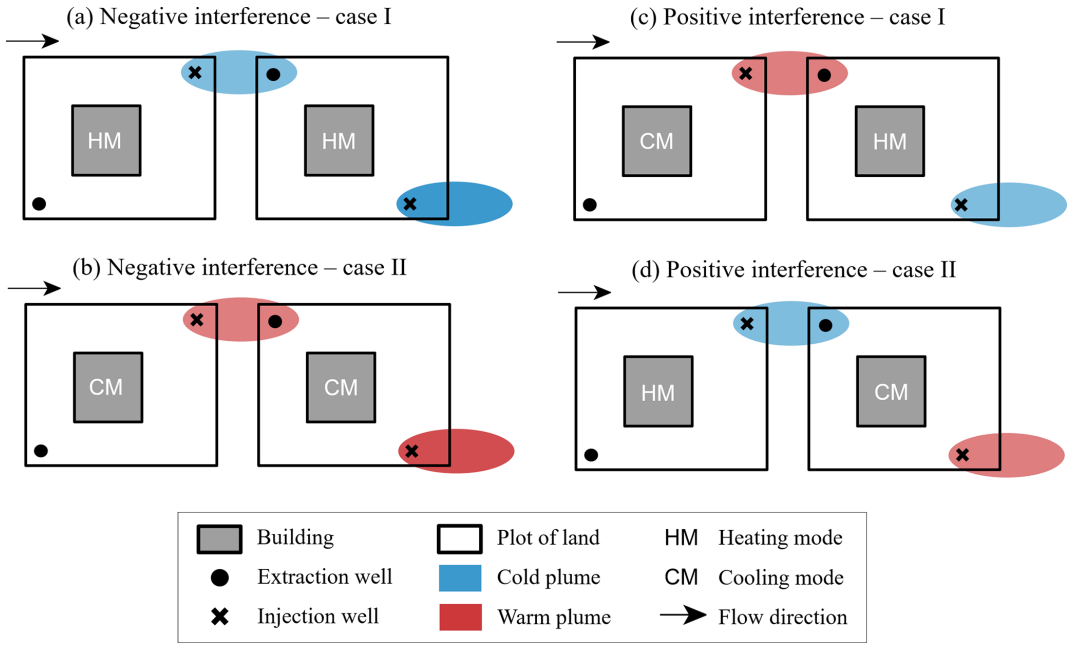

Figure 1. Possible thermal interference (interactions) between neighboring GWHP systems.

even maximize their positive interference (García-Gil et al., 2020). Hence, optimization of multiple neighboring systems plays an important role in urban planning strategies aimed at enhancing sustainability. In addition, optimization of GWHP systems is crucial for managing groundwater resources and maintaining the current state of groundwater, i.e. preventing adverse changes in its physical, chemical, and biological properties. Furthermore, it is essential to ensure adequate spacing between wells within the same GWHP to prevent hydraulic and thermal breakthroughs (Böttcher et al., 2019). Thus, optimization of individual systems is also important to maximize their efficiency and sustainability. Optimization of individual GWHP systems and concurrent optimization of multiple neighboring systems are challenging due to the complexity of the resulting optimization problems and the necessity for novel and efficient optimization approaches to solve them.

This paper presents a comprehensive overview of optimization approaches for the design and operation of GWHP systems. The approaches are critically evaluated and compared based on several criteria, and a novel classification scheme is introduced to effectively categorize these approaches. Furthermore, the current status of the approaches found in the literature is presented and possible future research directions are discussed.

2 Simulation models

GWHP systems affect the groundwater body both hydraulically and thermally (García Gil et al., 2022), which can also affect its chemical and biological conditions to a minor degree (Blum et al., 2021). The hydraulic head increases around injection wells and decreases around extraction wells, which also changes the hydraulic gradient and groundwater flow patterns. Thermal impacts are present due to the previously described thermal plumes. To analyze these impacts of GWHP systems on groundwater conditions, simulation models are commonly used. For a particular system design and operation, a simulation model can quantify its impacts on groundwater and, based on that, analyze the performance of the system. Therefore, simulation models play a crucial role for the computation of the resulting groundwater temperature field and serve as an integral component within the optimization procedures.

These simulation models generally fall into three categories: numerical, analytical, and data-driven. Numerical models use partial differential equations (PDEs) to describe the underlying physical phenomena, i.e. groundwater flow and heat transport in aquifers. The resulting system of PDEs can be solved with general PDE solving software or computational fluid dynamics (CFD) software, but there are also several software packages that include specialized domains of numerical simulation for shallow geothermal resources, such as: FEFLOW (Diersch, 2014) – based on the finite element method (FEM) or PFLOTRAN (Hammond et al., 2012) – based on the finite volume method (FVM). Numerical models can incorporate various complex subsurface conditions, including spatially heterogeneous groundwater parameters (e.g. hydraulic conductivity) and conditions (e.g. velocity, temperature, hydraulic head), complex boundary conditions, coupled physical processes, multiple subsurface layers, etc.,

while simultaneously simulating thermal and hydraulic effects of GWHP systems on the groundwater body. Therefore, they are closest to reality given sufficient quality of input data, but are generally computationally expensive.

The second category of models uses analytical formulas to approximate numerical solutions and is commonly applied to estimate thermal plumes associated with smaller GWHPs, whose energy consumption is less than 45 000 kWh per year (Ohmer et al., 2022). Due to their analytical nature, these models offer significant computational advantages over numerical models. In Pophillat et al. (2020) three prominent analytical models for estimating GWHP thermal plumes were analyzed and compared. These models include the radial heat transport model (RHM) (Guimerà et al., 2007), the linear advective heat transport model (LAHM) (Kinzelbach, 1992), and the planar advective heat transport model (PAHM) (Hähnlein et al., 2010). The authors concluded that although analytical solutions are less accurate compared to numerical models, they still have value for evaluating the thermal impact of GWHPs. Analytical solutions are particularly useful for performing initial assessments of potential negative interference between neighboring GWHPs (Pophillat et al., 2020).

Finally, data-driven models are gaining popularity in this area of research, primarily due to the emergence of machine learning. A common example is the use of neural networks (NNs) to predict thermal plumes (Russo et al., 2014; Leiteritz et al., 2022; Davis et al., 2023). Data-driven models, such as NNs, offer the advantage of fast evaluation, but rely on extensive training data and require additional time for the training process. Acquiring this training data is often challenging due to the limited measurement and monitoring of hydrogeological data. One possible solution is the use of physics-informed neural networks (PINNs) that integrate physical laws driven by PDEs, mitigating the need for extensive training data (Raissi et al., 2017).

3 Optimization of GWHPs

This section provides a comprehensive analysis of two key aspects related to the optimization of GWHP systems. First, in Sect. 3.1, the underlying optimization problems are discussed. Second, in Sect. 3.2, a detailed overview of the approaches for solving these optimization problems is provided. In the following section, we present a generalized problem related to the optimization of GWHP systems, which prepares the way for further analysis in subsequent sections.

3.1 Optimization problems

The high-level optimization problem concerning GWHP systems can be formulated as follows:

$$\min_{\boldsymbol{x}_\mathrm{d},\boldsymbol{x}_\mathrm{o}} f_\mathrm{obj}\left(\boldsymbol{x}_\mathrm{d},\boldsymbol{x}_\mathrm{o}\right) = \alpha_1 \cdot f_\mathrm{cost}\left(\boldsymbol{x}_\mathrm{d},\boldsymbol{x}_\mathrm{o}\right) + \alpha_2 \cdot f_\mathrm{env}\left(\boldsymbol{x}_\mathrm{d},\boldsymbol{x}_\mathrm{o}\right) \tag{1a}$$

$$\text{subject to } \mathcal{F}_\mathrm{sim}\left(\boldsymbol{x}_\mathrm{d},\boldsymbol{x}_\mathrm{o}\right) = 0 \tag{1b}$$

$$\boldsymbol{g}\left(\boldsymbol{x}_\mathrm{d},\boldsymbol{x}_\mathrm{o}\right) \leq 0 \tag{1c}$$

$$\boldsymbol{h}\left(\boldsymbol{x}_\mathrm{d},\boldsymbol{x}_\mathrm{o}\right) = 0 \tag{1d}$$

where $\boldsymbol{x}_\mathrm{d}$ is the vector of optimization variables related to the design of GWHP system(s), $\boldsymbol{x}_\mathrm{o}$ is the vector of optimization variables related to the operation of GWHP system(s), f_obj is the objective function to be minimized, f_cost is the function describing technical costs, f_env is the function describing negative environmental impacts, α_1 and α_2 are the weighting factors, $\mathcal{F}_\mathrm{sim}$ is the simulation model in a residual form, $\boldsymbol{g}$ are the inequality constraints, $\boldsymbol{h}$ are the equality constraints.

In this generalized problem, we differentiate between two types of optimization variables: design variables $\boldsymbol{x}_\mathrm{d}$ and operational variables $\boldsymbol{x}_\mathrm{o}$. An example of design variables are the number and spatial layout of GWHP wells, while an example of operational variables are the pumping rates of each well. The design variables are constant in time, whereas the operational variables are usually time-dependent.

The objective function f_obj contains two parts: f_cost, accounting for the technical costs of GWHP systems, and f_env, accounting for the negative environmental impacts. The term f_cost can represent various costs associated with the installation and operation of GWHPs, which can be reduced through different means, such as proper sizing of systems (reduced investment costs) or optimal operation of systems (increased efficiency and lifetime). On the other hand, the term f_env covers different environmental categories, such as negative impacts on groundwater or CO_2 emissions indirectly caused by the operation of GWHP systems. It should be noted that environmental considerations are usually incorporated into the problem through constraints and not directly within the objective function.

The simulation model $\mathcal{F}_\mathrm{sim}$ (see Sect. 2) that describes the subsurface phenomena is incorporated into the optimization as a single or multiple equality constraints. This model can be of any type discussed previously: numerical, analytical, or data-driven, and it can also have an explicit form, such as PDEs or algebraic equations, or an implicit "black-box" form, such as numerical simulation tools or NNs.

In addition to the simulation model, other inequality $\boldsymbol{g}$ or equality $\boldsymbol{h}$ constraints may be present in the optimization problem. These can be technical constraints, such as upper and lower limits on pumping rates, regulatory constraints, such as the maximum allowed change in groundwater temperatures, or any other additional constraints.

Depending on how certain elements are specified in the generalized problem (Eq. 1), the resulting optimization problems can be classified according to different criteria:

- *Optimization variables*: if the only optimization variables are the design parameters $\boldsymbol{x}_\mathrm{d}$ and the operation

of the system(s) is predefined, i.e. $\boldsymbol{x}_o$ is fixed, the problem (Eq. 1) becomes a design optimization problem. On the other hand, the problem becomes an optimal control problem when the system design is specified and the operating parameters $\boldsymbol{x}_o$ are the optimization variables. Finally, simultaneous optimization of the design and operation of GWHP systems is possible, i.e. considering both $\boldsymbol{x}_d$ and $\boldsymbol{x}_o$ as optimization variables. This generally leads to improved optimal solutions since there are more degrees of freedom to be optimized, but the resulting problems are usually more difficult to solve due to increased problem complexity (e.g. from linear to nonlinear).

– *Objective function*: in problem (Eq. 1), the objective function f_{obj} is a weighted sum of technical costs f_{cost} and quantified negative environmental impacts f_{env}. Setting one of the weights α to 0, the problem becomes either a purely economic or an ecological optimization problem, i.e. a single-objective optimization problem. If both weighting factors are kept positive, then both the cost and the environmental impact are minimized simultaneously and the problem becomes a type of multi-objective optimization. This means that by changing the values of α_1 and α_2, different Pareto-optimal solutions are obtained (Marler and Arora, 2010).

– *Application*: the application types can be divided into two main groups: optimization of a single standalone system and optimization of multiple neighboring GWHP systems. The application type directly changes the format of the optimization variables and the objective function. In addition, different applications may involve different optimization constraints, such as the threshold for negative interference between neighboring systems in the case of optimizing multiple systems.

– *Simulation model*: in the mathematical sense, the choice of simulation model $\mathcal{F}_{sim}$ fundamentally changes the type of the optimization problem. These optimization problem types belong to different branches of optimization and therefore require corresponding optimization approaches to be solved efficiently. For this reason, the entire following section is dedicated to the optimization approaches for the problem (Eq. 1).

3.2 Optimization approaches

In this study, the term "optimization approach" is considered to encompass not only the specific methodology used to solve a given optimization problem, such as the choice of an algorithm, but also the way in which the problem is formulated, which includes the selection of a groundwater simulation model. The classification of optimization approaches is shown in Fig. 2, where four different classes are identified. The categorization is based on the simulation model

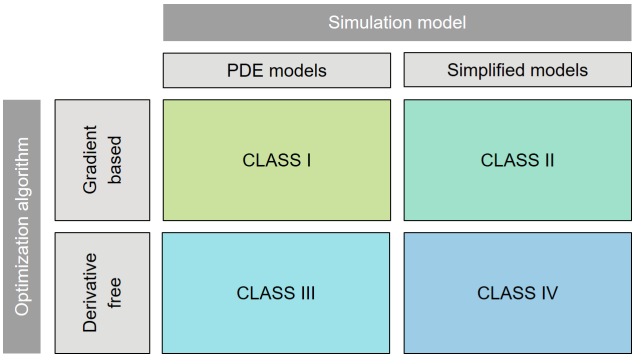

Figure 2. Proposed classification of the optimization approaches.

used, whether it is a PDE model or a simplified model, and the optimization algorithm employed, either gradient-based or derivative-free algorithms. In the following, each of these four classes is explained and references to relevant literature sources are provided.

Class I comprises optimization approaches where the simulation model is a numerical PDE model, and the optimization is performed using gradient-based algorithms. These approaches are referred to as PDE-constrained optimization (PDECO) problems, which are recognized as the most mathematically complex problems of the four classes considered. The complexity arises due to the multidisciplinary nature of these problems, necessitating expertise in several areas, including computational optimization, functional analysis, and numerical analysis. For example, state-of-the-art groundwater simulation tools usually lack the automatic provision of gradient information, requiring users to estimate gradients manually. There are two main methods to solve this problem: automatic differentiation of existing simulation tools (Naumann, 2011) or the development of custom numerical simulators within frameworks such as Firedrake (Rathgeber et al., 2017) and FEniCS (Logg et al., 2012), which can automatically provide the required gradients. Therefore, a comprehensive understanding of PDE solving is essential in the initial stages of developing a Class I approach. Various strategies exist for solving PDECO problems, including full-space and reduced-space methods, as well as discretize-then-optimize and optimize-then-discretize approaches (Hinze et al., 2008). For more information on PDECO, the reader is referred to the books by Hinze et al. (2008) and Tröltzsch (2010).

Class II includes approaches that utilize simplified models for groundwater simulation and employ gradient-based optimization algorithms to solve the underlying optimization problems. In this context, the simplified models primarily take the form of analytical models (see Sect. 2). These models are expressed through analytical formulas, allowing for direct integration into the optimization problem. The conceptualization of the overall optimization problem determines the resulting problems, which typically correspond to

well-established types of mathematical programming (optimization) problems, such as linear programming (LP), mixed-integer linear programming (MILP), quadratic programming (QP), and similar types. These problems are extensively studied in the optimization community, and consequently, efficient algorithms and solvers (software implementations of the algorithms) are readily available. Comprehensive information on these types of optimization problems can be found in numerous literature sources, including the books by Nocedal and Wright (1999), Schrijver (1998) and Bonnans et al. (2006).

Class III encompasses approaches that combine PDE simulation models with derivative-free optimization (DFO) algorithms. This form of optimization is commonly referred to as simulation-based optimization, where the simulation model is treated as a black-box, meaning that only the inputs and outputs of the simulator are observed and used by the optimization algorithm to guide the optimization process. As a result, the term black-box optimization (BBO) can also be used, which refers to optimization problems where either the objective function or some constraints are treated as black-boxes. However, it is important to note that the black-box in BBO is not limited to numerical simulation models. For instance, Class IV also falls under the umbrella of BBO. Furthermore, the terms BBO and DFO are closely interconnected and can be used interchangeably in certain contexts. These distinct terminologies have emerged over time, highlighting different aspects: the conceptual characteristics of BBO, and the algorithmic features of DFO. DFO algorithms, as the name suggests, do not rely on derivative information during optimization iterations to determine optimal solutions; instead, they use only the values of the objective function and constraints. These algorithms include: heuristic methods, e.g. genetic algorithms, particle swarm optimization, simulated annealing, etc. (Bozorg-Haddad et al., 2017); direct search methods, e.g. MADS algorithm (Le Digabel, 2011); and model-based methods, e.g. model-based trust-region (Conn et al., 2000). For more detailed information on DFO and BBO, interested readers are referred to Audet and Hare (2017) and Conn et al. (2009).

Class IV comprises optimization approaches that involve the coupling of simplified groundwater simulation models, such as analytical models or NNs, with DFO algorithms. Similar to Class III, Class IV falls into the DFO and BBO branches of optimization. Consequently, the same or similar optimization algorithms can be applied to both classes. The main difference between the two classes lies in the fidelity of the simulation models used. Class III uses high-fidelity models, while Class IV relies on low-fidelity models. Thus, the computational cost associated with evaluating potential solution candidates during optimization iterations is significantly lower in Class IV. It is important to note that Class IV has similarities to situations where model-based DFO algorithms are applied in Class III. The difference is that the approximate models in Class III are constructed dynamically during the optimization iterations, based on evaluations of the PDE model. In contrast, in Class IV, the simplified models are predefined and remain constant throughout the optimization process.

Finally, it should be mentioned that the four introduced classes do not encompass all conceivable approaches, since combined approaches also exist. For example, the solution obtained from Class II can serve as an initialization for the optimization process in Class I. However, within the context of this study, the division into four distinct classes seems both logical and practical, since there are substantial differences between these classes. The following section reviews previous research studies on the optimization of GWHP systems.

3.2.1 Current status of the approaches used for GWHP systems

Despite the increasing importance of GWHP optimization as a research area, the number of existing studies on this topic remains limited. Park et al. (2020) propose a simulation-based optimization approach to optimize pumping rates for a single GWHP system. The approach couples a numerical groundwater simulation model with a genetic optimization algorithm. Furthermore, the same approach was extended in Park et al. (2021) to optimize both well locations and pumping rates within a single system. Since the approach in these two studies uses a PDE simulation model along with a DFO algorithm, it falls under Class III of the proposed classification.

To date, only one research study has been identified that applies the approach of Class I, i.e. the PDECO framework. This study (Halilovic et al., 2022a) introduces a novel approach for concurrently optimizing the well locations of multiple neighboring systems. The approach was illustrated using a case study with ten systems, where the optimization objective is to minimize negative interactions between systems and maximize the overall efficiency of all systems. The proposed approach uses the adjoint method to efficiently compute gradients from the numerical simulation model, which are required by the optimization algorithm.

There is also only one research study that implements the approach belonging to Class II. In Halilovic et al. (2023), the authors introduce an approach that integrates an analytical groundwater simulation model directly into the optimization problem. Specifically, the analytical model used to calculate thermal plumes is the LAHM model (Kinzelbach, 1992) and the resulting optimization problem is formulated as an MILP problem. The study applies this approach to optimize the locations of systems and their associated wells within an urban area comprising 56 potential systems. The objective is to satisfy relevant regulations while maximizing heat extraction from the aquifer. An open-source implementation of the proposed approach can be accessed at Halilovic and Böttcher (2022).

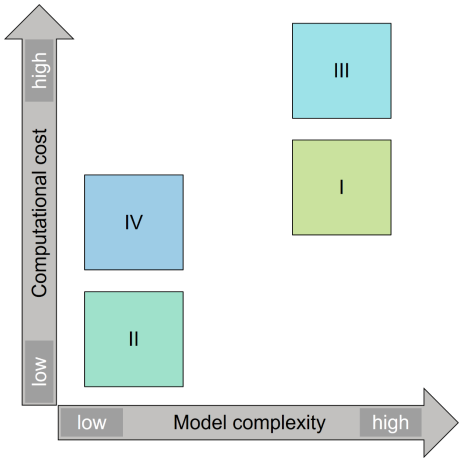

Figure 3. Qualitative comparison of the optimization approaches.

No research studies have been identified that apply the approach of Class IV, which involves the combination of simplified models with DFO algorithms. It should be noted that other studies on GWHP optimization exist, focusing on aspects such as optimizing the components of a heat pump or determining optimal control strategies. However, these studies do not consider underground processes and are therefore outside the scope of this work. Furthermore, there are other research studies (e.g. Zhou and Zhou, 2009; Lo Russo and Civita, 2009; Gao et al., 2013) that address the optimal design or operation of GWHPs using methods such as scenario comparison or sensitivity analysis. However, these methods are not optimization methods, and as such, they are not further discussed in the present study. In the subsequent section, a comparative analysis is conducted between optimization approaches, i.e. the identified four classes.

3.2.2 Comparison of the optimization approaches

The primary factors for comparing optimization approaches, i.e. their respective classes, are the computational cost and applicability criteria. Figure 3 shows a qualitative comparison of these classes, considering two dimensions. The vertical axis represents the computational cost required to solve optimization problems with the approaches of the respective class. The computational cost of an approach is of major importance, since in practical planning procedures a relatively fast solution is required. Moreover, the computational cost increases proportionally with the number of optimization parameters (variables) and the size of the simulation domain. Consequently, approaches with high computational costs are limited to scenarios with a small number of optimization parameters and small domains. As the number of optimization parameters increases, inefficient approaches quickly become computationally impractical, even when using high-performance computers.

The horizontal axis represents the complexity (fidelity) of the groundwater simulation model used in these approaches. In the context of this study, the complexity of a simulation model refers to the level of detail in representing physical phenomena in the subsurface, such as the propagation of thermal plumes, that are relevant to the optimization problem under consideration. Assuming that the required input data, such as groundwater parameters, are available in sufficient quality, more complex simulation models are more accurate, i.e. closer to reality. However, it is important to recognize that data on groundwater parameters and conditions are often limited, which limits the use of complex models. Model complexity is essentially limited by the available data, making the use of highly complex models impractical in the absence of the necessary data. Nevertheless, simpler PDE simulation models, such as a 2D model with uniform groundwater conditions, are applicable even with restricted data availability and generally offer higher accuracy than analytical models with identical input data. Since simulation models are an integral component of optimization approaches, their complexity directly affects the applicability of the obtained optimization results. For instance, the results of an approach that uses a complex groundwater simulation model provided with high-quality data can be applied in practice with greater confidence than the results of an approach based on less accurate models.

In the context of computational costs, two key aspects deserve attention: the convergence rate and the computational cost associated with the evaluation of each candidate solution (a unique combination of optimization variables). The former quantifies the number of optimization iterations required to reach the optimal solution, while the latter describes the runtime required for each model simulation used to evaluate the current candidate solution within the optimization iterations. In general, gradient-based algorithms significantly outperform derivative-free algorithms in terms of convergence rate and therefore it is recommended to use gradient-based algorithms when gradient information is readily available and can be obtained at a reasonable cost (Audet and Hare, 2017; Conn et al., 2009). As a result, Class II will almost always outperform Class IV, and Class I will outperform Class III, due to the use of gradient-based algorithms in the former classes (I and II) and derivative-free algorithms in the latter classes (III and IV). Another disadvantage of Classes III and IV is that derivative-free algorithms generally only find near-optimal solutions and do not guarantee optimality (Audet and Hare, 2017). Furthermore, classes that use simplified simulation models (II and IV) commonly have lower computational costs than classes that use PDE models (I and III). This is a direct consequence of the computational costs associated with evaluating the simulation model during optimization iterations. Considering all of the above, a hierarchy of classes based on overall computational cost can be established. Class II entails the least computational cost, while Class III is the most computationally demanding. Classes I

and IV fall somewhere in between, with Class IV usually outperforming Class I, although the specific problem characteristics (number of optimization variables, size of the simulation domain, etc.) can also influence this comparative performance. Despite the computationally demanding nature of Class III, this class is frequently used in the simulation community owing to its user-friendly nature. By coupling standard standalone simulation software with an existing implementation of a DFO algorithm, typically an evolutionary algorithm, users can develop and apply such approaches relatively quickly.

In terms of the complexity/fidelity of the simulation model used in optimization approaches, it is evident that the classes employing PDE models (I and III) outperform those employing simplified models (II and IV). The complexity of the simulation model directly influences the validity of the optimization results, thereby affecting the applicability of the corresponding classes. Consequently, it is reasonable to use approaches from different classes for different application scenarios. For instance, the classes with more complex models (I and III) are suitable for detailed planning of large GWHP systems, while the other two classes (II and IV) can be applied for initial assessments of potential negative interactions between neighboring systems or estimations of geothermal potential on a larger scale.

4 Discussion and outlook

While there are a limited number of research studies (see Sect. 3.2.1) that address the optimization of GWHP systems, the research area remains insufficiently explored, which provides an opportunity to pose new research questions and develop novel optimization approaches. The existing approaches in this field have certain limitations and do not cover all relevant applications. For example, the approach of Class III presented in Park et al. (2020, 2021) is limited by the number of optimization variables it can efficiently handle, since the computational cost increases exponentially as the number of variables increases. Similarly, the only study (Halilovic et al., 2022a) using the approach of Class I does not cover all relevant aspects of GWHP optimization, such as optimizing the number of wells in a large GWHP system, optimizing pumping rates, or simultaneously optimizing pumping rates and well locations.

Class I (PDECO) seems to be the most promising among the four classes because it uses PDE simulation models and has lower computational costs compared to Class III. Here, the complexity level of the PDE model can be selected based on data availability, as discussed in Sect. 3.2.2. However, this class presents significant challenges due to its mathematical complexity and multidisciplinary nature. To overcome the challenges associated with developing new approaches within Class I and facilitate their further advancement, collaboration within multidisciplinary teams will be required in the future.

The limitations of the classes that use simplified simulation models (Class II and IV) are directly related to the limitations of the simulation models employed. Consequently, improving the simplified simulation models directly enhances the approaches within these classes. The main goal is to maintain the simulation models as fast and simple to evaluate while enhancing their closeness to reality. By further improving the accuracy of these simplified models, their scope can be extended to new applications, such as detailed design of large GWHP systems comprising multiple extraction and injection wells. Moreover, the simplified models are well-suited for integration into energy system optimization models (ESOMs), where GWHP systems play an important role (Halilovic et al., 2022c). This is because the coupling of a numerical groundwater simulation with an ESOM is impractical and computationally demanding (Halilovic et al., 2022b). By using simplified models, the computational cost can be significantly reduced while still capturing the essential aspects of GWHP systems in the broader context of energy system optimization. This further enables the development of automated urban planning tools, which will increase sustainability.

Another important consideration in GWHP optimization is the inherent uncertainty associated with subsurface parameters and conditions. The complex nature of aquifers and the limited availability of measurement and monitoring data contribute to the presence of uncertainties (Gelhar et al., 1992). Incorporating these uncertainties into optimization approaches leads to stochastic programming problems (Birge and Louveaux, 2011), which constitute a separate field of optimization. The inherent stochastic nature of these problems significantly increases the complexity and computational cost compared to deterministic problems. Stochastic problems are often solved with modified deterministic optimization approaches or by using a deterministic equivalent of the stochastic problem (Hannah, 2015; Li and Grossmann, 2021). By minimizing the computational cost of deterministic optimization approaches, researchers can better address the challenges of stochastic problems and develop efficient approaches to such problems. Therefore, it is crucial for the deterministic optimization approaches discussed in this study to reduce their computational cost. Several strategies can be employed to reduce the computational cost of the existing approaches. For instance, the Class III approach (Park et al., 2020) may improve its efficiency by using model-based algorithms instead of a genetic algorithm. Similarly, the Class I approach (Halilovic et al., 2022a) can improve its efficiency by using suitable (re)meshing techniques or by fine-tuning optimization algorithm parameters.

It is important to note that the classification and comparison of optimization approaches presented in Sect. 3.2 is not limited to the optimization of GWHP systems, but can be applied to any optimization problem where the underlying

physical phenomena are described by PDEs. Moreover, the approaches developed for GWHP systems (see Sect. 3.2.1) and their future advancements or new approaches in this area can be extended to other applications. First, they can be extended to applications that share the same underlying physics, such as optimization of aquifer thermal energy storage (ATES) systems, calibration of numerical hydro-thermal groundwater simulation models, and optimization of observation well placement. Second, these approaches can be extended to other areas of shallow geothermal energy, including optimization of vertical and horizontal closed-loop shallow geothermal systems and optimization of borehole thermal energy storage (BTES) systems. Lastly, these approaches can be further extended to areas involving different physical phenomena, such as the optimization of wind farms or tidal power plants. Nevertheless, it is important to note that advances in these other areas, particularly in the area of shallow geothermal energy, can reciprocally contribute to the improvement of optimization approaches for GWHP systems. Namely, optimization approaches and principles used in other areas have the potential to be adapted and applied to GWHP systems.

5 Conclusions

This paper presents a comprehensive analysis and overview of approaches for optimizing the design and operation of GWHP systems. First, the optimization problems arising from this research and practice question were investigated, using a generalized problem as a basis. Then, optimization approaches were identified and compared, and a novel classification of the approaches is proposed. The identified approaches were divided into four distinct classes based on the type of groundwater simulation model used (PDE-based or simplified models) and the optimization algorithm applied (gradient-based or derivative-free). Finally, the paper includes a thorough review of the existing approaches in the literature, highlighting their limitations and outlining opportunities for future improvements.

Based on the analysis performed, several conclusions can be drawn:

- Optimization approaches that rely on gradient-based optimization algorithms are preferable, as they consistently outperform derivative-free algorithms.
- The choice of a simulation model used in an optimization approach has a significant impact on its applicability. For example, approaches using PDE models are more suitable for detailed design of large-scale GWHPs, while simplified models offer practical advantages for assessing the geothermal potential of large areas. However, it is important to note that the degree of model complexity is limited by the availability of hydrogeological data.
- The existing research on GWHP optimization is limited, with only a few studies addressing this topic.
- Existing approaches have certain limitations and do not cover all relevant applications and research questions in GWHP optimization. One of the main limitations is the high computational cost, which limits the number of optimization parameters and the size of the simulation domain that can be effectively considered. In addition, some approaches are limited in applicability due to the use of simplified groundwater simulation models. Moreover, applications such as optimizing the number and placement of wells in large GWHP systems or simultaneous optimization of pumping rates and well placements remain unexplored. Consequently, there is an ongoing need to develop new and improve existing approaches to address these limitations and fill the research gaps.
- The efficient optimization approaches developed for GWHP systems have the potential to be extended to other shallow geothermal applications as well as to other optimization problems where the underlying physical phenomena are described by PDEs. At the same time, approaches from other areas can be adapted and used for GWHP optimization in the future.

Finally, this study can provide a valuable foundation for researchers and practitioners involved in the management and optimization of shallow geothermal energy systems. In particular, it provides valuable insights and recommendations for the application and development of optimization approaches for GWHP systems. Despite its challenging nature, optimization of GWHP systems is of utmost importance to improve thermal management of groundwater and to unlock the full potential and attractiveness of GWHP technology.

Data availability. No data sets were used in this article.

Author contributions. SH: Conceptualization, Writing – original draft, Methodology, Investigation, Visualization. FB: Writing – reviewing and editing. KZ: Writing – reviewing and editing. TH: Writing – reviewing and editing, Supervision.

Competing interests. The contact author has declared that none of the authors has any competing interests.

Disclaimer. Publisher's note: Copernicus Publications remains neutral with regard to jurisdictional claims made in the text, published maps, institutional affiliations, or any other geographical representation in this paper. While Copernicus Publications makes every effort to include appropriate place names, the final responsibility lies with the authors.

Special issue statement. This article is part of the special issue "European Geosciences Union General Assembly 2023, EGU Division Energy, Resources & Environment (ERE)". It is a result of the EGU General Assembly 2023, Vienna, Austria, 23–28 April 2023.

Acknowledgements. No external funding was received for conducting this study. We would like to thank Jannis Epting for reviewing the paper and providing valuable comments that improved its quality.

Financial support. This work was supported by the Technical University of Munich (TUM) in the framework of the Open Access Publishing Program.

Review statement. This paper was edited by Michael Kühn and Giorgia Stasi, and reviewed by Jannis Epting and one anonymous referee.

References

Audet, C. and Hare, W.: Derivative-free and black-box optimization, Springer, ISBN 978-3-319-68913-5, https://doi.org/10.1007/978-3-319-68913-5, 2017.

Birge, J. R. and Louveaux, F.: Introduction to stochastic programming, Springer Science & Business Media, ISBN 978-1-4614-0237-4, https://doi.org/10.1007/978-1-4614-0237-4, 2011.

Blum, P., Menberg, K., Koch, F., Benz, S. A., Tissen, C., Hemmerle, H., and Bayer, P.: Is thermal use of groundwater a pollution?, J. Contam. Hydrol., 239, 103791, https://doi.org/10.1016/j.jconhyd.2021.103791, 2021.

Bonnans, J.-F., Gilbert, J. C., Lemaréchal, C., and Sagastizábal, C. A.: Numerical optimization: theoretical and practical aspects, Springer Science & Business Media, ISBN 978-3-540-35447-5, https://doi.org/10.1007/978-3-540-35447-5, 2006.

Böttcher, F. and Zosseder, K.: Thermal influences on groundwater in urban environments – A multivariate statistical analysis of the subsurface heat island effect in Munich, Sci. Total Environ., 810, 152193, https://doi.org/10.1016/j.scitotenv.2021.152193, 2021.

Böttcher, F., Casasso, A., Götzl, G., and Zosseder, K.: TAP – Thermal aquifer Potential: A quantitative method to assess the spatial potential for the thermal use of groundwater, Renew. Energy, 142, 85–95, https://doi.org/10.1016/j.renene.2019.04.086, 2019.

Bozorg-Haddad, O., Solgi, M., and Loáiciga, H. A.: Meta-heuristic and evolutionary algorithms for engineering optimization, John Wiley & Sons, ISBN 978-1-119-38705-3, 2017.

Conn, A. R., Gould, N. I., and Toint, P. L.: Trust region methods, SIAM, ISBN 978-0-89871-460-9, 2000.

Conn, A. R., Scheinberg, K., and Vicente, L. N.: Introduction to derivative-free optimization, SIAM, ISBN 978-0-89871-668-9, 2009.

Davis, K., Leiteritz, R., Pflüger, D., and Schulte, M.: Deep learning based surrogate modeling for thermal plume prediction of groundwater heat pumps, arXiv [preprint], arXiv:2302.08199, https://doi.org/10.48550/arXiv.2302.08199, 2023.

Diersch, H.-J. G.: FEFLOW, Springer, Berlin, Heidelberg, ISBN 978-3-642-38738-8, https://doi.org/10.1007/978-3-642-38739-5, 2014.

Epting, J. and Huggenberger, P.: Unraveling the heat island effect observed in urban groundwater bodies – Definition of a potential natural state, J. Hydrol., 501, 193–204, https://doi.org/10.1016/j.jhydrol.2013.08.002, 2013.

Epting, J., Böttcher, F., Mueller, M. H., García-Gil, A., Zosseder, K., and Huggenberger, P.: City-scale solutions for the energy use of shallow urban subsurface resources – Bridging the gap between theoretical and technical potentials, Renew. Energy, 147, 751–763, https://doi.org/10.1016/j.renene.2019.09.021, 2020.

Florides, G. and Kalogirou, S.: Ground heat exchangers – A review of systems,models and applications, Renew. Energy, 32, 2461–2478, https://doi.org/10.1016/j.renene.2006.12.014, 2007.

Gao, Q., Zhou, X.-Z., Jiang, Y., Chen, X.-L., and Yan, Y.-Y.: Numerical simulation of the thermal interaction between pumping and injecting well groups, Appl. Therm. Eng., 51, 10–19, https://doi.org/10.1016/j.applthermaleng.2012.09.017, 2013.

García-Gil, A., Mejías Moreno, M., Garrido Schneider, E., Marazuela, M. Á., Abesser, C., Mateo Lázaro, J., and Sánchez Navarro, J. Á.: Nested Shallow Geothermal Systems, Sustainability, 12, 5152, https://doi.org/10.3390/su12125152, 2020.

García Gil, A., Garrido Schneider, E. A., Mejías Moreno, M., and Santamarta Cerezal, J. C.: Shallow Geothermal Energy, Springer, https://doi.org/10.1007/978-3-030-92258-0, 2022.

Gelhar, L. W., Welty, C., and Rehfeldt, K. R.: A Critical Review of Data on Field-Scale Dispersion in Aquifers, Water Resour. Res., 28, 1955–1974, https://doi.org/10.1029/92WR00607, 1992.

Guimerà, J., Ortuño, F., Ruiz, E., Delos, A., and Pérez-Paricio, A.: Influence of ground-source heat pumps on groundwater, in: Conference Proceedings: European Geothermal Congress, 30 May–1 June 2007, Unterhaching, Germany, https://www.geothermal-energy.org/pdf/IGAstandard/EGC/2007/250.pdf (last access: 18 December 2023), 2007.

Hähnlein, S., Molina-Giraldo, N., Blum, P., Bayer, P., and Grathwohl, P.: Ausbreitung von Kältefahnen im Grundwasser bei Erdwärmesonden, Grundwasser, 15, 123–133, https://doi.org/10.1007/s00767-009-0125-x, 2010.

Halilovic, S. and Böttcher, F.: Optimization of GWHP well layouts using analytic models, Zenodo [code], https://doi.org/10.5281/zenodo.7230875, 2022.

Halilovic, S., Böttcher, F., Kramer, S. C., Piggott, M. D., Zosseder, K., and Hamacher, T.: Well layout optimization for groundwater heat pump systems using the adjoint approach, Energ. Convers. and Manag., 268, 116033, https://doi.org/10.1016/j.enconman.2022.116033, 2022a.

Halilovic, S., Odersky, L., Böttcher, F., Davis, K., Schulte, M., Zosseder, K., and Hamacher, T.: Optimization of an Energy System Model Coupled with a Numerical Hydrothermal Groundwater Simulation, in: Mapping the Energy Future – Voyage in Uncharted Territory, 43rd IAEE International Conference, 31 July–3 August 2022, International Association for Energy Economics, http://www.iaee.org/proceedings/article/17725 (last access: 18 December 2023), 2022b.

Halilovic, S., Odersky, L., and Hamacher, T.: Integration of groundwater heat pumps into energy sys-

tem optimization models, Energy, 238, 121607, https://doi.org/10.1016/j.energy.2021.121607, 2022c.

Halilovic, S., Böttcher, F., Zosseder, K., and Hamacher, T.: Optimizing the spatial arrangement of groundwater heat pumps and their well locations, Renew. Energy, 217, 119148, https://doi.org/10.1016/j.renene.2023.119148, 2023.

Hammond, G., Lichtner, P., Lu, C., and Mills, R. T.: PFLOTRAN: Reactive flow & transport code for use on laptops to leadership-class supercomputers, Groundwater React. Trans. Models, 5, 141–159, 2012.

Hannah, L. A.: Stochastic optimization, Int. Encycloped. Social Behav. Sci., 2, 473–481, 2015.

Hinze, M., Pinnau, R., Ulbrich, M., and Ulbrich, S.: Optimization with PDE constraints, in: vol. 23, Springer Science & Business Media, ISBN 978-1-4020-8839-1, https://doi.org/10.1007/978-1-4020-8839-1, 2008.

Kim, J. and Nam, Y.: A Numerical Study on System Performance of Groundwater Heat Pumps, Energies, 9, 4, https://doi.org/10.3390/en9010004, 2016.

Kinzelbach, W.: Numerische Methoden zur Modellierung des Transports von Schadstoffen im Grundwasser, Oldenbourg, ISBN 9783486263473, 1992.

Le Digabel, S.: Algorithm 909: NOMAD: Nonlinear optimization with the MADS algorithm, ACM Trans. Math. Softw., 37, 1–15, https://doi.org/10.1145/1916461.1916468, 2011.

Leiteritz, R., Davis, K., Schulte, M., and Pflüger, D.: A Deep Learning Approach for Thermal Plume Prediction of Groundwater Heat Pumps, arXiv [preprint], arXiv:2203.14961, https://doi.org/10.48550/arXiv.2203.14961, 2022.

Li, C. and Grossmann, I. E.: A review of stochastic programming methods for optimization of process systems under uncertainty, Front. Chem. Eng., 2, 34, https://doi.org/10.3389/fceng.2020.622241, 2021.

Logg, A., Mardal, K., and Wells, G. N.: Automated Solution of Differential Equations by the Finite Element Method, Springer, https://doi.org/10.1007/978-3-642-23099-8, 2012.

Lo Russo, S. and Civita, M. V.: Open-loop groundwater heat pumps development for large buildings: A case study, Geothermics, 38, 335–345, https://doi.org/10.1016/j.geothermics.2008.12.009, 2009.

Marler, R. T. and Arora, J. S.: The weighted sum method for multi-objective optimization: new insights, Struct. Multidiscip. Optimiz., 41, 853–862, https://doi.org/10.1007/s00158-009-0460-7, 2010.

Menberg, K., Bayer, P., Zosseder, K., Rumohr, S., and Blum, P.: Subsurface urban heat islands in German cities, Sci. Total Environ., 442, 123–133, https://doi.org/10.1016/j.scitotenv.2012.10.043, 2013.

Naumann, U.: The Art of Differentiating Computer Programs, Society for Industrial and Applied Mathematics, https://doi.org/10.1137/1.9781611972078, 2011.

Nocedal, J. and Wright, S. J.: Numerical optimization, Springer, ISBN 978-0-387-22742-9, https://doi.org/10.1007/b98874, 1999.

Ohmer, M., Klester, A., Kissinger, A., Mirbach, S., Class, H., Schneider, M., Lindenlaub, M., Bauer, M., Liesch, T., Menberg, K., and Blum, P.: Berechnung von Temperaturfahnen im Grundwasser mit analytischen und numerischen Modellen, Grundwasser, 27, 113–129, https://doi.org/10.1007/s00767-022-00509-2, 2022.

Park, D., Lee, E., Kaown, D., Lee, S.-S., and Lee, K.-K.: Determination of optimal well locations and pumping/injection rates for groundwater heat pump system, Geothermics, 92, 102050, https://doi.org/10.1016/j.geothermics.2021.102050, 2021.

Park, D. K., Kaown, D., and Lee, K.-K.: Development of a simulation-optimization model for sustainable operation of groundwater heat pump system, Renew. Energy, 145, 585–595, https://doi.org/10.1016/j.renene.2019.06.039, 2020.

Perego, R., Dalla Santa, G., Galgaro, A., and Pera, S.: Intensive thermal exploitation from closed and open shallow geothermal systems at urban scale: unmanaged conflicts and potential synergies, Geothermics, 103, 102417, https://doi.org/10.1016/j.geothermics.2022.102417, 2022.

Pophillat, W., Attard, G., Bayer, P., Hecht-Méndez, J., and Blum, P.: Analytical solutions for predicting thermal plumes of groundwater heat pump systems, Renew. Energy, 147, 2696–2707, https://doi.org/10.1016/j.renene.2018.07.148, 2020.

Raissi, M., Perdikaris, P., and Karniadakis, G. E.: Physics Informed Deep Learning (Part I): Data-driven Solutions of Nonlinear Partial Differential Equations, arXiv [preprint], arXiv:1711.10561, https://doi.org/10.48550/arXiv.1711.10561, 2017.

Rathgeber, F., Ham, D. A., Mitchell, L., Lange, M., Luporini, F., Mcrae, A. T. T., Bercea, G.-T., Markall, G. R., and Kelly, P. H. J.: Firedrake, ACM Trans. Math. Softw., 43, 1–27, https://doi.org/10.1145/2998441, 2017.

Russo, S. L., Taddia, G., and Verda, V.: Development of the thermally affected zone (TAZ) around a groundwater heat pump (GWHP) system: A sensitivity analysis, Geothermics, 43, 66–74, https://doi.org/10.1016/j.geothermics.2012.02.001, 2012.

Russo, S. L., Taddia, G., Gnavi, L., and Verda, V.: Neural network approach to prediction of temperatures around groundwater heat pump systems, Hydrogeol. J., 22, 205–216, https://doi.org/10.1007/s10040-013-1072-2, 2014.

Schrijver, A.: Theory of linear and integer programming, John Wiley & Sons, ISBN 978-0-471-98232-6, 1998.

Stauffer, F., Bayer, P., Blum, P., Giraldo, N. M., and Kinzelbach, W.: Thermal use of shallow groundwater, CRC Press, Boca Raton, Florida, ISBN 9781466560192, 2014.

Tröltzsch, F.: Optimal control of partial differential equations: theory, methods, and applications, in: Graduate Studies in Mathematics, Band 112, American Mathematical Society, ISBN 978-0821849040, 2010.

Zhou, Y.-z. and Zhou, Z.-f.: Simulation of Thermal Transport in Aquifer: A GWHP System in Chengdu, China, J. Hydrodynam., 21, 647–657, https://doi.org/10.1016/S1001-6058(08)60196-1, 2009.

4.2 Optimization using analytical models

As discussed in the previous section, the incorporation of groundwater-related factors, which include groundwater conditions and interactions between GWHP systems and groundwater, into an optimization framework can be achieved either through the use of numerical PDE models or simplified models. This section is dedicated to the latter case and focuses on optimization approaches that use analytical models to describe groundwater conditions. In this context, the section includes **Publications 3** [95] **and 4** [33], which present two new optimization approaches, referred to as Approach I and Approach II, respectively. These approaches belong to Class II within the classification taxonomy introduced in Section 4.1, as shown in Figure 4.1.

Approach I represents a novel methodological framework developed for optimizing the spatial arrangement of GWHP systems and associated wells within a designated area. The optimization objective is to maximize the thermal potential of groundwater, i.e. the heat extracted from the aquifer, while complying with a set of technical and regulatory constraints. These constraints include spatial limitations, such as the minimum prescribed spacing between wells within the same GWHP system, and regulations to avoid negative thermal interactions between neighboring systems. The inclusion of the latter consideration in the optimization process is based on an analytical model for simulating thermal plumes in groundwater. This model is an extended version of the original linear advective heat transport (LAHM) model [96].

Approach II is another developed methodological framework for comprehensive optimization of GWHP systems. In this approach, the scope of optimization is extended beyond the spatial arrangement of wells to include the sizing of extraction-injection well doublets, i.e. the pumping rates of wells. That is, Approach II treats pumping rates as optimization variables, in contrast to Approach I, which uses predefined pumping rates based on heating demand estimates. The optimization objective of Approach II is to maximize the technical potential of thermal groundwater use within the designated area. This objective translates into maximizing the total amount of groundwater extracted from the area.

While Approach I focuses primarily on thermal groundwater aspects that include thermal interactions between neighboring systems, Approach II focuses on hydraulic groundwater considerations. Consequently, the constraints in Approach II include technical and regulatory conditions associated with the hydraulic aspects of GWHP operation, such as restrictions on groundwater drawdown in extraction wells and groundwater level rise in injection wells. Furthermore, the available space for GWHP installations is limited primarily by the propagation of thermal plumes in Approach I and by the hydraulic footprint of GWHP wells in Approach II. In the latter, hydraulic considerations are integrated into the optimization process by using analytical expressions derived from the thermal aquifer potential (TAP) method [45].

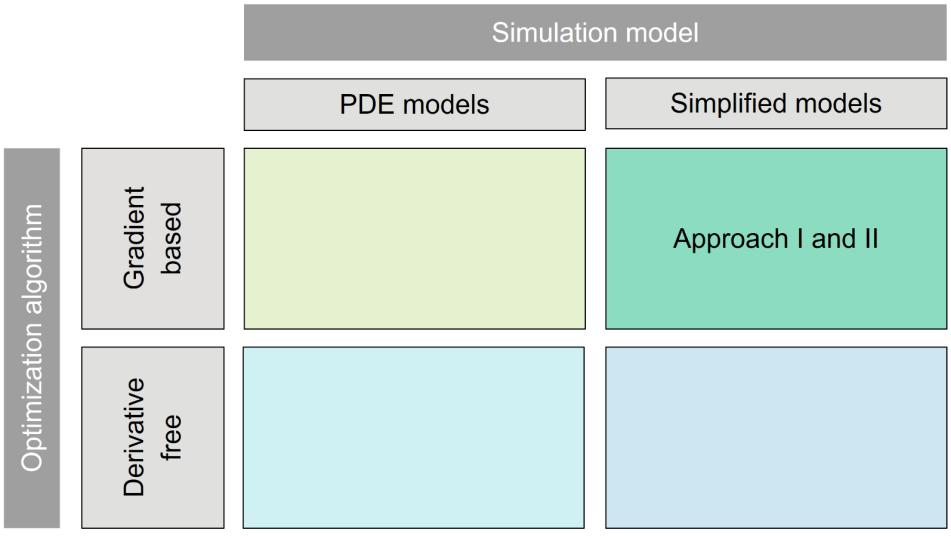

Figure 4.1 Approaches I and II in the classification scheme from Section 4.1

Both optimization approaches have been successfully demonstrated using real case studies involving areas within the city of Munich. The approaches can be used in various applications, such as active thermal

groundwater management, assessment of shallow geothermal potential, or strategic planning of 4th and 5th generation district heating systems. To support their practical usage, implementations (source code) of the approaches along with working examples are made openly available at [97] and [98] for Approach I and II, respectively. Approach I has already been integrated into practical applications by the Department of Climate and Environmental Protection (RKU) of the City of Munich in two ways: (1) using the extended LAHM model from Publication 3 within a GIS-based tool [99] for monitoring and licensing of GWHP installations, and (2) for assessing the city-wide thermal potential of groundwater, in particular for the preparation of the city's shallow geothermal potential map.

Publication 3 - Optimizing the spatial arrangement of groundwater heat pumps and their well locations

Authors: Smajil Halilović, Fabian Böttcher, Kai Zosseder, Thomas Hamacher

Journal: Renewable Energy (Elsevier)

Status: Published - November 2023

Digital object identifier: https://doi.org/10.1016/j.renene.2023.119148

Source code: https://github.com/SHalilovic/GWHP-analytic-optimization

Author	Contribution
Smajil Halilović	Conceptualization, Methodology, Writing – original draft, Software, Investigation, Visualization
Fabian Böttcher	Conceptualization, Writing – original draft, Data curation, Visualization
Kai Zosseder	Funding acquisition, Writing - reviewing and editing
Thomas Hamacher	Funding acquisition, Supervision

Renewable Energy 217 (2023) 119148

Contents lists available at ScienceDirect

Renewable Energy

journal homepage: www.elsevier.com/locate/renene

Optimizing the spatial arrangement of groundwater heat pumps and their well locations

Smajil Halilovic [a,*], Fabian Böttcher [b], Kai Zosseder [b], Thomas Hamacher [a]

[a] Chair of Renewable and Sustainable Energy Systems, Technical University of Munich, Lichtenbergstr. 4a, 85748 Garching, Germany
[b] Chair of Hydrogeology, Technical University of Munich, Arcisstr. 21, 80333 Munich, Germany

ARTICLE INFO

Keywords:
Optimization
Well layout
Heat pump
Groundwater
Geothermal potential

ABSTRACT

Increasing numbers of groundwater heat pump systems in urban areas can lead to negative thermal interference between neighboring systems. These systems and their associated wells can be optimally positioned so as to minimize such interactions and maximize the use of the shallow geothermal potential. This paper presents a new method that determines the optimal positioning of groundwater heat pumps and their wells by concurrently considering relevant technical and regulatory constraints. The method is based on an improved analytical model for estimating thermal anomalies in groundwater, i.e. thermal plumes, and integer linear programming optimization. The method is tested using a neighborhood with 56 parcels, i.e. potential systems, in two optimization cases: steady and dynamic. In both cases, the method successfully determines both the systems to be installed and the optimal locations of the wells such that relevant spatial regulations are satisfied and the energy extracted from the aquifer is maximized. The dynamic case is somewhat more restrictive, as 43 of 56 potential systems are installed, compared to 44 in the steady case. This method represents a significant improvement over existing ones, since it is able to efficiently optimize the locations and well layouts of a large number of systems simultaneously.

1. Introduction

The heating and cooling sector in the European Union relies mainly on fossil fuels [1] and as such requires further decarbonization in order to achieve the CO_2 neutrality target by 2050 [2]. Shallow geothermal energy (SGE) systems are a highly promising technology that can be used to increase the share of renewable resources in this sector [3,4]. There are two types of SGE installation [5]: closed-loop systems or ground source heat pumps (GSHP) and open-loop systems or groundwater heat pumps (GWHP). In GSHP systems, a heat carrier fluid circulates in a closed loop and transfers the heat from the ground to the heat pump [6], while GWHP systems use groundwater directly to extract heat from an aquifer [7]. These systems pump groundwater from extraction wells and return it to the same aquifer at injection wells once the heat has been exchanged within the heat pump.

The efficiency of GWHPs is relatively high compared to other heating systems [8] and depends primarily on the temperature of the pumped groundwater [9]. The efficiency is particularly high in urban areas, where groundwater temperatures are elevated due to the subsurface urban heat island (SSUHI) effect [10–12]. This favors the further diffusion of the technology in cities [13,14]. However, an increased number of GWHP installations can lead to negative thermal interference between neighboring systems [15]. Such interference occurs when a thermal plume, i.e. thermally altered groundwater, from the injection well of an upstream system reaches the extraction well of a neighboring downstream system, which can significantly affect the efficiency and operation of the downstream system [16]. At the same time, it is important to maintain sufficient internal distance between the extraction and injection wells of the same system to prevent thermal breakthroughs [17]. Active resource management is required to avoid negative interference between GWHP systems and maximize the potential and sustainability of the shallow geothermal resource groundwater [18].

A potential assessment is required for quantifying the opportunities and limitations of GWHPs in the area of interest and also represents the first step in resource management. It is necessary to distinguish between the theoretical potential – the total amount of available energy – and the technical potential – the proportion of the total energy that can be used by GWHPs [19]. Numerous research studies have evaluated geothermal aquifer potentials in various locations around the world,

* Corresponding author.
E-mail address: smajil.halilovic@tum.de (S. Halilovic).

https://doi.org/10.1016/j.renene.2023.119148
Received 2 December 2022; Received in revised form 6 August 2023; Accepted 9 August 2023
Available online 11 August 2023

Nomenclature

Latin letters

B	Aquifer thickness [m]
COP	Coefficient of performance
C_{m}	Volumetric heat capacity of medium [J/m^3 K]
C_{w}	Volumetric heat capacity of water [J/m^3 K]
d_{ext}	Decision variables for extraction wells
d_{inj}	Decision variables for injection wells
E_{ext}	Heat extracted from groundwater [J]
M	Total number of time steps
m	Linearization parameter [–]
N	Number of injection wells
N_p	Number of parcels
P	Set of all parcels/plots
q	Pumping rates [m^3/s]
R	Retardation factor [–]
r	Radial distance factor [m]
T	Groundwater temperature [K]
t	Time [s]
ΔT	Groundwater temperature change/difference [K]
Δt	Time step length [s]
ΔT_{inj}	Difference between inlet and natural groundwater temperature [K]
ΔT_{max}	Maximum groundwater temperature change [K]
t_M	Final time [s]
T_{n}	Natural groundwater temperature [K]
v_a	Seepage velocity [m/s]
x, y	Coordinates of the observed point [m]
Δx	Spatial distance in x direction [m]
Δy	Spatial distance in y direction [m]

Greek letters

β_{L}	Longitudinal dispersivity [m]
β_{T}	Transverse dispersivity [m]
Δ_{min}	Regulatory minimum distance [m]
$\Delta_{i,j}$	Euclidean distance between points i and j [m]
ω	Response factor
θ	Continuous optimization variables
ε	Porosity [–]

Subscripts and superscripts

ext	Extraction
inj	Injection
max	Maximum
min	Minimum
j	Counter for extraction wells
k, i	Counters for injection wells
l	Counter for time steps
p	Counter for parcels

including Switzerland [20,21], Spain [22], Australia [23], Finland [24,25] and Germany [26]. When assessing the technical potential, most of these studies do not consider possible negative interferences between neighboring GWHPs. However, for a comprehensive estimate of technical potential, it is necessary to take such interferences into account, as they limit the space available for GWHP installations.

Several research studies have addressed the question of how to manage, i.e. prevent or minimize, negative thermal interferences between GWHPs. García-Gil et al. [27] propose a relaxation factor for new GWHP systems to improve the fairness and sustainability of thermal groundwater use. Attard et al. [28] introduce thermal protection perimeters around extraction wells of GWHPs to prevent negative interferences. García-Gil et al. [29] define a balanced sustainability index to quantify the sustainability of each GWHP, i.e. its potential to cause negative interferences. These studies focus on how to better manage the installation of individual systems, so as to reduce the probability of negative interference with other systems. However, to fully maximize the technical geothermal potential of a particular area, all associated GWHPs should be considered and optimized cooperatively.

GWHP systems, i.e. their extraction and injection wells, can be optimally placed to avoid or minimize any negative interference and thus maximize the technical potential. In addition, wells in a single system can be optimally positioned to prevent hydraulic [30] and thermal breakthroughs [17] within the system. However, there is only limited literature that considers the optimal placement of GWHP wells [31]. Existing research studies typically focus on single GWHPs and compare a few predefined well layouts based on numerical simulations: Zhou and Zhou [32], Gao et al. [33] and Lo Russo and Civita [34]. This leads to suboptimal well layouts, since the design possibilities are not as fully explored as they are with numerical optimization methods. To date, the only studies that use numerical optimization to determine optimal GWHP well layouts are the works of Park et al. [35] and Halilovic et al. [36]. In [35] the authors use a genetic optimization algorithm with numerical groundwater simulations to optimize the well positions and pumping rates of a single GWHP system. This approach is an extension of the method from Park et al. [37], in which only the pumping rates of an individual system are optimized. On the other hand, Halilovic et al. [36] use gradient-based optimization to simultaneously determine optimal well positions for multiple neighboring GWHP systems. The underlying approach is based on adjoints for the efficient calculation of gradients and numerical groundwater simulations. However, both of these approaches [35,36] have their limitations when it comes to optimizing GWHP well layouts. The first [35] is limited by the number of optimization variables, i.e. the number of wells being optimized, due to the use of genetic algorithms. These algorithms require a large number of evaluations, which in this case are computationally intensive numerical groundwater simulations. Therefore, this approach is not suitable for the simultaneous optimization of well positions of multiple neighboring GWHPs. The second approach [36] is not limited by the number of wells considered and can be applied to multiple systems. However, the limiting factor here is the size of the computational domain, since the method requires a refined finite element mesh in the areas where wells can be placed. Consequently, as the size of the domain (area under consideration) increases, the computational cost of each optimization iteration increases significantly. Moreover, both approaches [35,36] are not yet adapted for determining the optimal GWHPs that should be installed in a given area under certain conditions, for instance, without negative interference. Thus, existing methods are not suitable for maximizing the technical potential of large areas.

The main aim of this paper is to present a new optimization method that can overcome the identified limitations of existing methods. The new method can optimize well locations of a large number, e.g. 100, of GWHP systems simultaneously, i.e. it can minimize the negative interference between all systems. The method can also be used to determine the GWHPs to be installed and their well locations in a given area without any negative interference above a certain threshold, for instance 1 K. The proposed optimization method uses integer linear programming with an upgraded analytical model for estimating the thermal plumes caused by GWHPs. This structure makes the

new method significantly less computationally expensive than existing methods, and it can therefore be applied to large areas. To demonstrate its effectiveness, the method is used to maximize the technical potential of a real-world urban region in the city of Munich, Germany. The GWHPs to be installed are determined and their wells placed so as to prevent negative interference and maximize the heat extracted from the aquifer.

The paper is organized as follows. The proposed method and its implementation are described in Sections 2 and 3, respectively. The results are presented and discussed in Section 4, and a critical reflection and outlook are given in Section 5. Finally, conclusions are presented in Section 6.

2. Methodology

The overall methodology consists of two components: simulating the impacts of GWHP on groundwater temperatures (Section 2.1) and optimizing the GWHP well layouts (Section 2.2).

2.1. Analytical computation of the groundwater temperature field

Numerical models can be used to assess the impact of GWHPs by computing the resulting thermal plumes. These models are time consuming to build and computationally expensive to run [38]. Over the years, multiple analytical solutions have been developed to predict the thermal plumes caused by GWHP systems. Pophillat et al. [38] compared numerical simulations with three analytical models: radial heat transport, linear advective heat transport and planar advective heat transport. The authors concluded that the considered analytical solutions were sufficient for a first-instance assessment of potential thermal interferences between neighboring systems. In addition, analytical models are more suitable for optimization processes, since optimization usually requires numerous simulation runs, and analytical models are significantly less computationally expensive than numerical simulations. Due to the form of their equation, analytical models can also be directly integrated into optimization models, which speeds up the optimization process. Such integration is carried out in this paper, using the linear advective heat transport model as an analytical solution to predict the thermal plumes of GWHPs.

2.1.1. Linear advective heat transport model

The linear advective heat transport model (LAHM) is a 2D analytical model used for the licensing of smaller systems (<45,000 kWh per year) in the German state of Baden-Württemberg [39]. The model was originally introduced in [40] and describes the heat propagation from a single injection well considering background flow in a homogeneous aquifer. The LAHM is defined as follows [41]:

$$\Delta T(\Delta x, \Delta y, t) = \frac{q \cdot \Delta T_{\mathrm{inj}}}{4\varepsilon\, B\, v_a \sqrt{\pi \beta_{\mathrm{T}}}} \exp\!\left(\frac{\Delta x - r}{2\,\beta_{\mathrm{L}}}\right) \frac{1}{\sqrt{r}} \operatorname{erfc}\!\left(\frac{r - v_a t/R}{2\sqrt{v_a \beta_{\mathrm{L}} t/R}}\right), \tag{1}$$

$$r = \sqrt{\Delta x^2 + \Delta y^2 \frac{\beta_{\mathrm{L}}}{\beta_{\mathrm{T}}}}, \tag{2}$$

where: ΔT is the change in groundwater temperature caused by a GWHP, i.e. the difference between the actual groundwater temperature T and the natural (undisturbed) temperature T_{n}; $\Delta x = (x - x_k)$ and $\Delta y = (y - y_k)$ are the distances of the observed point (x, y) from the injection well (x_k, y_k) in x and y direction, respectively; t is the observation time, i.e. the time from the commencement of the groundwater (re)injection; q is the pumping rate of the injection well; ΔT_{inj} is the difference between the inlet temperature and the undisturbed groundwater temperature; ε is the porosity; B is the aquifer thickness; v_a is the seepage velocity; β_{T} and β_{L} are the transverse and longitudinal dispersivity, respectively; r is the radial distance factor; $R = C_{\mathrm{m}}/(\varepsilon \cdot C_{\mathrm{w}})$ is the retardation factor, where C_{m} and C_{w} are the volumetric heat capacities of the porous medium and water, respectively. It should be noted that (1) only applies to the coordinate system in which the x-axis is in the direction of the groundwater flow and the y-axis is perpendicular to the flow direction.

2.1.2. Spatial and temporal superposition

The LAHM in its original form (1) can only be used for a single injection well, which has a constant pumping rate over the entire observation period. Accordingly, the "original" LAHM cannot be used to estimate groundwater temperature differences caused by multiple wells or wells with pumping rates that vary over time. However, due to the linear relationship between ΔT and q in (1) and since energy is an additive and extensive variable [42], the model can be extended by applying superposition principles. A similar approach was used in the series of works [43–46] to extend analytical models used for estimating temperature fields around borehole heat exchangers.

The LAHM can be applied to multiple wells using spatial superposition as follows:

$$\Delta T_{x,y}(t, q_{k=1\ldots N}) = \sum_{k=1}^{N} \Delta T_k(x - x_k, y - y_k, t, q_k), \tag{3}$$

where $\Delta T_{x,y}$ is the total temperature change at the observed point (x, y) caused by all wells; ΔT_k is the temperature change at the observed point due to the well k located at (x_k, y_k) with pumping rate q_k; N is the number of wells. Fig. 1(a) illustrates the principle of spatial superposition in the case of two injection wells with the same constant pumping rates.

The LAHM can also be extended to the dynamic case, in which pumping rates vary over time, by applying temporal superposition. The variable pumping rate of a single well can be regarded as a series of pulses, i.e. subdivided into time steps with constant pumping rates, similar to the approach in [43]:

$$\Delta T(\Delta x, \Delta y, t, q_{l=1\ldots M}) = \sum_{l=1}^{M} \frac{(q_l - q_{l-1}) \cdot \Delta T_{\mathrm{inj}}}{4\varepsilon\, B\, v_a \sqrt{\pi \beta_{\mathrm{T}}}} \exp\!\left(\frac{\Delta x - r}{2\,\beta_{\mathrm{L}}}\right) \frac{1}{\sqrt{r}} \times \operatorname{erfc}\!\left(\frac{r - v_a(t_M - t_l)/R}{2\sqrt{v_a \beta_{\mathrm{L}}(t_M - t_l)/R}}\right), \tag{4}$$

where M is the total number of time steps; q_l is the constant pumping rate during the time step l which runs from t_{l-1} to t_l; $(t_M - t_l)$ is the time remaining until the final time t_M; $t_0 = 0$ and $q_0 = 0$. Fig. 1(b) shows the principle of temporal superposition, applied to a single well with a time-varying pumping rate.

The spatial and temporal superpositions described above can be combined with one another so that the LAHM is able to calculate the groundwater temperature anomalies caused by multiple wells whose pumping rates, i.e. the extracted energy, vary over time:

$$\Delta T_{x,y}(t, q_{1\ldots N, 1\ldots M}) = \sum_{l=1}^{M} \sum_{k=1}^{N} q_{k,l}\, \omega_{k,l}^{t,x,y}(x - x_k, y - y_k), \tag{5}$$

with:

$$\omega_{k,l}^{t,x,y}(x - x_k, y - y_k) = \frac{\Delta T_{\mathrm{inj}}}{4\varepsilon\, B\, v_a \sqrt{\pi \beta_{\mathrm{T}}}} \exp\!\left(\frac{\Delta x - r}{2\,\beta_{\mathrm{L}}}\right) \frac{1}{\sqrt{r}} \times \left[\operatorname{erfc}\!\left(\frac{r - v_a(t - t_{l-1})/R}{2\sqrt{v_a \beta_{\mathrm{L}}(t - t_{l-1})/R}}\right) - \operatorname{erfc}\!\left(\frac{r - v_a(t - t_l)/R}{2\sqrt{v_a \beta_{\mathrm{L}}(t - t_l)/R}}\right)\right], \tag{6}$$

where $\omega_{k,l}^{t,x,y}$ is the response factor of the well k at the observed point (x, y) at time step $l \in \{1, \ldots, M\}$ with reference to the current time step $t \in \{1, \ldots, M\}$ and $l \le t$; $q_{k,l}$ is the constant pumping rate of the well k during the time step l, and the other parameters are the same as previously defined. Fig. 1(c) shows the combined superposition in the case of two wells with time-dependent pumping rates.

2.2. Optimization

The main optimization goal is to maximize the spatial thermal aquifer potential, i.e. to place those GWHPs that are able to extract the maximum energy in a given region such that there is no negative interference between them in terms of the defined regulations. The optimized placement of GWHPs and their wells is based on the selection of predefined (potential) well locations.

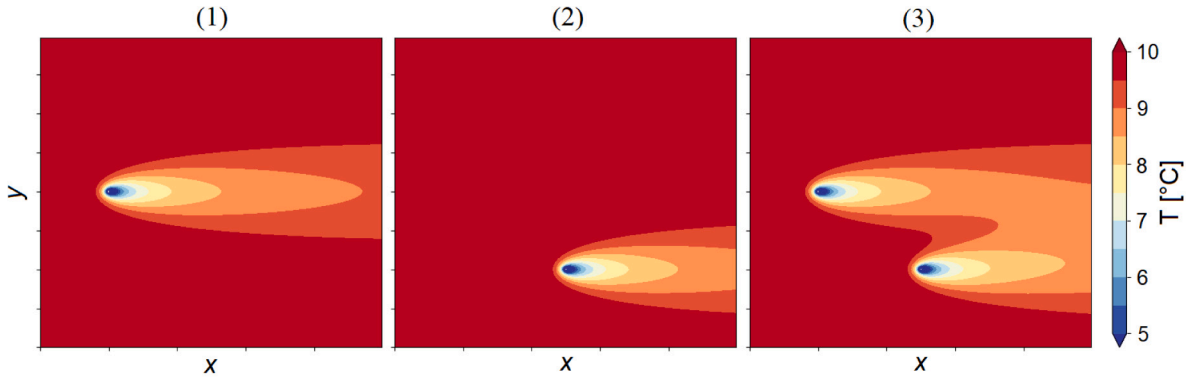

(a) Spatial superposition

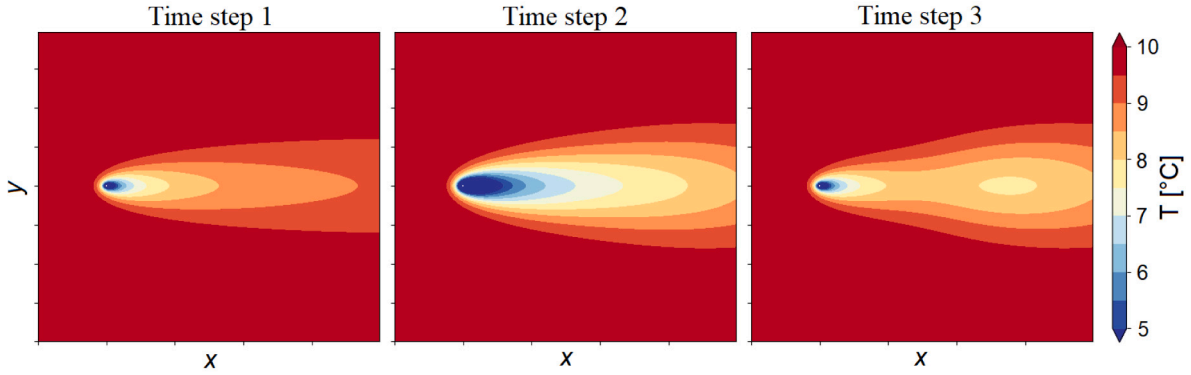

(b) Temporal superposition

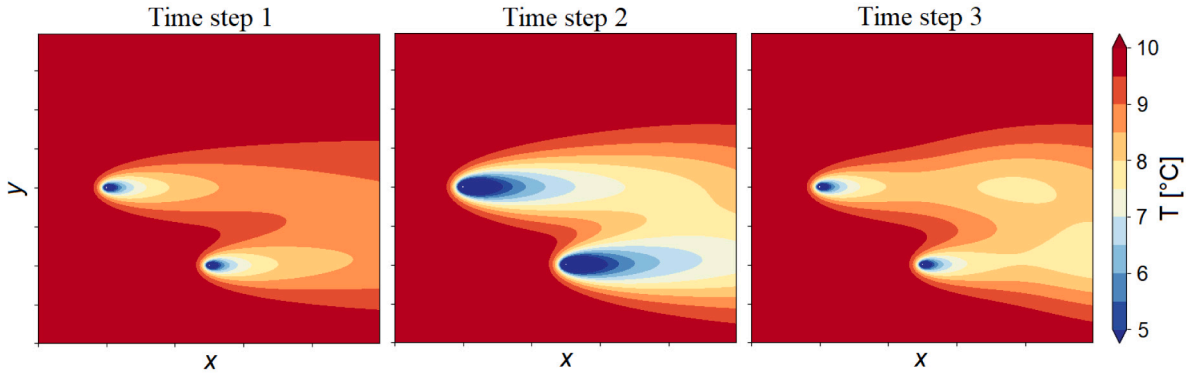

(c) Combined superposition

Fig. 1. Superposition principles: (a) Spatial superposition: (1) and (2) Individual temperature fields obtained for each well independently with the LAHM. (3) Resulting temperature field when both wells are in operation, obtained with spatial superposition. (b) Temporal superposition: Temporal evolution of the temperature field, i.e. groundwater temperatures after each of three time steps. The well has double the pumping rate in the second time step compared to the first and third time steps. (c) Spatial and temporal superpositions combined: Temperature anomalies over time caused by two wells. Both wells have double the pumping rate in the second time step compared to the first and third time steps.

2.2.1. Definition of potential well locations

Potential well locations are determined in a preprocessing step which considers legislative constraints, the existing building structure and the direction of groundwater flow in the study area. The initial spatial constraint of the chosen area is the minimum 3 m distance between the wells and the plot borders and buildings. Buffer zones are applied accordingly to clip the suitable well placement area within a parcel (cf. Fig. 2). The placement areas of extraction and injection wells are predefined by the direction of groundwater flow. In general, it is beneficial to place the extraction well up-gradient and the injection well down-gradient to avoid thermal recycling, which would reduce the GWHP's efficiency. The up-gradient and down-gradient areas are delineated by dividing the area deemed suitable for well placement normally to the groundwater flow direction in the centroid of the respective polygon. The extraction wells are placed on the up-gradient border and the injection wells on the down-gradient border within their specific polygon at a constant distance of 5 m to each other. Therefore, the preprocessing process enables the hydro-geologically and legally sound generation of potential well locations that are suitable for optimization.

2.2.2. Selection of well locations

It is assumed that one GWHP corresponds to one parcel in the area under consideration, with locations of potential wells being determined in a preprocessing process (see Section 2.2.1). As there are multiple potential well positions, there is a certain degree of freedom for each

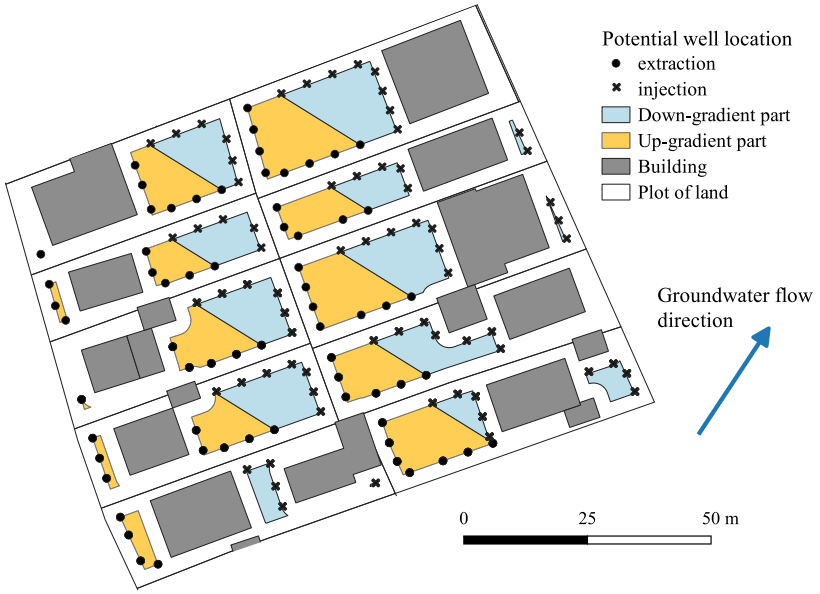

Fig. 2. Potential well locations with spatial and legal constraints.

GWHP regarding the spatial placement of the wells within the respective parcel. This means that the optimization process determines which systems should be installed and where the respective wells should be placed. The selection of GWHPs in the optimization process is as follows:

- each GWHP has a predefined number of potential extraction and injection wells,
- for a GWHP installation, one well pair is selected, i.e. one extraction and one injection well is selected,
- if GWHP is not installed, all of its potential wells are deselected,
- the selection of wells is modeled with binary optimization variables d_i: if $d_i = 1$, the well i is selected, otherwise $d_i = 0$, and the well is rejected.

Fig. 3 shows the concept by which GWHP wells are placed (selected). Potential extraction and injection wells are shown on the left with the corresponding optimization (decision) variables $d_{\text{ext},j}$ and $d_{\text{inj},i}$. An example of a well selection for an installed GWHP is shown in the right. In this case, the optimization variables have the following values: $d_{\text{ext},1} = d_{\text{inj},1} = d_{\text{inj},3} = 0$ and $d_{\text{ext},2} = d_{\text{inj},2} = 1$. More details on optimal well selection, i.e. the values of the decision variables, are given in Section 2.2.3.

The pumping rate q_p of each GWHP system, i.e. for each parcel p, can be expressed using the binary optimization variables as follows:

$$q_p = \sum_{i=1}^{N_{\text{inj}}^p} d_{\text{inj},i}\, q_i\,, \tag{7}$$

where N_{inj}^p is the total number of potential injection wells on the parcel p; $d_{\text{inj},i} \in \{0, 1\}$ is the decision variable for injection well i; q_i is the predefined pumping rate of the injection well i. If all decision variables in (7) are set to 0, all injection wells are deselected and the pumping rate of the GWHP is then also 0, which means that the system is not installed. On the other hand, if some of the decision variables are 1, the pumping rate of the GWHP is non-zero, which means it is installed. Thus, it is sufficient to use binary decision variables rather than pump rates as optimization variables in order to install or remove GWHP systems. The binary decision variables can be incorporated into the LAHM by introducing (7) into (5) as follows:

$$\Delta T_{x,y}(t, q_{1\ldots N,1\ldots M}) = \sum_{l=1}^{M}\sum_{k=1}^{N} d_{\text{inj},k}\, q_{k,l}\, \omega_{k,l}^{t,x,y}(x - x_k, y - y_k)\,, \tag{8}$$

$$N = \sum_{p=1}^{N_p} N_{\text{inj}}^p\,, \tag{9}$$

where N is the total number of potential injection wells in the area under consideration; N_p is the number of parcels (GWHP systems) in the area. The total temperature change of the groundwater is linear with respect to the optimization variables $d_{\text{inj},k}$, which is necessary to ensure that the optimization problem remains linear.

2.2.3. Objective function and constraints

In order to formulate the optimization problem, the objective function and the constraints must be defined. The optimization goal is to maximize the thermal energy obtained from the aquifer via GWHPs by determining an optimal placement that complies with regulatory conditions. The objective function is defined as follows:

$$E_{\text{ext}} = \sum_{l=1}^{M}\sum_{k=1}^{N} d_{\text{inj},k}\, q_{k,l} \cdot \Delta T_{\text{inj}} \cdot C_{\text{w}} \cdot \Delta t\,, \tag{10}$$

where E_{ext} is the total heat extracted from the groundwater by all GWPHs in the area under consideration and over the entire time horizon, discretized in time steps of length Δt. The goal is to maximize the objective function (10) while meeting the optimization constraints.

The first set of constraints describes the assumption that each GWHP, if installed, consists of a single well doublet, i.e. one extraction and one injection well. Therefore, a maximum of one extraction and one injection well can be installed on each parcel (plot) p, and the corresponding constraints read:

$$\sum_{i=1}^{N_{\text{inj}}^p} d_{\text{inj},i} \le 1 \quad \forall p \in P\,, \tag{11}$$

$$\sum_{j=1}^{N_{\text{ext}}^p} d_{\text{ext},j} \le 1 \quad \forall p \in P\,, \tag{12}$$

where N_{ext}^p is the total number of potential extraction wells on the parcel p and P the set of all parcels.

If an extraction well is installed in a particular parcel, an injection well must also be installed in that parcel and vice versa. Similarly, if there are no extraction wells in the parcel, there are no injection wells in that parcel, and vice versa. Thus, the number of injection and

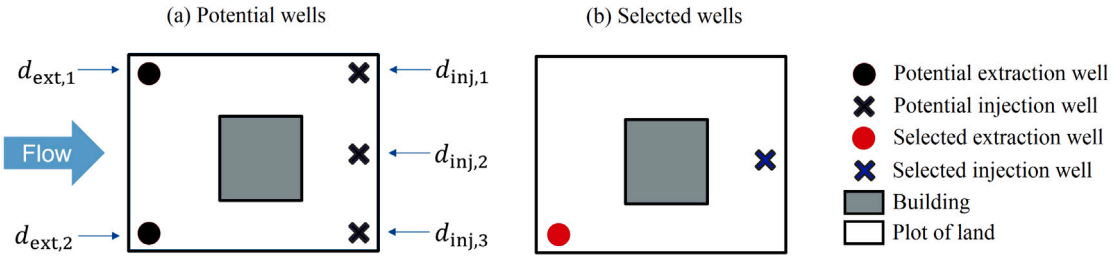

Fig. 3. Selection of optimal GWHP well positions: (a) Potential wells. (b) Optimal (selected) wells.

extraction wells installed in the same parcel must be equal, which is defined by the following constraint:

$$\sum_{i=1}^{N_{\text{inj}}^p} d_{\text{inj},i} = \sum_{j=1}^{N_{\text{ext}}^p} d_{\text{ext},j} \quad \forall p \in P\,. \tag{13}$$

Since the constraint (12) is a direct result of (11) and (13), it is sufficient to include only constraints (11) and (13) in the optimization problem.

The next set of constraints corresponds to the minimum distance requirement between extraction and injection wells of the same GWHP system. This distance is defined to avoid hydraulic and thermal breakthroughs within the system [17] and is 10 m [47] in the federal state of Bavaria, where the case study is located (see Section 3.1). In the optimization context, this means that if two wells, extraction and injection, are selected on the same parcel, they must be at least 10 m apart. The respective constraints read as follows:

$$d_{\text{inj},i} + d_{\text{ext},j} \leq 1 \quad \text{if} \quad \Delta_{i,j} < \Delta_{\min} \quad \forall i \in \{1,\dots,N_{\text{inj}}^p\},$$
$$\forall j \in \{1,\dots,N_{\text{ext}}^p\},\ \forall p \in P\,, \tag{14}$$

where $\Delta_{i,j} = \sqrt{(x_i - x_j)^2 + (y_i - y_j)^2}$ is the Euclidean distance between the potential injection and extraction wells (x_i, y_i) and (x_j, y_j), respectively; $\Delta_{\min} = 10$ m is the defined minimum distance. The constraints (14) are not set for all potential injection–extraction well pairs (i, j) on each plot p, but only for those whose distance is smaller than $\Delta_{\min}$. If the distance $\Delta_{i,j}$ is smaller than $\Delta_{\min}$, the constraint ensures that at most one of these wells can be installed. Since the locations of all potential wells are predefined, the distances between them can be precalculated and the constraints generated accordingly.

The final optimization constraint describes the regulation with regard to the negative influence on neighboring GWHPs. In the case of a new GWHP installation, this regulation protects the downstream systems from a significant drop in the groundwater temperature and, in turn, in their efficiency. In Bavaria, the temperature decrease compared to the natural groundwater temperature at the extraction well of a neighboring downstream system is limited to 1 K [47]. The corresponding constraint, which describes the prior regulation, holds for every potential extraction well j, and at the end of each time step $t \in \{1,\dots,M\}$:

$$d_{\text{ext},j} \cdot \Delta T_{x_j,y_j}(t,\overline{q}) \leq \Delta T_{\max}\,, \tag{15}$$

where $\Delta T_{\max} = 1$K is the maximum temperature change defined by the regulation; (x_j, y_j) are the coordinates of the extraction well j; $\Delta T_{x_j,y_j}(t,\overline{q}) = \Delta T_{x_j,y_j}(t, q_{1\dots N,1\dots M})$ as defined in (8). It depends on the value of the optimization variable $d_{\text{ext},j}$, whether the regulatory condition will be tested or not. If the extraction well j is selected ($d_{\text{ext},j} = 1$), the temperature change at this well must satisfy the regulation.

The constraint (15) is nonlinear, since the term $\Delta T_{x_j,y_j}(t,\overline{q})$, which already contains optimization variables $d_{\text{inj},k}$, is multiplied by the optimization variables $d_{\text{ext},j}$. However, all other optimization constraints and the objective function are linear w.r.t. the defined optimization variables. Thus, in order to keep the optimization problem linear, the constraint (15) is linearized in the following. First, the constraint is rewritten as:

$$\Delta T_{x_j,y_j}(t,\overline{q}) \leq \frac{1}{d_{\text{ext},j}} \cdot \Delta T_{\max}\,, \tag{16}$$

which is then linearized as:

$$\Delta T_{x_j,y_j}(t,\overline{q}) \leq (-m \cdot d_{\text{ext},j} + m + 1) \cdot \Delta T_{\max}\,, \tag{17}$$

where m is a sufficiently large number, so that (17) holds when $d_{\text{ext},j} = 0$. In this paper, $m = 99$, and it is a simple matter to verify that (17) has the same meaning as (15) for $d_{\text{ext},j} \in \{0,1\}$. Another linearization possibility is to introduce a set of new binary optimization variables $z_{j,k} = d_{\text{ext},j} \cdot d_{\text{inj},k}$ with additional constraints, which would replace the nonlinear terms (products) in (15). However, this approach introduces a significant number of new variables and constraints into the optimization problem, making it difficult to solve, and is therefore omitted.

Based on the previous definitions of the objective function and constraints, the optimization problem can be summarized as:

$$\max_{d_{\text{ext},j}, d_{\text{inj},k}} \quad E_{\text{ext}} \tag{18a}$$

$$\text{subject to} \quad (11), (13), (14), (17) \tag{18b}$$

with E_{ext} as defined in (10) and optimization variables $d_{\text{ext},j}, d_{\text{inj},k} \in \{0,1\}$, $j \in \{1,\dots,N_{\text{ext}}\}$, $k \in \{1,\dots,N\}$; where N_{ext} is the total number of potential extraction wells in the considered area. This constitutes an integer linear optimization problem, i.e. integer linear programming (ILP), with binary variables only. In general, linear programs are the simplest constrained optimization problems, in which finding the global optimum is both relatively quick and guaranteed. Finally, there are other alternatives to defining the objective function and formulating the optimization problem. For instance, the objective can be to maximize the efficiency, i.e. the groundwater temperature at extraction wells, of all the selected GWHPs. Details of this alternative problem formulation are given in Appendix A.

3. Implementation

The optimization method is implemented using Python-MIP [48], an open-source package for modeling and solving mixed-integer linear programs. The Python code, along with a working example, is accessible from [49]. Preprocessing of potential well locations is performed in PostgreSQL using the open-source spatial database extender PostGIS [50]. The case study area and the optimization cases are presented in the following.

3.1. Case study

The methodology described in Section 2.2 is applied to a neighborhood of approx. 6 ha in the city of Munich (see Fig. 4). Munich is generally well-suited to the thermal exploitation of groundwater, as it is located on a productive and shallow gravel aquifer, which was formed during the Pleistocene period. More detailed information on the

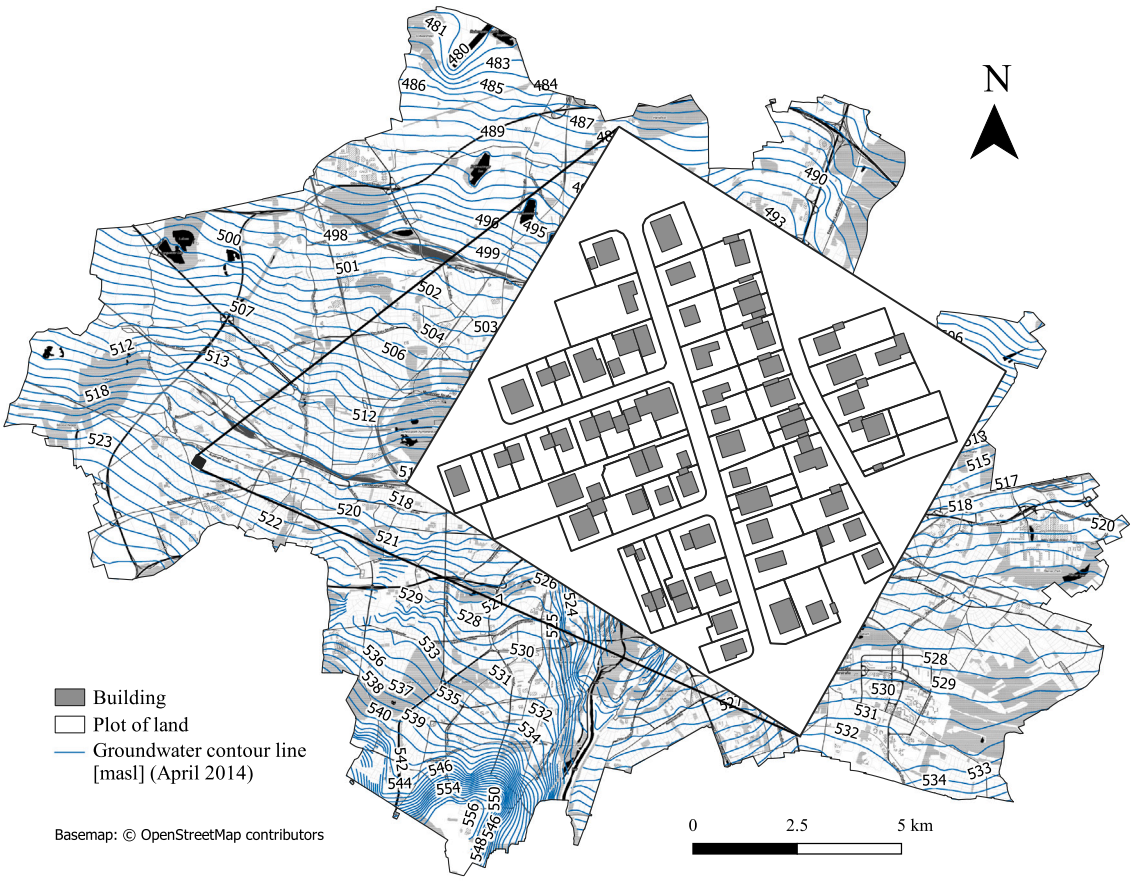

Fig. 4. Location of the case study neighborhood in the city of Munich with groundwater contour lines of the mean low water situation.

datasets used can be obtained from Böttcher et al. [26] and Zosseder et al. [51]. The known hydro-geological parameters in the chosen area, i.e. aquifer thickness, seepage velocity and flow direction, show only little variation. Therefore, we assume that the application of isotropic and constant hydraulic conditions does not lead to any significant bias in (1). A summary of the values applied to the case study neighborhood is given in Table 1. In addition, a homogeneous building structure of detached and semi-detached houses with predominantly sufficient drilling space on the plots provides suitable conditions for a dense cluster of potential GWHP users.

The pumping rates required for the 56 potential GWHPs are derived from a heat demand simulation using UrbanHeatPro [52], an open-source tool used for estimating the heating demands of buildings. It is assumed that one GWHP system supplies all buildings on a plot, so loads are merged for plots with more than one building. With a monthly resolution of required heating energy E_{heat}, and assuming a constant coefficient of performance (COP) of 4 and a constant source temperature difference (ΔT_{inj}) in the heat pump of 5 K, monthly pumping rates q_p were calculated with:

$$q_p = \frac{E_{\text{heat}}}{C_{\text{w}} \cdot \Delta T \cdot t_{\text{m}}} \cdot \frac{COP - 1}{COP}, \tag{19}$$

where t_{m} is the time period of one month. The aggregation of the monthly pumping rates for the various optimization cases is described in the following section.

3.2. Optimization cases

As previously mentioned, analytical formulas are used for licensing purposes of GWHPs in the German state of Baden-Württemberg. Two simulation cases are provided in the government guideline [41] describing the use of these formulas and the corresponding open source tool. The "annual mean value load" case describes the long-term impact that would result from continuous operation of a system, assuming a constant extraction rate and temperature spread ΔT_{inj} throughout the year. This case applies to stationary conditions, i.e. the assumption that the temperature field has theoretically reached its final expansion. It is also assumed that unaffected and constant temperatures prevail in the initial state. The purpose of the second case, "winter operation load", is to check whether the seasonal increase in the use of a system during the heating period has a greater effect than assuming annual mean values. For example, the double pumping rate compared to the annual mean value can be assumed, and 120 days can be set as the duration of the period of increased use [41].

In analogy to these definitions, two optimization cases are analyzed in this paper, these being the steady (winter) case and the dynamic (annual) case. The steady case is based on the "winter operation load" described above, in which all potential GWHPs have a constant pumping rate during the 120 days under consideration, which is twice the annual mean value. Therefore, only the spatial superposition of

Table 1
Hydro-geological parameters of the analyzed case study.

Parameter	Value	Unit
Aquifer thickness	8.5	m
Seepage velocity	$4 \cdot 10^{-5}$	m/s
Porosity	0.3	–
Longitudinal dispersivity	5	m
Transverse dispersivity	0.5	m
Volumetric heat capacity of the medium	$2.888 \cdot 10^{6}$	J/m^3 K
Volumetric heat capacity of water	$4.185 \cdot 10^{6}$	J/m^3 K
Flow direction (clockwise from North)	32	°

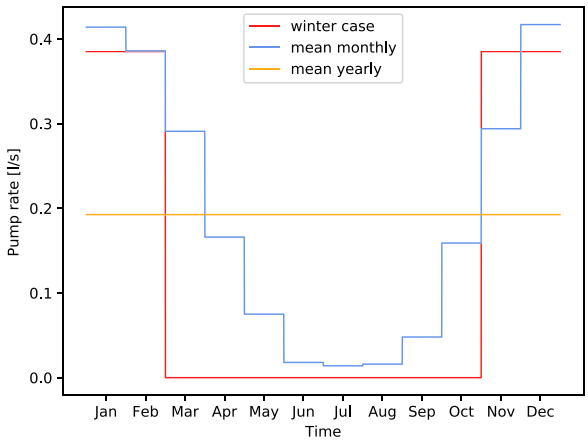

Fig. 5. Pumping rates of a potential GWHP used in two optimization cases.

Table 2
Optimization results.

Scenario	Nr. of GWHPs			Extracted heat	
	Total	Installed	Non-installed	Amount [J]	Share [%]
Winter (steady) case	56	44	12	$\sim 2.43 \cdot 10^{12}$	82.40
Annual (dynamic) case	56	43	13	$\sim 3.40 \cdot 10^{12}$	81.33

the LAHM is required in this case. On the other hand, the dynamic case should more realistically reflect the behavior of GWHPs over the course of the year. In this optimization case, the observation period is set to one year, with monthly time steps and averaged pumping rates for each month. To account for this dynamic behavior, both temporal and spatial superposition are needed. Fig. 5 shows the pumping rates of an example GWHP for the two optimization cases. The blue line denotes the dynamic case with average monthly values, while the red line denotes the steady case. It should be noted that the time window of the dynamic case begins in August, at which time the groundwater temperature is assumed to have recovered from the previous heating season and returned to its natural state.

4. Results

This section presents and analyzes the results of the optimization. Table 2 summarizes the results of the two optimization cases. It shows the total number of GWHP systems, i.e. the maximum number of systems potentially in the area, and the numbers of both installed and non-installed systems for each case. In the steady (winter) case, 44 out of 56 potential GWHPs are installed, only one more than in the dynamic (annual) case. The maximum heat extracted from the groundwater, which corresponds to the value of the objective function, is shown for both cases. This value represents the amount of heat extracted over the whole year and over the 4 months (with increased pumping rate) for the dynamic and steady cases, respectively. Consequently, the heat quantities for the dynamic and steady case should not be compared. These values are normalized by the corresponding theoretical maximum values that would result if all 56 potential GWHPs were installed. The normalized values, i.e. the heat fractions, are about 80% in both cases and approximately 1% more in the steady case. This demonstrates that negative interferences significantly limit the available space for GWHP installations and are an important factor when evaluating the technical potential in an area with a high building density.

Optimal well layouts for both optimization cases, including their comparison, are shown in Fig. 6. It can be seen that each plot with an installed GWHP has one extraction–injection well pair, which means that constraints (11) and (13) are satisfied. The minimum distance of 10 m between wells of a single system is also maintained for all installed systems, which corresponds to constraint (14). It is also notable that GWHPs are installed on almost the same parcels in both cases, but with different well locations. To better understand the differences in well layouts between the two cases, it is necessary to visualize the resulting groundwater temperature fields, i.e. the thermal plumes.

Fig. 7 shows the resulting thermal plumes, i.e. the groundwater temperature anomalies, for the optimal well layout in both cases. The thermal plumes shown correspond to those after four months for the steady (winter) case and at the end of February for the dynamic (annual) case. The end of February is shown for the dynamic case, because this is when the thermal plumes are at their maximum and have the greatest impact on well selection. The GWHPs have been heating during the previous winter months, while from March onward, the heating loads, and thus the intensity of the thermal plumes, start to decrease. This is illustrated in Fig. 8, which shows the evolution of the thermal plumes in the dynamic case. The figure also confirms the assumption about the recovery of groundwater temperatures at the beginning of August.

Fig. 7 shows that none of the optimally selected extraction wells are located in an area where the groundwater temperature changes by more than 1 K. This means that the negative thermal interference between the installed GWHPs is minimized, i.e. the constraint (17) is satisfied. Comparison of the thermal plumes in each of the cases shows that they are similar, while some of the differences are due to the different well selections. Therefore, the steady case is a relatively good approximation to the more realistic dynamic case. However, although only one GWHP fewer is installed in the dynamic case and virtually the same parcels are chosen for the installed GWHPs, it should be noted that the selected well locations differ significantly between the two cases. The observed difference in optimal well layouts can be attributed to the "confined" nature of the problem solution. For example, in the dynamic case, one optimal extraction well location from the steady state case might be within the area of thermal plumes. As a result, the entire solution is forced to transition to the next best feasible well arrangement. This transition can be significant, especially given the relatively large distance of 5 m between potential wells. Furthermore, the aforementioned "confinement" of the problem makes its solution sensitive to the choice of potential well locations. Minor changes in potential well locations can result in substantial variations in optimal well layouts. To mitigate this sensitivity of the solution to potential well locations, one viable approach is to implement smaller spacing between potential wells. Appendix B provides further details about this aspect. Finally, we compare the computational cost. The optimization process takes about 5 and 35 s for the steady and dynamic cases, respectively, when performed on a computer with the following configuration: Intel Xeon(R) Gold 6140 CPU @ 2.30 GHz × 72, 320 GB RAM.

5. Discussion and outlook

The results demonstrate that the optimization method presented here can efficiently determine the optimal locations for GWHPs and their wells for maximizing the technical geothermal potential. In both cases, wells are successfully placed to minimize negative thermal interferences and meet all regulatory requirements. Therefore, the proposed method covers the research gaps identified in Section 1 and is suitable for use in spatial energy planning, for example, in urban districts. However, the new method also has its limitations. These will now be discussed along with some possible future advancements and applications.

The main limiting factor is that an analytical model is used, which provides a less accurate calculation of thermal plumes than numerical models. Pophillat et al. [38] demonstrated that the LAHM tends to overestimate thermal plumes, and thus its application is a conservative assumption that tends to underestimate the spatial potential. The upgraded LAHM incorporates the following simplifications due to the

Fig. 6. Optimal well locations: (a) The steady case. (b) The dynamic case. (c) Comparison between two cases.

embedded properties of the original LAHM: the groundwater flow is in only one direction throughout the domain, aquifer properties are homogeneous, there is no hydraulic influence from the wells and there is no heat exchange with the atmosphere or conductive processes. However, conditions in aquifers are normally heterogeneous. For instance, the spatially heterogeneous porosity can significantly influence thermal retardation and consequently increase the uncertainty of the thermal plume estimation [53]. Numerical models based on partial differential equations (PDEs) are required in order to obtain more accurate estimates of groundwater temperatures and to incorporate heterogeneous aquifer conditions. Nevertheless, the original LAHM has already demonstrated its suitability for licensing purposes [39] as well as for initial assessments of negative thermal interferences between GWHPs [38]. Hence, its upgraded version and the presented optimization method can be used to estimate the technical geothermal potential of an aquifer. In the future, the new method can be combined with a PDE-based optimization method to improve the representation of aquifer conditions, while still keeping the computational cost at a reasonable level. This combined method can then be used in a detailed design optimization of multiple neighboring GWHPs, large standalone GWHPs or even nested systems with positive thermal interactions [54].

In this work, it is assumed that each installed GWHP system consists of a single well pair. This is generally the case for smaller systems, but not for large ones in which there may be multiple extraction and injection wells. Thus, one of the future advancements will be to accommodate systems with multiple extraction and/or injection wells. The formulation of the optimization problem needs to be slightly modified in this case, since the total pumping rate of a system will be distributed among several wells, depending on the number of installed wells.

The new method can also be used to make an economic and environmental comparison of two installation strategies for GWHP systems, these being either small individual or large communal systems. This would require additional modifications to the optimization problem. For instance, drilling costs for wells, pumping and piping costs, and operational and installation costs of the heat pumps have to be taken into consideration. Nevertheless, such a comparison would provide urban planners and individual users with valuable decision support regarding the optimal thermal use of groundwater.

Finally, in the future, the method presented can be integrated into urban energy system optimization models (ESOMs). The ESOMs are used to analyze future energy scenarios, i.e. to determine the optimal technology mixes to achieve CO_2 reduction targets. If GWHPs are among the technologies considered, the spatial thermal potential

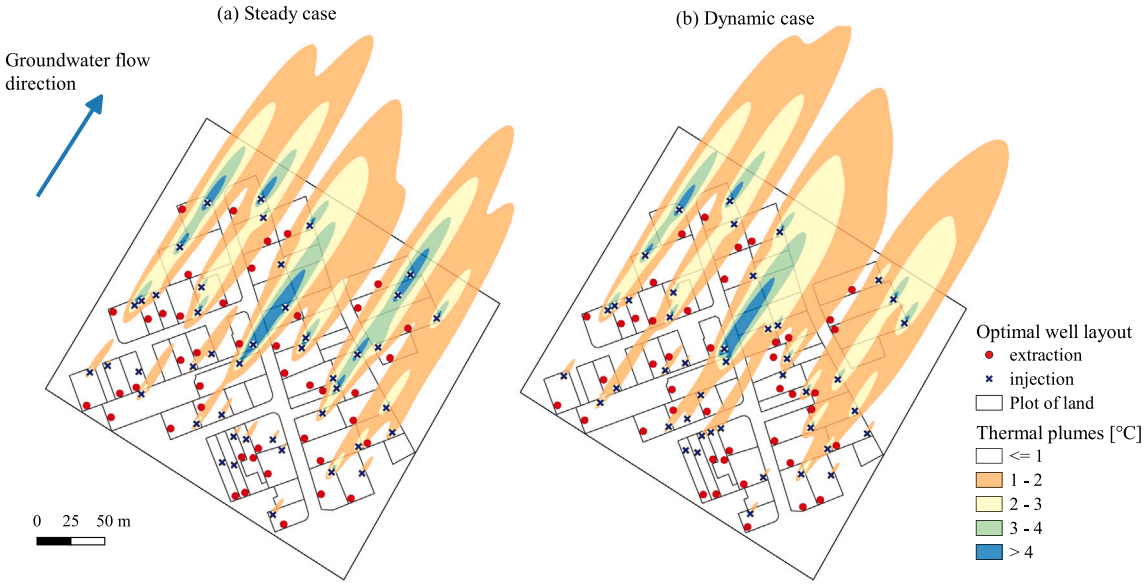

Fig. 7. Thermal plumes for the two cases: (a) The steady case. (b) The dynamic case (end of February).

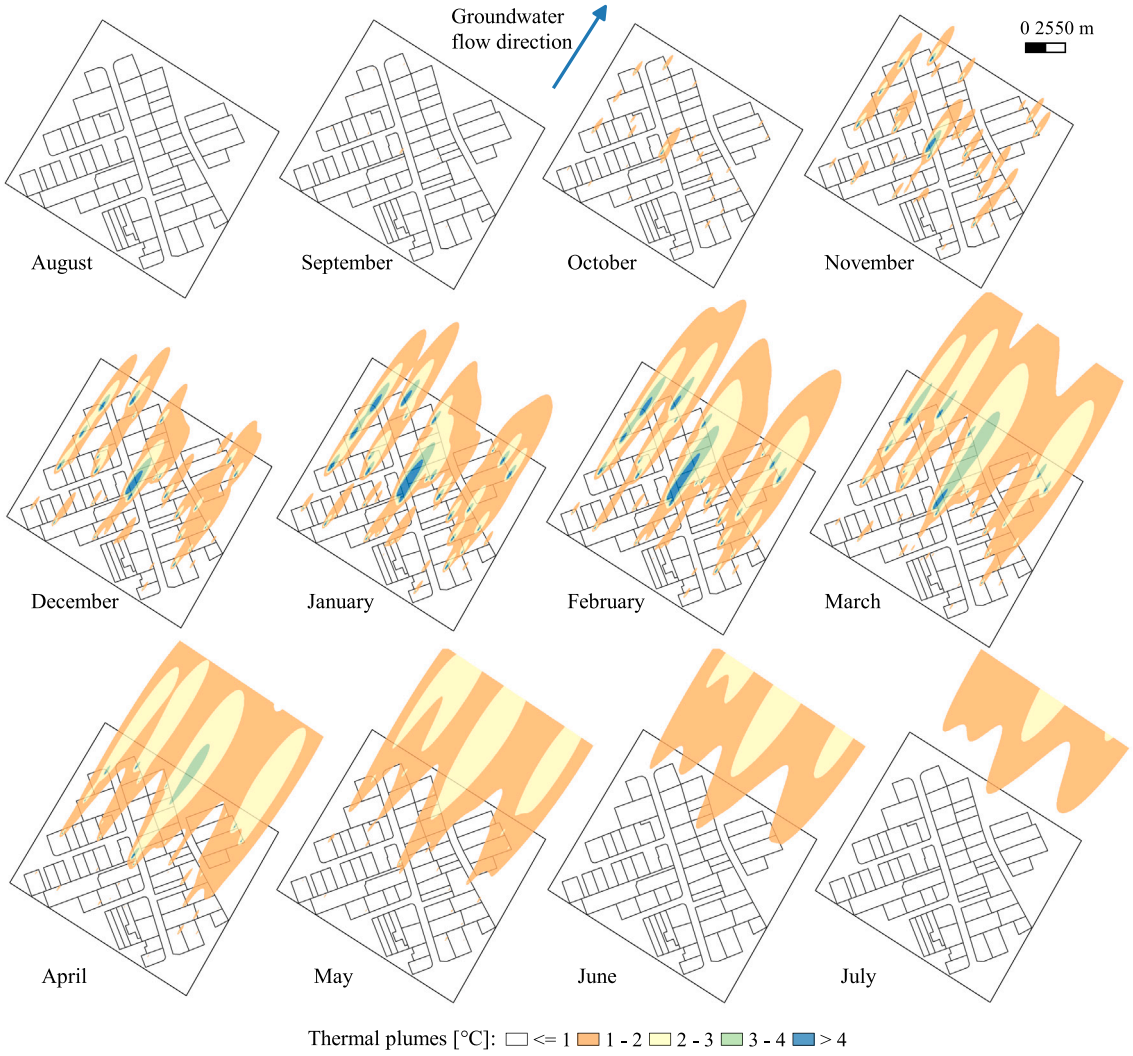

Fig. 8. Development of thermal plumes in the dynamic case: Thermal plumes at the end of each month.

of groundwater should be integrated into the ESOM [55]. The new method is particularly suitable for this purpose due to its analytical and linear properties. On the other hand, numerical groundwater simulation models are computationally intensive and require additional solvers, making the process of coupling them with ESOMs significantly more complex [56]. In addition, the upgraded LAHM is, thanks to its low computational cost, well suited for integration into GIS-supported online management tools, such as the web app developed in the GEO.KW project [57,58].

6. Conclusions

This paper presents a new method of optimizing the spatial arrangement of groundwater heat pumps and their well locations with the overall aim of maximizing the technical geothermal potential of groundwater. The method is based on an analytical estimation of thermal plumes using an upgraded LAHM model that supports dynamic simulation and multiple injection wells. Optimal placement of GWHP wells is attained through the selection of predefined potential well locations, such that negative thermal interferences between installed GWHPs are minimized. The overall optimization problem is an integer linear program that can be solved efficiently for a large number of optimization variables.

To demonstrate the applicability of the method, it was tested on a real case study comprising an area in the city of Munich (Germany) with 56 parcels, i.e. potential GWHPs. Two optimization cases were considered, each differing in GWHP their representation: the steady (winter) case with constant pumping rates over a period of four months and the dynamic (annual) case with average monthly pumping rates. The results for both cases show that the method successfully determines the GWHPs to be installed and their optimal well locations such that all regulatory conditions are met and negative interferences are minimized. The results also demonstrate that about 80% of the total heat demand can be met, which means that potential negative interferences are a significant limiting factor for the installation of GWHPs.

The method presented is the first method to determine the optimal installation of GWHPs in a given area such that the energy extracted from the aquifer is maximized and there are no negative interferences above a certain threshold. In addition, the new method can be applied to determine optimal locations for a large number of GWHPs and their wells at relatively low computational cost, which is a significant improvement over existing methods. Furthermore, the method can be extended to several other applications in the future, such as well size and location optimization for large GWHPs, economic analysis of GWHP installation strategies, and optimization of nested GWHP systems. The proposed method is especially suitable for integration in energy system optimization models that are used to analyze the energy transition in the heating and cooling sector. Finally, the method can be used in GIS-based tools for energy planning and geothermal groundwater management.

CRediT authorship contribution statement

Smajil Halilovic: Conceptualization, Methodology, Writing – original draft, Software, Investigation, Visualization. **Fabian Böttcher:** Conceptualization, Writing – original draft, Data curation, Visualization. **Kai Zosseder:** Funding acquisition, Writing – review & editing. **Thomas Hamacher:** Funding acquisition, Supervision.

Declaration of competing interest

The authors declare that they have no known competing financial interests or personal relationships that could have appeared to influence the work reported in this paper.

Acknowledgments

The work presented in this paper was supported by the German Federal Ministry for Economic Affairs and Energy (BMWi) within the scope of the research project GEO.KW (01184143/1).

Appendix A. Alternative objective function

Instead of maximizing the total amount of extracted energy, the goal can be to maximize the efficiency of all selected GWHPs. In this case, the groundwater temperature at the extraction wells of selected GWHPs is maximized and the objective function reads as follows:

$$\sum_{t=1}^{M}\sum_{j=1}^{N_{\text{ext}}} d_{\text{ext},j}\cdot\left(T_{\text{n}}^{j}(t)-\Delta T_{x_j,y_j}(t,\overline{q})\right), \tag{A.1}$$

where $T_{\text{n}}^{j}(t)$ is the natural (undisturbed) groundwater temperature at the considered location (x_j, y_j) and at the time step t, $t \in \{1,\dots,M\}$. The natural groundwater temperatures have predefined constant values, which means that the first term in (A.1) is linear. However, the second term:

$$\sum_{t=1}^{M}\sum_{j=1}^{N_{\text{ext}}} d_{\text{ext},j}\cdot\Delta T_{x_j,y_j}(t,\overline{q}) \tag{A.2}$$

is nonlinear and similar to the left-hand side of the constraint (15). Hence, the optimization problem can be linearized as follows:

$$\max_{d_{\text{ext},j},d_{\text{inj},k},\theta_j(t)} \quad \sum_{t=1}^{M}\sum_{j=1}^{N_{\text{ext}}}\left(d_{\text{ext},j}\cdot T_{\text{n}}^{j}(t)-\theta_j(t)\right) \tag{A.3a}$$

$$\text{subject to} \quad (11),\ (13),\ (17) \tag{A.3b}$$

$$\Delta T_{x_j,y_j}(t,\overline{q}) \le -m\cdot d_{\text{ext},j}+m+\theta_j(t), \tag{A.3c}$$

where the constraint (A.3c) must hold $\forall t \in \{1,\dots,M\}$ and $\forall j \in \{1,\dots,N_{\text{ext}}\}$; $\theta_j(t) \in \mathbb{R}_0^+$ are new non-negative continuous optimization variables needed for the linearization; $m = 99$ and other parameters are the same as before. For the selected extraction wells, i.e. when $d_{\text{ext},j} = 1$, (A.3c) becomes:

$$\Delta T_{x_j,y_j}(t,\overline{q}) \le \theta_j(t), \tag{A.4}$$

which means that by minimizing $\theta_j(t)$, the temperature drops at these extraction wells are also minimized. Since this matches the optimization goal, which is to maximize the efficiency of the selected GWHPs, the objective function becomes (A.3a). On the other hand, when $d_{\text{ext},j} = 0$, the optimizer will set the corresponding variables $\theta_j(t)$ to zero without influencing the selection of optimal wells. Thus, by introducing the new set of optimization variables $\theta_j(t)$ and the corresponding constraints, the problem can be formulated as a mixed-integer linear program (A.3).

Appendix B. Initialization of the optimization problem

The spatial arrangement of potential well locations can have a considerable impact on the optimization problem (18) and the resulting optimal well layouts. Notably, when the potential wells are spaced at relatively large distances, minor alterations in their locations can result in significant changes in the final selection of optimal well locations. Fig. B.9 illustrates this phenomenon by showing the optimal well layouts for two slightly different initial arrangements of potential wells. The original initialization, i.e. the arrangement of potential well locations, is the one used to analyze the potential of the case study area. The new initialization is derived from the original one by randomly moving the location of each potential well within a radius of 0.5 m from its original position. The optimal well locations for both initializations are then determined using the steady state optimization scenario.

Despite the relatively small differences in the potential well locations, the resulting optimal well layouts exhibit considerable variation.

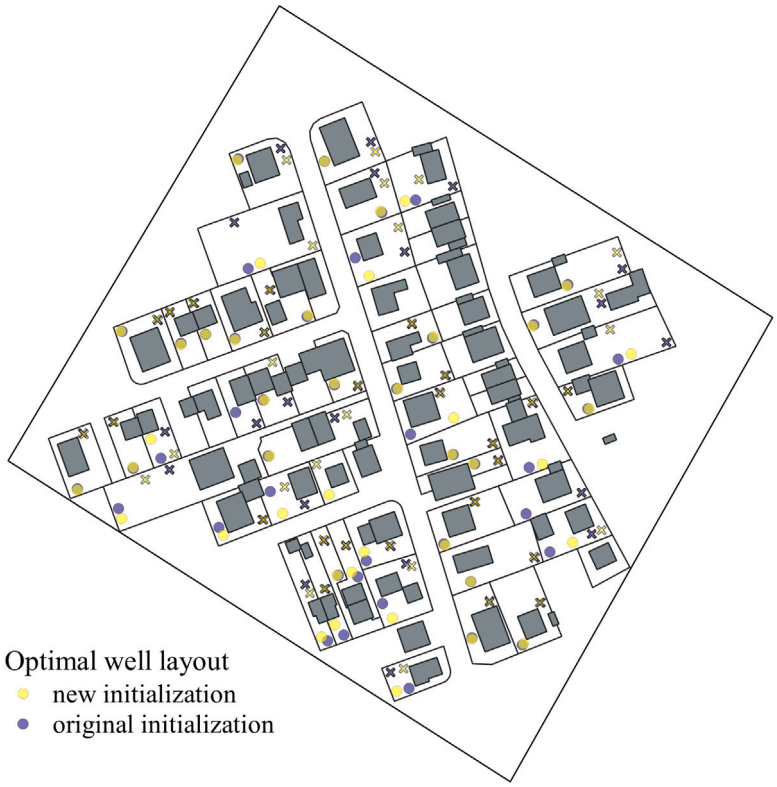

Fig. B.9. Comparison of optimal well layouts for two different potential well arrangements.

This sensitivity of the solution to potential well locations can be attributed to the narrowness of the problem solution due to the constraint on negative thermal interference and the prevailing geometric relationships. In particular, certain optimal well locations are located exactly at the boundaries of the thermal plumes indicated by the 1 K thermal isolines. Consequently, even a slight deviation of one of the optimal well locations into an infeasible region during re-initialization causes the problem solution to switch to the next best feasible optimal well layout. This can lead to significant differences in the new optimal well layout compared to the original one, especially if the potential wells are relatively far apart, as the solution is forced to make significant adjustments or "jumps" between different well layouts during the optimization process.

References

[1] European Commission. Joint Research Centre. Institute for Energy and Transport., European Technology Platform on Renewable Heating and Cooling., Strategic research and innovation agenda for renewable heating and cooling: European technology platform on renewable heating and cooling, Publications Office, 2013, http://dx.doi.org/10.2790/88750.

[2] European Commission, 2050 Long-term strategy: Climate action, 2020, URL https://ec.europa.eu/clima/eu-action/climate-strategies-targets/2050-long-term-strategy_en.

[3] J.W. Lund, A.N. Toth, Direct utilization of geothermal energy 2020 worldwide review, Geothermics 90 (2021) 101915, http://dx.doi.org/10.1016/j.geothermics.2020.101915, URL https://www.sciencedirect.com/science/article/pii/S0375650520302078.

[4] J. Hou, M. Cao, P. Liu, Development and utilization of geothermal energy in China: Current practices and future strategies, Renew. Energy 125 (2018) 401–412, http://dx.doi.org/10.1016/j.renene.2018.02.115.

[5] F. Stauffer, P. Bayer, P. Blum, N.M. Giraldo, W. Kinzelbach, Thermal use of shallow groundwater, CRC Press, Boca Raton, Fla., 2014.

[6] S. Haehnlein, P. Bayer, P. Blum, International legal status of the use of shallow geothermal energy, Renew. Sustain. Energy Rev. 14 (9) (2010) 2611–2625, http://dx.doi.org/10.1016/j.rser.2010.07.069.

[7] G. Florides, S. Kalogirou, Ground heat exchangers—A review of systems, models and applications, Renew. Energy 32 (15) (2007) 2461–2478, http://dx.doi.org/10.1016/j.renene.2006.12.014.

[8] S.J. Self, B.V. Reddy, M.A. Rosen, Geothermal heat pump systems: Status review and comparison with other heating options, Appl. Energy 101 (2013) 341–348, http://dx.doi.org/10.1016/j.apenergy.2012.01.048.

[9] J. Kim, Y. Nam, A numerical study on system performance of groundwater heat pumps, Energies 9 (1) (2016) 4, http://dx.doi.org/10.3390/en9010004.

[10] F. Böttcher, K. Zosseder, Thermal influences on groundwater in urban environments – A multivariate statistical analysis of the subsurface heat island effect in Munich, Sci. Total Environ. 810 (January 2022) (2021) 152193, http://dx.doi.org/10.1016/j.scitotenv.2021.152193, URL https://doi.org/10.1016/j.scitotenv.2021.152193.

[11] K. Menberg, P. Bayer, K. Zosseder, S. Rumohr, P. Blum, Subsurface urban heat islands in german cities, Sci. Total Environ. 442 (2013) 123–133, http://dx.doi.org/10.1016/j.scitotenv.2012.10.043.

[12] J.A. Rivera, P. Blum, P. Bayer, Increased ground temperatures in urban areas: Estimation of the technical geothermal potential, Renew. Energy 103 (2017) 388–400, http://dx.doi.org/10.1016/j.renene.2016.11.005.

[13] K.P. Tsagarakis, L. Efthymiou, A. Michopoulos, A. Mavragani, A.S. Anđelković, F. Antolini, M. Bacic, D. Bajare, M. Baralis, W. Bogusz, S. Burlon, J. Figueira, M.S. Genç, S. Javed, A. Jurelionis, K. Koca, G. Ryżyński, J.F. Urchueguia, B. Žlender, A review of the legal framework in shallow geothermal energy in selected European countries: Need for guidelines, Renew. Energy 147 (2020) 2556–2571, http://dx.doi.org/10.1016/j.renene.2018.10.007.

[14] J. Epting, P. Huggenberger, Unraveling the heat island effect observed in urban groundwater bodies–definition of a potential natural state, J. Hydrol. 501 (2013) 193–204, http://dx.doi.org/10.1016/j.jhydrol.2013.08.002.

[15] V. Somogyi, V. Sebestyén, E. Domokos, A. Zseni, Z. Papp, Thermal impact assessment with hydrodynamics and transport modeling, Energy Convers. Manage. 104 (2015) 127–134, http://dx.doi.org/10.1016/j.enconman.2015.04.045.

[16] E. Milnes, P. Perrochet, Assessing the impact of thermal feedback and recycling in open-loop groundwater heat pump (GWHP) systems: a complementary design tool, Hydrogeol. J. 21 (2) (2013) 505–514, http://dx.doi.org/10.1007/s10040-012-0902-y.

[17] D. Banks, Thermogeological assessment of open-loop well-doublet schemes: a review and synthesis of analytical approaches, Hydrogeol. J. 17 (5) (2009) 1149–1155, http://dx.doi.org/10.1007/s10040-008-0427-6.

[18] A. García Gil, E.A. Garrido Schneider, M. Mejías Moreno, J.C. Santamarta Cerezal, Management and governance of shallow geothermal energy resources, in: Shallow Geothermal Energy, Springer, 2022, pp. 237–272.

[19] P. Bayer, G. Attard, P. Blum, K. Menberg, The geothermal potential of cities, Renew. Sustain. Energy Rev. 106 (2019) 17–30, http://dx.doi.org/10.1016/j.rser.2019.02.019.

[20] J. Epting, M.H. Müller, D. Genske, P. Huggenberger, Relating groundwater heat-potential to city-scale heat-demand: A theoretical consideration for urban groundwater resource management, Appl. Energy 228 (2018) 1499–1505, http://dx.doi.org/10.1016/j.apenergy.2018.06.154.

[21] J. Epting, F. Böttcher, M.H. Mueller, A. García-Gil, K. Zosseder, P. Huggenberger, City-scale solutions for the energy use of shallow urban subsurface resources – bridging the gap between theoretical and technical potentials, Renew. Energy 147 (2020) 751–763, http://dx.doi.org/10.1016/j.renene.2019.09.021.

[22] A. García-Gil, E. Vázquez-Suñe, M.M. Alcaraz, A.S. Juan, J.Á. Sánchez-Navarro, M. Montlleó, G. Rodríguez, J. Lao, GIS-supported mapping of low-temperature geothermal potential taking groundwater flow into account, Renew. Energy 77 (2015) 268–278, http://dx.doi.org/10.1016/j.renene.2014.11.096.

[23] M. Pujol, L.P. Ricard, G. Bolton, 20 Years of exploitation of the yarragadee aquifer in the perth basin of western Australia for direct-use of geothermal heat, Geothermics 57 (2015) 39–55, http://dx.doi.org/10.1016/j.geothermics.2015.05.004.

[24] T. Arola, K. Korkka-Niemi, The effect of urban heat islands on geothermal potential: examples from quaternary aquifers in Finland, Hydrogeol. J. 22 (8) (2014) 1953–1967, http://dx.doi.org/10.1007/s10040-014-1174-5.

[25] T. Arola, L. Eskola, J. Hellen, K. Korkka-Niemi, Mapping the low enthalpy geothermal potential of shallow quaternary aquifers in Finland, Geotherm. Energy 2 (1) (2014) 1–20, http://dx.doi.org/10.1186/s40517-014-0009-x.

[26] F. Böttcher, A. Casasso, G. Götzl, K. Zosseder, TAP - thermal aquifer potential: A quantitative method to assess the spatial potential for the thermal use of groundwater, Renew. Energy 142 (2019) 85–95, http://dx.doi.org/10.1016/j.renene.2019.04.086.

[27] A. García-Gil, E. Vázquez-Suñe, E.G. Schneider, J.Á. Sánchez-Navarro, J. Mateo-Lázaro, Relaxation factor for geothermal use development – criteria for a more fair and sustainable geothermal use of shallow energy resources, Geothermics 56 (2015) 128–137, http://dx.doi.org/10.1016/j.geothermics.2015.04.003.

[28] G. Attard, P. Bayer, Y. Rossier, P. Blum, L. Eisenlohr, A novel concept for managing thermal interference between geothermal systems in cities, Renew. Energy 145 (2020) 914–924, http://dx.doi.org/10.1016/j.renene.2019.06.095.

[29] A. García-Gil, S. Muela Maya, E. Garrido Schneider, M. Mejías Moreno, E. Vázquez-Suñé, M.Á. Marazuela, J. Mateo Lázaro, J.Á. Sánchez-Navarro, Sustainability indicator for the prevention of potential thermal interferences between groundwater heat pump systems in urban aquifers, Renew. Energy 134 (2019) 14–24, http://dx.doi.org/10.1016/j.renene.2018.11.002.

[30] C.G. Clyde, G.V. Madabhushi, Spacing of wells for heat pumps, J. Water Resour. Plann. Manag. 109 (3) (1983) 203–212, http://dx.doi.org/10.1061/(ASCE)0733-9496(1983)109:3(203).

[31] S. Halilovic, F. Böttcher, K. Zosseder, T. Hamacher, Optimization approaches for the design and operation of open-loop shallow geothermal systems, 2023, http://dx.doi.org/10.48550/arXiv.2307.11244, arXiv preprint arXiv:2307.11244.

[32] Y.-z. Zhou, Z.-f. Zhou, Simulation of Thermal Transport in Aquifer: A GWHP System in Chengdu, China, J. Hydrodyn. 21 (5) (2009) 647–657, http://dx.doi.org/10.1016/S1001-6058(08)60196-1.

[33] Q. Gao, X.-Z. Zhou, Y. Jiang, X.-L. Chen, Y.-Y. Yan, Numerical simulation of the thermal interaction between pumping and injecting well groups, Appl. Therm. Eng. 51 (1–2) (2013) 10–19, http://dx.doi.org/10.1016/j.applthermaleng.2012.09.017.

[34] S. Lo Russo, M.V. Civita, Open-loop groundwater heat pumps development for large buildings: A case study, Geothermics 38 (3) (2009) 335–345, http://dx.doi.org/10.1016/j.geothermics.2008.12.009.

[35] D. Park, E. Lee, D. Kaown, S.-S. Lee, K.-K. Lee, Determination of optimal well locations and pumping/injection rates for groundwater heat pump system, Geothermics 92 (2021) 102050, http://dx.doi.org/10.1016/j.geothermics.2021.102050.

[36] S. Halilovic, F. Böttcher, S.C. Kramer, M.D. Piggott, K. Zosseder, T. Hamacher, Well layout optimization for groundwater heat pump systems using the adjoint approach, Energy Convers. Manage. 268 (2022) 116033, http://dx.doi.org/10.1016/j.enconman.2022.116033.

[37] D.K. Park, D. Kaown, K.-K. Lee, Development of a simulation-optimization model for sustainable operation of groundwater heat pump system, Renew. Energy 145 (2020) 585–595, http://dx.doi.org/10.1016/j.renene.2019.06.039.

[38] W. Pophillat, G. Attard, P. Bayer, J. Hecht-Méndez, P. Blum, Analytical solutions for predicting thermal plumes of groundwater heat pump systems, Renew. Energy 147 (2020) 2696–2707, http://dx.doi.org/10.1016/j.renene.2018.07.148.

[39] Umweltministerium Baden-Württemberg, Leitfaden zur Nutzung von Erdwärme mit Grundwasserwärmepumpen, 2009.

[40] W. Kinzelbach, Numerische Methoden Zur Modellierung Des Transports Von Schadstoffen Im Grundwasser, Oldenbourg, 1987.

[41] Umweltministerium Baden-Württemberg, Arbeitshilfe zum Leitfaden zur Nutzung von Erdwärme mit Grundwasserwärmepumpen, 2009.

[42] D. Marcotte, P. Pasquier, F. Sheriff, M. Bernier, The importance of axial effects for borehole design of geothermal heat-pump systems, Renew. Energy 35 (4) (2010) 763–770, http://dx.doi.org/10.1016/j.renene.2009.09.015.

[43] M. de Paly, J. Hecht-Méndez, M. Beck, P. Blum, A. Zell, P. Bayer, Optimization of energy extraction for closed shallow geothermal systems using linear programming, Geothermics 43 (2012) 57–65, http://dx.doi.org/10.1016/j.geothermics.2012.03.001.

[44] P. Bayer, M. de Paly, M. Beck, Strategic optimization of borehole heat exchanger field for seasonal geothermal heating and cooling, Appl. Energy 136 (2014) 445–453, http://dx.doi.org/10.1016/j.apenergy.2014.09.029.

[45] J. Hecht-Méndez, M. de Paly, M. Beck, P. Bayer, Optimization of energy extraction for vertical closed-loop geothermal systems considering groundwater flow, Energy Convers. Manage. 66 (2013) 1–10, http://dx.doi.org/10.1016/j.enconman.2012.09.019.

[46] M. Beck, P. Bayer, M. de Paly, J. Hecht-Méndez, A. Zell, Geometric arrangement and operation mode adjustment in low-enthalpy geothermal borehole fields for heating, Energy 49 (2013) 434–443, http://dx.doi.org/10.1016/j.energy.2012.10.060.

[47] Bayerisches Landesamt für Umwelt, Planung und Erstellung von Erdwärmesonden: LfU, 2012, URL https://www.lfu.bayern.de/wasser/merkblattsammlung/teil3_grundwasser_und_boden/doc/nr_372.pdf.

[48] H.G. Santos, T.A. Toffolo, Mixed integer linear programming with python, 2020.

[49] S. Halilovic, F. Böttcher, Optimization of GWHP well layouts using analytic models, 2022, http://dx.doi.org/10.5281/zenodo.7230875, URL https://github.com/SHalilovic/GWHP-analytic-optimization.

[50] PostGIS Team, PostGIS, 2022, http://dx.doi.org/10.5281/zenodo.5879631, URL https://postgis.net/.

[51] K. Zosseder, M. Kerl, A. Albarrán-Ordás, M. Gossler, A. Kiecak, L. Chavez-Kus, Die hydraulischen Grundwasserverhältnisse des quartären und des oberflächennahen tertiären Grundwasserleiters im Großraum München, Geol. Bavar. 122 (2022) URL https://www.bestellen.bayern.de/shoplink/91122.htm.

[52] A. Molar-Cruz, UrbanHeatPro, 2020, https://github.com/tum-ens/UrbanHeatPro.

[53] M.A. Gossler, P. Bayer, K. Zosseder, Experimental investigation of thermal retardation and local thermal non-equilibrium effects on heat transport in highly permeable, porous aquifers, J. Hydrol. 578 (2019) 124097, http://dx.doi.org/10.1016/j.jhydrol.2019.124097.

[54] A. García-Gil, M. Mejías Moreno, E. Garrido Schneider, M.Á. Marazuela, C. Abesser, J. Mateo Lázaro, J.Á. Sánchez Navarro, Nested shallow geothermal systems, Sustainability 12 (12) (2020) 5152, http://dx.doi.org/10.3390/su12125152.

[55] S. Halilovic, L. Odersky, T. Hamacher, Integration of groundwater heat pumps into energy system optimization models, Energy 238 (2022) 121607, http://dx.doi.org/10.1016/j.energy.2021.121607.

[56] S. Halilovic, L. Odersky, F. Böttcher, K. Davis, M. Schulte, K. Zosseder, T. Hamacher, Optimization of an energy system model coupled with a numerical hydrothermal groundwater simulation, in: Mapping the Energy Future-Voyage in Uncharted Territory-, 43rd IAEE International Conference, July 31-August 3, 2022, International Association for Energy Economics, 2022.

[57] K. Zosseder, F. Böttcher, K. Davis, C. Haas, S. Halilovic, T. Hamacher, H. Heller, L. Odersky, V. Pauw, T. Schramm, S.M. and, Schlussbericht zum Verbundprojekt GEO-KW: Kopplung des geothermischen Speicherpotenzials mit den wechselnden Anforderungen des urbanen Energiebedarfs zur effizienten Nutzung der regenerativen Energiequelle Grundwasser für die dezentrale Kälte- und Wärmebereitstellung in der Stadt, Technical Report, Bundesministerium für Wirtschaft und Klimaschutz, 2022, http://dx.doi.org/10.14459/2022md1692003.

[58] F. Böttcher, K. Davis, S. Halilovic, L. Odersky, V. Pauw, T. Schramm, K. Zosseder, Optimising the thermal use of groundwater for a decentralized heating and cooling supply in the city of Munich, Germany, 2021, http://dx.doi.org/10.5194/egusphere-egu21-14929, URL https://doi.org/10.5194/egusphere-egu21-14929.

Publication 4 - Spatial analysis of thermal groundwater use based on optimal sizing and placement of well doublets

Authors: Smajil Halilović, Fabian Böttcher, Kai Zosseder, Thomas Hamacher

Journal: Energy (Elsevier)

Status: Published (online) - June 2024

Digital object identifier: https://doi.org/10.1016/j.energy.2024.132058

Source code: https://github.com/SHalilovic/Well-doublet-optimization

Author	Contribution
Smajil Halilović	Conceptualization, Methodology, Writing - original draft, Software, Formal analysis, Investigation, Visualization
Fabian Böttcher	Conceptualization, Writing - reviewing and editing, Data curation
Kai Zosseder	Writing - reviewing and editing
Thomas Hamacher	Writing - reviewing and editing, Supervision

Energy 304 (2024) 132058

Contents lists available at ScienceDirect

Energy

journal homepage: www.elsevier.com/locate/energy

Spatial analysis of thermal groundwater use based on optimal sizing and placement of well doublets

Smajil Halilovic [a,*], Fabian Böttcher [b,c], Kai Zosseder [b], Thomas Hamacher [a]

[a] Technical University of Munich, Chair of Renewable and Sustainable Energy Systems, Germany
[b] Technical University of Munich, Chair of Hydrogeology, Germany
[c] Department for Climate and Environmental Protection (RKU), City of Munich, Germany

ARTICLE INFO

Keywords:
Shallow geothermal energy
Groundwater heat pump
Optimization
Geothermal potential
Well placement
Spatial energy planning

ABSTRACT

This paper proposes an approach to optimize the technical potential of thermal groundwater use by determining the optimal sizing and placement of extraction–injection well doublets. The approach quantifies the maximum technically achievable volume of extracted groundwater in a given area and, hence, the amount of heat exchanged with the aquifer, considering relevant regulatory and hydraulic constraints. The hydraulic constraints ensure acceptable drawdown and rise of groundwater in extraction and injection wells for sustainable use, respectively, prevention of internal hydraulic breakthroughs, and adequate spacing between neighboring doublets. Analytical expressions representing these constraints are integrated into a mixed-integer linear optimization framework allowing efficient application to relatively large areas. The applicability of the approach is demonstrated by a real case study in Munich, where the geothermal potential of each city block is optimized independently. Six optimization scenarios, differing in terms of required minimum installed doublet capacity and spacings between doublets, underline the adaptability of the approach. The approach provides a comprehensive and optimized potential assessment and can be readily applied to other geographic locations. This makes it a valuable tool for thermal groundwater management and spatial energy planning, such as the planning of fourth and fifth generation district heating systems.

1. Introduction

Shallow geothermal energy (SGE) plays an increasingly important role in the decarbonization of the heating and cooling sector [1]. Especially in the context of 4th generation district heating (4GDH) systems [2] and 5th generation district heating and cooling (5GDHC) systems [3], SGE systems represent a promising technology as their application is expanded from individual users to communities in this case. One way of SGE utilization is through open-loop systems, commonly referred to as groundwater heat pumps (GWHPs). Fig. 1 shows a typical GWHP system with its main components. These systems directly exploit the thermal energy of groundwater through extraction–injection well doublets by pumping groundwater from extraction wells and returning it to the same shallow aquifer through injection wells after thermal exchange [4]. Consequently, the properties of groundwater, including its quantity, quality, depth, and temperature, are the most important factors affecting the feasibility and performance of GWHP systems [5,6]. Accurate characterization and consideration of these groundwater properties is essential for ensuring sustainable and efficient operation of GWHPs [7]. It should be noted that GWHPs are mainly used in areas with high ambient groundwater velocity, which limits the application of aquifer thermal energy storage (ATES) systems, another type of SGE systems for thermal groundwater utilization. In this paper, we focus only on GWHP systems, i.e. on areas with high groundwater velocity.

In the context of groundwater utilization for GWHP systems, it is crucial to recognize that groundwater availability and properties exhibit significant spatial variation [8]. In addition, spatial availability for GWHP well installations in urban areas is limited due to extensive building development. Therefore, conducting a spatial analysis is essential to identify adequate well locations and sizing for well doublets. The goal of such an analysis is to quantify suitable groundwater extraction values for the targeted urban energy planning level, such as a plot of land or city block [9]. Accurate estimation of groundwater extraction and injection rates, can ensure sustainable GWHP operation based on the local hydrogeological conditions and in compliance with relevant legal and technical constraints. The technical potential derived from such an analysis is a basis for active thermal groundwater management and the development of urban energy strategies [10], including the planning of 4GDH and 5GDHC systems.

* Corresponding author.
E-mail address: smajil.halilovic@tum.de (S. Halilovic).

https://doi.org/10.1016/j.energy.2024.132058
Received 12 November 2023; Received in revised form 31 May 2024; Accepted 11 June 2024
Available online 13 June 2024

Nomenclature

Latin letters

B	Saturated aquifer thickness [m]
C	Condition for relative well placement
d	Decision variables for doublets
d_{ext}	Decision variables for extraction wells
d_{inj}	Decision variables for injection wells
E	Set of potential extraction wells
$\mathbf{g}_1$	Equality constraints
$\mathbf{g}_2$	Inequality constraints
∇h	Hydraulic gradient [-]
h_{max}	Maximum allowed groundwater level [m]
h_{n}	Natural groundwater level [m]
I	Set of potential injection wells
K	Hydraulic conductivity [m/s]
m	Interference parameter [m]
N	Number of potential doublets
n_{doublet}	Number of installed doublets in city block [-]
q	Pump rate of a doublet [m^3/s]
q_{b}	Pump rate at the hydraulic breakthrough threshold [m^3/s]
q_{block}	Pump rate per city block [m^3/s]
q_{d}	Pump rate at the drawdown threshold [m^3/s]
q_{f}	Injection rate at the upconing threshold [m^3/s]
q_{max}	Pre-computed maximum pump rate of a doublet [m^3/s]
q_{min}	Predefined minimum pump rate of a doublet [m^3/s]
q_{total}	Total pump rate [m^3/s]
r_{Δ}	External–internal well distance ratio [-]
S	Set of potential doublets
$\boldsymbol{u}$	Optimization variables
v_D	Darcy velocity [m/s]
x, y	Coordinates of a well [m]

Greek letters

α	Hydraulic breakthrough parameter [m^2/s]
χ	Line length [m]
Δ	Distance between two wells or two doublets [m]
Δ_{min}	Regulatory minimum distance [m]

Subscripts and superscripts

ext	Extraction
inj	Injection
max	Maximum
min	Minimum
$\tilde{a}$	Median of a
i	Counter for injection wells
j	Counter for extraction wells
k, p	Counters for doublets

Several research studies assess the potential of thermal groundwater use at different locations and considering various constraints [11–19]. Some studies focus on specific technical and/or regulatory constraints,

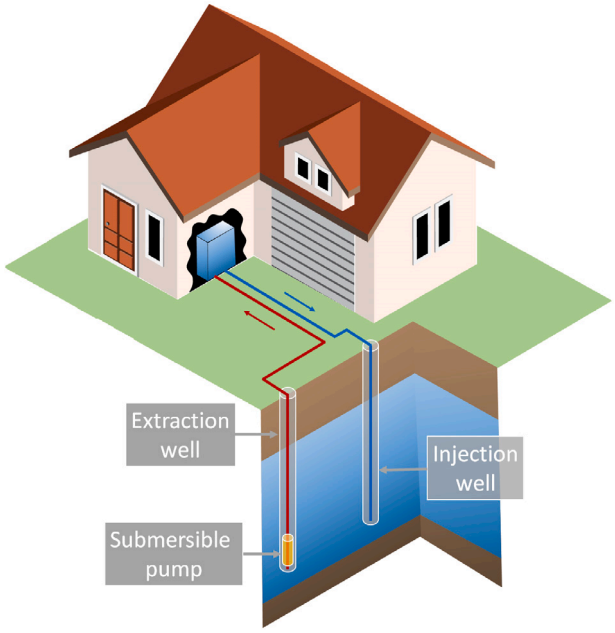

Fig. 1. Typical GWHP system with its main components.

while others combine multiple constraints to estimate the technical potential, i.e. technically feasible groundwater pumping rates, at a given spatial resolution. In general, their aim is to estimate the local geothermal potential, but not to optimize the technical potential. However, the geothermal potential can be maximized through strategic sizing and placement of well doublets within the considered area. As the thermal use of groundwater with well doublets induces hydraulic and thermal changes in the aquifer, each operating doublet consumes space and obstructs the installation of additional doublets. In the vicinity of wells, pumping may create a considerable drawdown and injection an upconing of groundwater, respectively. Especially in the planning stage of larger GWHP systems with multiple well doublets, a consideration of hydraulic influences is crucial for a sustainable well arrangement, as each well doublet leaves its own hydraulic footprint in the aquifer. These characteristics of multi-doublet systems have not been addressed in the existing potential assessment studies. This aspect is particularly important when the spatial planning level allows flexibility in the arrangement of doublets and associated wells. For instance, analyzing the geothermal potential for large GWHPs in the context of future 4GDH and 5GDHC systems requires determining the optimal size and placement of multiple wells simultaneously. To answer the question of optimal well count, sizing and placement in the potential assessment, it is necessary to integrate optimization methods into the analysis.

Halilovic et al. [20] recently reviewed optimization approaches for GWHP systems and concluded that there are only a few studies addressing the topic of optimal well placement and/or sizing. Some of the existing optimization approaches employ numerical groundwater simulation models and are therefore not suitable for integration into large-scale potential assessments due to their high computational costs [21–23]. In contrast, optimization approaches based on analytical models prove to be more suitable for such integration, as they generally require less computational cost while providing reasonably accurate and conservative estimates. To date, only one research study has implemented an optimization approach based on an analytical groundwater simulation model [24]. The approach uses the linear advective heat transport model (LAHM) to estimate thermal plumes caused by GWHPs [25]. The developed approach optimally places GWHPs and their associated wells in the considered area in order to minimize thermal interactions between the systems and simultaneously maximize the heat extracted from the groundwater, thereby

maximizing the spatial potential of thermal groundwater use. This optimization approach is promising for potential estimation studies and is already applied on city-scale supporting the municipal heat planning of Munich [24], but has certain limitations.

The main limitations of the approach proposed in Halilovic et al. [24] arise from the characteristics of the LAHM model, which assumes homogeneous groundwater conditions throughout the entire study area. Additionally, the approach does not consider any hydraulic aspects, such as pumping limits due to induced groundwater drawdowns in extraction wells and the resulting hydraulic footprint that prevents additional wells of the same type to be installed nearby. Furthermore, systems' pumping rates are predefined based on the estimated energy demand of the corresponding plots, which means that only the placement of the systems and their wells is optimized and their sizing remains unchanged. This makes the approach unsuitable for certain applications, such as potential analysis for large multi-doublet GWHPs in 4GDH and 5GDHC systems, since hydraulic constraints are crucial in this case. Therefore, there is a need for an optimization approach that accounts for aspects not covered in Halilovic et al. [24], particularly hydraulic constraints and spatial heterogeneity of groundwater parameters.

The main objective of this paper is to introduce a novel approach for maximizing the technical potential of thermal groundwater use. The proposed approach simultaneously optimizes the sizing and placement of doublets and associated wells within feasible areas, with the goal of maximizing the geothermal potential, i.e. the extracted heat from groundwater. To achieve this, the approach considers multiple important factors, including regulatory constraints, spatial heterogeneity of groundwater properties, and relevant hydraulic constraints. The latter includes considerations of drawdown in extraction wells, groundwater rise in injection wells, internal hydraulic breakthroughs, and spacing between adjacent well doublets based on their hydraulic footprints [26]. To effectively include these constraints, the method integrates analytical expressions for pumping rate limits from Böttcher et al. [19] into a mixed-integer linear optimization problem. This type of optimization problems is well established in the optimization community and can be solved efficiently with modern solvers [27]. The new approach provides a comprehensive and robust potential estimation, as demonstrated by using a real case study wherein the technical potential of thermal groundwater use of each city block of Munich is optimized.

The paper is organized as follows: Section 2 describes the methodology, followed by its implementation and a case study in Section 3. Section 4 presents and analyzes the results. Section 5 discusses the advantages, limitations and possible future improvements and applications of the approach. The paper concludes with a summary in Section 6.

2. Methodology

The proposed approach combines analytical expressions that describe groundwater pumping limits (Section 2.1) with mixed-integer linear programming techniques (Section 2.2) to optimize the placement and sizing of extraction–injection well doublets.

2.1. The thermal aquifer potential (TAP) method

Böttcher et al. [19] developed the Thermal Aquifer Potential (TAP) method to analyze the technical potential of thermal groundwater use in shallow phreatic aquifers. This method is based on empirical analytic formulas that describe the maximum pumping rates of a well doublet with respect to three different constraints: maximum drawdown in the extraction well, upconing threshold at the injection well, and hydraulic breakthrough between the two wells.

The TAP method estimates the maximum pumping rate of a doublet at the drawdown threshold q_d as follows [19]:

$$q_d = 0.195 \cdot K \cdot B^2, \tag{1}$$

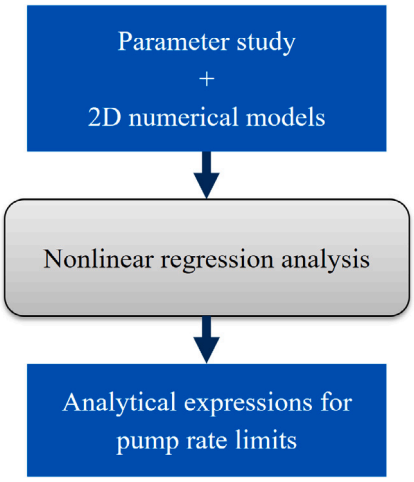

Fig. 2. Flowchart of the TAP method.

where K is the hydraulic conductivity and B is the saturated aquifer thickness. The considered threshold for drawdown is one-third of the saturated aquifer thickness as defined by the regulatory state of the art in Bavaria, Germany [19]. The maximum injection rate at the upconing (flooding) threshold q_f is estimated with [19]:

$$q_f = (h_{max} - h_n) \cdot K \cdot B^{0.798} \cdot \exp(29.9 \cdot \nabla h), \tag{2}$$

where h_{max} and h_n are the maximum allowed and the natural groundwater level, respectively, and ∇h is the hydraulic gradient. Finally, the TAP method calculates the maximum pumping rate at the hydraulic breakthrough threshold q_b of the well doublet using the following equation [19]:

$$q_b = \frac{\pi}{1.96} \cdot v_D \cdot B \cdot \Delta_{wells}, \tag{3}$$

where v_D is the Darcy velocity and Δ_{wells} is the internal distance between the extraction and injection well of the doublet. In this work, to simplify the description of the optimization problem in later sections, (3) is rewritten as follows:

$$q_b = \alpha \cdot \Delta_{wells}, \tag{4}$$

where $\alpha = (\pi/1.96) \cdot v_D \cdot B$ is the hydraulic breakthrough parameter of the considered well doublet. It should be noted that the TAP method does not consider thermal breakthrough directly, but only indirectly by considering hydraulic breakthrough. Since the hydraulic breakthrough occurs before the thermal one, its prevention will also prevent the internal thermal breakthrough [28]. The TAP method defines the technical pumping rate of a well doublet as the minimum of the three previously specified pumping rates q_d, q_f and q_b.

The analytical formulas (1)–(3) in the TAP method are derived from the results of numerical parameter studies using nonlinear regression analysis. Fig. 2 shows the overall flowchart of the TAP method. In the first phase, idealized 2D box models are prepared for numerical groundwater simulations in the parameter study. In this study, important parameters are varied within a reasonable range of values, and steady-state simulations are performed to gain conservative results. The extraction and injection wells are placed in the center of the 2D models parallel to the groundwater flow direction and at different distances from each other. Subsequently, the results of the numerical simulations from the parameter study are used in a nonlinear regression analysis to fit the analytical expressions (1)–(3).

In addition to the threshold pumping rates q_d, q_f, and q_b, the authors of the TAP method also analyzed the hydraulic footprint of a well doublet using idealized 2D models in a similar manner. This analysis is necessary for estimating technical potential because neighboring

systems limit the available water budget and therefore increase the likelihood of hydraulic breakthrough within the system if they are located too close. Thus, the authors determined a correlation between the percentage of cycled water (inter-flow) in a well doublet and the external–internal well distance ratio r_A, i.e. the ratio between the distance to neighboring doublets and the inner well spacing [19].

2.2. Optimization

An optimization procedure can be used to maximize the technical potential of thermal groundwater use through optimal placement and sizing of well doublets. The proposed optimization approach integrates the equations from the TAP method into a mixed-integer linear program (MILP) to maximize the thermal aquifer potential while satisfying technical and legal constraints. In MILP problems, the goal is to optimize a linear objective function subject to a set of linear constraints, where some of the optimization variables are integer and others are continuous. There are multiple powerful solvers for this type of optimization problems that can be readily applied [27]. The placement of doublets and their wells is based on a selection of predefined potential well locations, which are defined in a pre-processing step as described in the following.

2.2.1. Definition of potential well locations and doublets

In the pre-processing phase, potential well locations are determined taking into account ground plans of the existing buildings, legal constraints and groundwater flow direction in the considered area. To determine a feasible area for well placement, a minimum distance of 3 m between wells and buildings is maintained in the first step, by applying corresponding buffer zones (see Fig. 3(a)). Within this delineated area, potential wells are strategically positioned at the nodes of a virtual grid that is oriented according to the groundwater flow direction at the centroid of the corresponding polygon. The grid is designed with a constant well-to-well spacing, with one of its axes aligned with the groundwater flow direction and the other axis perpendicular to it. The grid is then divided into lines parallel to groundwater flow, which are denoted as doublet lines in Fig. 3(a), and wells are grouped based on the lines they lie on. The simplifying assumption of this procedure is that only wells placed on the same line are allowed to be installed as an extraction–injection well doublet for the potential multi-well system. This ensures that the installed wells are aligned with the groundwater flow direction, which is a prerequisite for applying the TAP method (see Section 2.1). The pre-processing step results in hydrogeologically and legally viable potential well locations, which are further used in the optimization procedure.

2.2.2. Optimization concept

As described previously, each line in Fig. 3(a) corresponds to one potential well doublet, i.e. one upstream extraction and one downstream injection well which are installed according to the groundwater flow direction. There are multiple potential well locations on each line and multiple potential doublets (lines) in a city block, which gives a high degree of freedom in the layout (installation) of a large multi-doublet system and the placement of its wells. In addition, the size of a doublet, i.e. its pumping rate, is interdependent with the well locations due to the hydraulic breakthrough limits. Therefore, an optimization procedure is required to determine the optimal combination of doublets to be installed in a city block, i.e. the size and placement of the doublets and the placement of the corresponding wells. The optimization concept is described below:

- the area of interest has a predefined number of potential well doublets (lines),
- each doublet (line) has a predefined number of potential well locations, which can be extraction or injection wells,
- for each potential doublet (line) there are two optimization variables: the binary variable d corresponding to the decision whether to install ($d = 1$) or not ($d = 0$) this doublet, and the continuous variable $q \in \mathbb{R}_0^+$ representing the pumping rate of the doublet,
- for each potential well location, there are two binary optimization variables: d_{ext} and d_{inj}, which represent the selection decision for the extraction and injection well, respectively,
- if an extraction well is installed (selected) at the considered well location, then $d_{\text{ext}} = 1$ and $d_{\text{inj}} = 0$, and vice versa, in case of an injection well, $d_{\text{ext}} = 0$ and $d_{\text{inj}} = 1$,
- if neither an extraction nor an injection well is selected at the considered potential well location, then $d_{\text{ext}} = d_{\text{inj}} = 0$,
- if the well doublet is installed ($d = 1$), one extraction well and one injection well is selected from the potential well locations on the corresponding line,
- if doublet is not installed ($d = 0$), all potential wells on that line are deselected.

Fig. 3(b) shows an example of a city block with two installed doublets and the placement (selection) of their wells. It is important to point out that the proposed approach does not consider thermal interactions between doublets, specifically the propagation of thermal plumes in groundwater induced by GWHPs. Therefore, the approach focuses on optimizing the technical potential of smaller areas (e.g. city blocks) separately and does not address the optimization of the spatial potential of multiple areas jointly. In the next section, further details on the relations between the optimization variables described previously, as well as on other optimization constraints, are provided.

2.2.3. Objective function and constraints

The optimization objective is to maximize the technical potential of thermal aquifer utilization in a city block, i.e. to maximize groundwater extraction by well doublets while meeting the corresponding technical and legal constraints. Thus, the objective function to be maximized is defined as:

$$q_{\text{total}} = \sum_{k=1}^{N} q_k \,, \tag{5}$$

where q_{total} is the total pumping rate of all doublets, q_k is the pumping rate of a single doublet k and N is the number of potential doublets. The maximization of the volume of extracted groundwater simultaneously maximizes the thermal energy exchange with the aquifer.

The problem also includes several optimization constraints related to the installation and operation of doublets and their wells. The first set of constraints ensures that only installed doublets can be operated:

$$q_k \leq q_{\text{max},k} \cdot d_k \quad \forall k \in S \,, \tag{6}$$

where $q_{\text{max},k}$ is the pre-computed maximum pumping rate of a doublet k and $S = \{1, \dots, N\}$ is the set of all potential well doublets. If a doublet is not installed ($d_k = 0$), it cannot pump groundwater ($q_k = 0$), otherwise its pumping rate is limited by $q_{\text{max},k}$, which is calculated in the pre-processing as follows:

$$q_{\text{max},k} = \min\left(\max_{j \in E_k} q_{\text{d},j}, \max_{i \in I_k} q_{\text{f},i}\right), \tag{7}$$

where $q_{\text{d},j}$ and $q_{\text{f},i}$ are the "threshold" pumping and injection rates from the TAP method, i.e. Eqs. (1) and (2), respectively, and E_k and I_k are the sets of all potential extraction and injection wells of the doublet k, respectively. Thus, $q_{\text{max},k}$ represents the minimum between the two: the maximum pumping rate of all potential extraction wells j, based on the drawdown threshold, and the maximum injection rate of all potential injection wells i, based on the upconing threshold, of the doublet k (see Section 2.1). This initial estimate of the theoretical upper bound for the pumping rates is used in the optimization constraints to reduce the exploratory design space and thereby speed up the overall optimization process.

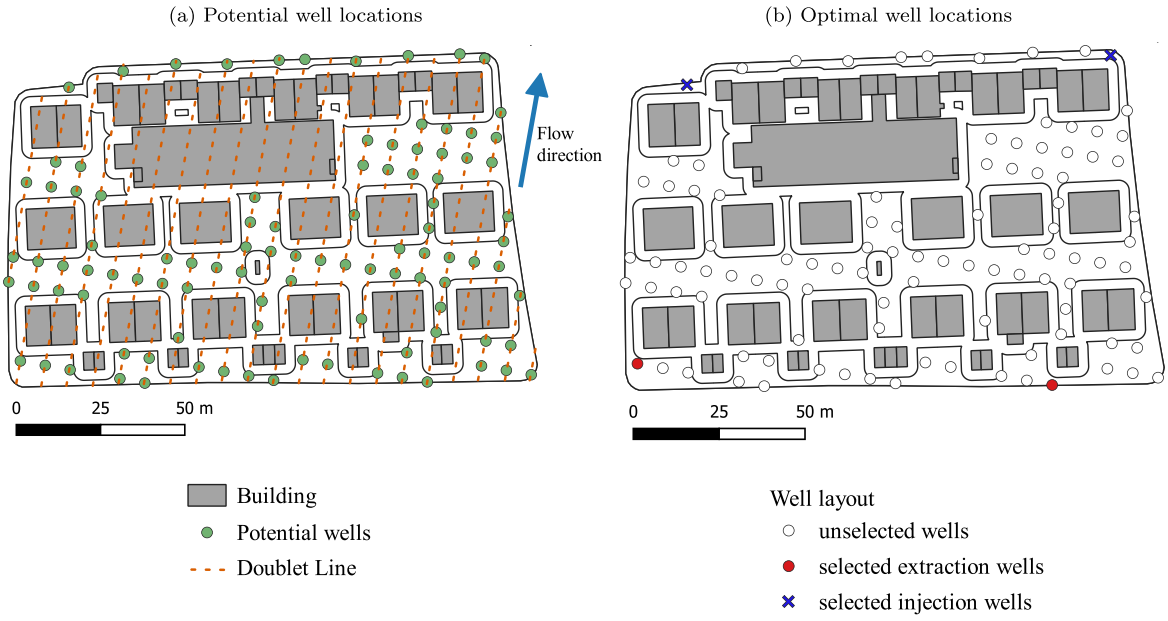

Fig. 3. Selection of optimal well locations: (a) Potential wells. (b) Optimal (selected) wells and corresponding doublets.

The second set of constraints specifies a minimum pumping rate for installed well doublets:

$$q_{\min} \cdot d_k \leq q_k \quad \forall k \in S\,, \tag{8}$$

where $q_{\min}$ is the predefined minimum pumping rate of a doublet. These constraints serve to prevent the installation of too small doublets, which are not economically viable in practice.

The third set of constraints corresponds to the fact that each doublet consists of a single extraction–injection well pair:

$$\sum_{i \in I_k} d_{\text{inj},i} = d_k \quad \forall k \in S\,, \tag{9}$$

$$\sum_{j \in E_k} d_{\text{ext},j} = d_k \quad \forall k \in S\,. \tag{10}$$

This also implies that the number of installed extraction and injection wells of the same doublet must be the same, i.e. 0 or 1, depending on whether the doublet is installed or not.

The next set of constraints are limitations on the pumping rates of well doublets based on the TAP method. The first group of such constraints ensures that none of the installed extraction wells (doublets) exceeds the drawdown threshold defined in the TAP method:

$$q_k \leq d_{\text{ext},j} \cdot q_{\text{d},j} + q_{\max,k} \cdot (1 - d_{\text{ext},j}) \quad \forall j \in E_k\,, \forall k \in S\,. \tag{11}$$

Depending on which extraction well j is selected ($d_{\text{ext},j} = 1$), the pumping rate q_k of the doublet is limited by the pumping rate at the drawdown threshold of this well $q_{\text{d},j}$. If the well j is not selected ($d_{\text{ext},j} = 0$), the constraint reads as $q_k \leq q_{\max,k}$, which should hold in any case. The form of the constraint (11) is necessary to ensure that only the selected extraction wells set an upper limit on the pumping rate based on the drawdown threshold. The other constraints in connection with the TAP method are formulated in a similar manner.

The second group of TAP-related constraints limits the injection rates based on the upconing threshold:

$$q_k \leq d_{\text{inj},i} \cdot q_{\text{f},i} + q_{\max,k} \cdot (1 - d_{\text{inj},i}) \quad \forall i \in I_k\,, \forall k \in S\,. \tag{12}$$

Similar to (11), these constraints enforce that the selected injection wells, and thus the corresponding doublets, do not exceed the upconing threshold.

The next group of TAP-related constraints ensures that an internal hydraulic breakthrough is prevented by limiting the doublet's pumping rate:

$$q_k \leq \alpha_{i,j} \cdot \Delta_{i,j} + q_{\max,k} \cdot (2 - d_{\text{ext},j} - d_{\text{inj},i}) \quad \forall j \in E_k\,, \forall i \in I_k\,, \forall k \in S\,, \tag{13}$$

where $\Delta_{i,j}$ is the distance between injection and extraction wells i and j, respectively, and $\alpha_{i,j} = (\alpha_i + \alpha_j)/2$ is the averaged hydraulic breakthrough parameter α of these two wells. The constraint (13) is activated, i.e. it becomes $q_k \leq \alpha_{i,j} \cdot \Delta_{i,j}$, only for the selected (i,j) well pair ($d_{\text{ext},j} = d_{\text{inj},i} = 1$). In all other cases, the constraint does not introduce additional, more stringent upper limits on the pumping rate q_k.

In addition to the relation between pumping rate and internal well distance defined by the constraint (13), the well placement must also comply with the regulatory minimum internal distance and the natural order (upstream-downstream) of well placement:

$$d_{\text{inj},i} + d_{\text{ext},j} \leq 1 \quad \text{if} \quad (\Delta_{i,j} < \Delta_{\min} \text{ or } \neg C_{i,j}) \quad \forall j \in E_k\,, \forall i \in I_k\,, \forall k \in S\,, \tag{14}$$

where $\Delta_{\min}$ is the defined regulatory minimum distance and $C_{i,j}$ is the relative well placement condition for the (i,j) well pair, which states that the injection well should be placed downstream relative to the extraction well. If the internal distance of the considered well pair (i,j) is smaller than $\Delta_{\min}$ or if the condition $C_{i,j}$ is not satisfied, these two wells cannot be installed together as a doublet. The regulatory distance $\Delta_{\min}$ between extraction and injection wells of the same doublet is defined to avoid hydraulic and thermal breakthroughs within the system [28]. This distance is 10 m in the case study (see Section 3.1), which is located in the German state of Bavaria [29].

The remaining optimization constraints address the spacing and sizing of neighboring doublets. The first group of such constraints guarantees sufficient distance between two neighboring doublets considering their hydraulic footprint derived from the TAP method. The pumping rates of two neighboring doublets k and p are limited based on their mutual distance $\Delta_{k,p}$ as follows:

$$\frac{q_k}{\tilde{\alpha}_k} + \frac{q_p}{\tilde{\alpha}_p} \leq \frac{2}{r_\Delta} \cdot \Delta_{k,p} + m_{k,p} \cdot (2 - d_k - d_p) \quad \text{if} \quad \chi_k + \chi_p > \frac{2}{r_\Delta} \cdot \Delta_{k,p} \quad \forall k, p \in S\,, \tag{15}$$

where: $\tilde{\alpha}_k$ and $\tilde{\alpha}_p$ are the hydraulic breakthrough parameters for the doublets k and p, respectively; $m_{k,p} = q_{\max,k}/\tilde{\alpha}_k + q_{\max,p}/\tilde{\alpha}_p$ is the interference parameter between these two doublets; χ_k and χ_p are the line lengths representing the doublets k and p, respectively, i.e. the maximum possible internal well distances for the doublets; and r_Δ is the previously defined external–internal well distance ratio. The hydraulic breakthrough parameter $\tilde{\alpha}$ for each doublet is defined as the median value of this parameter among all potential wells within that doublet. To reduce computational complexity and avoid excessive constraints, the constraint is applied only to pairs of potential doublets that are relatively close to each other, since mutual hydraulic influence is relevant in this case. The relative closeness of two doublets is determined by comparing their distance $\Delta_{k,p}$ with the averaged maximum possible internal well spacing of the doublets $(\chi_k + \chi_p)/2$, multiplied by the chosen external–internal spacing ratio r_Δ. If $\Delta_{k,p} \geq r_\Delta \cdot (\chi_k + \chi_p)/2$, the doublets are sufficiently far apart and the constraint (15) is not applied. Otherwise, the constraint is activated.

When the doublet pair (k, p) is installed, i.e. $d_k = d_p = 1$, the constraint (15) takes the following form:

$$\frac{q_k}{\tilde{\alpha}_k} + \frac{q_p}{\tilde{\alpha}_p} \leq \frac{2}{r_\Delta} \cdot \Delta_{k,p}\,, \tag{16}$$

which imposes a limit on the weighted sum of the pumping rates of the doublets based on their distance. The formulation of (16) is derived from the constraint for the internal hydraulic breakthrough of a doublet (13) and using the definition of the ratio r_Δ. In all other cases, i.e. when one or both doublets are not installed, the parameter $m_{k,p}$ ensures that the constraint (15) is always satisfied, thus avoiding the introduction of any additional limitations on the pumping rates.

The second set of constraints for neighboring doublets specifies a minimum distance between two installed doublets, which is determined by the regulatory internal distance $\Delta_{\min}$ between wells within the same doublet:

$$d_k + d_p \leq 1 \quad \text{if} \quad \Delta_{k,p} < r_\Delta \cdot \Delta_{\min} \quad \forall k, p \in S\,. \tag{17}$$

If the distance between two potential doublets is smaller than $r_\Delta \cdot \Delta_{\min}$, these doublets cannot be installed jointly. This constraint guarantees that neighboring doublets maintain an adequate spacing even for smaller doublet sizes (pumping rates), which is not addressed by the constraint (15).

Based on the previously defined objective function and constraints, the underlying optimization problem can be formulated as follows,

$$\max_{\boldsymbol{u}} \quad q_{\text{total}}(\boldsymbol{u}) \tag{18a}$$

$$\text{subject to} \quad \mathbf{g}_1(\boldsymbol{u}) = 0, \tag{18b}$$

$$\mathbf{g}_2(\boldsymbol{u}) \leq 0, \tag{18c}$$

where: $\boldsymbol{u}$ represents the vector of all optimization variables, which includes the binary variables $\boldsymbol{d}_{\text{ext}}$, $\boldsymbol{d}_{\text{inj}}$, $\boldsymbol{d}$ and the continuous variables $\boldsymbol{q}$; $\mathbf{g}_1$ represents all the equality constraints defined by (9) and (10); $\mathbf{g}_2$ represents all the inequality constraints defined by (6), (8), (11), (12), (13), (14), (15) and (17). The optimization problem (18) is a mixed-integer linear program that is solved independently for each city block, as described in the following.

3. Implementation

The introduced optimization approach is implemented using Python-MIP [30], an open-source package specifically designed for modeling and solving mixed-integer linear programs. The Python code, including a functional example, is freely available at [31]. Preprocessing of potential well locations and pumping rate limits is conducted in Python using geopandas and dependent libraries [32]. In the following sections, the case study area and the considered optimization scenarios are described.

3.1. Case study

The presented optimization approach is applied on a city block level in the entire city area of Munich (see Fig. 4). This means that the optimization problem (18) is formulated and solved for each city block, thereby optimizing the potential of each block independently from other blocks. The city block level is selected because it is aligned with the energy planning scale relevant to future 4GDH and 5GDHC systems. Munich offers favorable conditions for exploiting thermal energy from groundwater due to its location on a productive and shallow gravel aquifer. Extensive studies have been conducted to characterize key hydro-geological parameters, such as hydraulic conductivity, aquifer thickness, and groundwater flow direction, within the city area. Detailed information on these parameters are provided by Böttcher et al. [19] and Zosseder et al. [33].

In the pre-processing step (see Section 2.2.1), potential well locations are determined for each city block by initially using a constant distance of 5 m between wells. Due to the large area of some city blocks, this results in a high number of potential well locations in those blocks. Thus, to simplify the calculation and reduce computational time, an iterative approach is used to reduce the number of potential wells per city block. The constant distance between wells is iteratively increased by 2.5 m for each block until the number of potential wells within the block is reduced to 100 or less. Once the potential well locations are determined, the relevant values from the TAP method q_{d}, q_{f}, and α are calculated for each location using the available groundwater parameter data for the city of Munich. In addition, a filtering process is used during pre-processing to exclude potential well locations with limited potential. Specifically, potential wells with pre-calculated pumping rates at drawdown or upconing thresholds (q_{d} or q_{f}) below 1 [l/s] are removed. The value of 1 [l/s] is used in this work because the focus here is on large multi-well systems that can be used in 4GDH or 5GDHC systems. This process ensures that areas (blocks) lacking sufficient potential due to groundwater conditions are excluded from further analysis. The potential analysis (optimization) is then performed for the remaining 8751 city blocks of Munich, as shown in Fig. 4.

3.2. Optimization scenarios

In total, six distinct optimization scenarios were investigated, each representing different combinations of two parameters: the external–internal well distance ratio r_Δ and the predefined minimum pumping rate of an installed doublet $q_{\min}$. Three values were considered for r_Δ: 1.5, 2, and 3. These values correspond to about 10%, 5%, and 2.5%, respectively, of the inter-flow according to the TAP method (see Section 2.1). The last case, with $r_\Delta = 3$, is the most conservative and is characterized by the lowest level of interaction between neighboring doublets. These r_Δ values were paired with two values for $q_{\min}$: 1 and 5 [l/s]. In the latter case, the use of larger doublets, e.g. for 4GDH and 5GDHC grids, is particularly emphasized.

4. Results

The results obtained from the optimization scenarios are presented and analyzed in this section. Table 1 provides a summary of the results for all optimization scenarios introduced in Section 3.2. The table includes the following results: the total number of installed well doublets in the city of Munich, the maximum and mean number of installed doublets per city block, the average of pumping rates of the largest installed doublets in city blocks (i.e. the average of maximum pumping rates of installed doublets per city block), the mean value of pumping rates of all installed doublets (excluding non-installed doublets), the number of city blocks with and without installed doublets, the total installed pumping rate for the entire city, and the maximum and mean values of installed pumping rates per city block.

Fig. 4. Case study with considered city blocks.

Table 1
Results of the six optimization scenarios for the city of Munich.

Scenario		Nr. of installed doublets			Doublet pumping rates [l/s]		Nr. of blocks		Block pumping rates [l/s]		
q_{min} [l/s]	r_Δ	Total	Max	Mean	Average Max per block	Mean	With doublets	Without doublets	Total	Max	Mean
1	1.5	24 802	27	2.8	20.7	10.7	8232	519	274 149.2	971.4	31.3
	2	19 134	20	2.2	21.3	12.0	8232	519	241 056.5	762.8	27.5
	3	14 139	18	1.6	21.9	14.3	8232	519	212 419.2	639.7	24.3
5	1.5	14 255	23	1.6	26.2	17.4	6342	2409	256 201.4	971.4	29.3
	2	11 435	16	1.3	26.9	18.9	6342	2409	227 090.8	762.7	25.9
	3	8905	10	1.0	27.6	21.7	6342	2409	202 045.0	639.7	23.1

It is evident that scenarios with larger values of r_Δ and the same q_{min} have a smaller number of installed well doublets with larger capacities (pumping rates). At the same time, as the r_Δ value increases, the installed capacities per city block decrease. This result conforms with expectations, as these scenarios follow a more conservative approach that requires larger distances between neighboring doublets. Furthermore, for a given r_Δ, the maximum installed pumping rate per city block remains unchanged regardless of the q_{min} value. This shows that the city block with the highest installed capacity is identical in both q_{min} scenarios and does not contain any well doublets with capacities between 1 and 5 [l/s].

The number of city blocks with and without installed doublets remains constant for scenarios with the same q_{min} value. This is due to the fact that the parameter r_Δ controls the spacing between neighboring doublets and does not influence whether at least one single doublet is installed within a city block. From the scenarios with $q_{min} = 1$ [l/s] to $q_{min} = 5$ [l/s], the count of city blocks without installed doublets rises from 519 to 2409, respectively, of the total 8751 blocks considered. The difference of 1890 city blocks results from areas with low potential for thermal groundwater use mainly due to a lower groundwater thickness and corresponds to the blocks containing doublets with flow rates between 1 and 5 [l/s]. This observation is further evident in Fig. 5, which shows the optimized potential of GWHP systems for two scenarios: $q_{min} = 1$ [l/s], $r_\Delta = 2$ (top) and $q_{min} = 5$ [l/s], $r_\Delta = 3$ (bottom). The second scenario is more conservative, requiring more spacing between neighboring well doublets and considering only larger doublets, and this is also evident in the results (see Table 1). Moreover, the results show that certain city regions exhibit an extensive potential for the thermal use of groundwater, making them especially well suited for the use of large multi-well GWHPs in 4GDH or 5GDHC systems. Conversely, areas in the inner city zone and around the city river Isar (see Fig. 4) with lower potential for thermal groundwater use (marked in red colors) are also observed to be less suitable for larger GWHPs. These results are the consequence of unfavorable hydrogeologic conditions in the inner city zone, which were also observed in the original TAP publication [19].

Fig. 6 shows the statistical results for two optimization scenarios: $q_{min} = 1$ [l/s], $r_\Delta = 2$ and $q_{min} = 5$ [l/s], $r_\Delta = 2$. The figure depicts the distributions of installed capacities q_{block} and the number of installed doublets $n_{doublet}$ per city block, along with the correlation between these two variables. The distribution plots reveal that both parameters, q_{block} and $n_{doublet}$, mostly follow an exponential distribution pattern. This means that the frequency (count) of city blocks increases exponentially with decreasing capacity q_{block} and number of doublets $n_{doublet}$ installed per block. Moreover, the number of blocks with only one installed doublet is the highest, followed by blocks with two or no doublets, depending on the scenario. The scenario with $q_{min} = 5$ [l/s] contains more blocks without doublets compared to the scenario with $q_{min} = 1$ [l/s] because the first scenario excludes all blocks with only one doublet that has a capacity between 1 and 5 [l/s]. Similarly, due to the exclusion of smaller doublets in the first scenario, there are also fewer blocks in this scenario that contain a larger number of installed

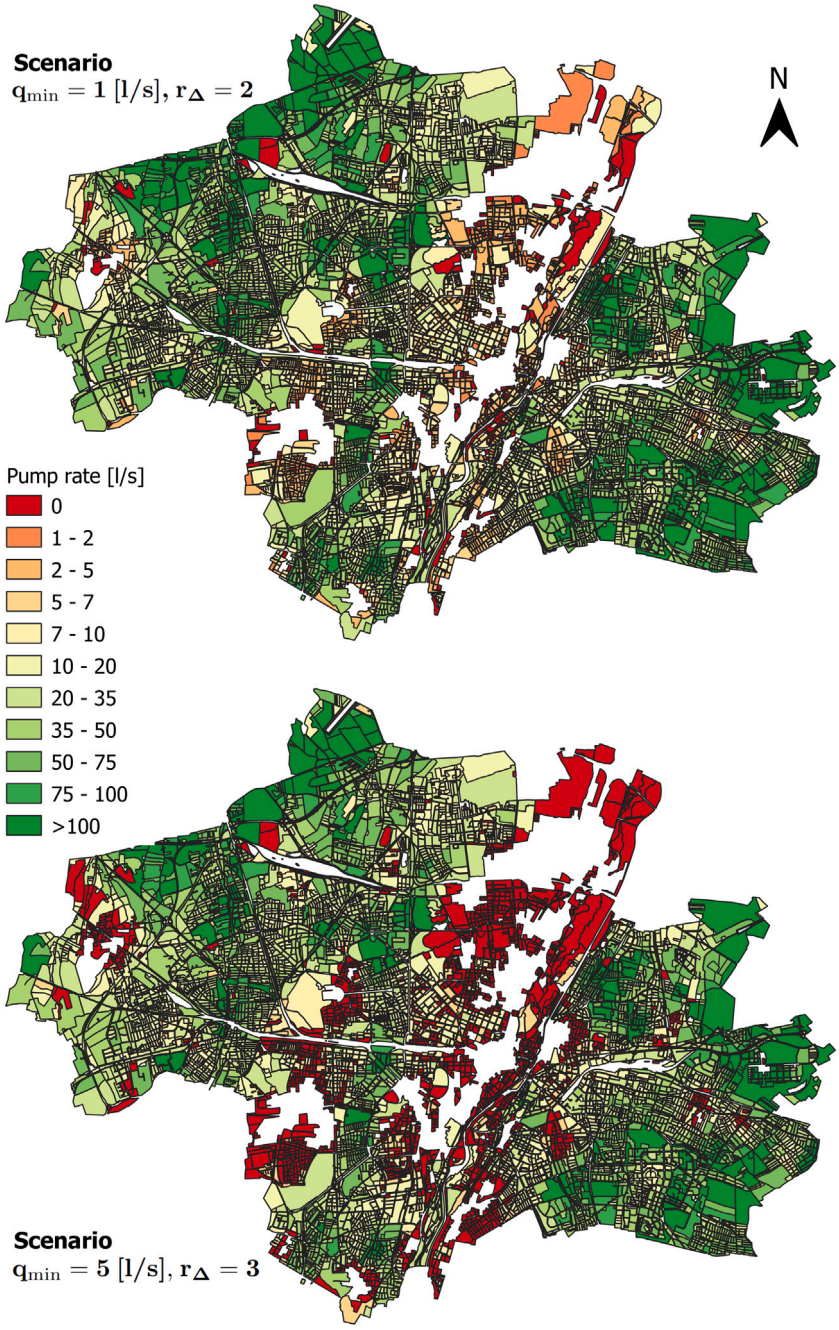

Fig. 5. Optimized pumping rates per city block for two scenarios $q_{min} = 1$ [l/s], $r_{\Delta} = 2$ (top) and $q_{min} = 5$ [l/s], $r_{\Delta} = 3$ (bottom).

doublets (e.g. 10 doublets per block). This is further supported by the central graph that illustrates the relationship between the number of doublets $n_{doublets}$ in a block and its capacity q_{block}.

Fig. 7 presents an example of the optimal positioning of well doublets in four city blocks. The optimal well arrangements for two scenarios are depicted: $q_{min} = 1$ [l/s], $r_{\Delta} = 2$ and $q_{min} = 5$ [l/s], $r_{\Delta} = 2$. As discussed previously, only larger doublets are included in the second scenario. Consequently, certain city blocks in the second scenario have fewer but larger doublets compared to the first scenario, as can be seen in Fig. 7.

5. Discussion and outlook

The presented optimization approach can effectively analyze the technical potential of thermal groundwater use by determining optimal arrangements of well doublets, their sizing, and well locations within the designated area. The approach can successfully quantify the maximum technically achievable groundwater pumping rate, and thus the exchanged thermal energy with the aquifer, taking into account relevant regulatory and hydraulic constraints. Moreover, the considered optimization scenarios demonstrate the approach's versatility through the selection of specific optimization parameters. For example, by increasing the ratio r_{Δ}, more conservative results are obtained, indicating reduced interaction between neighboring doublets. Similarly, selecting a larger value for the minimum capacity q_{min} focuses the analysis on large GWHP systems, which is particularly useful for investigating the potential for 4GDH and 5GDHC systems. The approach can also be used to study the potential of smaller systems, such as distributed GWHPs for individual households, by setting an upper threshold for the installed capacity of an individual well doublet. Therefore, the presented approach can serve as a valuable basis for

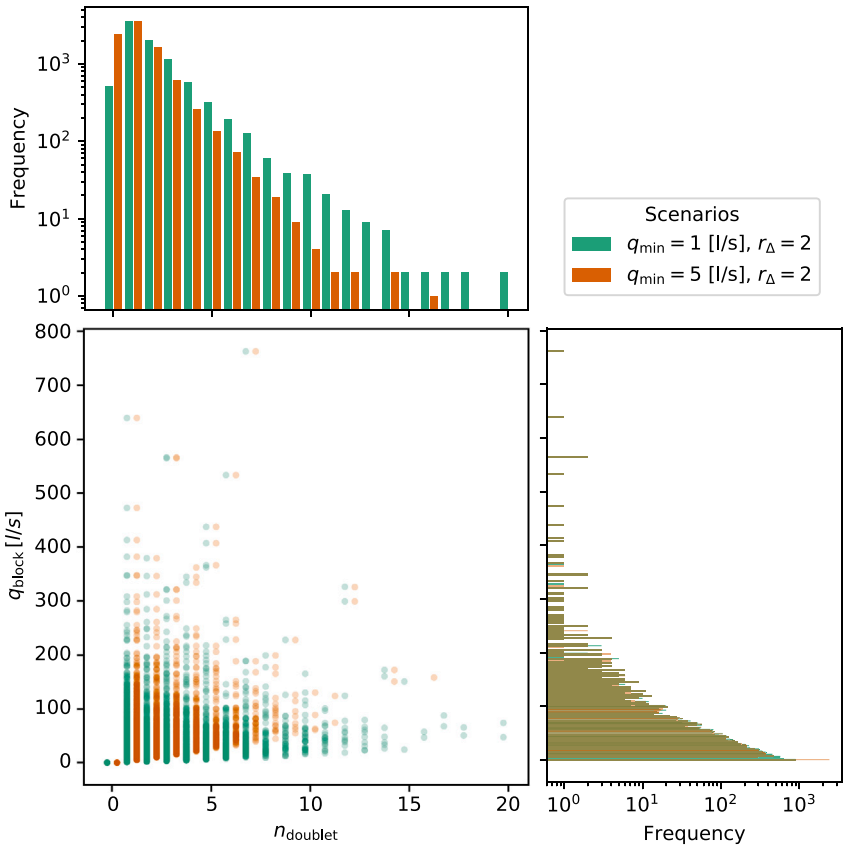

Fig. 6. Result comparison for two optimization scenarios.

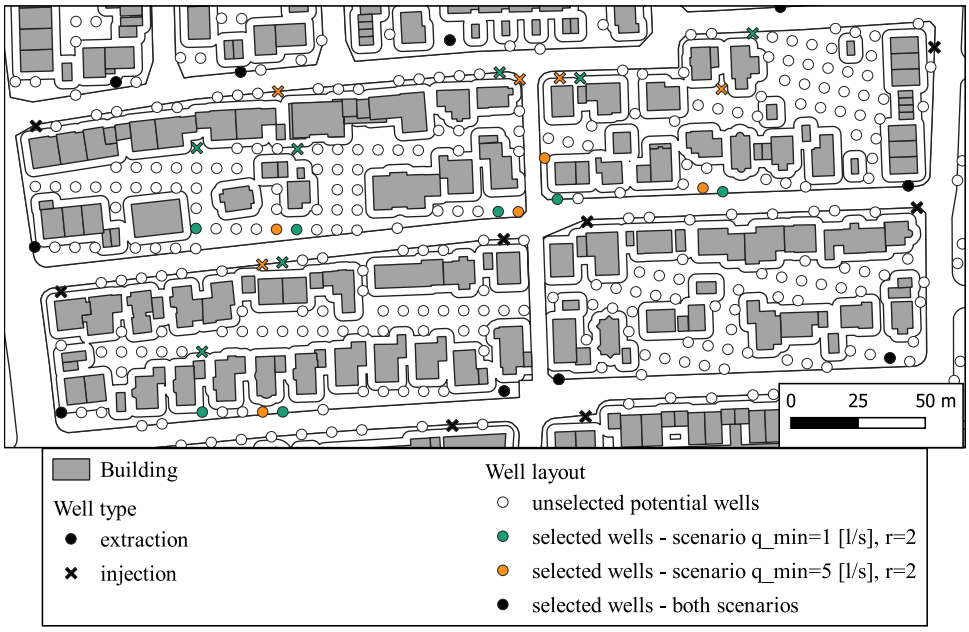

Fig. 7. Optimal well placement for two scenarios. It should be noted that the city blocks are optimized/considered separately and the figure shows several independent optimization results – one per city block – for both scenarios.

both thermal groundwater management and urban energy planning. The new approach offers several advantages over existing methods, including simultaneous optimization of well placement and size, consideration of spatial heterogeneity of groundwater parameters, and hydraulic constraints for determining optimal pumping rates. However, it has certain limitations, which are discussed in the following together with possible future improvements.

In this approach, the analytical formulas of the TAP method are incorporated into an optimization framework. As a result, certain limitations are inherited from the integration of the TAP method. The

first one is that the wells of a doublet are fully aligned with the groundwater flow direction. In reality, this need not be the case, as wells can be placed in various configurations, such as in the corners of a city block, without strictly following the groundwater flow direction. To address this limitation, one of the first future improvements is to extend the approach to such cases. This extension involves using new analytical expressions applicable to well pairs that are not aligned with groundwater flow direction.

The second limitation relates to having the same number of extraction and injection wells in a potential multi-well system. The proposed approach already provides flexibility in the design of multi-well systems because the doublets within a city block can be connected in different configurations. For example, multiple doublets can be combined into a larger system or several smaller single-doublet systems can be used. In practice, however, systems may have unbalanced combinations of extraction and injection wells due to hydrogeological conditions, such as one extraction well paired with two or more injection wells. Therefore, the approach can be further extended in the future to accommodate such scenarios.

It should be mentioned that the potential analysis study presented in this work did not consider existing systems within the city. Nevertheless, the approach presented is fully capable of including existing systems into the potential analysis. Including existing systems in the optimization problem (18) is a straightforward process. One method is to set the optimization variables of the installed systems and wells to constant values using equality constraints. In particular, binary decision variables can be set to 1, representing the presence of the installed wells, while capacities can be set to their actual installed capacity values. Alternatively, optimization variables for existing systems need not be used, and their values can be substituted directly into the associated constraints with corresponding constant numerical values. By using either of these methods, the approach can efficiently account for existing systems and contribute to a more comprehensive analysis of thermal aquifer potential.

Furthermore, as stated in Section 2.2.2, the proposed approach does not directly consider thermal anomalies in the groundwater. However, certain aspects related to heat transport are addressed indirectly within the optimization approach. First, the prevention of internal hydraulic breakthrough within each system is achieved by applying the constraint (13). Since thermal breakthrough normally occurs after hydraulic breakthrough, this constraint also ensures the prevention of internal thermal breakthrough [28]. Second, the constraints (15) and (17) ensure sufficient spacing between neighboring well doublets, accounting for the hydraulic footprint of each doublet. Additionally, a potential doublet is defined on each line within a city block, and additional doublets are installed on parallel lines that are aligned with the groundwater flow direction. This geometric arrangement of potential doublets within a city block, along with the required spacing between neighboring doublets, results in a lower possibility of mutual thermal interference. Consequently, the new approach indirectly accounts for thermal effects such as thermal breakthroughs or negative thermal interactions between neighboring doublets. This only holds true for every city block individually without considering interactions with neighboring blocks.

On the other hand, when jointly optimizing multiple neighboring city blocks, it is crucial to consider the propagation of thermal plumes, since upstream systems can directly affect downstream ones. To account for this, an analytical model for estimating thermal plumes can be incorporated into the proposed optimization approach. One possible solution is to combine our approach with optimization concepts from the study by Halilovic et al. [24], where the spatial potential is optimized using the LAHM analytical model for thermal plume estimations. By incorporating these thermal aspects into the optimization process, the approach can be extended to the combined optimization of large areas, such as several neighboring city blocks or entire city districts. Moreover, there is the potential to combine the approach with energy system optimization models (ESOMs) used for optimal planning of urban energy systems. For urban areas where thermal use of groundwater is a viable option, accurate representation of thermal potential in ESOMs is crucial [34], especially in the context of optimal planning of future 4GDH and 5GDHC systems. In general, potential analysis methods based on analytical formulas are more suitable for integration into ESOMs because they are significantly less computationally demanding and complex compared to methods based on numerical groundwater simulations [35].

Finally, the approach can be extended to cost-related considerations, allowing for a holistic analysis that addresses both economic and environmental aspects of energy planning. This is particularly relevant for large groundwater uses with multiple wells for heating or cooling, as drilling costs become a significant factor. The challenge is to find the optimal balance between fewer, more expensive wells with larger diameters and multiple wells with smaller diameters. Additionally, the proposed approach can be fully integrated into GIS-based online management and energy planning tools, such as the web tool developed as part of the GEO.KW project [36,37] .

6. Conclusion

This paper presents a novel approach for determining the optimal sizing and placement of well doublets, with the overall goal of maximizing the technical potential of thermal groundwater use, i.e. the volume of pumped groundwater. The approach incorporates regulatory conditions, spatial variability of groundwater parameters, and key hydraulic constraints into the potential assessment process. The considered hydraulic constraints ensure acceptable drawdown levels in extraction wells and groundwater rise in injection wells, prevention of internal hydraulic breakthroughs, and adequate spacing between neighboring doublets. Analytic expressions describing these hydraulic constraints are integrated into a mixed-integer linear optimization problem allowing efficient application to relatively large areas. The positioning of well doublets is based on the selection of predefined potential locations.

The proposed approach is applied to a real case study involving the optimization of the geothermal potential for each city block in Munich. To demonstrate the adaptability of the approach, six different optimization scenarios are used, differing in two parameters: the minimum capacity of a single installed doublet (1 and 5 [l/s]) and the external–internal well distance ratio (1.5, 2, and 3). The results prove the effectiveness and efficiency of the approach in identifying urban areas, or in this case city blocks, with favorable potential for large-scale GWHP systems as well as those unsuitable for such installations. Furthermore, the presented method provides comprehensive and optimized potential estimates that can be readily extended to other geographic locations. Thus, it is a valuable tool for thermal groundwater management and the integration of thermal groundwater potential into spatial energy planning, including the development of future 4GDH and 5GDHC systems. In addition, the method can provide valuable insights for well drilling and construction companies and housing associations. Finally, by coupling optimization techniques with potential analysis, the new method enables more thorough exploration and exploitation of the shallow geothermal potential, leading to an improved use of groundwater for heating and cooling purposes.

CRediT authorship contribution statement

Smajil Halilovic: Conceptualization, Formal analysis, Investigation, Methodology, Software, Visualization, Writing – original draft. **Fabian Böttcher:** Conceptualization, Data curation, Writing – review & editing. **Kai Zosseder:** Writing – review & editing. **Thomas Hamacher:** Supervision, Writing – review & editing.

Declaration of competing interest

The authors declare that they have no known competing financial interests or personal relationships that could have appeared to influence the work reported in this paper.

Data availability

Data will be made available on request.

Acknowledgments

No external funding was received for conducting this study. We would like to thank Jannis Epting for reviewing the paper and providing valuable comments that improved its quality.

References

[1] Lund JW, Toth AN. Direct utilization of geothermal energy 2020 worldwide review. Geothermics 2021;90:101915. http://dx.doi.org/10.1016/j.geothermics.2020.101915.
[2] Lund H, Werner S, Wiltshire R, Svendsen S, Thorsen JE, Hvelplund F, Mathiesen BV. 4Th generation district heating (4GDH): Integrating smart thermal grids into future sustainable energy systems. Energy 2014;68:1–11. http://dx.doi.org/10.1016/j.energy.2014.02.089.
[3] Boesten S, Ivens W, Dekker SC, Eijdems H. 5Th generation district heating and cooling systems as a solution for renewable urban thermal energy supply. Adv Geosci 2019;49:129–36. http://dx.doi.org/10.5194/adgeo-49-129-2019.
[4] Stauffer F, Bayer P, Blum P, Giraldo NM, Kinzelbach W. Thermal use of shallow groundwater. Boca Raton, Fla: CRC Press; 2014.
[5] Banks D. An introduction to thermogeology: ground source heating and cooling. John Wiley & Sons; 2012.
[6] Lee J-Y, Won J-H, Hahn J-S. Evaluation of hydrogeologic conditions for groundwater heat pumps: analysis with data from national groundwater monitoring stations. Geosci J 2006;10:91–9. http://dx.doi.org/10.1007/BF02910336.
[7] Busby J, Lewis M, Reeves H, Lawley R. Initial geological considerations before installing ground source heat pump systems. Q J Eng Geol Hydrogeol 2009;42:295–306. http://dx.doi.org/10.1144/1470-9236/08-092.
[8] Fry V. Lessons from London: regulation of open-loop ground source heat pumps in central London. Q J Eng Geol Hydrogeol 2009;42:325–34. http://dx.doi.org/10.1144/1470-9236/08-087.
[9] Schiel K, Baume O, Caruso G, Leopold U. GIS-based modelling of shallow geothermal energy potential for CO2 emission mitigation in urban areas. Renew Energy 2016;86:1023–36. http://dx.doi.org/10.1016/j.renene.2015.09.017.
[10] García Gil A, Garrido Schneider EA, Mejías Moreno M, Santamarta Cerezal JC. Management and governance of shallow geothermal energy resources. In: Shallow geothermal energy. Springer; 2022, p. 237–72.
[11] Epting J, Müller MH, Genske D, Huggenberger P. Relating groundwater heat-potential to city-scale heat-demand: A theoretical consideration for urban groundwater resource management. Appl Energy 2018;228:1499–505. http://dx.doi.org/10.1016/j.apenergy.2018.06.154.
[12] Epting J, Böttcher F, Mueller MH, García-Gil A, Zosseder K, Huggenberger P. City-scale solutions for the energy use of shallow urban subsurface resources – bridging the gap between theoretical and technical potentials. Renew Energy 2020;147:751–63. http://dx.doi.org/10.1016/j.renene.2019.09.021.
[13] Casasso A, Sethi R. Assessment and mapping of the shallow geothermal potential in the province of Cuneo (Piedmont, NW Italy). Renew Energy 2017;102:306–15. http://dx.doi.org/10.1016/j.renene.2016.10.045.
[14] Muñoz M, Garat P, Flores-Aqueveque V, Vargas G, Rebolledo S, Sepúlveda S, Daniele L, Morata D, Ángel Parada M. Estimating low-enthalpy geothermal energy potential for district heating in Santiago basin–Chile (33.5 °S). Renew Energy 2015;76:186–95. http://dx.doi.org/10.1016/j.renene.2014.11.019.
[15] García-Gil A, Vázquez-Suñe E, Alcaraz MM, Juan AS, Sánchez-Navarro JÁ, Montlleó M, Rodríguez G, Lao J. Gis-supported mapping of low-temperature geothermal potential taking groundwater flow into account. Renew Energy 2015;77:268–78. http://dx.doi.org/10.1016/j.renene.2014.11.096.
[16] Pujol M, Ricard LP, Bolton G. 20 Years of exploitation of the yarragadee aquifer in the perth basin of western australia for direct-use of geothermal heat. Geothermics 2015;57:39–55. http://dx.doi.org/10.1016/j.geothermics.2015.05.004.
[17] Arola T, Korkka-Niemi K. The effect of urban heat islands on geothermal potential: examples from quaternary aquifers in finland. Hydrogeol J 2014;22:1953–67. http://dx.doi.org/10.1007/s10040-014-1174-5.
[18] Arola T, Eskola L, Hellen J, Korkka-Niemi K. Mapping the low enthalpy geothermal potential of shallow quaternary aquifers in finland. Geotherm Energy 2014;2:1–20. http://dx.doi.org/10.1186/s40517-014-0009-x.
[19] Böttcher F, Casasso A, Götzl G, Zosseder K. Tap - thermal aquifer potential: A quantitative method to assess the spatial potential for the thermal use of groundwater. Renew Energy 2019;142:85–95. http://dx.doi.org/10.1016/j.renene.2019.04.086.
[20] Halilovic S, Böttcher F, Zosseder K, Hamacher T. Optimization approaches for the design and operation of open-loop shallow geothermal systems. 2023, http://dx.doi.org/10.48550/arXiv.2307.11244, arXiv preprint arXiv:2307.11244.
[21] Park D, Lee E, Kaown D, Lee S-S, Lee K-K. Determination of optimal well locations and pumping/injection rates for groundwater heat pump system. Geothermics 2021;92:102050. http://dx.doi.org/10.1016/j.geothermics.2021.102050.
[22] Park DK, Kaown D, Lee K-K. Development of a simulation–optimization model for sustainable operation of groundwater heat pump system. Renew Energy 2020;145:585–95. http://dx.doi.org/10.1016/j.renene.2019.06.039.
[23] Halilovic S, Böttcher F, Kramer SC, Piggott MD, Zosseder K, Hamacher T. Well layout optimization for groundwater heat pump systems using the adjoint approach. Energy Convers Manage 2022;268:116033. http://dx.doi.org/10.1016/j.enconman.2022.116033.
[24] Halilovic S, Böttcher F, Zosseder K, Hamacher T. Optimizing the spatial arrangement of groundwater heat pumps and their well locations. Renew Energy 2023;217:119148. http://dx.doi.org/10.1016/j.renene.2023.119148.
[25] Kinzelbach W. Numerische methoden zur modellierung des transports von schadstoffen im grundwasser. Oldenbourg; 1987.
[26] Clyde CG, Madabhushi GV. Spacing of wells for heat pumps. J Water Resour Plan Manage 1983;109:203–12. http://dx.doi.org/10.1061/(ASCE)0733-9496(1983)109:3(203).
[27] Vielma JP. Mixed integer linear programming formulation techniques. SIAM Rev. 2015;57:3–57.
[28] Banks D. Thermogeological assessment of open-loop well-doublet schemes: a review and synthesis of analytical approaches. Hydrogeol J 2009;17:1149–55. http://dx.doi.org/10.1007/s10040-008-0427-6.
[29] Bayerisches Landesamt für Umwelt. Planung und erstellung von erdwärmesonden: Lfu. 2012, URL: https://www.lfu.bayern.de/wasser/merkblattsammlung/teil3_grundwasser_und_boden/doc/nr_372.pdf.
[30] Santos HG, Toffolo TA. Mixed integer linear programming with python. 2020.
[31] Halilovic S, Böttcher F. Optimization of thermal groundwater use. 2023, http://dx.doi.org/10.5281/zenodo.10031559, URL: https://github.com/SHalilovic/Well-doublet-optimization.
[32] Jordahl K, den Bossche JV, Fleischmann M, Wasserman J, McBride J, Gerard J, Tratner J, Perry M, Badaracco AG, Farmer C, Hjelle GA, Snow AD, Cochran M, Gillies S, Culbertson L, Bartos M, Eubank N, maxalbert, Bilogur A, Rey S, Ren C, Arribas-Bel D, Wasser L, Wolf LJ, Journois M, Wilson J, Greenhall A, Holdgraf C, Filipe, Leblanc F. geopandas/geopandas: v0.8.1. 2020, http://dx.doi.org/10.5281/zenodo.3946761.
[33] Zosseder K, Kerl M, Albarrán-Ordás A, Gossler M, Kiecak A, Chavez-Kus L. Die hydraulischen grundwasserverhältnisse des quartären und des oberflächennahen tertiären grundwasserleiters im großraum münchen. Geol Bavar 2022;122. URL: https://www.bestellen.bayern.de/shoplink/91122.htm.
[34] Halilovic S, Odersky L, Hamacher T. Integration of groundwater heat pumps into energy system optimization models. Energy 2022;238:121607. http://dx.doi.org/10.1016/j.energy.2021.121607.
[35] Halilovic S, Odersky L, Böttcher F, Davis K, Schulte M, Zosseder K, Hamacher T. Optimization of an energy system model coupled with a numerical hydrothermal groundwater simulation. In: Mapping the energy future-voyage in uncharted territory-, 43rd IAEE international conference, July 31-August 3, 2022. International Association for Energy Economics; 2022.
[36] Zosseder K, Böttcher F, Davis K, Haas C, Halilovic S, Hamacher T, Heller H, Odersky L, Pauw V, Schramm T, and SM. Des geothermischen speicherpotenzials mit den wechselnden anforderungen des urbanen energiebedarfs zur effizienten nutzung der regenerativen energiequelle grundwasser für die dezentrale kälte- und wärmebereitstellung in der stadt. Technical report, Bundesministerium für Wirtschaft und Klimaschutz; 2022, http://dx.doi.org/10.14459/2022md1692003.
[37] Böttcher F, Davis K, Halilovic S, Odersky L, Pauw V, Schramm T, Zosseder K. Optimising the thermal use of groundwater for a decentralized heating and cooling supply in the city of Munich, Germany. 2021, http://dx.doi.org/10.5194/egusphere-egu21-14929.

4.3 PDE-based optimization

This section is dedicated to the PDE-based optimization of GWHP systems, which involves the use of PDE (numerical) models to simulate groundwater flow and heat transport within an aquifer. The theoretical background for this section regarding numerical groundwater simulation models and PDE-constrained optimization is provided in Sections 2.1.2 and 2.2, respectively. The section includes the last publication of this thesis, **Publication 5** [100], which presents a novel PDE-constrained optimization framework for GWHPs, hereafter referred to as Approach III. This approach uses the adjoint method to efficiently obtain the required gradients for optimization. Consequently, it falls into Class I of the classification scheme presented in Section 4.1, as shown in Figure 4.2.

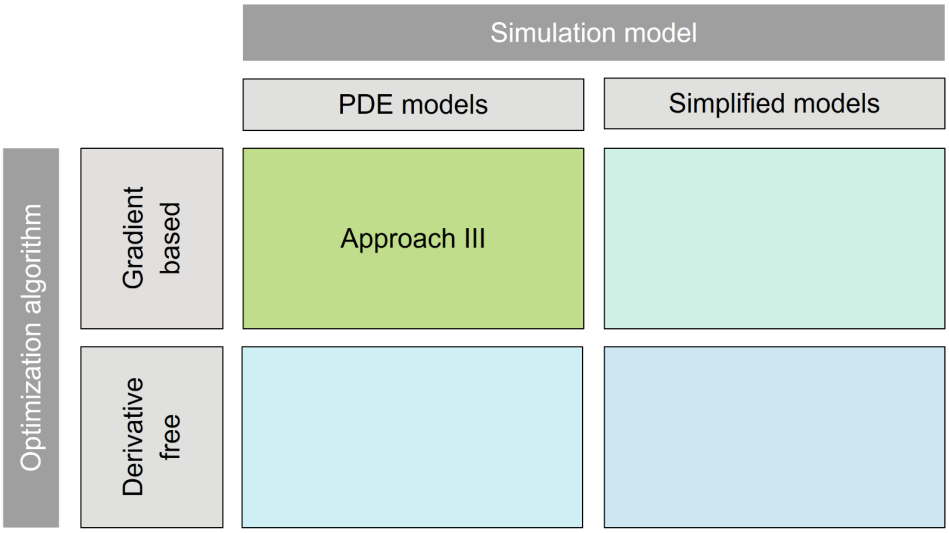

Figure 4.2 Approach III in the classification scheme from Section 4.1

Approach III can effectively determine optimal well placements for multiple neighboring GWHP systems concurrently, with the goal of maximizing the efficiency of all of these systems while minimizing the negative thermal interactions between them. In contrast to Approaches I and II presented in the previous section, Approach III allows for the placement of GWHP wells at any location within a feasible area, rather than being limited to predefined discrete locations. In addition, Approach III can account for various complexities present in aquifers because of its use of a numerical groundwater simulation model. It is therefore particularly suitable for detailed design and optimization of GWHP systems. The applicability of the approach is demonstrated using a real case study comprising 10 neighboring GWHP systems.

Publication 5 - Well layout optimization for groundwater heat pump systems using the adjoint approach

Authors: Smajil Halilović, Fabian Böttcher, Stephan C. Kramer, Matthew D. Piggott, Kai Zosseder, Thomas Hamacher

Journal: Energy Conversion and Management (Elsevier)

Status: Published - September 2022

Digital object identifier: https://doi.org/10.1016/j.enconman.2022.116033

Author	Contribution
Smajil Halilović	Conceptualization, Methodology, Writing - original draft, Software, Investigation, Visualization
Fabian Böttcher	Conceptualization, Writing - original draft, Data curation, Visualization
Stephan C. Kramer	Methodology, Software, Writing - reviewing and editing
Matthew D. Piggott	Methodology, Writing - reviewing and editing
Kai Zosseder	Funding acquisition, Writing - reviewing and editing
Thomas Hamacher	Funding acquisition, Supervision

Energy Conversion and Management 268 (2022) 116033

Contents lists available at ScienceDirect

Energy Conversion and Management

journal homepage: www.elsevier.com/locate/enconman

Well layout optimization for groundwater heat pump systems using the adjoint approach

Smajil Halilovic [a,*], Fabian Böttcher [b], Stephan C. Kramer [c], Matthew D. Piggott [c], Kai Zosseder [b], Thomas Hamacher [a]

[a] Technical University of Munich, Chair of Renewable and Sustainable Energy Systems, Germany
[b] Technical University of Munich, Chair of Hydrogeology, Germany
[c] Imperial College London, Department of Earth Science and Engineering, United Kingdom

ARTICLE INFO

Keywords:
Optimization
Well layout
Heat pump
Groundwater
Adjoint

ABSTRACT

Groundwater heat pump systems cause thermal anomalies in the aquifer that can impact upon downstream systems and reduce their efficiency. Therefore, it is important to optimally position the extraction and injection wells of such systems to avoid negative interactions and maximize the thermal potential of the aquifer. This paper presents a new method to determine optimal well layouts of groundwater heat pumps using the adjoint approach, which is an efficient way to solve the underlying PDE-constrained optimization problem. An integral part of the method is the numerical groundwater simulation, which here is based on the finite element method. In addition, a multi-start initialization strategy is introduced in an attempt to better reach the global optimum. The method is applied to a real case study with 10 groundwater heat pumps, i.e. 20 wells, and two optimization scenarios with different natural groundwater temperatures. In both scenarios, the optimization method successfully determines a well layout that maximizes groundwater temperatures at all extraction wells. Comparing the results from these scenarios demonstrates that hydro-geological conditions can have a significant impact on the optimal well layout. The proposed method is equally applicable to systems with multiple extraction and injection wells and can be extended to various other shallow geothermal applications, such as combined heating and cooling systems.

1. Introduction

The European Union has set itself the goal of being climate neutral by 2050 [1]. This implies the decarbonization of all energy-related sectors, including residential heating and cooling. One of the key technologies to decarbonize this sector are heat pumps [2], as they use renewable resources, are highly efficient and can provide additional flexibility to the electricity system [3]. In particular, shallow geothermal heat pumps are gaining in importance due to their higher efficiency compared to air–water heat pumps [4].

Groundwater heat pumps (GWHPs), along with ground source heat pumps, are one of two main types of geothermal heat pumps. GWHPs are open-loop systems, which means that they use heat directly from the groundwater and, in contrast to closed-loop systems, do not require any additional heat carrier fluid. Residential GWHP systems usually have a single pair of wells in which the groundwater is pumped from the extraction well and, after the energy (heat) exchange, the cooled water is returned into the same aquifer at the injection well. The returned water causes thermal anomalies, so-called thermal plumes, which spread in the aquifer according to the natural groundwater flow direction and can reach neighboring downstream GWHP systems [5]. Potential negative interaction events such as this must be avoided because the efficiency of GWHPs depends significantly on the groundwater temperature [6].

On the other hand, urban areas have high shallow geothermal potential, since ground temperatures are anthropologically elevated by the subsurface urban heat island (SSUHI) effect [7,8]. Therefore, in addition to being a climate-friendly technology, there is an incentive to install more GWHP systems in urban areas due to the potentially increased efficiency and the need to mitigate further groundwater temperature rise. However, an increased number of GWHPs can lead to negative interactions between neighboring systems. In order to avoid such negative effects, an optimal management of the resource is required [9]. GWHP systems can be carefully positioned in an attempt to minimize any negative interactions, i.e. to maximize the efficiency of all systems, and at the same time to maximize the shallow geothermal potential of a specific region.

* Corresponding author.
E-mail address: smajil.halilovic@tum.de (S. Halilovic).

https://doi.org/10.1016/j.enconman.2022.116033
Received 4 April 2022; Received in revised form 25 June 2022; Accepted 18 July 2022
Available online 1 August 2022

Nomenclature

Latin letters

$\mathbf{A}$	Coefficient matrix of constraints
a, b	Coefficients of linear constraints
B	Saturated aquifer thickness [m]
$\mathbf{b}$	Coefficient vector of constraints
C_{m}	Volumetric heat capacity of medium [J/m^3 K]
C_{w}	Volumetric heat capacity of water [J/m^3 K]
D	Feasible area for wells
d	Distance [m]
$\mathbf{D}_{\mathrm{mech}}$	Tensor of mechanical dispersion [m^2/s]
d_R	Regulatory distance [m]
$\mathcal{F}$	Residual of equations
f_μ	Viscosity relation function [–]
f^{B}	Aquifer bottom [m]
G	Penalty field
g	Inequality constraints
h	Hydraulic head [m]
h_{n}	Natural groundwater head [m]
$\mathbf{I}$	Unity or identity matrix [–]
J	Functional of interest
$\hat{J}$	Reduced functional of interest
$\mathbf{K}$	Tensor of hydraulic conductivity [m/s]
$\boldsymbol{m}$	Design/control variables
N	Number of heat pumps
N^{cst}	Number of constraints
n_{iter}	Number of optimization iterations
p	Penalty function
P_R, P_T	Penalty terms
$\overline{P}_{\mathrm{t}}$	Depth integrated heat source/sink terms [W/m^2]
$\mathbf{q}$	Darcy velocity [m/s]
$\overline{Q}$	Depth integrated liquid source/sink terms [m/s]
q	Pumping rates [m^3/s]
R	Restricted area for wells
r	Radius of approximate delta function [m]
r^{p}	Radius of restricted area [m]
S_0	Aquifer storativity [1/m]
T	Groundwater temperature [K]
t	Time [s]
T^{inj}	Temperature of reinjected water [K]
$\boldsymbol{u}$	State variables
V_{norm}	Normalization volume [m^3]
$\mathbf{x}^{\mathrm{ext}}$	Coordinates of extraction wells [m]
$\mathbf{x}^{\mathrm{inj}}$	Coordinates of injection wells [m]
$\mathbf{x}^{\mathrm{p}}$	Coordinates of penalty center [m]

Greek letters

α, γ	Penalty scaling factors [–]
β_L	Longitudinal dispersivity [m]
β_T	Transverse dispersivity [m]
$\boldsymbol{\varphi}$	Adjoint variables
δ	2D Dirac delta function [1/m^2]
Λ	Coefficient of thermal conductivity of liquid [J/m K s]
Λ^s	Coefficient of thermal conductivity of solid [J/m K s]
$\mathbf{\Lambda}$	Tensor of hydrodynamic thermodispersion [W/m K]
Ω	Computational domain
$\partial\Omega$	Domain boundary
ψ	Approximate delta function [1/m^2]
ε	Porosity [–]
ε_e	Specific yield [–]

Subscripts and superscripts

ext	Extraction
inj	Injection
in	Inflow
min	Minimum
i, j	Counters

A few research studies discuss negative interactions between GWHPs and their connection to the shallow geothermal potential. Attard et al. [10] introduced a new concept to prevent thermal interference between neighboring GWHPs based on thermal protection perimeters, which are defined around existing GWHPs. These protection zones ensure minimum distances between new and existing systems in order to avoid negative interactions. On the other hand, García-Gil et al. [11] proposed a new management policy for GWHPs based on numerical models and a relaxation factor. The factor ensures that part of the geothermal potential is available for future GWHP systems and thus prevents its monopolization. Epting et al. [12] presented a method for evaluating the theoretical and technical shallow geothermal potential on an urban scale. The technical potential is based on the TAP method (Thermal Aquifer Potential) [13], which takes into account the legal and operational framework conditions for GWHPs. However, possible negative thermal interactions between neighboring GWHPs are not part of the TAP method and are therefore only qualitatively discussed in [12]. None of these studies consider any optimization method, but there is a clear need for such methods to maximize the shallow geothermal potential through optimal placement of GWHP systems, i.e. their wells.

In general, well placement is important for a single GWHP system to avoid hydraulic and thermal breakthroughs [14] within the system, but optimal well placement can also be used to reduce negative interactions with neighboring systems. However, while there exist several research studies on the optimization of borehole heat exchanger (BHE) fields [15,16], there is still a lack of research on the optimization of well layouts for GWHPs. Most of the existing studies only use simulation methods to analyze a few possible spatial patterns of wells. Zhou and Zhou [17] numerically simulated a GWHP with one well doublet using several different spacings between wells (20–100 m) and cooling load variations (±20%). Gao et al. [18] performed a numerical investigation of four different predefined well configurations of a single GWHP system. Similarly, Lo Russo and Civita [19] compared five exploration scenarios to find a suitable design, including the spatial pattern of extraction and injection wells, for a GWHP serving a large commercial building. All previously described scenario (simulation) based designs of well layouts have two major drawbacks: only inferior designs are found compared to the fully optimized designs, and additional manual work is required for each new system to define suitable scenarios. More recently, Park et al. [20] developed a simulation–optimization model to find optimal pumping rates of a GWHP system. Their approach is based on the coupling of a numerical groundwater simulator with a genetic optimization algorithm. Park et al. [21] further developed this model to

determine optimal well locations and pumping rates of a single GWHP. Optimal well locations are found in such a way that the extraction well is fixed and the injection well is optimally selected from a set of predefined locations. The existing methods either evaluate only a relatively small number of predefined well layouts using simulation scenarios [17–19], or, due to the underlying optimization method, enable optimization over a small number of discrete (predefined) well positions [21]. As a result, possible well layout designs are not fully explored, i.e. only sub-optimal well positions are determined, which can reduce the efficiency and lifespan of GWHPs. Furthermore, research so far has only focused on finding optimal well locations for a single GWHP system, but has not considered the case of multiple GWHPs in order to reduce their mutual negative interactions and thus maximize the geothermal potential of a given area. Therefore, existing methods have several limitations and are not suitable to fully optimize well layouts of GWHP systems, especially in cases where multiple wells need to be optimized simultaneously.

The main objective of this paper is to introduce a new method for optimizing well layouts of GWHP systems that closes the previously identified research gaps. The new method is a significant improvement over existing methods because both a continuous variation and large numbers of well locations can be considered within the optimization procedure. In addition, the newly proposed method can optimize well locations of multiple systems simultaneously, since the number of optimized wells is not a limiting factor. The underlying method is a gradient-based optimization and relies on an efficient computation of gradients using the adjoint approach. As an integral part of this optimization concept, the numerical simulation of the groundwater flow and heat transport is performed using the finite element method (FEM). The applicability of the method is demonstrated using a case study where negative interactions between several neighboring GWHP systems are minimized, i.e. wells are placed to maximize groundwater temperatures at all extraction wells. It should be emphasized that the method can also be directly applied to find optimal well arrangements of individual systems.

The paper is structured as follows. Section 2 describes the methodology, i.e. the new optimization method. Section 3 provides information about the implementation of the method, as well as the selected case study, followed by the results, which are presented and analyzed in Section 4. In Section 5, limitations and possible improvements of the method, including future applications, are discussed. Finally, Section 6 provides conclusions for this work.

2. Methodology

The methodology can be divided into two parts: simulation and optimization. The forward simulation (Section 2.1) is a numerical calculation to evaluate a specific well layout, i.e. to calculate the corresponding thermal and hydraulic groundwater conditions. The optimization (Section 2.2), on the other hand, finds the best (optimal) well layout for a given objective, such as maximizing the temperatures at the extraction wells.

2.1. Forward simulation model

To analyze the impacts of GWHPs on an aquifer, a forward model describing flow and heat transport in the groundwater (porous media) is required. This simulation model can be formulated as a system of coupled partial differential equations (PDEs), which reads as follows [22]:

$$(BS_0 + \varepsilon_e)\frac{\partial h}{\partial t} + \nabla \cdot (B\mathbf{q}) = \overline{Q}, \tag{1a}$$

$$\mathbf{q} = -\mathbf{K} f_\mu \cdot \nabla h, \tag{1b}$$

$$B = h - f^{\mathrm{B}}, \tag{1c}$$

$$BC_{\mathrm{m}}\frac{\partial T}{\partial t} - \nabla \cdot (B\mathbf{\Lambda} \cdot \nabla T) + BC_{\mathrm{w}}\mathbf{q} \cdot \nabla T = \overline{P}_{\mathrm{t}}. \tag{2}$$

The given PDE system describes 2D vertically averaged, i.e. horizontal, flow and heat transport in an unconfined aquifer. The first set of Eqs. (1) represents flow in porous media, whereas the third PDE (2) represents heat transport in porous media, written here in convective form. All symbols from the PDE system are described in the nomenclature. The physical meaning of the PDEs as well as the modifications and assumptions used in this work are described in the following.

The first PDE (1a) corresponds to the mass conservation law, where the hydraulic head h and the Darcy velocity $\mathbf{q}$ are dependent variables. The aquifer's thickness B is defined as a difference between h and the bottom of the aquifer f^{B}. The term $\overline{Q}$ represents the depth integrated liquid source/sink terms. In this work, it is assumed that the only source and sink terms correspond with the wells of GWHPs, i.e. $\overline{Q} = \sum_{i=1}^{N} \overline{Q}_i$, where $\overline{Q}_i$ is the source/sink term of the GWHP i, with N the number of GWHPs. Furthermore, it is assumed that each GWHP has two wells: an extraction well (sink term) and an injection well (source term). Wells can be modeled (idealized) with well-type singular point sinks or sources at their locations $\mathbf{x}_i = (x_i, y_i) \in \mathbb{R}^2$ [22]. Based on this, for each GWHP i:

$$\overline{Q}_i = q_i(t)\delta(\mathbf{x} - \mathbf{x}_i^{\mathrm{inj}}) - q_i(t)\delta(\mathbf{x} - \mathbf{x}_i^{\mathrm{ext}}), \tag{3}$$

where $q_i(t)$ is the pumping rate of the GWHP, and "inj" and "ext" stand for injection and extraction, respectively.

The second PDE (1b) represents Darcy's law, which has the same dependent variables as (1a). The PDEs (1a)–(1b) can be solved simultaneously or sequentially by introducing (1b) into (1a). To simplify the computation, the second approach is followed in this work, where the unknown h is computed first and thereafter $\mathbf{q}$ is obtained directly from (1b). Moreover, to linearize (1a) and reduce computational costs, the effect of wells on the saturated aquifer's thickness B is neglected, i.e. it is assumed that B only depends on the natural groundwater head h_{n}:

$$B = h_{\mathrm{n}} - f^{\mathrm{B}}. \tag{4}$$

This is an acceptable assumption since the GWHP systems considered in this work are relatively small and have low pumping rates, which leads to low groundwater depression cones. It should be noted that the effects of wells on the state h are still taken into account in the PDEs, and are only neglected in the term B used for vertical averaging.

The third PDE (2) describes the heat transport in a two-phase (liquid and solid) medium, i.e. groundwater. The main dependent variable here is the groundwater temperature T, whereas other terms are constant parameters or solutions from the previous PDEs. The second term in (2) describes the heat conduction and dispersion, and the third term the thermal advection, respectively. The parameter $\mathbf{\Lambda}$ in the second term is the hydrodynamic thermal dispersion, which can be calculated using the following equations [22]:

$$\mathbf{\Lambda} = (\varepsilon \Lambda + (1 - \varepsilon)\Lambda^s)\mathbf{I} + C_{\mathrm{w}}\mathbf{D}_{\mathrm{mech}}, \tag{5}$$

$$\mathbf{D}_{\mathrm{mech}} = \beta_T \|\mathbf{q}\|\mathbf{I} + (\beta_L - \beta_T)\frac{\mathbf{q} \otimes \mathbf{q}}{\|\mathbf{q}\|}, \tag{6}$$

with symbols' descriptions given in the nomenclature. The term $\overline{P}_{\mathrm{t}}$ in (2) represents vertically averaged heat sink/source terms. In this work, it is assumed that the only heat sinks/sources correspond with the wells of GWHPs, i.e. $\overline{P}_{\mathrm{t}}$ is given by:

$$\overline{P}_{\mathrm{t}} = \sum_{i=1}^{N} q_i(t) C_{\mathrm{w}} [T_i^{\mathrm{inj}}(t) - T]\delta(\mathbf{x} - \mathbf{x}_i^{\mathrm{inj}}), \tag{7}$$

where $T_i^{\mathrm{inj}}(t)$ is the temperature of re-injected water at the injection well of GWHP i. It should also be noted that since the energy exchange only takes place at injection wells of GWHPs, only the injection wells appear as heat sinks in (7).

The flow PDEs (1) and the heat transport PDE (2) are coupled only in one direction. Hence, they can be solved sequentially, first the flow problem, and then the heat problem. Strictly speaking this

is not realistic as the water density and hydraulic conductivity also depend on the temperature of the groundwater. However, neglecting these dependencies simplifies the problem significantly and is a reasonable assumption for the considered application since temperature differences occur over a small range of approximately 5 K [23]. Finally, it should be emphasized that in this initial work only the steady state is considered within the optimization process. Thus, all the time dependent components in the previously described system of PDEs are discarded. This means that the PDEs (1a) and (2) take the following form:

$$\nabla \cdot (B\mathbf{q}) = \overline{Q}, \tag{8}$$

$$-\nabla \cdot (B\boldsymbol{\Lambda} \cdot \nabla T) + BC_{\mathrm{w}}\mathbf{q} \cdot \nabla T = \overline{P}_{\mathrm{t}}, \tag{9}$$

whereas (1b) remains the same.

2.2. Optimization

The optimization objective is to maximize the groundwater temperatures at extraction wells of GWHPs, since the efficiency of GWHPs increases with increasing groundwater temperature at those wells. The underlying problem can be described as a PDE-constrained optimization (PDECO) problem, since the groundwater flow and heat transport are modeled with the previously described system of PDEs. In general, PDECO problems can be formulated as follows:

$$\min_{\boldsymbol{u},\boldsymbol{m}} \quad J(\boldsymbol{u},\boldsymbol{m}), \tag{10a}$$

$$\text{subject to} \quad \mathcal{F}(\boldsymbol{u},\boldsymbol{m}) = 0, \tag{10b}$$

$$g(\boldsymbol{u},\boldsymbol{m}) \leq 0, \tag{10c}$$

where $J(\boldsymbol{u},\boldsymbol{m}) \in \mathbb{R}$ is the functional of interest and is used to describe mathematically the objective of the optimization, $\boldsymbol{u}$ are the state variables that are the solution of a PDE or a system of PDEs represented in a residual form by $\mathcal{F}(\boldsymbol{u},\boldsymbol{m}) = 0$, $\boldsymbol{m}$ are the design/control variables, and g any additional inequality constraints on controls and/or states.

The problem (10) can be solved in two ways: using full space or reduced space methods [24]. In the former, states and controls are considered both as optimization variables within the optimization algorithm (solver) and changed directly and simultaneously in each optimization iteration. In the latter, the mapping $\boldsymbol{m} \mapsto \boldsymbol{u}(\boldsymbol{m})$, which is implicitly defined by the PDE constraint(s) $\mathcal{F}(\boldsymbol{u},\boldsymbol{m}) = 0$, is used to obtain the reduced problem [24]:

$$\min_{\boldsymbol{m}} \quad \hat{J}(\boldsymbol{m}) := J(\boldsymbol{u}(\boldsymbol{m}),\boldsymbol{m}), \tag{11a}$$

$$\text{subject to} \quad g(\boldsymbol{u}(\boldsymbol{m}),\boldsymbol{m}) \leq 0, \tag{11b}$$

where $\hat{J}(\boldsymbol{m})$ is termed the reduced functional of interest. The reduced problem is suitable for use with the adjoint approach for computing functional gradients. In this work, a gradient-based optimization is used together with the adjoint approach, which is the most efficient technique of computing the required gradients in each optimization iteration [25].

In each iteration, gradient-based optimization algorithms require computation of the gradient of the functional with respect to the control variables:

$$\frac{\mathrm{d}\hat{J}}{\mathrm{d}\boldsymbol{m}} = \frac{\mathrm{d}J(\boldsymbol{u}(\boldsymbol{m}),\boldsymbol{m})}{\mathrm{d}\boldsymbol{m}} = \frac{\partial J}{\partial \boldsymbol{m}} + \frac{\partial J}{\partial \boldsymbol{u}}\frac{\mathrm{d}\boldsymbol{u}}{\mathrm{d}\boldsymbol{m}}. \tag{12}$$

The partial derivatives $\partial J/\partial \boldsymbol{m}$ and $\partial J/\partial \boldsymbol{u}$ can be computed analytically and are, thus, computationally cheap to evaluate. On the other hand, the derivative $\mathrm{d}\boldsymbol{u}/\mathrm{d}\boldsymbol{m}$ is computationally expensive for high-dimensional states $\boldsymbol{u}$ and controls $\boldsymbol{m}$. In general, the discretized state space is high-dimensional in PDECO problems, whereas the dimension of the control space depends on the number and type (a constant, or a spatially or time-varying function) of controls. In the adjoint approach, the direct computation of $\mathrm{d}\boldsymbol{u}/\mathrm{d}\boldsymbol{m}$ is avoided and the functional gradient is obtained as follows [24]:

$$\frac{\mathrm{d}\hat{J}}{\mathrm{d}\boldsymbol{m}} = \frac{\partial J}{\partial \boldsymbol{m}} - \boldsymbol{\varphi}^* \frac{\partial \mathcal{F}}{\partial \boldsymbol{m}}, \tag{13}$$

where $\boldsymbol{\varphi}$ are the adjoint variables, and * denotes the Hermitian operator. The adjoints are obtained from the adjoint equation:

$$\frac{\partial \mathcal{F}}{\partial \boldsymbol{u}}^* \boldsymbol{\varphi} = \frac{\partial J}{\partial \boldsymbol{u}}^*. \tag{14}$$

Therefore, the computation of the functional gradient involves two steps: solving (14) for the adjoint variables and using the obtained values in (13). Since the adjoint equation does not contain derivatives with respect to controls and is a linear PDE, the computational effort for its solution is independent of the size of the control and if implemented efficiently is generally less or as expensive as solving the forward problem described by $\mathcal{F}$. As a result, the adjoint approach enables an efficient computation of functional gradients independent of the dimension of the control variables.

2.2.1. Optimization variables and the functional of interest

The main objective of the optimization procedure is to design the placement of the GWHP systems, i.e. their extraction and injection wells, in a way that the efficiency of all GWHPs is maximized and all regulatory conditions are met. Therefore, the **control optimization variables** are the Cartesian coordinates (positions) of wells: $\mathbf{x}_i^{\mathrm{ext}} = (x_i^{\mathrm{ext}}, y_i^{\mathrm{ext}}) \in \mathbb{R}^2$ represents the extraction well coordinates of the heat pump i and $\mathbf{x}_i^{\mathrm{inj}} = (x_i^{\mathrm{inj}}, y_i^{\mathrm{inj}}) \in \mathbb{R}^2$ represents the injection well coordinates of the same heat pump. All control variables can be described using the following vector:

$$\boldsymbol{m} = [x_1^{\mathrm{ext}}, \dots, x_N^{\mathrm{ext}}, y_1^{\mathrm{ext}}, \dots, y_N^{\mathrm{ext}}, x_1^{\mathrm{inj}}, \dots, x_N^{\mathrm{inj}}, y_1^{\mathrm{inj}}, \dots, y_N^{\mathrm{inj}}]^T. \tag{15}$$

The **state optimization variables** are the solutions of the governing PDEs, i.e. the hydraulic head h, Darcy velocity $\mathbf{q}$ and the groundwater temperature T.

The optimization goal is to maximize the groundwater temperatures at all extraction wells. Thus, the corresponding functional of interest J_0 reads as follows:

$$J_0(\boldsymbol{u},\boldsymbol{m}) = \sum_{i=1}^{N} T(\mathbf{x}_i^{\mathrm{ext}}) = \sum_{i=1}^{N} \int_{\Omega} T(\mathbf{x}) \cdot \delta(\mathbf{x} - \mathbf{x}_i^{\mathrm{ext}})\, \mathrm{d}\Omega. \tag{16}$$

The point evaluation of the function T, i.e. sampling of the groundwater temperature field at the extraction well, can be formulated as an integral of the product of the function T and the corresponding 2D Dirac delta function. In this work, the short notation for the point evaluations of functions (states) will be used from now on, but the implementation is based on the previously described multiplication with delta functions.

2.2.2. Optimization constraints

The underlying PDECO problem includes control constraints, which are based on the regulations and physical conditions when placing (installing) new GWHP systems. The first set of constraints corresponds to the fact that the wells of a GWHP can be placed only inside a plot (property) that belongs to the owner of that GWHP. In addition, approval regulations for new systems usually stipulate a minimum distance between the wells and the plot boundaries. For instance, this distance is 3 meters in Bavaria (Germany) [26], where the considered case study is located. Thus, for each GWHP i the constraints state that both wells, extraction and injection, must be restricted to the feasible area D_i that corresponds to the plot area excluding a minimum-distance buffer zone:

$$\mathbf{x}_i^{\mathrm{ext}}, \mathbf{x}_i^{\mathrm{inj}} \in D_i, \quad \forall i \in \{1, \dots, N\}. \tag{17}$$

In the case of idealized rectangular plots aligned with the coordinate system, these constraints would take a particularly simple form as

upper and lower bounds on controls. However, in this work, a more realistic and general case with convex plots is considered. The constraints are then formulated as follows:

$$g_i^j(x_i^w, y_i^w) = a_{i,1}^j x_i^w + a_{i,2}^j y_i^w \leq b_i^j, \quad \forall i \in \{1, \dots, N\}, \forall j \in \{1, \dots, n_i\}, \quad (18)$$

where w stands for extraction or injection, i.e. $w \in \{\text{ext}, \text{inj}\}$; i is the counter for plots (GWHPs); j counts the linear segments of the plot boundary, assumed to be a polygon; n_i is the total number of boundary segments for plot i; $a_{i,1}^j$, $a_{i,2}^j$, b_i^j are the coefficients of the linear inequality constraint that corresponds to the boundary segment j of plot i. These constraints can be also written in matrix form:

$$\mathbf{A}\boldsymbol{m} \leq \mathbf{b}, \quad (19)$$

where the matrix $\mathbf{A}$ contains the coefficients $a_{i,1}^j$ and $a_{i,2}^j$, and the vector $\mathbf{b}$ the coefficients b_i^j. The total number of constraints in (18), N_1^{cst}, depends on the number of segments of plot boundaries and is given as:

$$N_1^{\text{cst}} = \sum_{i=1}^{N} n_i. \quad (20)$$

The coefficients in (18) are derived using analytical formulae and geometric relations, as described in Appendix A.

The second set of constraints corresponds to regulation over the minimum distance between wells of the same GWHP system. The injection well is usually placed downstream and far enough from the extraction well to avoid hydraulic and thermal breakthroughs [14]. Breakthroughs reduce the efficiency of GWHPs because the altered groundwater circulates back to the extraction well [27]. For this reason, there is usually a defined minimum distance between two wells of a system. For example, in Bavaria, Germany, this distance is 10 meters according to current best practice in local water protection authorities. The corresponding constraints can be defined as follows:

$$d(\mathbf{x}_i^{\text{ext}}, \mathbf{x}_i^{\text{inj}})^2 = (x_i^{\text{ext}} - x_i^{\text{inj}})^2 + (y_i^{\text{ext}} - y_i^{\text{inj}})^2 \geq d_{\min}^2, \quad \forall i \in \{1, \dots, N\}, \quad (21)$$

where d is the distance function and $d_{\min} = 10$ [m] is the predefined minimum distance. The total number of these control constraints is equal to the number of considered GWHPs, i.e. $N_2^{\text{cst}} = N$.

The regulations also specify minimum distances between GWHP wells and existing objects on a property, such as a house or a garage. The wells cannot be placed within such objects and the minimum distance provides a buffer zone that is necessary from a safety and technical point of view. This regulatory distance d_R is 3 meters [26] in the area of interest (see Section 3.1). The corresponding constraints can be summarized as follows:

$$\mathbf{x}_i^{\text{ext}}, \mathbf{x}_i^{\text{inj}} \notin R_i^j, \quad \forall i \in \{1, \dots, N\}, \forall j \in \{1, \dots, r_i\}, \quad (22)$$

where R_i^j is the restricted area j for wells within the plot i, which is for example a house and its surrounding 3-meter buffer zone; r_i the number of restricted areas in the plot i. Fig. 1 shows an example plot with a restricted area and minimum-distance buffer zones. The control constraints in (22) cannot be mathematically formulated as convex linear constraints, such as (18), even when the restricted areas R_i^j are convex polygons. For this reason, these constraints are integrated into the optimization problem via penalty terms, as explained in the following section.

Finally, it should be noted that if the order of installation of GWHPs is defined, i.e. there are some existing GWHPs in the area and the new ones should be optimally placed accordingly, an additional set of constraints is required. These constraints correspond to regulations over negative interference between neighboring GWHPs. The details of such constraints and how they can be included in the optimization are given in Appendix B, but they are not considered further in the present study.

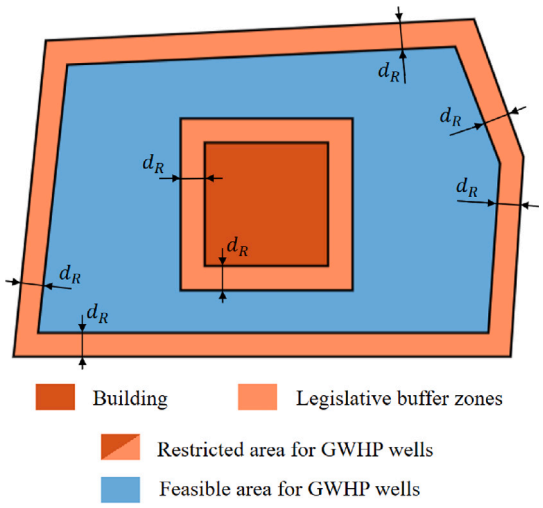

Fig. 1. Example of a plot with one building and the corresponding buffer zones ($d_R = 3$ m).

2.2.3. Penalty terms

In general, penalty terms (functions) can be used to convert constrained optimization problems into unconstrained ones or to replace only a certain number of constraints. These functions are added to the original objective function and are formulated in such a way that they become zero if the corresponding constraint is met, or otherwise take a positive value in the case of a minimization problem [28]. In the PDECO framework, the penalty functions can be used to replace state constraints or control constraints that are difficult to express in a suitable form for the selected optimization algorithm and/or its software implementation.

Since the control constraints (22) cannot be formulated mathematically as convex linear constraints, they are replaced by penalty functions. The corresponding penalty term P_R, which is added to the functional of interest (16), contains penalty functions for the positions of all extraction and injection wells:

$$P_R = \alpha \cdot \sum_{i=1}^{N} \left(p(\mathbf{x}_i^{\text{ext}}) + p(\mathbf{x}_i^{\text{inj}}) \right), \quad (23)$$

where p denotes the penalty function, and α is a penalty scaling factor that determines how severely the objective will be penalized if the constraints are not met. The penalty function p should be positive if the well under consideration lies within one of the restricted areas R_i^j and otherwise be zero. In this work, the functions p are defined as a point evaluation of a predefined penalty field:

$$p(\mathbf{x}_i) = \int_{\Omega} G(\mathbf{x}) \cdot \delta(\mathbf{x} - \mathbf{x}_i) \, \mathrm{d}\Omega, \quad (24)$$

where $G(\mathbf{x})$ is the penalty field constructed using the restricted areas R_i^j. The penalty field is defined as follows:

$$G(\mathbf{x}) = \begin{cases} 0 & \text{if} \quad \mathbf{x} \notin R_i^j, \\ & \quad \forall i \in \{1, \dots, N\}, \forall j \in \{1, \dots, r_i\} \\ 1 + \cos\left[\frac{d(\mathbf{x}, \mathbf{x}_{i,j}^{\text{p}})}{r_{i,j}^{\text{p}}} \cdot \frac{\pi}{2} \right] & \text{if} \quad \mathbf{x} \in R_i^j, \end{cases} \quad (25)$$

where $\mathbf{x} = (x, y) \in \Omega$ is an arbitrary point in the domain Ω; d the distance function from (21); $\mathbf{x}_{i,j}^{\text{p}}$ and $r_{i,j}^{\text{p}}$ are the penalty center and the radius of the corresponding restricted area R_i^j, respectively. The penalty field G for an example restricted area is depicted in Fig. 2. The idea behind this particular choice of shape for G is that the more a well is within a restricted area, the larger the penalty term and, conversely, the penalty should be smaller the closer the well is to the boundary of

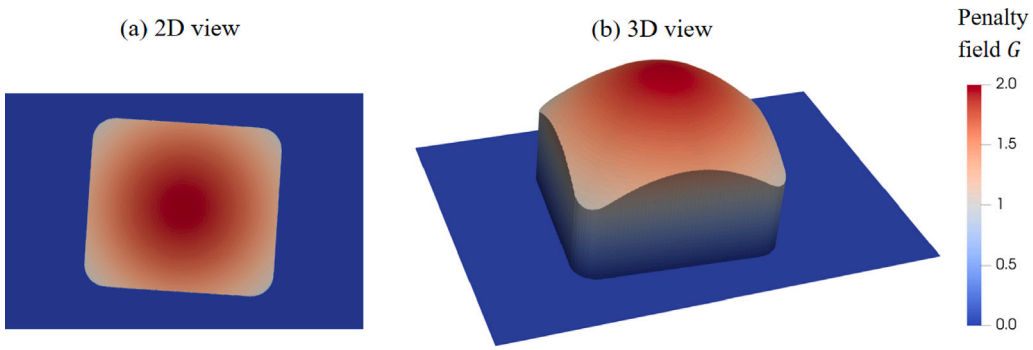

Fig. 2. Penalty field for an example restricted area plotted in 2D (a) and 3D (b). If a well is placed in the feasible part (blue color), the penalty field G is 0, otherwise the penalty has a positive value if a well is within the restricted area (red colors).

the area. This leads to a non-zero gradient, which is important for the gradient-based optimization approach. The radii $r^{\mathrm{p}}_{i,j}$ are selected as the maximum distance between any point belonging to the corresponding area R^j_i and its penalty center $\mathbf{x}^{\mathrm{p}}_{i,j}$. This ensures that the minimum value of $G(\mathbf{x})$ inside restricted areas is $1 + \cos(\pi/2) = 1$. On the other hand, the selection of the centers $\mathbf{x}^{\mathrm{p}}_{i,j}$ is a non-trivial task, since it depends on the relative positions of the restricted areas R^j_i and the corresponding plots D_i. The centers must be chosen in such a way that the points representing the well positions are not "trapped" in a restricted area during the optimization iterations. This type of situation is depicted in Fig. 3, where the well i cannot escape the restricted area anymore and reach the feasible part of the domain. Therefore, a distinction is made between three baseline scenarios, as depicted in Fig. 4, when selecting penalty centers:

1. the restricted area R^j_i overlaps with only one edge (boundary section) of the plot D_i: the penalty center corresponds to the middle point of overlapping section of that edge;
2. the restricted area R^j_i overlaps with exactly two edges of the plot D_i, including the corner of the plot that is between those two edges: the penalty center corresponds to that particular corner;
3. all other cases: the penalty center corresponds to the geometrical centroid of R^j_i.

These baseline scenarios are usually sufficient to cover many cases, but also provide the general concept for selecting penalty centers in all other cases.

It should be emphasized that by combining penalty functions for restricted areas and inequality constraints for convex plots, any type of plot geometry can be defined. For example, if the original plots are non-convex, they can be converted to convex hulls first and then additional restricted areas can be defined to cover the difference between the original plots and the new (convex) ones. This is important because in the real world, plots have many different geometries, including non-convex ones.

Finally, it should be noted that the penalty factor α is usually applied in an iterative way. The iterative optimization procedure means that α is increased at the end of each "outer" iteration, i.e. after the optimization algorithm has converged or reached the predefined number of optimization iterations. The solution from the previous outer iteration is used as the starting point for the next iteration. The whole procedure starts with a relatively small value of α and ends when α is considered to be sufficiently large. In general, this iterative approach should help to improve the convergence of optimization algorithms and ideally has the same solution as the original optimization problem, which includes constraints instead of penalties [28]. Also in this work, an iterative optimization with increasing penalty factors is applied (see Section 3).

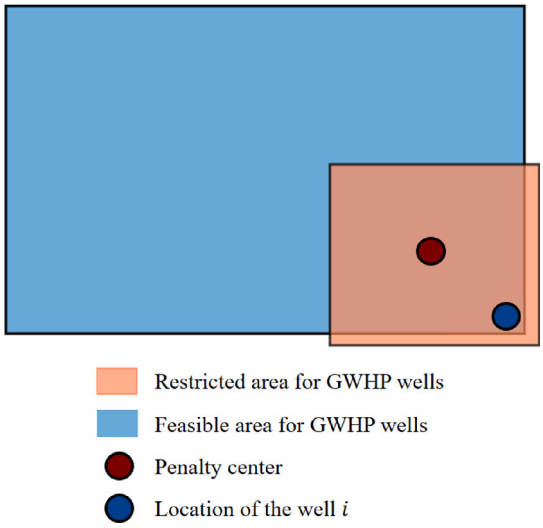

Fig. 3. Example of improper selection of a penalty center. The well i cannot reach the feasible area because of the selected position of the penalty center and the underlying shape of the penalty functions.

2.2.4. Approximated delta functions

The Dirac delta functions are present in two places in the underlying PDECO problem: in the representation of wells, i.e. sink and source terms in PDEs, as well as in the sampling of functions (states and penalty fields), such as the evaluation of the groundwater temperature at extraction wells. The delta function is a non-smooth function and is therefore problematic for gradient-based optimization, which requires information about gradients in each iteration. One approach to address this problem is to replace the delta function with a smooth approximation. A similar approach is used in [29] to represent production wells of a deep geothermal system. In other energy-related applications, such as the layout optimization of wind [30] and tidal turbines [31], the approach of representing the corresponding turbines with approximate smooth functions is already well established. These smooth approximations are usually based on exponential functions and are often referred to as bump functions. The one used in this work is depicted in Fig. 5 and defined as follows:

$$\delta(\mathbf{x} - \mathbf{x}_i) \approx \psi(x, y, x_i, y_i) = \mathrm{e}^{-\frac{(x-x_i)^2+(y-y_i)^2}{r^2}}, \tag{26}$$

where $\mathbf{x}_i = (x_i, y_i)$ is the center of the bump function ψ and r its radius. The radius $r = 0.1$ [m] is chosen based on the well dimensions of real GWHPs. For this reason, it can be argued that the well representation in this work is actually more realistic than the usual use of single point sources for wells. Finally, the volume V_{norm} below the surface of the

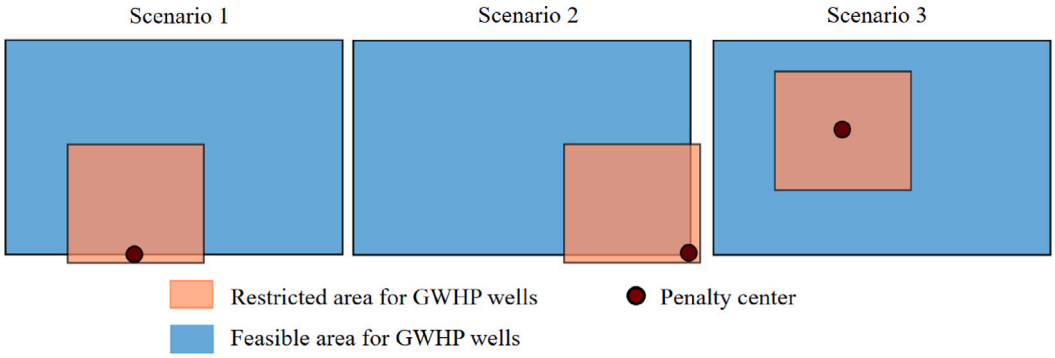

Fig. 4. Baseline scenarios for the selection of penalty centers.

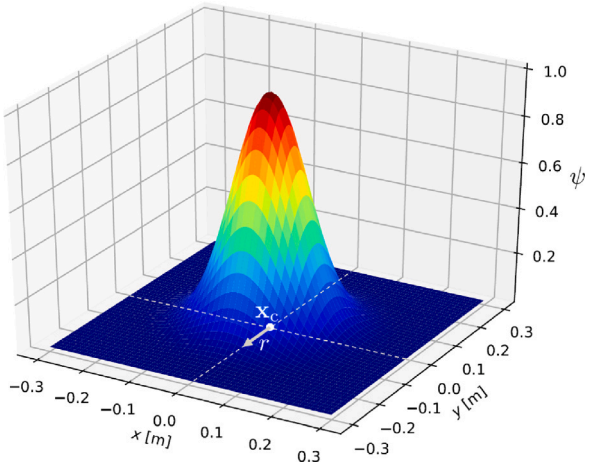

Fig. 5. Smooth approximation ψ of the Dirac delta function with center $\mathbf{x}_c = (0, 0)$ and radius $r = 0.1$ [m].

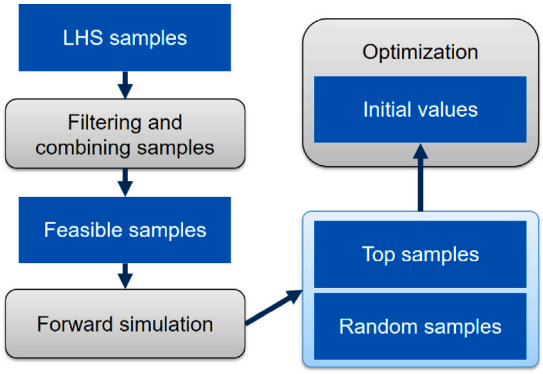

Fig. 6. Multi-start initialization strategy.

function ψ must be used to normalize the values of the "smoothed" delta function:

$$V_{\text{norm}} = \int_{-\infty}^{\infty}\int_{-\infty}^{\infty} \psi(x, y, x_i, y_i)\,\mathrm{d}x\mathrm{d}y = r^2\pi. \tag{27}$$

2.2.5. Problem formulation

Based on the previous definitions of constraints, penalty functions and the functional of interest, the optimization problem reads as follows:

$$\min_{\boldsymbol{m}} \quad -\hat{J}_0(\boldsymbol{m}) + P_R(\boldsymbol{m}), \tag{28a}$$

$$\text{subject to} \quad g_1(\boldsymbol{m}) \le 0, \tag{28b}$$

$$g_2(\boldsymbol{m}) \le 0, \tag{28c}$$

where $\hat{J}_0(\boldsymbol{m}) = J_0(\boldsymbol{u}(\boldsymbol{m}), \boldsymbol{m})$ is the reduced form of the functional of interest J_0 defined in (16); $P_R(\boldsymbol{m})$ the penalty term from (23); $g_1(\boldsymbol{m}) = \mathbf{A}\boldsymbol{m} - \mathbf{b}$ corresponds to the linear inequality constraints (19), and $g_2(\boldsymbol{m})$ to the minimum distance constraints (21). Since the sense of optimization is changed from maximization in (16) to minimization in (28), a negative sign is introduced in front of $\hat{J}_0$. The underlying problem represents a PDECO problem with control constraints.

2.2.6. Problem initialization

The underlying optimization problem is non-convex, which means that gradient-based algorithms converge towards a local optimum. Therefore, the selection of the initial optimization candidate is important, as those that are close to the global optimum are more likely to converge to it. Fig. 6 shows the multi-start initialization strategy used in this work to achieve the global optimum or to come sufficiently close to it. In the first step, different combinations of initial GWHP well positions, i.e. samples, are generated using the Latin Hypercube Sampling (LHS) method [32]. The LHS implementation in Python [33] provides only lower and upper limits on sampling points, i.e. well coordinates in this case. Therefore, the obtained LHS samples are in general not feasible, since they do not satisfy the optimization constraints (17), (21) and (22). In the second step, the LHS samples are filtered and mutually combined to obtain feasible samples that meet all optimization constraints. The feasible samples are combinations of well positions that are within feasible areas (plots), with sufficient spacing between wells of the same GWHP and outside of restricted areas. In addition, for each well pair, it is required that the injection well is located downstream of the extraction well for the samples to be considered feasible. In the third step, a forward simulation is carried out for each feasible sample and the functional of interest (16) is computed. Based on the value of this functional, all samples are sorted in ascending order. Finally, two smaller sets of feasible samples are selected for the initialization: the top-most samples, which have the smallest functional values, and a set of random samples. In addition to improving the optimal solution, these different starting points are also used to investigate the influence of the initialization on the optimization process. To adequately explore the design space, 1000 feasible samples are generated in this work and then the top 10 top samples and 5 random samples are used for initialization.

3. Implementation

The forward simulation model is implemented in Firedrake [34], which is an open-source tool for solving PDEs using the finite element method (FEM). Firedrake provides high-level abstractions for defining and solving PDE problems in the Python environment. Further advantages are MPI parallelization and compatibility with dolfin-adjoint [35], which can automatically provide adjoint solution fields

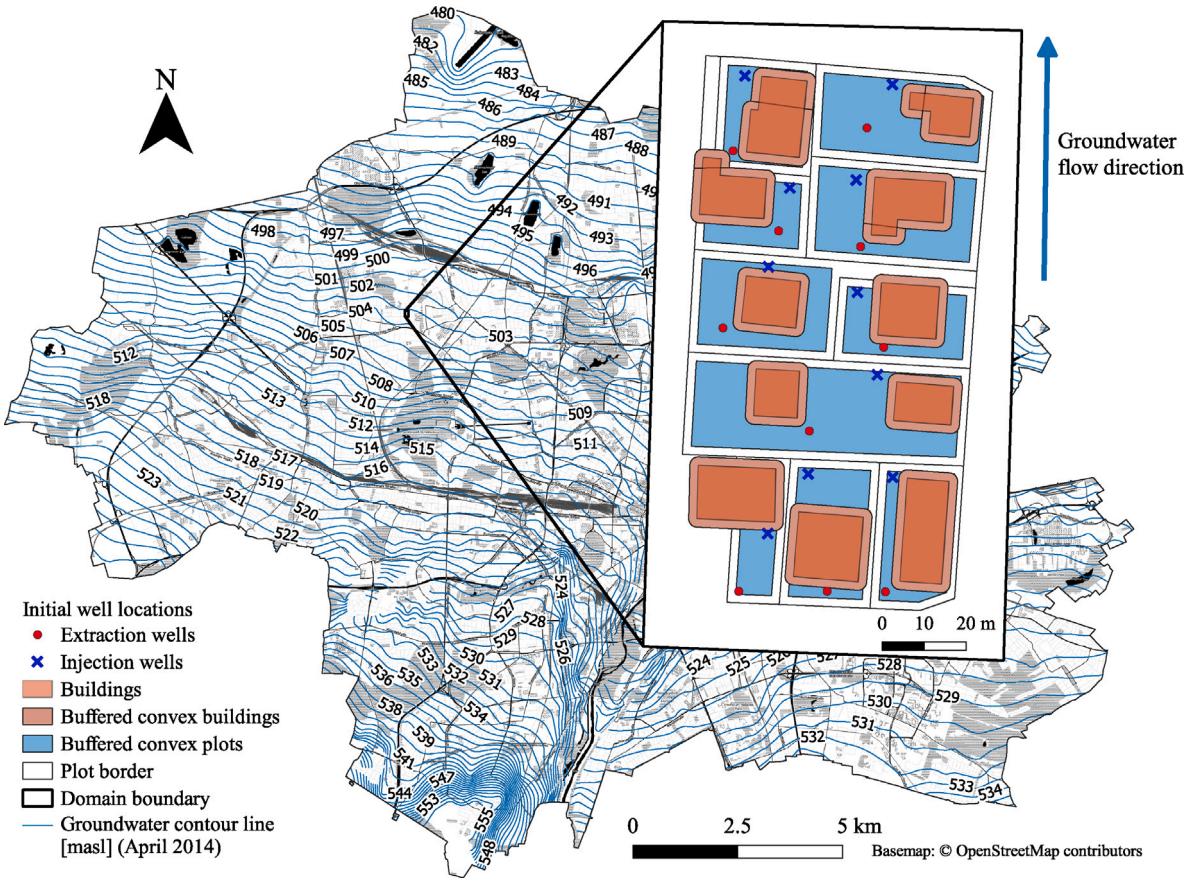

Fig. 7. Location of the case study domain in Munich with a detailed view of the relevant features.

based purely on the forward numerical model defined in Firedrake. These two tools are used to implement and solve the PDECO problem (28), where dolfin-adjoint provides interface to optimization algorithms. The implemented forward model is verified against corresponding simulation results obtained using FEFLOW [22,36], an established commercial software package for groundwater simulations. The Sequential Least SQuares Programming (SLSQP) algorithm [37] and its implementation in the SciPy Python library [38] are used to solve the underlying optimization problem. The penalty factor α is applied iteratively as described previously in Section 2.2.3, using the following increasing values: 0, 0.1, 1, 10, 100. For each of the five α values, the maximum number of optimization iterations is set to 50.

3.1. Case study

The method is applied in a 1.3-hectare study area in the City of Munich, Germany. Munich offers an exceptional hydro-geological database acquired in predecessor projects, namely GEPO and GeoPot [39]. As shown in Fig. 7, the study area comprises 10 plots of land with a typical building structure of 11 single-family detached houses. With the simplifying assumption that the heat demand of every plot can be supplied and re-injected by one extraction and one injection well, the optimal positions of 10 well pairs are determined in the case study. Geologically, the case study area is situated in the so-called Munich Gravel Plain which provides favorable conditions for the thermal use of groundwater [13]. Generally, the fluvio-glacial sandy gravels have a high hydraulic conductivity and they host a productive shallow aquifer (cf. Fig. 8). Beneath the Quaternary gravels, intersecting Tertiary sandy, silt and clay layers confine the aquifer to the bottom [40]. The study area was selected because it offers favorable hydro-geological conditions and a low depth to groundwater of around 3.5 m that would additionally support an economical installation of groundwater heat pumps. The elongated shape from south to north was chosen for this test case so as to trigger negative thermal interactions between injection and extraction wells of potential systems, as groundwater flow is also directed towards the North, and thus to demonstrate the value of an PDE-constrained optimization based design approach.

Fig. 8a shows the penalty field for restricted areas in the study case (see Section 2.2.3). In addition, the saturated thickness of the Quaternary aquifer, the groundwater contours and the hydraulic conductivity are depicted in Fig. 8b and Fig. 8c, respectively. The aquifer basis was derived by geostatistical relief modeling of the entire Munich Gravel Plain [41]. Within the domain of the case study, a northward directed groundwater flow with a homogeneous hydraulic gradient of 2.8 per mill is present. The saturated thickness is computed by subtracting the base of the Quaternary aquifer from the shown groundwater table, which was measured at mean low water conditions in April 2014. As observable in Fig. 7, this represents the common regional conditions in the Northwest of Munich. The saturated thickness decreases from 9 m to 7 m towards the Northwest. Thus, the domain offers slightly higher values compared to the median thickness of 6.3 m over the entire city area. The hydraulic conductivity of the domain was derived by an interpolation of pumping test data and represents the highly conductive and homogeneous gravels of the area [42].

To solve the underlying PDE system that describes the heat transport and groundwater flow in the aquifer, the pumping rates of all 10 GWHPs have to be defined. These are calculated from the annual heating demand and assuming 2400 full load hours per year, as well as a constant annual performance factor of 4 and a temperature difference of −5 K at the injection well. The heating demand of each system, i.e. each building, is estimated using an open source tool UrbanHeatPro [43]. The obtained values of pumping rates and the heating power

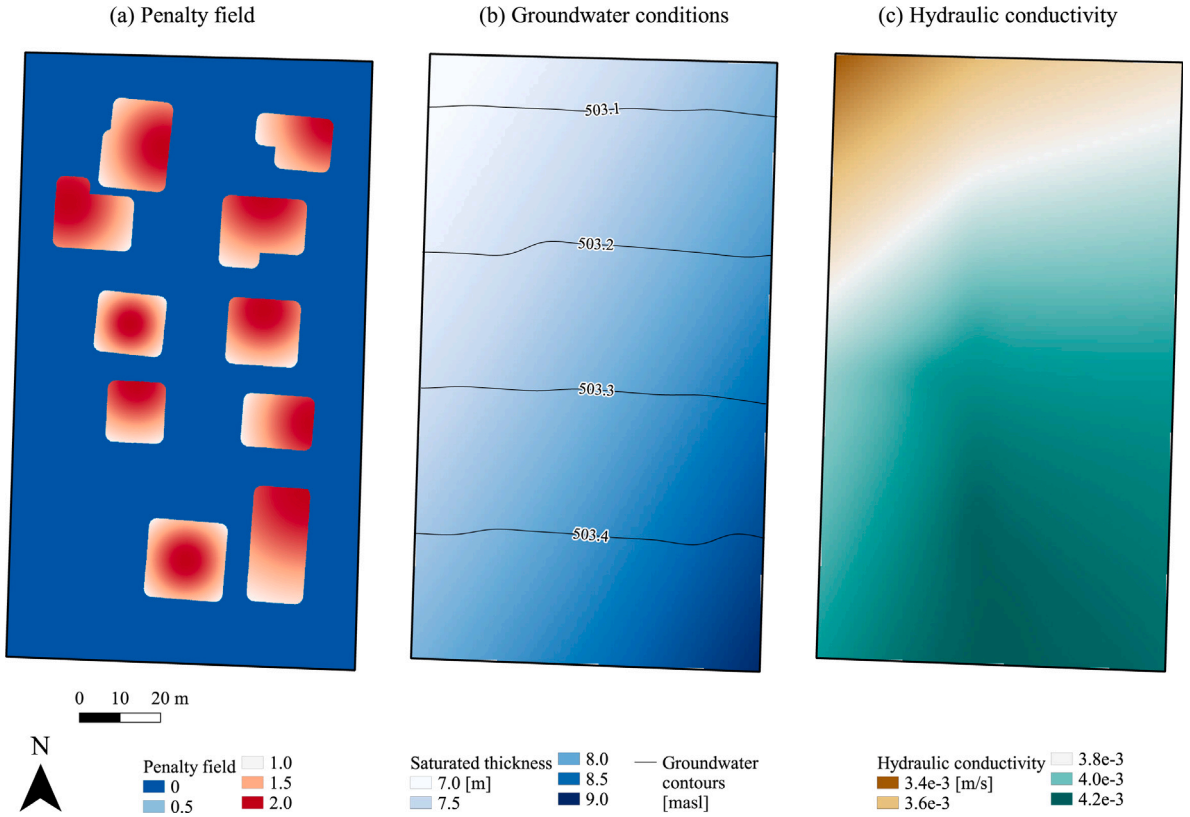

Fig. 8. Case study domain with penalty field, initial groundwater conditions and hydraulic conductivity.

Table 1
Constant pumping rates and the heating power of the domain's 10 GWHP systems.

Plot ID	1	2	3	4	5	6	7	8	9	10
Pumping rate [L/s]	0.65	0.49	0.42	1.03	0.84	0.51	0.76	0.56	0.58	0.44
Heating power [kW]	13.65	10.29	8.82	21.63	17.64	10.71	15.96	11.76	12.18	9.24

are summarized in Table 1, with the system labels corresponding to those in Fig. 9.

For the numerical modeling of the groundwater source, the domain is discretized with approximately $3 \cdot 10^6$ triangular elements using the open source mesh generator Gmsh [44]. Element sizes range from 0.08 m within plots to 3 m further away from plots, as shown in Fig. 9. The fine mesh resolution within plots is necessary because the wells can be placed anywhere in plots during the optimization iterations, and the approximated delta functions representing wells require a relatively fine spatial discretization. Mesh sensitivity testing shows that the element size of 0.08 m is required to generate an acceptable discretization error for the delta functions and the application considered in this work. Piece-wise linear finite element basis functions (P1) are used for all state variables, as they provide sufficiently accurate results and are computationally less expensive than higher-order basis functions. For the interpolation of the smooth delta functions (cf. (26)), piece-wise quadratic basis functions (P2) prove to be sufficient.

As shown in Fig. 9, Dirichlet type boundary conditions were assigned at the upstream $\partial\Omega_{\text{in}}$ and downstream $\partial\Omega_{\text{out}}$ border to represent a constant hydraulic head at 503.492 masl for inflow and 503.064 masl for outflow, respectively. At the remaining borders parallel to the groundwater streamlines, no boundary condition was assigned, which corresponds to a Neumann type boundary condition without fluid flux [22]. Extraction and injection wells are hydraulically represented through single node sink and source terms approximated by smooth delta functions (see Section 2.2.4), where abstraction and injection rates are always equal within one well pair. Due to the assumption of a constant natural groundwater temperature, the heat transport simulation can be solved with only one Dirichlet type boundary condition at the upstream border $\partial\Omega_{\text{in}}$. The assigned temperature depends on the optimization scenario, as described in Section 3.2. The thermal impact of the injection wells is represented with an assignment of 5 °C to the temperature of re-injected water at those wells T_i^{inj} (cf. (7)). Normally, injection well temperatures are assigned based on extraction well temperatures by subtracting a constant predefined temperature difference. However, since the extraction well temperatures are changing with the well positions during the optimization, it is assumed for the sake of simplicity that the injection well temperatures T_i^{inj} are independent of the extraction well temperatures. The predefined value of 5 °C is based on the expected average extraction well temperatures of 10 °C (see Section 3.2) and a temperature difference of −5 K.

3.2. Optimization scenarios

Two optimization scenarios are used to demonstrate the ability of the optimization process to produce suitable results based on different hydro-geological conditions, as well as to show how these conditions affect the optimal well layout. These two scenarios differ in the natural temperature of the inflowing groundwater. In the first scenario, the groundwater temperature at the inflow boundary of the domain is set to be constant, i.e. $T_{\text{in}} = 10$ °C. In the second scenario, the groundwater temperature is higher in the middle of the inflow boundary and lower at its edges:

$$T_{\text{in}}(\mathbf{x}) = T_{\text{in}}^{\min} + \Delta T_{\text{in}} \cdot \cos\left[\frac{d(\mathbf{x}, \mathbf{x}_{\text{in}})}{r_{\text{in}}} \cdot \frac{\pi}{2}\right], \quad \mathbf{x} \in \partial\Omega_{\text{in}}, \tag{29}$$

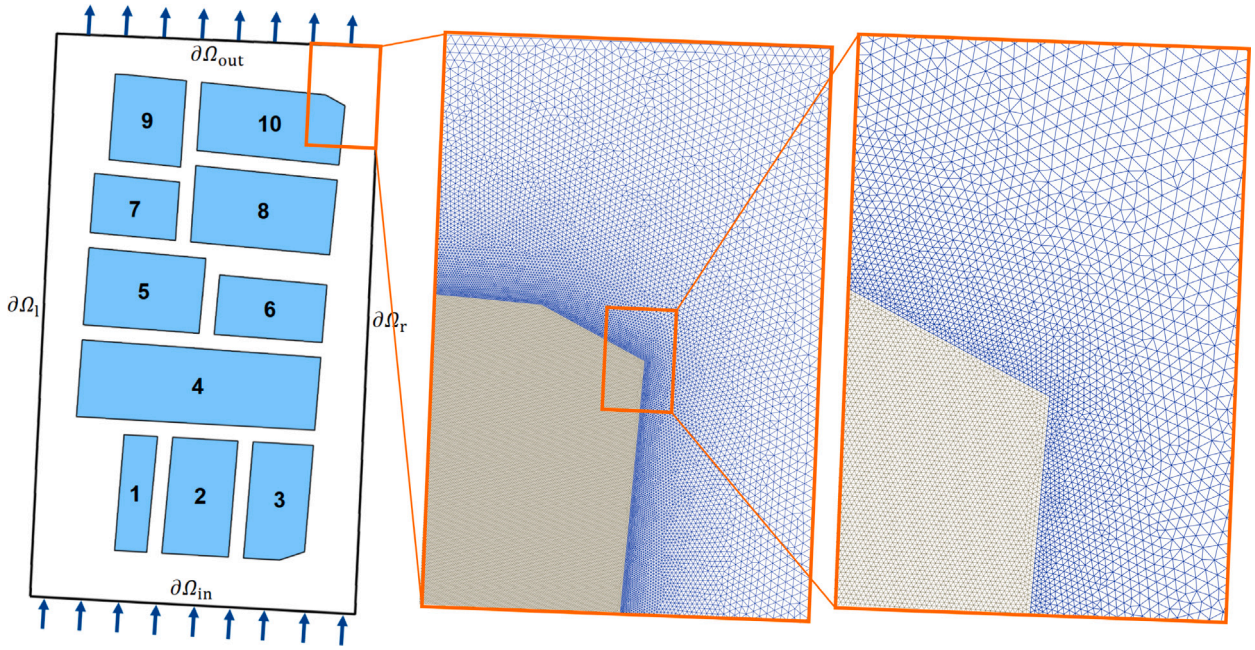

Fig. 9. Case study area with its boundary and GWHP (plot) labels and sections of the corresponding finite element mesh.

where $T_{in}^{min} = 8$ °C is the temperature at the boundary edges, $\Delta T_{in} = 4$ °C the temperature difference between the maximum and minimum temperature at the boundary, $d(\mathbf{x}, \mathbf{x}_{in})$ distance between a point $\mathbf{x}$ at the inflow boundary $\partial\Omega_{in}$ and its geometric center $\mathbf{x}_{in}$, and r_{in} the "radius" of the boundary, i.e. the distance between its center point and one of the edges. The groundwater temperature at the boundary center corresponds to the maximum temperature of 12 °C. Conceptually, optimization scenario 2 represents the case where groundwater flowing into the domain has been altered in the upstream area, for example, by other GWHPs, while scenario 1 represents the case where no GWHPs are present in the upstream area.

4. Results

In this section, the results of the optimization scenarios are presented and analyzed. Table 2 summarizes the results of the optimization scenario 1. For all 15 different initializations, i.e. the first 10 top and 5 random LHS samples (see Section 2.2.6), the number of optimization iterations n_{iter} as well as the initial and final values of the functional of interest are provided. In addition to the total number of iterations, the number of iterations for each value of the penalty factor α is also given. For the first two values of α, i.e. $\alpha = 0$ and $\alpha = 0.1$, the number of iterations almost always reaches the predefined maximum number of 50. Thereafter, the number of iterations tends to decrease as the value of α increases, and is usually lowest for the largest α. This means that the main progress in optimization, i.e. the largest changes in the well layout, are achieved during the stages with smallest penalty factor, where violation of the constraints related to restricted areas (see 2.2.3) carries little or no penalty. Considering the functional of interest, its final values are always smaller than the initial values. Since the functional is defined as the negative sum of the groundwater temperatures at all extraction wells, this means that the sum of these temperatures is maximized and increases by a few degrees, e.g. from approx. 89 °C to 93 °C for the 1st top sample. The only exception to functional improvement is the 6th top sample, where the final value is positive. This means that the solution is not feasible and some of the wells are located within restricted areas, resulting in an increased penalty and therefore shifting the functional into positive range. A further analysis of this special case is carried out later in this section with the help of visualizations. The blue color in Table 2 indicates the

Table 2
Results for optimization scenario 1.

Sample		Nr. of iterations						Functional of interest	
Type	Nr.	$\alpha = 0$	$\alpha = 0.1$	$\alpha = 1$	$\alpha = 10$	$\alpha = 100$	Total	Initial	Final
Top	1	50	47	4	14	1	116	−89.0773	−93.0678
	2	50	50	50	27	8	185	−88.4074	−92.7604
	3	50	50	37	14	12	163	−88.2872	−92.2075
	4	50	50	33	4	5	142	−87.8936	−88.6561
	5	50	50	50	25	6	181	−87.8581	−91.6815
	6	50	50	50	37	6	193	−87.6945	14.8968
	7	50	50	50	50	16	216	−87.6555	−92.3777
	8	50	50	18	50	18	186	−87.5232	−92.8066
	9	50	50	50	50	44	244	−87.4092	−91.9520
	10	50	50	42	7	7	156	−87.4081	−92.1422
Random	1	50	50	44	3	5	152	−84.8632	−90.0143
	2	50	50	50	48	6	204	−85.3343	−90.6592
	3	50	50	50	37	9	196	−85.8546	−92.7686
	4	50	50	25	14	1	140	−87.3253	−93.0817
	5	50	50	33	4	5	142	−82.7233	−88.6561

two best optimal solutions, which are obtained for the 1st top and the 4th random initialization samples. While these two samples lead to almost identical solutions, it is evident that initialization plays a significant role and that the problem has many local minima. However, using multiple top samples for initialization seems to be a good strategy for reliably reaching or getting close to the global optimum. This is further supported by the fact that the 4th random sample in this case is actually equal to the 13th top sample, which means that this sample would also be one of the top initialization samples if 15 instead of first 10 top samples were used for initialization.

The well layout changes during the optimization iterations for the 1st top sample in optimization scenario 1 are depicted in Fig. 10(a). Extraction and injection wells are denoted with circles and crosses, and the dark blue and yellow colors represent the first and last iterations, respectively. This notation of wells and iterations is used throughout the work. The corresponding groundwater temperature field and well locations for the initial and final (optimal) well layout are presented in Fig. 10(b). In the optimal solution, wells are placed mainly on the edges of the plots or in their corners. The extraction wells are placed within the regions of high groundwater temperature. To establish such regions,

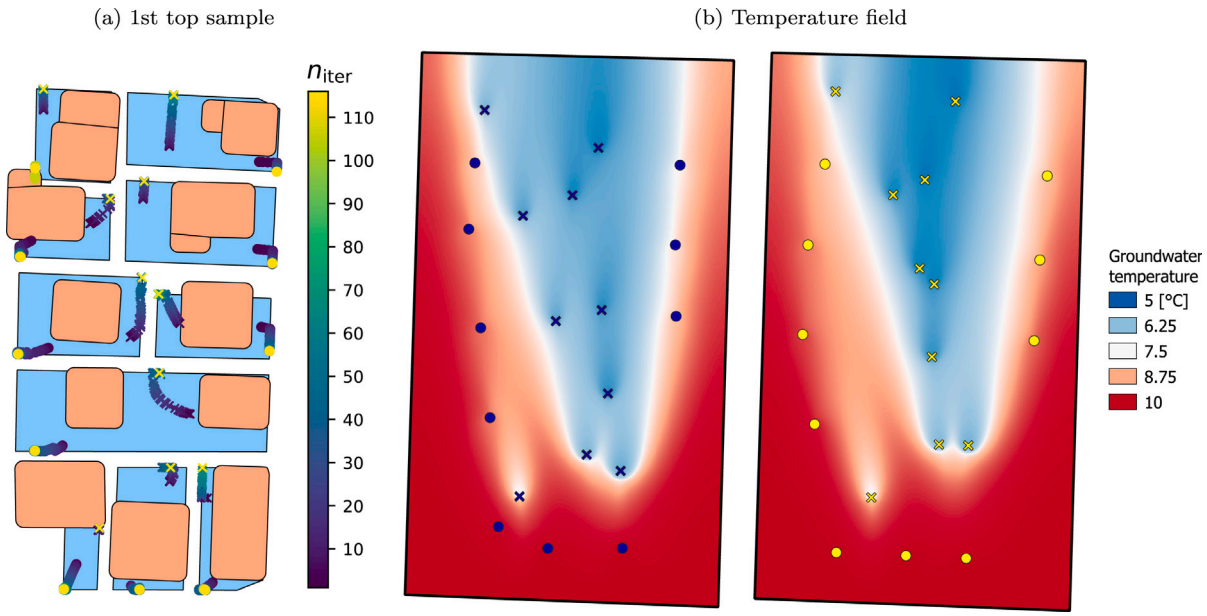

Fig. 10. Optimal well layout for optimization scenario 1: (a) Well positions through optimization iterations. Extraction and injection wells are depicted with circles and crosses, respectively. The colors in the legend represent optimization iterations, with dark blue and yellow corresponding to the first and last iteration (solution), respectively. (b) Groundwater temperature field and well locations for the initial (left) and final/optimal (right) well layout.

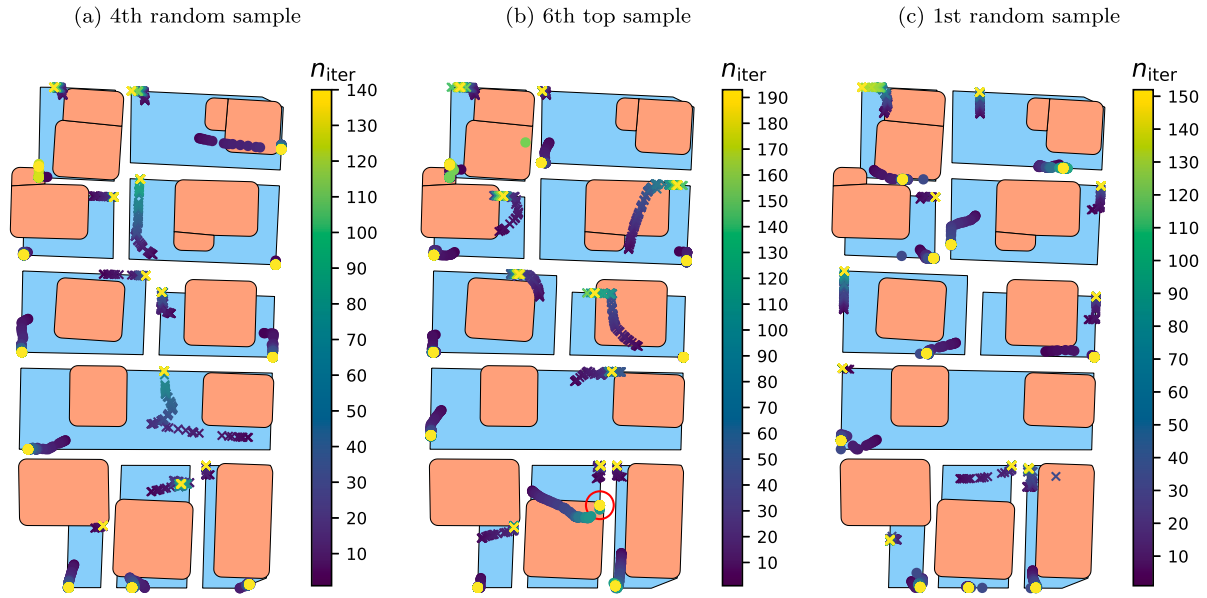

Fig. 11. Well positions through optimization iterations for optimization scenario 1. Extraction and injection wells are depicted with circles and crosses, respectively. The colors in the legend represent optimization iterations, with dark blue and yellow corresponding to the first and last iteration (solution), respectively.

in the optimal well layout all injection wells are grouped within an interior region of the domain. As a result, negative well interactions are minimized and temperatures at the extraction wells are maximized, which is the optimization goal.

To further compare different initialization patterns, changes in well layout during optimization for three samples are shown in Fig. 11. The following samples are presented: 4th random, which yields one of the two best optimal solutions in addition to the 1st top sample; 6th top, where the solution is not feasible; and 1st random, with one of the inferior feasible solutions. Comparing the 4th random (see Fig. 11(a)) and 1st top (see Fig. 10(a)) samples, it can be seen that they result in nearly identical optimal well layouts, particularly in the case of extraction wells. For this reason, the final value of the functional of interest is almost the same for the two cases. As mentioned earlier, the 6th top initialization sample produces a positive final functional of interest, i.e. an infeasible solution. The extraction well of system 2, which is marked with a red circle in Fig. 11(b), is placed within the restricted area, i.e. too close to a building. This causes a large penalty and thus increases the functional of interest. The reason why the extraction well is "captured" in a restricted area is the combination of hard and soft optimization constraints. The hard constraints, such as the minimum distance constraint (21), are those that are imposed directly within the optimization algorithm and, therefore, must be satisfied in each optimization iteration. The soft constraints, such as the constraint over restricted areas (22), are represented with penalty terms and do not have to be satisfied in all optimization iterations. Nevertheless, by increasing the penalty factor, soft constraints should be also met in the final solution. This can be seen in Fig. 11(b), where the considered

Table 3
Results for optimization scenario 2.

Sample		Nr. of iterations						Functional of interest	
Type	Nr.	$\alpha = 0$	$\alpha = 0.1$	$\alpha = 1$	$\alpha = 10$	$\alpha = 100$	Total	Initial	Final
Top	1	50	50	41	34	3	178	−94.9388	−99.0102
	2	50	50	32	23	1	156	−94.2972	−98.1109
	3	50	50	13	25	1	139	−93.8563	−98.2430
	4	50	50	50	35	8	193	−93.5070	−97.9084
	5	50	50	32	50	50	232	−93.4840	−99.6244
	6	50	50	7	50	22	179	−93.4203	−99.4235
	7	50	50	50	7	47	204	−93.3522	−99.6396
	8	50	50	28	1	1	130	−93.3488	−97.1548
	9	50	50	24	22	1	147	−93.3085	−98.7915
	10	50	50	7	50	11	168	−93.2896	−99.1492
Random	1	50	50	43	38	6	187	−91.8329	−97.9626
	2	50	50	50	50	12	212	−91.4544	−97.4910
	3	50	47	2	40	8	147	−91.7123	−98.8106
	4	50	50	10	50	22	182	−92.2810	−98.9850
	5	50	50	45	7	6	158	−88.8350	−97.4986

extraction well initially "moves" more into the restricted area and after a certain number of iterations tries to leave it. However, the "escape" is not successful, since the distance between the extraction and the corresponding injection well reaches the minimum value, which is represented by a hard constraint and must be always fulfilled. Fig. 11(c) shows the optimal well layout for one of the inferior local optima. Compared to the best optimal solutions, i.e. the 4th random and 1st top, the final well layout differs significantly.

Table 3 summarizes the results of the optimization scenario 2 (see Section 3.2). The number of optimization iterations and the initial and final functional of interest are provided for all 15 initialization samples. Similar to optimization scenario 1, the number of iterations almost always reaches the maximum for the two lowest penalty factors, $\alpha = 0$ and $\alpha = 0.1$, and thereafter tends to decrease as α increases. The two best optimal solutions are indicated in blue color and correspond to the 7th and 5th top samples. In addition, the three subsequent best solutions are also obtained from the top samples, namely: 6th, 10th and 1st, respectively. These results reaffirm that using multiple top samples for initialization rather than randomly selecting feasible samples is a valid strategy leading to the global optimum. A feasible solution is found for all 15 samples and the functional of interest has evidently improved. The sum of groundwater temperatures at all extraction wells increases by a several degrees, e.g. from approx. 93.3 °C to 99.6 °C for the 7th top sample. Comparing initial and final functional, the improvement in scenario 2 is larger on average than in scenario 1. This means that the potential for improving well layouts is generally influenced by hydro-geological conditions. However, it should be noted that the final functional values between the two scenarios are not comparable, as the temperature of the groundwater flowing into the area is different.

Changes in well layout during optimization for the 7th top sample, which results in the best optimum in optimization scenario 2, are shown in Fig. 12(a). The accompanying initial and optimal temperature fields, including well locations, are presented in Fig. 12(b). Similar to optimization scenario 1, the injection wells are grouped in an interior region of the domain. The only exception is the injection well of the system 1, which does not belong to this cold region. The extraction wells are "moved" to regions with higher groundwater temperatures. The extraction wells on the left side of the domain are not placed in the plot corners as in scenario 1, but follow the patterns in the groundwater temperature field, as shown in Fig. 13(a). These results demonstrate that: first, hydro-geological conditions, such as the natural groundwater temperature, can significantly influence the optimal well layout; and second, the proposed optimization approach successfully integrates such conditions. Moreover, the temperature fields shown in Figs. 10(b) and 12(b) indicate that thermal advection plays a significant role in heat transport, which was expected given that the groundwater velocity is relatively high in the study area.

Fig. 13 also depicts changes in well layout during optimization for the following two samples: 1st top, which has the best initial functional but does not yield the best optimal solution and 3rd random that delivers an inferior feasible solution. The example in Fig. 13(c) also demonstrates that wells, such as the injection well of GWHP 8, can switch sides of the restricted areas during optimization. This is an advantage in the context of global optimization, since the well placement is not limited by the initial relative position to restricted areas.

Fig. 14 shows the optimization progress over all iterations. Results obtained with the 1st and 7th top initialization samples are presented for optimization scenarios 1 and 2, respectively. In addition to the evolution of the functional of interest J, changes in groundwater temperatures T at all extraction wells during the optimization are displayed. Iterations with different penalty factors α are indicated with different background colors. Comparing the initial values (iteration 0) with the final values, it is noticeable that the temperatures at extraction wells have increased and at the same time the functional has decreased. This inverse behavior of temperatures and the functional follows from the definition of the functional. According to its definition in (28a), the functional of interest consists of a negative sum of the temperatures at all extraction wells and a penalty term related to restricted areas. The main advance in temperature rise takes place during the $\alpha = 0$ and partially during the $\alpha = 0.1$ stages. Thereafter, the temperatures change only slightly for higher α values. The largest value drop of the functional also occurs at $\alpha = 0$. Additionally, oscillations occur in the functional for some larger α values. The reason for this is that the optimization algorithm uses too large an optimization step and some of wells end up in one of restricted areas, which activates the penalty and increases the functional drastically. However, the algorithm automatically reacts to this and quickly reduces the functional again. Furthermore, it should be noted that the computational cost increases with increasing α values. As an indicative example, one optimization iteration takes about 2 min and up to 7–9 min for $\alpha = 0$ and $\alpha = 100$, respectively, when running in parallel on 20 cores of Intel Xeon Processor (Skylake, IBRS), 2394 MHz, 88 GB of RAM. There is potential for a further reduction in computational time by tuning the parameters of the optimization algorithm, improving the parallelization, or introducing mesh adaptivity techniques to more efficiently focus resolution where needed [45].

Finally, to quantify the well layout improvements after optimization, a benchmark, i.e. non-optimized well layout, is required. It should be noted here that the initial well layouts are generally not the non-optimized benchmark as they are part of the optimization, i.e. the strategy to reach the global optimum. Therefore, for each optimization scenario, the initial sample with the highest functional value of all feasible samples (see Section 2.2.6) is used as the non-optimized benchmark. Comparing this benchmark to the final solutions, the functional of interest has changed from approx. −79.3 °C to −93.1 °C and from −85.7 °C to −99.6 °C in the scenario 1 and 2, respectively. This means that the sum of groundwater temperatures at all extraction wells has increased by almost 14 °C in both scenarios after the optimization, which can significantly improve the efficiency of GWHPs.

5. Discussion

The results demonstrate that the proposed method can successfully determine the optimal well layout of multiple GWHPs that maximizes groundwater temperatures at all extraction wells. The comparison of the results between optimization scenarios shows that the hydro-geological conditions are an important factor for the optimal well layout and are correctly considered by the method. Furthermore, the proposed multi-start initialization strategy is successful in robustly supporting the attainment of an optimal solution that is closer to the global optima than that obtainable from a random or naively chosen starting configuration. However, the new method has some limitations, which are discussed in the following sections along with future work.

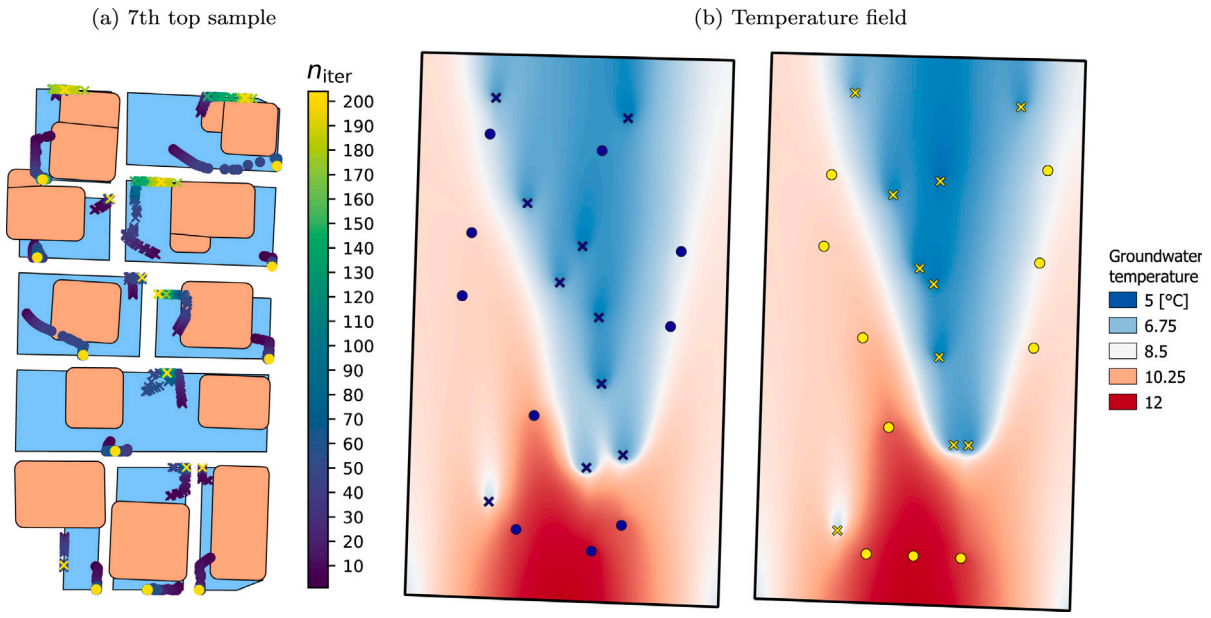

Fig. 12. Optimal well layout for optimization scenario 2: (a) Well positions through optimization iterations. Extraction and injection wells are depicted with circles and crosses, respectively. The colors in the legend represent optimization iterations, with dark blue and yellow corresponding to the first and last iteration (solution), respectively. (b) Groundwater temperature field and well locations for the initial (left) and final/optimal (right) well layout.

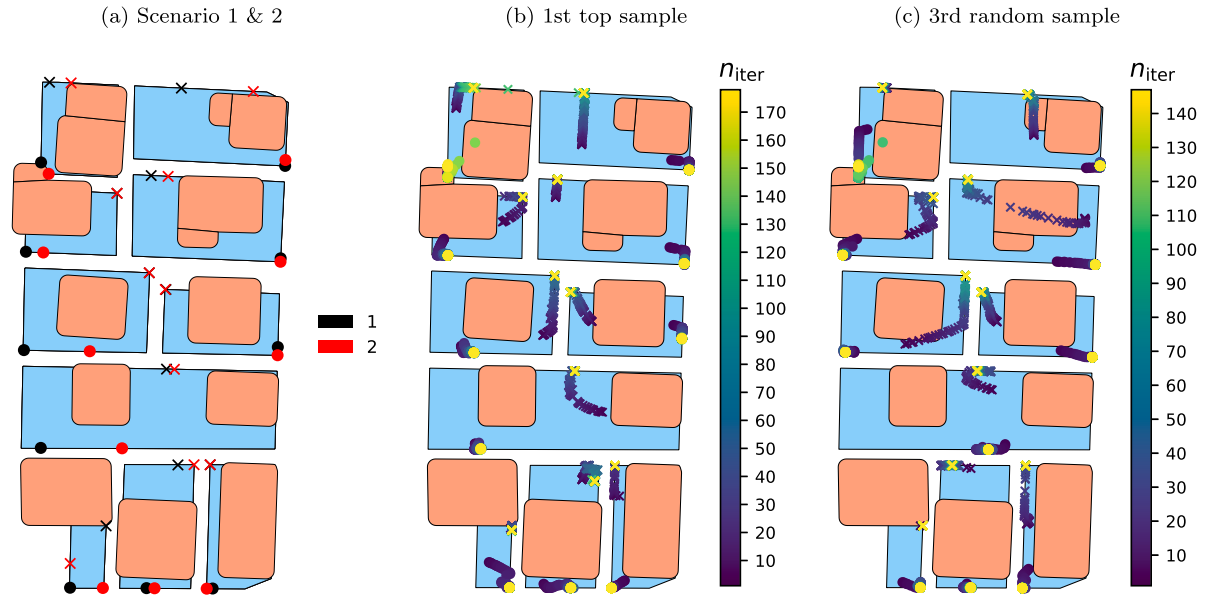

Fig. 13. Optimal well layout: (a) Final well positions for optimization scenario 1 (black) and 2 (red) for the samples top 1 and 7, respectively. (b) Well positions through optimization iterations for optimization scenario 2. Extraction and injection wells are depicted with circles and crosses, respectively. The colors in the legend represent optimization iterations, with dark blue and yellow corresponding to the first and last iteration (solution), respectively.

5.1. Critical reflection

The assumptions used to simplify the optimization problem in this work can be divided into two groups: those related to physical phenomena and the conceptual ones. The first are described in Section 2.1 and represent reasonable assumptions for the problem under consideration, such as the approximation that the water density remains constant. The conceptual assumptions are the main assumptions that significantly reduce the problem complexity and are therefore discussed in the following.

In this work only a steady state solution for the groundwater simulation is considered within the optimization procedure. This simplifies the optimization and speeds up the entire process considerably, since only stationary forward and adjoint PDEs are solved in each optimization iteration. In the time-dependent case, both the forward and adjoint PDEs are time-dependent and require appropriate time discretization. Depending on the selected time horizon and time steps, each optimization iteration becomes more time-consuming and memory-intensive compared to the steady state. The time-dependent case, however, is more realistic, as the seasonal changes in GWHP use, e.g. an increased heating demand in winter, as well as the environmental conditions, such as heat fluxes from the surface, can be taken into account [46]. Furthermore, this work assumes a constant, predefined temperature of the re-injected water at injection wells. This should be replaced by a constant temperature difference between extraction and injection wells of each system to improve the representation of GWHPs in the

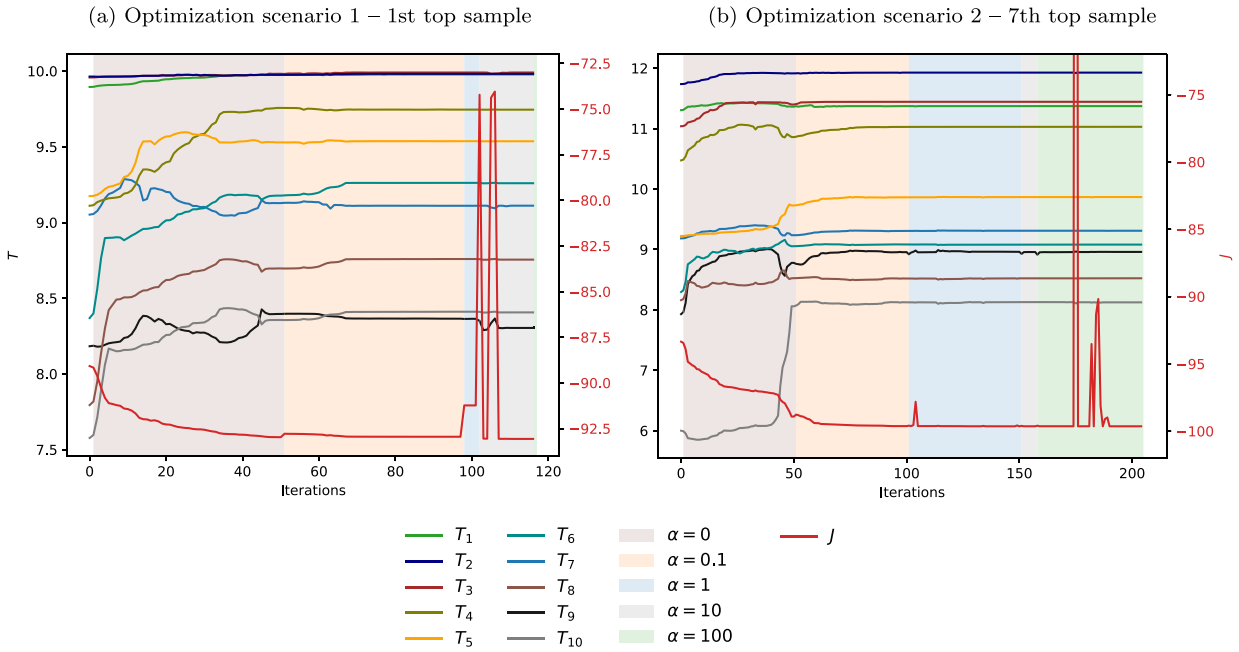

Fig. 14. Optimization progress: groundwater temperatures at all extraction wells and the functional of interest J through optimization iterations. Different background colors correspond to different values of the penalty factor α.

numerical simulation model [47]. If this temperature difference is kept constant, the heating power provided for each GWHP corresponds to that from Table 1.

The approach introduced here uses a vertically averaged 2D representation of the aquifer. To fully take into account all the complexities present in urban aquifers, a 3D numerical model is required [48]. However, the 2D model is, on the one hand, significantly less computationally complex and, on the other hand, should deliver sufficiently good results. It should also be noted that many aquifer parameters, such as the hydraulic conductivity or thermal dispersion factors, are based on indirect measurements and are therefore subject to uncertainties [49]. It is important to analyze how these parameter uncertainties affect the optimal solution. Such an analysis can be done in two ways, either by including the uncertainties in the optimization, i.e. solving a stochastic PDECO problem, or by performing a parameter-based sensitivity analysis with the optimal solution. This could help to find the minimum data quality required for optimization purposes or to define robust optimal solutions.

5.2. Outlook

One of the first future steps is to include the time dependencies into the optimization, i.e. to consider time-dependent PDECO problem. The solution to this problem can then be compared with the optimal solution from the stationary PDECO to assess how sufficient and robust the stationary case is for optimization purposes. Furthermore, since the groundwater simulation has been simplified by considering a 2D vertically averaged aquifer, a future goal is to use a full 3D model to analyze optimal solutions from the 2D model. For example, one can introduce random vertical heterogeneities in the aquifer to evaluate the robustness of the 2D-based optimal well layout.

Finally, the presented method has several other possible future applications, such as:

- Optimization of large GWHPs with more than one extraction and injection well, which means finding the optimal number and positioning of wells as well as optimal pumping rates. The method can already be used to find optimal well locations of an individual GWHP with any number of wells. However, if the number of wells and their pumping rates are unknown, these can also be defined as optimization variables.
- Optimization of aquifer thermal energy storage (ATES) systems as these systems have the same working principle as GWHPs, with the exception of utilizing the aquifer as energy storage. Similar to GWHPs, optimal well locations and their pumping rates can be found for ATES systems. In addition, the method can be used to find optimal locations of multiple ATES systems in the areas with high density of such systems [50,51].
- Finding optimal arrangements of neighboring GWHPs that operate in both modes, i.e. heating and cooling. Since these modes change the groundwater temperature in opposite directions, positive interactions between neighboring systems can arise [52]. Thus, it would be useful to optimally place wells so that the positive synergies are maximized. The method can be applied in this case by including the time dependencies and additional heat sources, i.e. cooling wells.
- Improved quantification of the thermal groundwater potential of the area of interest. This means, for example, determining the maximum number of GWPHs that can be installed in a certain area while complying with all regulatory conditions. Such potential assessments could be integrated into energy system optimization models [53], which are used to find optimal energy transition paths towards CO_2 reduction targets.

6. Conclusions

In this work, a new method for determining the optimal well layout of groundwater heat pumps is presented. The method is a gradient-based optimization that relies on an efficient calculation of the required gradients using the adjoint approach. This enables a large number of continuous optimization variables, i.e. well locations, to be considered simultaneously. An integral part of this optimization concept is the numerical simulation of the groundwater flow and heat transport based on finite elements. The new method is implemented using Firedrake and dolfin-adjoint, which are open-source frameworks for numerically solving PDEs using FEM and generating adjoints, respectively. Since the underlying PDE-constrained optimization problem is non-convex and has many local optima, a robust initialization strategy is also

proposed. The strategy is to use multiple starting well layouts, which are obtained from Latin Hypercube Sampling and have the best values of the functional of interest.

The new method is tested on a case study in Munich, Germany, with real data and 10 GWHPs, each with a single well pair. A total of 10 extraction and 10 injection wells are optimally placed to maximize groundwater temperature at all extraction wells. To analyze the influence of hydro-geological conditions on the optimization results, i.e. the optimal well layout, two optimization scenarios were considered, which differ in the temperature of the inflowing groundwater. The results show that the proposed methodology successfully finds optimal well layouts in both scenarios and that hydro-geological conditions can significantly alter the optimal well layout. In both scenarios, the sum of groundwater temperatures at all extraction wells in the optimal well layout is almost 14 °C higher than in the non-optimized benchmark.

It should be emphasized that the proposed method is the first well layout optimization method that allows for continuous well locations and is not limited by the number of wells. This is a significant improvement compared to the existing methods, which can only consider predefined (discrete) well locations and a small number of wells. In addition, this is the first method used to optimize the well layout of multiple neighboring GWHPs to maximize thermal groundwater potential. The method can also be applied to find optimal well layouts of individual systems with multiple extraction and injection wells. Moreover, the method can be used in various other applications in the future, such as the optimization of ATES systems or the quantification of the thermal potential of aquifers. Finally, the introduced method can serve as a basis for the future optimal management and planning of the geothermal resource groundwater.

CRediT authorship contribution statement

Smajil Halilovic: Conceptualization, Methodology, Writing – original draft, Software, Investigation, Visualization. **Fabian Böttcher:** Conceptualization, Writing – original draft, Data curation, Visualization. **Stephan C. Kramer:** Methodology, Software, Writing – review & editing. **Matthew D. Piggott:** Methodology, Writing – review & editing. **Kai Zosseder:** Funding acquisition, Writing - review & editing. **Thomas Hamacher:** Funding acquisition, Supervision.

Declaration of competing interest

The authors declare that they have no known competing financial interests or personal relationships that could have appeared to influence the work reported in this paper.

Data availability

Data will be made available on request.

Acknowledgments

The work presented in this paper has been supported by the German Federal Ministry for Economic Affairs and Energy (BMWi) within the scope of the research project GEO.KW (01184143/1). The authors also acknowledge the TUM Global Incentive Fund 2021 for supporting the collaboration between the Technical University of Munich and Imperial College London.

Appendix A. Coefficients for linear control constraints

Linear control constraints (18) are generated automatically in the code using the following steps:

1. The geometry of plots is read from shape files using the Python library GeoPandas [54]. The result is a list of vertices for each convex plot.
2. The vertices are then used to define linear functions that correspond to the edges of plots.
3. Inequality constraints are defined based on geometric relations and the linear functions obtained previously.

In the second step, the linear function corresponding to the edge e_{ij} between two vertices v_i and v_j is obtained from the equation of a line through two points:

$$y = k_{ij} \cdot x + n_{ij} \tag{A.1}$$

$$k_{ij} = \frac{y_j - y_i}{x_j - x_i} \tag{A.2}$$

$$n_{ij} = \frac{y_i \cdot x_j - y_j \cdot x_i}{x_j - x_i} \tag{A.3}$$

where $v_i = (x_i, y_i)$ and $v_j = (x_j, y_j)$. It should be noted that in the case of $x_i = x_j = x_\perp$ the previous formulas for k_{ij} and n_{ij} are not applicable since the function becomes $y = x_\perp$.

In the third step, the inequality constraint for each edge is obtained from the function (A.1) by replacing the equality sign with $\leq$ or $\geq$. The inequality sign is selected based on a relative geometric positions of the corresponding edge e_{ij} and an arbitrary point $p_c = (x_c, y_c)$ within the convex plot (polygon). An example plot with an internal point p_c and an edge e_{ij} is depicted in Fig. A.15a. If the edge e_{ij} lies "below" the point p_c then = in (A.1) is replaced by $\geq$ and, otherwise it is replaced by $\leq$ if the edge is "above" the point. The "below" and "above" means respectively negative and positive y-axis sections $m_c = y(x_c)$ of the function corresponding to that edge on an auxiliary coordinate system, whose origin is the point p_c (Fig. A.15b). The special case $y = x_\perp$ must be separately considered, since there is no intersection with y-axis here (Fig. A.15c). In this case, if $x_c \leq x_\perp$ the inequality constraint reads as $x \leq x_\perp$ and, otherwise, the constraints becomes $x \geq x_\perp$. It should be noted that the point p_c can be chosen arbitrarily as far as it is inside the plot, but here the geometrical centroids of plots are used since they are easy to obtain from shape files.

Appendix B. State constraints

Once the order of installation of GWHPs is established, a new set of constraints should be added to reflect the regulations on negative interference between neighboring GWHP systems. As already mentioned, neighboring GWHPs can influence each other in such a way that upstream GWHPs change the groundwater temperature at extraction wells of downstream GWHPs. In some countries, the approval ordinance stipulates that the temperature change (due to the new upstream systems) at the extraction well of an existing GWHP must be less than a specified constant threshold value T_{diff}. In this work, the area of interest is located in Bavaria, Germany, where $T_{diff} = 1$ [K] [26]. The corresponding constraints are given as follows:

$$T_n(\mathbf{x}_i^{ext}) - T(\mathbf{x}_i^{ext}) \leq T_{diff} \quad \forall i \in \{1, \dots, N_{exis}\} \tag{B.1}$$

where $T_n(\mathbf{x}_i^{ext})$ is the natural groundwater temperature at the extraction well of GWHP i; $T(\mathbf{x}_i^{ext})$ the temperature after new systems have been installed upstream; N_{exis} the number of existing GWHPs. The temperature field T_n can be obtained by solving the underlying PDE system without any new GWHPs and, thus, represents a constant parameter in the optimization problem. It is important to note that the current system for installing (licensing) new GWHPs works on a first-come-first-served basis. Therefore, the regulation described above is only

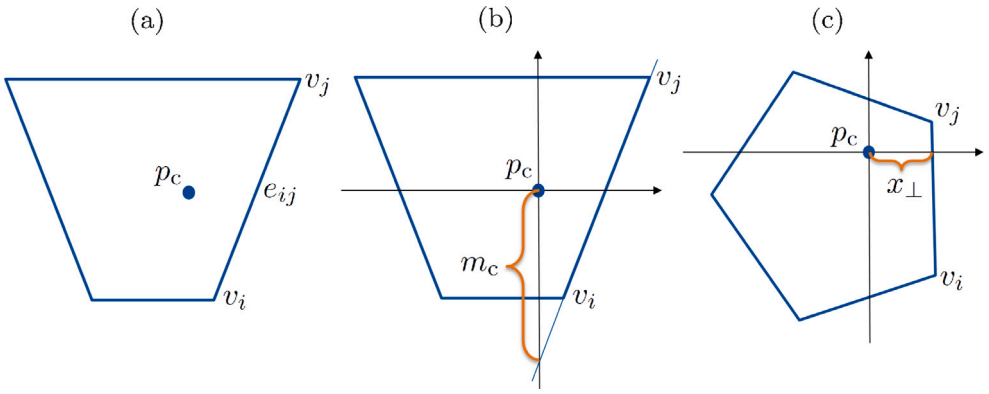

Fig. A.15. Geometric relations between an edge e_{ij} and a point p_c within the plot.

applied to new systems to check whether they have a negative impact on already existing downstream GWHPs.

In (B.1) the temperature fields (functions) are evaluated at the positions of extraction wells, which means that the Dirac delta function is applied in the same way as in (16). However, it should be noted that $\mathbf{x}_i^{\text{ext}}$ in (B.1) are no longer control variables, but only constant values, since the existing GWHPs are "fixed" and not part of the optimization. Moreover, the constraints (B.1) include the state T and, thus, cannot be explicitly defined in the reduced formulation (11). There are several approaches to dealing with state constraints in PDECO problems, including the penalty-based approach.

The state constraints (B.1) can be replaced by adding a penalty term P_T to the original functional of interest (16). In the first step, the constraints are reformulated as follows:

$$\int_\Omega s_1(\mathbf{x}_i^{\text{ext}})\,\mathrm{d}\Omega \leq \int_\Omega s_2(T,\mathbf{x}_i^{\text{ext}})\,\mathrm{d}\Omega \tag{B.2}$$

where $s_1(\mathbf{x}_i^{\text{ext}}) = (T_{\text{n}}(\mathbf{x}) - \mathrm{T}_{\text{diff}})\cdot\delta(\mathbf{x}-\mathbf{x}_i^{\text{ext}})$ and $s_2(T,\mathbf{x}_i^{\text{ext}}) = T(\mathbf{x})\cdot\delta(\mathbf{x}-\mathbf{x}_i^{\text{ext}})$. Thereafter, the penalty term is defined as:

$$P_T = \gamma\cdot\sum_{i=1}^{N}\int_\Omega (\max\{0, s_1^i - s_2^i\})^2\,\mathrm{d}\Omega \tag{B.3}$$

where $s_1^i = s_1(\mathbf{x}_i^{\text{ext}})$, $s_2^i = s_2(T,\mathbf{x}_i^{\text{ext}})$, and γ is a penalty scaling factor. This type of penalty is similar to the Moreau–Yosida type of regularization terms used in state-constrained optimization problems [55]. The penalty term P_T becomes zero when the constraints (B.1) are met, and otherwise scales quadratically with the constraints violation. The maximum function in (B.3) is squared to obtain a smooth function, which is advantageous for gradient-based optimization.

References

[1] European Commission. 2050 Long-term strategy: Climate action. 2020, URL: https://ec.europa.eu/clima/eu-action/climate-strategies-targets/2050-long-term-strategy_en.

[2] Bloess A, Schill W-P, Zerrahn A. Power-to-heat for renewable energy integration: A review of technologies, modeling approaches, and flexibility potentials. Appl Energy 2018;212:1611–26. http://dx.doi.org/10.1016/j.apenergy.2017.12.073.

[3] Rinaldi A, Soini MC, Streicher K, Patel MK, Parra D. Decarbonising heat with optimal PV and storage investments: A detailed sector coupling modelling framework with flexible heat pump operation. Appl Energy 2021;282:116110. http://dx.doi.org/10.1016/j.apenergy.2020.116110.

[4] Self SJ, Reddy BV, Rosen MA. Geothermal heat pump systems: Status review and comparison with other heating options. Appl Energy 2013;101:341–8. http://dx.doi.org/10.1016/j.apenergy.2012.01.048.

[5] Somogyi V, Sebestyén V, Domokos E, Zseni A, Papp Z. Thermal impact assessment with hydrodynamics and transport modeling. Energy Convers Manage 2015;104:127–34. http://dx.doi.org/10.1016/j.enconman.2015.04.045.

[6] Kim J, Nam Y. A numerical study on system performance of groundwater heat pumps. Energies 2016;9(1):4. http://dx.doi.org/10.3390/en9010004.

[7] Böttcher F, Zosseder K. Thermal influences on groundwater in urban environments – A multivariate statistical analysis of the subsurface heat island effect in Munich. Sci Total Environ 2021;810(January 2022):152193. http://dx.doi.org/10.1016/j.scitotenv.2021.152193.

[8] Menberg K, Bayer P, Zosseder K, Rumohr S, Blum P. Subsurface urban heat islands in German cities. Sci Total Environ 2013;442:123–33. http://dx.doi.org/10.1016/j.scitotenv.2012.10.043.

[9] Herbert A, Arthur S, Chillingworth G. Thermal modelling of large scale exploitation of ground source energy in urban aquifers as a resource management tool. Appl Energy 2013;109:94–103. http://dx.doi.org/10.1016/j.apenergy.2013.03.005.

[10] Attard G, Bayer P, Rossier Y, Blum P, Eisenlohr L. A novel concept for managing thermal interference between geothermal systems in cities. Renew Energy 2020;145:914–24. http://dx.doi.org/10.1016/j.renene.2019.06.095.

[11] García-Gil A, Vázquez-Suñe E, Schneider EG, Sánchez-Navarro JA, Mateo-Lázaro J. Relaxation factor for geothermal use development – Criteria for a more fair and sustainable geothermal use of shallow energy resources. Geothermics 2015;56:128–37. http://dx.doi.org/10.1016/j.geothermics.2015.04.003.

[12] Epting J, Böttcher F, Mueller MH, García-Gil A, Zosseder K, Huggenberger P. City-scale solutions for the energy use of shallow urban subsurface resources – Bridging the gap between theoretical and technical potentials. Renew Energy 2020;147:751–63. http://dx.doi.org/10.1016/j.renene.2019.09.021.

[13] Böttcher F, Casasso A, Götzl G, Zosseder K. TAP - Thermal aquifer Potential: A quantitative method to assess the spatial potential for the thermal use of groundwater. Renew Energy 2019;142:85–95. http://dx.doi.org/10.1016/j.renene.2019.04.086.

[14] Clyde CG, Madabhushi GV. Spacing of wells for heat pumps. J Water Resour Plan Manage 1983;109(3):203–12. http://dx.doi.org/10.1061/(ASCE)0733-9496(1983)109:3(203).

[15] Hecht-Méndez J, de Paly M, Beck M, Bayer P. Optimization of energy extraction for vertical closed-loop geothermal systems considering groundwater flow. Energy Convers Manage 2013;66:1–10. http://dx.doi.org/10.1016/j.enconman.2012.09.019.

[16] Beck M, Bayer P, de Paly M, Hecht-Méndez J, Zell A. Geometric arrangement and operation mode adjustment in low-enthalpy geothermal borehole fields for heating. Energy 2013;49:434–43. http://dx.doi.org/10.1016/j.energy.2012.10.060.

[17] Zhou Y-z, Zhou Z-f. Simulation of thermal transport in aquifer: A GWHP system in Chengdu, China. J Hydrodyn 2009;21(5):647–57. http://dx.doi.org/10.1016/S1001-6058(08)60196-1.

[18] Gao Q, Zhou X-Z, Jiang Y, Chen X-L, Yan Y-Y. Numerical simulation of the thermal interaction between pumping and injecting well groups. Appl Therm Eng 2013;51(1–2):10–9. http://dx.doi.org/10.1016/j.applthermaleng.2012.09.017.

[19] Lo Russo S, Civita MV. Open-loop groundwater heat pumps development for large buildings: A case study. Geothermics 2009;38(3):335–45. http://dx.doi.org/10.1016/j.geothermics.2008.12.009.

[20] Park DK, Kaown D, Lee K-K. Development of a simulation-optimization model for sustainable operation of groundwater heat pump system. Renew Energy 2020;145:585–95. http://dx.doi.org/10.1016/j.renene.2019.06.039.

[21] Park D, Lee E, Kaown D, Lee S-S, Lee K-K. Determination of optimal well locations and pumping/injection rates for groundwater heat pump system. Geothermics 2021;92:102050. http://dx.doi.org/10.1016/j.geothermics.2021.102050.

[22] Diersch H-JG. FEFLOW. Berlin, Heidelberg: Springer Berlin Heidelberg; 2014, http://dx.doi.org/10.1007/978-3-642-38739-5.

[23] Bundschuh J, Suárez Arriaga MC. Introduction to the numerical modeling of groundwater and geothermal systems: Fundamentals of mass, energy, and solute transport in poroelastic rocks. Multiphysics modeling, vol. 2, Boca Raton: CRC Press; 2010.

[24] Hinze M, Pinnau R, Ulbrich M, Ulbrich S. Optimization with PDE constraints, Vol. 23. Springer Science & Business Media; 2008, URL: http://swbplus.bsz-bw.de/bsz288078012cov.htm.

[25] Giles MB, Pierce NA. An introduction to the adjoint approach to design. Flow Turbul Combust 2000;65(3/4):393–415. http://dx.doi.org/10.1023/A:1011430410075, URL: https://link.springer.com/article/10.1023/a:1011430410075.
[26] Bayerisches Landesamt für Umwelt. Planung und Erstellung von Erdwärmesonden: LfU. 2012, URL: https://www.lfu.bayern.de/wasser/merkblattsammlung/teil3_grundwasser_und_boden/doc/nr_372.pdf.
[27] Milnes E, Perrochet P. Assessing the impact of thermal feedback and recycling in open-loop groundwater heat pump (GWHP) systems: a complementary design tool. Hydrogeol J 2013;21(2):505–14. http://dx.doi.org/10.1007/s10040-012-0902-y.
[28] Yeniay O. Penalty function methods for constrained optimization with genetic algorithms. Math Comput Appl 2005;10(1):45–56. http://dx.doi.org/10.3390/mca10010045, URL: https://www.mdpi.com/133758.
[29] Blank L, Meneses Rioseco E, Caiazzo A, Wilbrandt U. Modeling, simulation, and optimization of geothermal energy production from hot sedimentary aquifers. Comput Geosci 2021;25(1):67–104. http://dx.doi.org/10.1007/s10596-020-09989-8.
[30] King RN, Dykes K, Graf P, Hamlington PE. Optimization of wind plant layouts using an adjoint approach. Wind Energy Sci 2017;2(1):115–31. http://dx.doi.org/10.5194/wes-2-115-2017.
[31] Funke SW, Farrell PE, Piggott MD. Tidal turbine array optimisation using the adjoint approach. Renew Energy 2014;63:658–73. http://dx.doi.org/10.1016/j.renene.2013.09.031.
[32] Jin R, Chen W, Sudjianto A. An efficient algorithm for constructing optimal design of computer experiments. J Statist Plann Inference 2005;134(1):268–87. http://dx.doi.org/10.1016/j.jspi.2004.02.014.
[33] Bouhlel MA, Hwang JT, Bartoli N, Lafage R, Morlier J, Martins JR. A Python surrogate modeling framework with derivatives. Adv Eng Softw 2019;135:102662. http://dx.doi.org/10.1016/j.advengsoft.2019.03.005.
[34] Rathgeber F, Ham DA, Mitchell L, Lange M, Luporini F, Mcrae ATT, Bercea G-T, Markall GR, Kelly PHJ. Firedrake. ACM Trans Math Software 2017;43(3):1–27. http://dx.doi.org/10.1145/2998441.
[35] Mitusch S, Funke S, Dokken J. Dolfin-adjoint 2018.1: automated adjoints for FEniCS and Firedrake. J Open Source Softw 2019;4(38):1292. http://dx.doi.org/10.21105/joss.01292.
[36] Trefry MG, Muffels C. FEFLOW: A finite-element ground water flow and transport modeling tool. Ground Water 2007;45(5):525–8. http://dx.doi.org/10.1111/j.1745-6584.2007.00358.x.
[37] Kraft D, Schnepper K. SLSQP—a nonlinear programming method with quadratic programming subproblems, Vol. 545. Oberpfaffenhofen: DLR; 1989.
[38] Virtanen P, Gommers R, Oliphant TE, Haberland M, Reddy T, Cournapeau D, Burovski E, Peterson P, Weckesser W, Bright J, van der Walt SJ, Brett M, Wilson J, Millman KJ, Mayorov N, Nelson ARJ, Jones E, Kern R, Larson E, Carey CJ, Polat I, Feng Y, Moore EW, VanderPlas J, Laxalde D, Perktold J, Cimrman R, Henriksen I, Quintero EA, Harris CR, Archibald AM, Ribeiro AH, Pedregosa F, van Mulbregt P. SciPy 1.0: fundamental algorithms for scientific computing in Python. Nature Methods 2020;17(3):261–72. http://dx.doi.org/10.1038/s41592-019-0686-2, URL: https://www.nature.com/articles/s41592-019-0686-2?report=reader.
[39] Zosseder K, Kerl M, Albarrán-Ordás A, Gossler M, Kiecak A, Chavez-Kus L. Die hydraulischen Grundwasserverhältnisse des quartären und des oberflächennahen tertiären Grundwasserleiters im Großraum München. Geol Bavarica 2022;122(Umwelt Spezial):199, URL: https://www.bestellen.bayern.de/shoplink/91122.htm.
[40] Albarrán-Ordás A, Zosseder K. The di models method: geological 3-D modeling of detrital systems consisting of varying grain fractions to predict the relative lithological variability for a multipurpose usability. Bull Eng Geol Environ 2022;81(1). http://dx.doi.org/10.1007/s10064-021-02538-2.
[41] Albarrán-Ordás A, Zosseder K. Geostatistische Reliefmodellierung der quartären Grundwasserleiterbasis in der Münchener Schotterebene unter Verwendung von Massendaten. Z Deutsch Ges Geowiss 2020;171(1):1–19. http://dx.doi.org/10.1127/zdgg/2020/0206.
[42] Theel M, Huggenberger P, Zosseder K. Assessment of the heterogeneity of hydraulic properties in gravelly outwash plains: a regionally scaled sedimentological analysis in the Munich gravel plain, Germany. Hydrogeol J 2020;28(8):2657–74. http://dx.doi.org/10.1007/s10040-020-02205-y.
[43] Molar-Cruz A. UrbanHeatPro. 2020, https://github.com/tum-ens/UrbanHeatPro.
[44] Geuzaine C, Remacle J-F. Gmsh: A 3-D finite element mesh generator with built-in pre- and post-processing facilities. Internat J Numer Methods Engrg 2009;79(11):1309–31. http://dx.doi.org/10.1002/nme.2579.
[45] Wallwork J, Angeloudis A, Barral N, Mackie L, Kramer S, Piggott M. Tidal turbine array modelling using goal-oriented mesh adaptation. California Digital Library (CDL); 2022, http://dx.doi.org/10.31223/x5h06b.
[46] Stauffer F, Bayer P, Blum P, Giraldo NM, Kinzelbach W. Thermal use of shallow groundwater. Boca Raton, Fla.: CRC Press; 2014.
[47] Muela Maya S, García-Gil A, Garrido Schneider E, Mejías Moreno M, Epting J, Vázquez-Suñé E, Marazuela MA, Sánchez-Navarro JA. An upscaling procedure for the optimal implementation of open-loop geothermal energy systems into hydrogeological models. J Hydrol 2018;563:155–66. http://dx.doi.org/10.1016/j.jhydrol.2018.05.057.
[48] Epting J, Huggenberger P. Unraveling the heat island effect observed in urban groundwater bodies - Definition of a potential natural state. J Hydrol 2013;501:193–204. http://dx.doi.org/10.1016/j.jhydrol.2013.08.002.
[49] Gelhar LW, Welty C, Rehfeldt KR. A critical review of data on field-scale dispersion in aquifers. Water Resour Res 1992;28(7):1955–74. http://dx.doi.org/10.1029/92WR00607, arXiv:arXiv:1011.1669v3.
[50] Bloemendal M, Olsthoorn T, Boons F. How to achieve optimal and sustainable use of the subsurface for aquifer thermal energy storage. Energy Policy 2014;66:104–14. http://dx.doi.org/10.1016/j.enpol.2013.11.034.
[51] Bloemendal M, Jaxa-Rozen M, Olsthoorn T. Methods for planning of ATES systems. Appl Energy 2018;216:534–57. http://dx.doi.org/10.1016/j.apenergy.2018.02.068.
[52] García-Gil A, Mejías Moreno M, Garrido Schneider E, Marazuela MA, Abesser C, Mateo Lázaro J, Sánchez Navarro JA. Nested shallow geothermal systems. Sustainability 2020;12(12):5152. http://dx.doi.org/10.3390/su12125152.
[53] Halilovic S, Odersky L, Hamacher T. Integration of groundwater heat pumps into energy system optimization models. Energy 2022;238:121607. http://dx.doi.org/10.1016/j.energy.2021.121607.
[54] Jordahl K, den Bossche JV, Fleischmann M, Wasserman J, McBride J, Gerard J, Tratner J, Perry M, Badaracco AG, Farmer C, Hjelle GA, Snow AD, Cochran M, Gillies S, Culbertson L, Bartos M, Eubank N, maxalbert, Bilogur A, Rey S, Ren C, Arribas-Bel D, Wasser L, Wolf LJ, Journois M, Wilson J, Greenhall A, Holdgraf C, Filipe, Leblanc F. Geopandas/geopandas: v0.8.1. 2020, http://dx.doi.org/10.5281/ZENODO.3946761.
[55] Hintermüller M, Hinze M. Moreau–Yosida regularization in state constrained elliptic control problems: Error estimates and parameter adjustment. SIAM J Numer Anal 2009;47(3):1666–83. http://dx.doi.org/10.1137/080718735.

5 Conclusion and outlook

This thesis has developed and evaluated novel frameworks for the optimization of GWHP systems that are efficient and tailored to specific applications. In achieving this primary objective, the thesis effectively closes research gaps identified in the literature, resulting in both methodological and application-oriented advances. It should be highlighted that the optimization approaches for GWHP systems introduced in this thesis are pioneering work in this field, as the development of such approaches was almost non-existent before.

5.1 Conclusion

The publications included in this thesis introduce new approaches for the optimization of GWHPs at the system level, conduct a comparative analysis of different approaches, and present strategies for integrating GWHPs into ESOMs. Building on the findings from these publications, the central research questions formulated in Section 1.3 are answered in the following:

1. **What are the viable approaches for the optimization of GWHP systems, and how do they compare in terms of efficiency and applicability?**

   In Section 4.1, a comprehensive analysis was conducted to identify and compare GWHP optimization approaches and to propose a new classification scheme for them. The identified approaches were divided into four different classes based on the groundwater simulation model used (PDE-based or simplified) and the optimization algorithm used (gradient-based or derivative-free). In terms of computational efficiency, optimization approaches using gradient-based algorithms are preferable, since they consistently outperform derivative-free algorithms. On the other hand, the applicability of an optimization approach is significantly influenced by the choice of the groundwater simulation model. Approaches using PDE models are more suitable for detailed GWHP planning, while approaches based on simplified models offer practical advantages for assessing geothermal potential over large areas.

2. **How to optimize the design and operation of GWHP systems?**

   Sections 4.2 and 4.3 present three new approaches for optimizing the design and operation of GWHP systems. The overview of these approaches is depicted in Figure 5.1. Approaches I and II, introduced in Section 4.2, use simplified (analytical) models to represent groundwater conditions and interactions between GWHPs and groundwater. Conversely, Approach III, presented in Section 4.3, is based on a PDE model of groundwater flow and heat transport within an aquifer. The difference between Approaches I and II lies primarily in their focus: Approach I concentrates on thermal groundwater considerations, particularly negative thermal interactions between neighboring systems, while Approach II focuses on hydraulic groundwater considerations.

   The identified three sub-questions are answered below:

   a) **How to optimize well locations of GWHP systems?**

      This thesis contributes three new approaches to effectively determine optimal well locations of GWHP systems. In addition to the differences between these approaches described previously, they also differ in the concept of optimal well placement. In the first two approaches, well placement is based on the selection of predefined discrete well locations, whereas the last approach enables well placement anywhere within the feasible area. The practical application of the approaches is demonstrated with real case studies in the city of Munich. The choice of the most suitable approach depends on the specific application objective. Approaches I and II are computationally more efficient

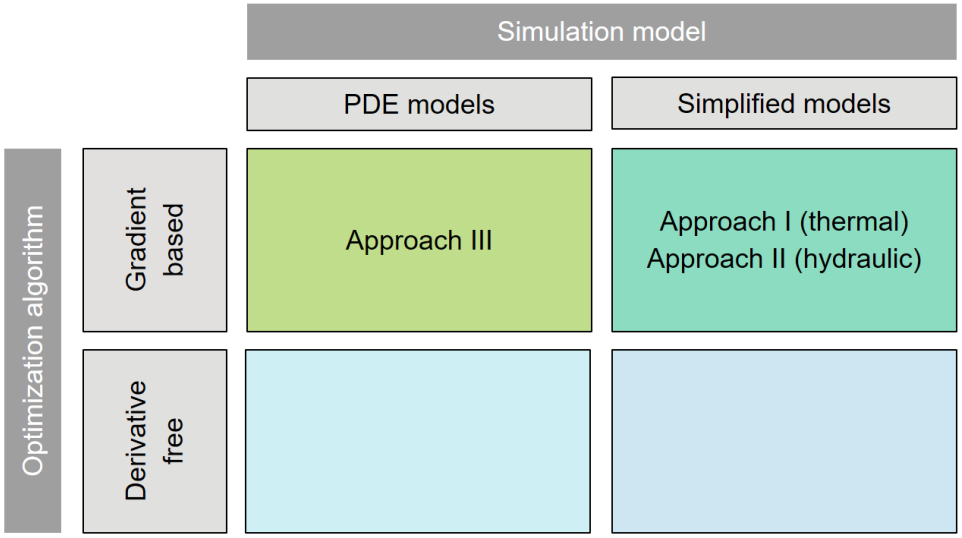

Figure 5.1 New optimization approaches in the classification scheme from Section 4.1

compared to Approach III, making them suitable for larger areas. However, this efficiency comes at the cost of neglecting multiple details and complexities associated with groundwater due to their reliance on simplified groundwater models. In contrast, Approach III can accommodate these complexities, which makes it the preferred option for applications that require detailed and accurate groundwater modeling.

b) **How to determine the optimal number of GWHP wells to be installed?**

Approaches I and II directly address this research question. These two approaches are able to not only identify optimal GWHP well locations, but also determine the optimal number of wells, i.e. the number and placement of GWHP systems or well doublets, within an area based on the overall objective. The presented approaches allow for various analyses, including determining the maximum number of systems and their locations without negative interactions within a given region or estimating the maximum technical geothermal potential of an area. The decision process on whether to install a particular GWHP (well doublet) differs slightly between the two approaches, but in both cases it involves selecting extraction-injection well pairs from a predefined set of well locations. As previously discussed, Approach I focuses on thermal groundwater considerations, while Approach II centers on hydraulic aspects. Consequently, the key factor limiting the available space for GWHP installations is the propagation of thermal plumes in the first case and the hydraulic footprint of wells in the second case. Therefore, the suitability of the two approaches depends on the requirements specific to a particular application.

c) **How to optimize the sizing (pumping rates) of GWHP wells?**

Approach II is formulated to determine the optimal sizing and placement of extraction-injection well doublets, with the aim to maximize the technical potential of thermal groundwater use. Methodologically, this is achieved by introducing additional continuous optimization variables that correspond to the pumping rates (sizes) of well doublets. This approach is tested using a real case study in the city of Munich, where the potential of each city block is optimized individually. The obtained results show that the optimal sizing strategy for well doublets depends on several factors, including the geometry of individual city blocks, their orientation with respect to the groundwater flow direction, the minimum pumping rate thresholds, and the constraints governing the distance between neighboring doublets. Approach II combines these various factors into a comprehensive optimization framework that enables the identification of the optimal strategy for maximizing geothermal potential within a given city block. This strategy can result in a small number of larger doublets (wells) or a larger number of comparatively smaller doublets.

3. **How to effectively integrate GWHPs into energy system optimization models?**

   Chapter 3 addresses this question by introducing and comparing three different approaches for integrating GWHPs into ESOMs. These approaches differ in their representation of GWHP efficiency: constant, time-dependent, and both time- and location-dependent. The comparison of the approaches is performed using a real case study in Munich, where the respective ESOM represents the residential heating sector of the city. The results reveal that assuming a constant efficiency of heat pumps throughout the year leads to misleading optimization results, while adding a spatial component to the temporal one does not significantly change the cumulative results. Therefore, the second approach (time-dependent COP) is the most suitable for analysis at the energy system level, as it is less computationally intensive than the last approach (time- and location-dependent COP). However, if spatially distributed results are needed, e.g. for urban planning, then the last approach is required.

Finally, the developed optimization approaches provide valuable tools for a variety of stakeholders, in particular for researchers and practitioners engaged in the management and optimization of open-loop shallow geothermal systems. Their potential applications span a wide spectrum, ranging from optimal design of individual GWHP systems to strategic planning of future district heating systems. Moreover, it should be emphasized that the proposed approaches can be adapted to other objective functions and constraints, extending their utility to other shallow geothermal applications and even to other energy applications where the underlying physical phenomena are governed by PDEs. In this context, the research presented here contributes to improving the understanding and optimization not only of GWHP systems, but also of other technical systems characterized by bidirectional interactions with their energy resources (environment).

5.2 Outlook

The novel optimization approaches introduced in this thesis significantly advance the research field of GWHP optimization. Nevertheless, these approaches have certain limitations, which are discussed in the following along with possible future improvements and new applications:

- Approaches I and II use analytical models to describe groundwater conditions, which leads to certain assumptions and simplifications inherent in these models. For instance, these models assume unidirectional groundwater flow in the study area or homogeneity of aquifer properties. Therefore, one potential avenue for advancement lies in the **enhancement of** these underlying **analytical models**, which would improve the corresponding optimization approaches.

- Approach I focuses on **thermal** groundwater considerations, while Approach II focuses on **hydraulic aspects**. In the future, a **combination** of these two approaches could lead to a comprehensive framework covering all relevant aspects, thus improving the analysis of the technical geothermal potential and enabling a more sophisticated thermal groundwater management.

- If GWHPs are regarded as relevant technologies in the considered region, the spatial thermal potential of groundwater should be integrated into the corresponding ESOM for the heating and/or cooling sector. Approaches I and II are particularly suitable for this task due to their analytical nature and computational efficiency, in contrast to the approaches based on PDE models [101]. This would directly improve the **representation of GWHPs in ESOMs** and the current integration methods presented in Chapter 3. In addition, Approaches I and II could also be integrated into GIS-based tools for energy planning and thermal groundwater management.

- Approach III (**PDE-based optimization**) could be extended to cover additional dimensions of GWHP optimization. This may include the consideration of **time-dependent** scenarios and the use of **3D subsurface models**, thereby going beyond the scope of the current analysis in Section 4.3, which focuses on steady-state PDEs and 2D models. In addition, the present approach optimizes only the placement of GWHP wells. Therefore, its scope could be extended to scenarios where the number of wells or systems

and their operating parameters (sizing) are also optimized. To realize such advances, mixed-integer PDE constrained optimization problems would need to be addressed.

- Through the inclusion of **economic factors**, all three approaches could be extended in the future to a comprehensive analysis that incorporates both economic and environmental dimensions of energy planning. This extended framework would provide urban planners and individual stakeholders with valuable decision support for the thermal use of groundwater.
- Groundwater (aquifer) **parameters** are often subject to **uncertainties** due to the lack of measurements or estimates from indirect measurements [102]. This thesis has not addressed the inclusion of these uncertainties in the optimization process or their impact on optimal solutions. Therefore, the optimization approaches could be extended in the future to also account for these aspects, e.g. by using stochastic optimization methods.
- The presented approaches have the potential to be extended to various **other applications** in the future. In the first instance, these are applications related to GWHP optimization that have not been addressed within the scope of this thesis. For example, we could consider optimization of a single large GWHP system with multiple extraction and injection wells, or simultaneous optimization of neighboring GWHPs operating in both heating and cooling modes. In the latter scenario, such modes can lead to positive thermal interactions between neighboring systems [103], providing the opportunity to maximize positive synergies and utilize groundwater as an energy carrier. Secondly, the approaches could be adapted for other shallow geothermal applications, e.g. optimization of ATES, GSHP, and BTES systems. Finally, the applicability of these approaches could be extended to a broader range of energy applications where the underlying physical phenomena are governed by PDEs, such as the optimization of wind or tidal energy systems.

Bibliography

[1] European Commission, "2050 long-term strategy: Climate action," 2020.

[2] European Commission. Joint Research Centre. Institute for Energy and Transport. and European Technology Platform on Renewable Heating and Cooling., *Strategic research and innovation agenda for renewable heating and cooling: European technology platform on renewable heating and cooling*. Publications Office, 2013.

[3] J. W. Lund and A. N. Toth, "Direct utilization of geothermal energy 2020 worldwide review," *Geothermics*, vol. 90, p. 101915, 2021.

[4] J. Hou, M. Cao, and P. Liu, "Development and utilization of geothermal energy in China: Current practices and future strategies," *Renewable energy*, vol. 125, pp. 401–412, 2018.

[5] S. J. Self, B. V. Reddy, and M. A. Rosen, "Geothermal heat pump systems: Status review and comparison with other heating options," *Applied Energy*, vol. 101, pp. 341–348, 2013.

[6] F. Stauffer, P. Bayer, P. Blum, N. M. Giraldo, and W. Kinzelbach, *Thermal use of shallow groundwater*. Boca Raton, Fla.: CRC Press, 2014.

[7] S. Haehnlein, P. Bayer, and P. Blum, "International legal status of the use of shallow geothermal energy," *Renewable and Sustainable Energy Reviews*, vol. 14, no. 9, pp. 2611–2625, 2010.

[8] G. Florides and S. Kalogirou, "Ground heat exchangers—a review of systems, models and applications," *Renewable Energy*, vol. 32, no. 15, pp. 2461–2478, 2007.

[9] A. García Gil, E. A. Garrido Schneider, M. Mejías Moreno, and J. C. Santamarta Cerezal, *Shallow Geothermal Energy*. Springer, 2022.

[10] D. Banks, *An introduction to thermogeology: ground source heating and cooling*. John Wiley & Sons, 2012.

[11] J.-Y. Lee, J.-H. Won, and J.-S. Hahn, "Evaluation of hydrogeologic conditions for groundwater heat pumps: analysis with data from national groundwater monitoring stations," *Geosciences Journal*, vol. 10, pp. 91–99, 2006.

[12] J. Kim and Y. Nam, "A numerical study on system performance of groundwater heat pumps," *Energies*, vol. 9, no. 1, p. 4, 2016.

[13] A. García Gil, E. A. Garrido Schneider, M. Mejías Moreno, and J. C. Santamarta Cerezal, "Management and governance of shallow geothermal energy resources," in *Shallow Geothermal Energy*, pp. 237–272, Springer, 2022.

[14] J. Epting, M. H. Müller, D. Genske, and P. Huggenberger, "Relating groundwater heat-potential to city-scale heat-demand: A theoretical consideration for urban groundwater resource management," *Applied Energy*, vol. 228, pp. 1499–1505, 2018.

[15] J. Epting, F. Böttcher, M. H. Mueller, A. García-Gil, K. Zosseder, and P. Huggenberger, "City-scale solutions for the energy use of shallow urban subsurface resources – bridging the gap between theoretical and technical potentials," *Renewable Energy*, vol. 147, pp. 751–763, 2020.

[16] S. Lo Russo and M. V. Civita, "Open-loop groundwater heat pumps development for large buildings: A case study," *Geothermics*, vol. 38, no. 3, pp. 335–345, 2009.

[17] Y.-z. Zhou and Z.-f. Zhou, "Simulation of Thermal Transport in Aquifer: A GWHP System in Chengdu, China," *Journal of Hydrodynamics*, vol. 21, no. 5, pp. 647–657, 2009.

[18] Q. Gao, X.-Z. Zhou, Y. Jiang, X.-L. Chen, and Y.-Y. Yan, "Numerical simulation of the thermal interaction between pumping and injecting well groups," *Applied Thermal Engineering*, vol. 51, no. 1-2, pp. 10–19, 2013.

[19] D. K. Park, D. Kaown, and K.-K. Lee, "Development of a simulation-optimization model for sustainable operation of groundwater heat pump system," *Renewable Energy*, vol. 145, pp. 585–595, 2020.

[20] D. Park, E. Lee, D. Kaown, S.-S. Lee, and K.-K. Lee, "Determination of optimal well locations and pumping/injection rates for groundwater heat pump system," *Geothermics*, vol. 92, p. 102050, 2021.

[21] C. Audet and W. Hare, *Derivative-free and blackbox optimization*. Springer, 2017.

[22] A. R. Conn, K. Scheinberg, and L. N. Vicente, *Introduction to derivative-free optimization*. SIAM, 2009.

[23] M. H. Dickson and M. Fanelli, *Geothermal energy*. Dec 1995.

[24] L. Rybach, "Geothermal energy: sustainability and the environment," *Geothermics*, vol. 32, no. 4-6, pp. 463–470, 2003.

[25] K. C. Lee, "Classification of geothermal resources - an engineering approach," 1996.

[26] K. C. Lee, "Classification of geothermal resources by exergy," *Geothermics*, vol. 30, no. 4, pp. 431–442, 2001.

[27] C. F. Williams, M. J. Reed, and A. F. Anderson, "Updating the classification of geothermal resources," in *Proceedings, Thirty-Sixth Workshop on Geothermal Reservoir Engineering*, p. 2011, 2011.

[28] A. M. Omer, "Ground-source heat pumps systems and applications," *Renewable and sustainable energy reviews*, vol. 12, no. 2, pp. 344–371, 2008.

[29] A. Carotenuto, M. Ciccolella, N. Massarotti, and A. Mauro, "Models for thermo-fluid dynamic phenomena in low enthalpy geothermal energy systems: A review," *Renewable and Sustainable Energy Reviews*, vol. 60, pp. 330–355, 2016.

[30] K. S. Lee, *Underground thermal energy storage*. Springer, 2013.

[31] H.-J. Diersch and D. Bauer, "Analysis, modeling and simulation of underground thermal energy storage (UTES) systems," in *Advances in Thermal Energy Storage Systems*, pp. 149–183, Elsevier, 2015.

[32] B. Sanner and B. Nordell, "Underground thermal energy storage with heat pumps: An international overview," *Newsletter/IEA Heat Pump Center*, vol. 16, no. 2, pp. 10–14, 1998.

[33] S. Halilovic, F. Böttcher, K. Zosseder, and T. Hamacher, "Spatial analysis of thermal groundwater use based on optimal sizing and placement of well doublets," *Energy*, vol. 304, p. 132058, 2024.

[34] D. L. Warner and U. Algan, "Thermal impact of residential ground-water heat pumps," *Groundwater*, vol. 22, no. 1, pp. 6–12, 1984.

[35] C. D. Palmer, D. W. Blowes, E. O. Frind, and J. W. Molson, "Thermal energy storage in an unconfined aquifer: 1. Field injection experiment," *Water Resources Research*, vol. 28, no. 10, pp. 2845–2856, 1992.

[36] V. Somogyi, V. Sebestyén, E. Domokos, A. Zseni, and Z. Papp, "Thermal impact assessment with hydrodynamics and transport modeling," *Energy Conversion and Management*, vol. 104, pp. 127–134, 2015.

[37] Bayerisches Landesamt für Umwelt, "Planung und Erstellung von Erdwärmesonden: LfU," 2012.

[38] S. Foster and P. Chilton, "Groundwater: the processes and global significance of aquifer degradation," *Philosophical Transactions of the Royal Society of London. Series B: Biological Sciences*, vol. 358, no. 1440, pp. 1957–1972, 2003.

[39] P. Blum, K. Menberg, F. Koch, S. A. Benz, C. Tissen, H. Hemmerle, and P. Bayer, "Is thermal use of groundwater a pollution?," *Journal of Contaminant Hydrology*, vol. 239, p. 103791, 2021.

[40] J. Adams and S. Bachu, "Equations of state for basin geofluids: algorithm review and intercomparison for brines," *Geofluids*, vol. 2, no. 4, pp. 257–271, 2002.

[41] H. Brielmann, C. Griebler, S. I. Schmidt, R. Michel, and T. Lueders, "Effects of thermal energy discharge on shallow groundwater ecosystems," *FEMS microbiology ecology*, vol. 68, no. 3, pp. 273–286, 2009.

[42] F. H. Chapelle, "The significance of microbial processes in hydrogeology and geochemistry," *Hydrogeology Journal*, vol. 8, pp. 41–46, 2000.

[43] P. C. Bennett, F. K. Hiebert, and J. R. Rogers, "Microbial control of mineral–groundwater equilibria: Macroscale to microscale," *Hydrogeology Journal*, vol. 8, pp. 47–62, 2000.

[44] S. Hähnlein, P. Blum, and P. Bayer, "Oberflächennahe Geothermie–aktuelle rechtliche Situation in Deutschland," *Grundwasser*, vol. 16, no. 2, pp. 69–75, 2011.

[45] F. Böttcher, A. Casasso, G. Götzl, and K. Zosseder, "Tap - thermal aquifer potential: A quantitative method to assess the spatial potential for the thermal use of groundwater," *Renewable Energy*, vol. 142, pp. 85–95, 2019.

[46] S. Bezelgues-Courtade, J.-C. Martin, S. Schomburgk, P. Monnot, D. Nguyen, M. Le Brun, A. Desplan, *et al.*, "Geothermal potential of shallow aquifers: decision-aid tool for heat-pump installation," in *World Geothermal Congress 2010*, pp. 9–p, 2010.

[47] H. Bouwer, "Artificial recharge of groundwater: hydrogeology and engineering," *Hydrogeology journal*, vol. 10, pp. 121–142, 2002.

[48] A. Casasso and R. Sethi, "Assessment and mapping of the shallow geothermal potential in the province of Cuneo (Piedmont, NW Italy)," *Renewable Energy*, vol. 102, pp. 306–315, 2017.

[49] D. Banks, "Thermogeological assessment of open-loop well-doublet schemes: a review and synthesis of analytical approaches," *Hydrogeology Journal*, vol. 17, no. 5, pp. 1149–1155, 2009.

[50] E. Milnes and P. Perrochet, "Assessing the impact of thermal feedback and recycling in open-loop groundwater heat pump (GWHP) systems: a complementary design tool," *Hydrogeology journal*, vol. 21, no. 2, pp. 505–514, 2013.

[51] C. G. Clyde and G. V. Madabhushi, "Spacing of wells for heat pumps," *Journal of Water Resources Planning and Management*, vol. 109, no. 3, pp. 203–212, 1983.

[52] W. Pophillat, G. Attard, P. Bayer, J. Hecht-Méndez, and P. Blum, "Analytical solutions for predicting thermal plumes of groundwater heat pump systems," *Renewable Energy*, vol. 147, pp. 2696–2707, 2020.

[53] H.-J. G. Diersch, *FEFLOW*. Berlin, Heidelberg: Springer Berlin Heidelberg, 2014.

[54] J. Bundschuh and M. C. Suárez Arriaga, *Introduction to the numerical modeling of groundwater and geothermal systems: Fundamentals of mass, energy, and solute transport in poroelastic rocks*, vol. 2 of *Multiphysics modeling*. Boca Raton: CRC Press, 2010.

[55] H. F. Wang and M. P. Anderson, *Introduction to groundwater modeling: finite difference and finite element methods*. Academic Press, 1995.

[56] S. Whitaker, "Flow in porous media I: A theoretical derivation of Darcy's law," *Transport in porous media*, vol. 1, pp. 3–25, 1986.

[57] M. Barackman and M. Brusseau, "Chapter 8 - groundwater sampling," in *Environmental Monitoring and Characterization* (J. F. Artiola, I. L. Pepper, and M. L. Brusseau, eds.), pp. 121–139, Burlington: Academic Press, 2002.

[58] R. N. King, K. Dykes, P. Graf, and P. E. Hamlington, "Optimization of wind plant layouts using an adjoint approach," *Wind Energy Science*, vol. 2, no. 1, pp. 115–131, 2017.

[59] W. Munters and J. Meyers, "Dynamic strategies for yaw and induction control of wind farms based on large-eddy simulation and optimization," *Energies*, vol. 11, no. 1, p. 177, 2018.

[60] J. P. Goit and J. Meyers, "Optimal control of energy extraction in wind-farm boundary layers," *Journal of Fluid Mechanics*, vol. 768, pp. 5–50, 2015.

[61] S. W. Funke, P. E. Farrell, and M. D. Piggott, "Tidal turbine array optimisation using the adjoint approach," *Renewable Energy*, vol. 63, pp. 658–673, 2014.

[62] A. Angeloudis, S. C. Kramer, A. Avdis, and M. D. Piggott, "Optimising tidal range power plant operation," *Applied energy*, vol. 212, pp. 680–690, 2018.

[63] R. Du Feu, S. Funke, S. Kramer, D. Culley, J. Hill, B. Halpern, and M. Piggott, "The trade-off between tidal-turbine array yield and impact on flow: A multi-objective optimisation problem," *Renewable Energy*, vol. 114, pp. 1247–1257, 2017.

[64] M. C. Steinbach, "On PDE solution in transient optimization of gas networks," *Journal of computational and applied mathematics*, vol. 203, no. 2, pp. 345–361, 2007.

[65] K. Ehrhardt and M. C. Steinbach, "Nonlinear optimization in gas networks," in *Modeling, Simulation and Optimization of Complex Processes: Proceedings of the International Conference on High Performance Scientific Computing, March 10–14, 2003, Hanoi, Vietnam*, pp. 139–148, Springer, 2005.

[66] M. Gugat, G. Leugering, A. Martin, M. Schmidt, M. Sirvent, and D. Wintergerst, "MIP-based instantaneous control of mixed-integer PDE-constrained gas transport problems," *Computational Optimization and Applications*, vol. 70, pp. 267–294, 2018.

[67] C. D. Laird, L. T. Biegler, and B. G. van Bloemen Waanders, "Real-time, large-scale optimization of water network systems using a subdomain approach," in *Real-time PDE-constrained optimization*, pp. 289–306, SIAM, 2007.

[68] P. Domschke, O. Kolb, and J. Lang, "Adjoint-based error control for the simulation and optimization of gas and water supply networks," *Applied Mathematics and Computation*, vol. 259, pp. 1003–1018, 2015.

[69] A. Martin, K. Klamroth, J. Lang, G. Leugering, A. Morsi, M. Oberlack, M. Ostrowski, and R. Rosen, *Mathematical optimization of water networks*, vol. 162. Springer, 2012.

[70] L. Blank, E. Meneses Rioseco, A. Caiazzo, and U. Wilbrandt, "Modeling, simulation, and optimization of geothermal energy production from hot sedimentary aquifers," *Computational Geosciences*, vol. 25, pp. 67–104, 2021.

[71] M. Chen, A. F. Tompson, R. J. Mellors, and O. Abdalla, "An efficient optimization of well placement and control for a geothermal prospect under geological uncertainty," *Applied energy*, vol. 137, pp. 352–363, 2015.

[72] G. Huang, X. Hu, H. Ma, L. Liu, J. Yang, W. Zhou, W. Liao, and B. Ningbo, "Optimized geothermal energy extraction from hot dry rocks using a horizontal well with different exploitation schemes," *Geothermal Energy*, vol. 11, no. 1, p. 5, 2023.

[73] J. Gao and Q. Shi, "A new mathematical modeling approach for thermal exploration efficiency under different geothermal well layout conditions," *Scientific Reports*, vol. 11, no. 1, p. 22930, 2021.

[74] A. Pizzolato, A. Sharma, K. Maute, A. Sciacovelli, and V. Verda, "Topology optimization for heat transfer enhancement in latent heat thermal energy storage," *International Journal of Heat and Mass Transfer*, vol. 113, pp. 875–888, 2017.

[75] A. Pizzolato, A. Sharma, K. Maute, A. Sciacovelli, and V. Verda, "Design of effective fins for fast pcm melting and solidification in shell-and-tube latent heat thermal energy storage through topology optimization," *Applied Energy*, vol. 208, pp. 210–227, 2017.

[76] C. Pan, N. Vermaak, C. Romero, S. Neti, S. Hoenig, and C.-H. Chen, "Efficient optimization of a longitudinal finned heat pipe structure for a latent thermal energy storage system," *Energy Conversion and Management*, vol. 153, pp. 93–105, 2017.

[77] R. Krug, V. Mehrmann, and M. Schmidt, "Nonlinear optimization of district heating networks," *Optimization and Engineering*, vol. 22, pp. 783–819, 2021.

[78] B. van der Heijde, M. Fuchs, C. R. Tugores, G. Schweiger, K. Sartor, D. Basciotti, D. Müller, C. Nytsch-Geusen, M. Wetter, and L. Helsen, "Dynamic equation-based thermo-hydraulic pipe model for district heating and cooling systems," *Energy Conversion and Management*, vol. 151, pp. 158–169, 2017.

[79] J. Mohring, D. Linn, M. Eimer, M. Rein, and N. Siedow, "District heating networks–dynamic simulation and optimal operation," *Mathematical Modeling, Simulation and Optimization for Power Engineering and Management*, pp. 303–325, 2021.

[80] P. Kolvenbach, O. Lass, and S. Ulbrich, "An approach for robust PDE-constrained optimization with application to shape optimization of electrical engines and of dynamic elastic structures under uncertainty," *Optimization and Engineering*, vol. 19, pp. 697–731, 2018.

[81] Z. Bontinck, O. Lass, S. Schöps, H. De Gersem, S. Ulbrich, and O. Rain, "Robust optimisation formulations for the design of an electric machine," *IET Science, Measurement & Technology*, vol. 12, no. 8, pp. 939–948, 2018.

[82] M. Merkel, P. Gangl, and S. Schöps, "Shape optimization of rotating electric machines using isogeometric analysis," *IEEE Transactions on Energy Conversion*, vol. 36, no. 4, pp. 2683–2690, 2021.

[83] P. Gangl and U. Langer, "Topology optimization of electric machines based on topological sensitivity analysis," *Computing and Visualization in Science*, vol. 15, pp. 345–354, 2012.

[84] V. Akçelik, G. Biros, O. Ghattas, J. Hill, D. Keyes, and B. van Bloemen Waanders, "Parallel algorithms for PDE-constrained optimization," in *Parallel processing for scientific computing*, pp. 291–322, SIAM, 2006.

[85] M. Hinze, R. Pinnau, M. Ulbrich, and S. Ulbrich, *Optimization with PDE constraints*, vol. 23. Springer Science & Business Media, 2008.

[86] F. Tröltzsch, *Optimal control of partial differential equations: theory, methods, and applications*, vol. 112. American Mathematical Soc., 2010.

[87] A. Manzoni, A. Quarteroni, and S. Salsa, *Optimal control of partial differential equations*. Springer, 2021.

[88] R. Herzog and K. Kunisch, "Algorithms for PDE-constrained optimization," *GAMM-Mitteilungen*, vol. 33, no. 2, pp. 163–176, 2010.

[89] M. D. Gunzburger, *Perspectives in flow control and optimization*. SIAM, 2002.

[90] G. Biros and O. Ghattas, "Parallel Lagrange–Newton–Krylov–Schur methods for PDE-constrained optimization. Part I: The Krylov–Schur solver," *SIAM Journal on Scientific Computing*, vol. 27, no. 2, pp. 687–713, 2005.

[91] S. W. Funke and P. E. Farrell, "A framework for automated PDE-constrained optimisation," *arXiv preprint arXiv:1302.3894*, 2013.

[92] M. B. Giles and N. A. Pierce, "An introduction to the adjoint approach to design," *Flow, Turbulence and Combustion*, vol. 65, no. 3/4, pp. 393–415, 2000.

[93] S. Halilovic, L. Odersky, and T. Hamacher, "Integration of groundwater heat pumps into energy system optimization models," *Energy*, vol. 238, p. 121607, 2022.

[94] S. Halilovic, F. Böttcher, K. Zosseder, and T. Hamacher, "Optimization approaches for the design and operation of open-loop shallow geothermal systems," *Advances in Geosciences*, vol. 62, pp. 57–66, 2023.

[95] S. Halilovic, F. Böttcher, K. Zosseder, and T. Hamacher, "Optimizing the spatial arrangement of groundwater heat pumps and their well locations," *Renewable Energy*, vol. 217, p. 119148, 2023.

[96] W. Kinzelbach, *Numerische Methoden zur Modellierung des Transports von Schadstoffen im Grundwasser*. 1987.

[97] S. Halilovic and F. Böttcher, "Optimization of GWHP well layouts using analytic models," 10 2022.

[98] S. Halilovic and F. Böttcher, "Optimization of thermal groundwater use," 10 2023.

[99] K. Zosseder, F. Böttcher, K. Davis, C. Haas, S. Halilovic, T. Hamacher, H. Heller, L. Odersky, V. Pauw, T. Schramm, and M. Schulte, "Schlussbericht zum Verbundprojekt GEO-KW: Kopplung des geothermischen Speicherpotenzials mit den wechselnden Anforderungen des urbanen Energiebedarfs zur effizienten Nutzung der regenerativen Energiequelle Grundwasser für die dezentrale Kälte-und Wärmebereitstellung in der Stadt," tech. rep., Bundesministerium für Wirtschaft und Klimaschutz, 2022.

[100] S. Halilovic, F. Böttcher, S. C. Kramer, M. D. Piggott, K. Zosseder, and T. Hamacher, "Well layout optimization for groundwater heat pump systems using the adjoint approach," *Energy Conversion and Management*, vol. 268, p. 116033, 2022.

[101] S. Halilovic, L. Odersky, F. Böttcher, K. Davis, M. Schulte, K. Zosseder, and T. Hamacher, "Optimization of an energy system model coupled with a numerical hydrothermal groundwater simulation," in *Mapping the Energy Future-Voyage in Uncharted Territory-, 43rd IAEE International Conference, July 31-August 3, 2022*, International Association for Energy Economics, 2022.

[102] L. W. Gelhar, C. Welty, and K. R. Rehfeldt, "A critical review of data on field-scale dispersion in aquifers," *Water Resources Research*, vol. 28, no. 7, pp. 1955–1974, 1992.

[103] A. García-Gil, M. Mejías Moreno, E. Garrido Schneider, M. Á. Marazuela, C. Abesser, J. Mateo Lázaro, and J. Á. Sánchez Navarro, "Nested shallow geothermal systems," *Sustainability*, vol. 12, no. 12, p. 5152, 2020.